

University of Southampton Research Repository ePrints Soton

Copyright © and Moral Rights for this thesis are retained by the author and/or other copyright owners. A copy can be downloaded for personal non-commercial research or study, without prior permission or charge. This thesis cannot be reproduced or quoted extensively from without first obtaining permission in writing from the copyright holder/s. The content must not be changed in any way or sold commercially in any format or medium without the formal permission of the copyright holders.

When referring to this work, full bibliographic details including the author, title, awarding institution and date of the thesis must be given e.g.

AUTHOR (year of submission) "Full thesis title", University of Southampton, name of the University School or Department, PhD Thesis, pagination

UNIVERSITY OF SOUTHAMPTON

FACULTY OF NATURAL AND ENVIRONMENTAL SCIENCES

Ocean and Earth Sciences



THE EVOLUTION OF VOLCANISM ON MONTSERRAT

by

Michael Cassidy

Thesis for the degree of Doctor of Philosophy

April 2012

UNIVERSITY OF SOUTHAMPTON
ABSTRACT

FACULTY OF NATURAL AND ENVIRONMENTAL SCIENCE
Ocean and Earth Sciences

Doctor of Philosophy

THE EVOLUTION OF VOLCANISM ON MONTSERRAT

By Michael Cassidy

Montserrat is a small volcanic island located in the Lesser Antilles. It hosts an active volcano, the Soufrière Hills volcano, which has affected, and continues to significantly affect, the local population. The thesis aims to examine the history of volcanism and related hazards on this island, to further understand the periodicity of eruptions, magmatic processes and potential future hazards, such as landslides. Uniquely, this work combines samples collected and sequences logged in both the subaerial and submarine realms.

A complete isotopic stratigraphy for the four different volcanic centres on Montserrat is presented, which includes high-precision double-spike Pb isotope data, combined with trace element and Sr-Nd isotope data for 2.5 Myr. These data show that the South Soufrière Hills volcanic centre falls along a different trend in Pb isotope space relative to the Silver Hills, Centre Hills and Soufrière Hills, which lie on the general trend common within the Lesser Antilles volcanics. The reason for this sudden magmatic source change is thought to be influenced by transtensional forces. The results suggest that Montserrat is not a simple two component system, but is affected by bulk sediment addition, sediment melt, slab fluids, altered oceanic crust and Galapagos plume components.

The previously understudied South Soufrière Hills volcanic centre is examined through subaerial sedimentological logging and sampling for geochemical analysis, together with submarine sediment core sedimentology, geochemistry and geophysical surveys. The results show that the South Soufrière Hills suffered a series of collapses, which successively cut back into older and chemically heterogeneous deposits, reversing the subaerial chemostratigraphy. The volcanic deposits show evidence for magma mingling, explosive andesitic eruptions and effusive eruptions of dacitic and basaltic lava flows.

Previously unrecognised volcanoclastic deposits are examined to constrain their age, source and emplacement mechanism. One such unit, the 8 ka Andesitic Volcanoclastic Unit resulted from a newly identified pyroclastic density current derived from a dome collapse of the Soufrière Hills volcano, which, upon entrance into the ocean, rapidly ingested water to become a water-supported turbidity current.

The marine sediment cores from Montserrat are comprehensively examined to produce an eruption history. Different tephra detection techniques were used to assess the most effective way of constructing volcanic records from marine sediment cores. The results show that fast, high spatial resolution and non-destructive techniques, such as XRF core scanning and magnetic susceptibility, are the best for detecting cryptotephra. Once the visible and cryptotephra have been identified, selected criteria are outlined to help distinguish primary eruption tephra from reworked volcanoclastic deposits. Such techniques were used to construct the record of eruptions from Montserrat in a time period from 130 to 37 ka. This work has significantly extended our understanding of this complex volcanic island and the thorough methodology used has potential implications for volcanism beyond Montserrat.

CONTENTS

	PAGE
List of Figures.....	x
List of Tables.....	xi
Authors Declaration.....	xiii
Acknowledgements.....	xv
 Chapter 1: INTRODUCTION.....	 1
1.1 Executive Summary and Project rationale	1
1.2 Geological Background of Montserrat.....	1
1.3 Overview of magma genesis at Lesser Antilles and Montserrat.....	4
1.4 Eruptive history of Montserrat overview.....	5
1.5 Geomorphology and mass movement events.....	8
Thesis overview	9
References.....	11
 Chapter 2: TRACKING THE MAGMATIC EVOLUTION OF AN ISLAND ARC VOLCANO: INSIGHTS FROM A HIGH- PRECISION Pb ISOTOPE RECORD OF MONTSERRAT, LESSER ANTILLES.....	 17
ABSTRACT.....	17
1.1 Introduction.....	18
1.2 Geological setting.....	19
2. Methods.....	22
2.1 Sample acquisition.....	22
2.2 Analytical techniques.....	22
3. Results.....	24
3.1 Provenance of Montserrat volcanics.....	24
3.2 Geochemical time series.....	27
3.2.1 Trace elements.....	27
3.2.2 Isotopic time series.....	30
4. Discussion.....	32
4.1 Montserrat and shallow level contamination.....	32
4.2 Age relations of the volcanic centres.....	33

4.3 Geochemical evolution of Montserrat.....	34
4.4 Slab and sediment contributions.....	36
4.5 Co-existence of two magmatic sources for Montserrat at ~130 ka....	41
4.6 Mantle enrichment.....	43
5. Summary and conclusions.....	44
References.....	45

CHAPTER 3 - MULTI-STAGE COLLAPSE EVENTS IN THE SOUTH SOUFRIÈRE HILLS, MONTSERRAT, AS RECORDED IN MARINE SEDIMENT CORES.....

Abstract.....	53
1. Introduction.....	54
1.1 Geological background.....	56
2. Methods.....	56
2.1 Marine core sampling, logging and fieldwork.....	56
2.2 Morphological and geophysical data.....	57
2.3 Geochemistry.....	57
3. Results.....	58
3.1 Subaerial stratigraphy of the SSH volcanic complex.....	58
3.2 Submarine morphology and geophysical data offshore from the SSH volcanic complex.....	64
3.3 Submarine stratigraphy and deposit characteristics.....	67
3.3.1 SSH Lower Unit.....	69
3.3.2 SSH Hemipelagic-rich Unit.....	73
3.3.3 SSH Upper Unit.....	73
3.4 Chemostratigraphy.....	73
4. Discussion.....	77
4.1 Emplacement of the subaerial SSH deposits.....	77
4.2 Emplacement of the submarine SSH deposits.....	79
4.3 Source of the submarine deposits, the geophysical evidence.....	80
4.4 Chemostratigraphic interpretations.....	81
4.5 Collapse model.....	82
5. Conclusions.....	84
References.....	84

CHAPTER 4 - A NEW LAVA DOME COLLAPSE INTO THE OCEAN AT THE SOUFRIÈRE HILLS VOLCANO,
MONTserrat, WEST INDIES AT CA 8 KA: HOW SUBMARINE STRATIGRAPHY CAN COMPLEMENT SUBAERIAL
ERUPTION HISTORIES.....91

Abstract.....	91
1. Introduction.....	92
1.1 Geological setting.....	94
2. Methods.....	97
2.1 Marine core sampling.....	97
2.2 AMS radiocarbon dating.....	97
2.3 Geochemical analyses.....	98
3. Results.....	98
3.1 Sea floor morphology and submarine facies architecture.....	98
3.2 Radiocarbon (AMS) dating constraints.....	101
3.3 Facies characteristics of the Mafic and Bioclastic-rich Unit.....	102
3.4 Facies characteristics of the 8 ka Andesitic Volcaniclastic Unit.....	108
4. Discussion.....	109
4.1 Source of the units.....	109
4.2 Reconstructing the emplacement mechanisms.....	110
4.2.1 The Mafic and Bioclastic-rich Unit.....	111
4.2.2 The 8 ka Andesitic Volcaniclastic Unit.....	111
4.3 Timing of events.....	113
5. Conclusions.....	113
References.....	114

CHAPTER 5 - ADVANCES IN THE CONSTRUCTION OF VOLCANIC RECORDS FROM MARINE SEDIMENT CORES: A
REVIEW AND CASE STUDY (MONTserrat, WEST INDIES).....118

Abstract.....	118
1. Introduction.....	120
1.1 Rationale and aims.....	120
1.2 Terminology.....	121
1.3 Volcanic sedimentation in oceanic settings.....	122
1.3.1 Primary airfall ash deposits.....	123
1.3.2 Primary Volcaniclastic flow deposits.....	123
1.3.3 Reworked Volcaniclastic deposits.....	124
1.4 Cryptotephra.....	125
1.5 Montserrat: the natural laboratory.....	126

2. Methods.....	131
2.1 Core sampling and sedimentological logging.....	131
2.2 Stable Oxygen isotopes.....	131
2.3 AMS radiocarbon dating.....	132
2.4 Component analysis.....	133
2.5 Scanning Electron Microscope (SEM).....	133
2.6 Magnetic susceptibility.....	134
2.7 Colour spectrophotometry.....	134
2.8 Grain size.....	134
2.9 XRF-core scanning.....	135
2.10 X-radiography.....	135
3. Results and Interpretations.....	136
3.1 Sea floor morphology.....	136
3.2 Core Chronology.....	136
3.3 Proximal core correlations south and south west offshore Montserrat.....	140
3.4 Stratigraphic Architecture.....	140
3.4.1 SSH Lower and Upper Units.....	140
3.4.2 75 ka Glass shard-rich Unit.....	141
3.4.3 75 Stratified Volcaniclastic Unit.....	141
3.4.4 8-35 ka Mafic and Bioclastic-rich Unit.....	142
3.4.5 8 ka Andesitic Volcaniclastic Unit.....	143
3.4.6 Current Soufrière Hills volcano eruptive products.....	145
3.5 Distal core stratigraphy.....	146
3.5.1 Component analysis by point counting.....	146
3.5.2 Magnetic susceptibility.....	148
3.5.3 Colour spectrophotometry.....	149
3.5.4 Grain size measurements.....	149
3.5.5 X-radiography.....	150
3.5.6 XRF core scanning.....	152
3.6 Cryptotephra detection.....	155
3.7 Primary or reworked.....	157
3.8 Nature of volcanic material.....	159
4. Discussion.....	161
4.1 What is the most effective way of detecting and identifying tephra layers.....	161

4.2 Inherent problems and limitations of detecting tephra in marine sediment records.....	161
4.3 Other tephra detection methods not explored in this study.....	163
5. Conclusions.....	166
References.....	167
CHAPTER 6: CONCLUSIONS AND FUTURE WORK.....	183
1. Key conclusions and returning to original thesis questions.....	183
1.1 Chapter 2.....	183
1.2 Chapter 3.....	184
1.3 Chapter 4.....	185
1.4 Chapter 5.....	186
2. Future perspectives.....	187
APPENDIX.....	189
Appendix A - Geochemical tables from Chapter 2.....	190
Appendix B - Data tables for Chapter 3.....	200
Appendix C - SEM images of the different components from Chapter 5.....	204
Appendix D - Conference Abstracts.....	205

LIST OF FIGURES

CHAPTER 1

Figure 1. Tectonic and geographical setting.....	4
Figure 2. Summary stratigraphic column of Montserrat.....	7
Figure 3. Submarine debris avalanche map.....	9

CHAPTER 2

Figure 1. Location and regional context map.....	21
Figure 2. Discriminant plots.....	26
Figure 3. Trace element time series.....	29
Figure 4. Isotopic time series.....	31
Figure 5. Differentiation versus isotopes.....	33
Figure 6. (La/Sm) _N plotted against Nd isotope.....	35
Figure 7. Pb isotopic diagrams.....	38
Figure 8. Trace element and isotopic plots and modelling.....	40
Figure 9. Schematic summary diagram.....	43

CHAPTER 3

Figure 1. Location map.....	56
Figure 2. East subaerial field section.....	61
Figure 3. Subaerial petrology.....	62
Figure 4. West subaerial field section.....	64
Figure 5. Geophysical imaging.....	66
Figure 6. 3D morphology images.....	67
Figure 7. Submarine transect of the units.....	69
Figure 8. Grain size statistics.....	71
Figure 9. Submarine clast petrology.....	73
Figure 10. Major element plot.....	75
Figure 11. Trace and isotopic discriminant plot.....	77
Figure 12. Block diagram summary.....	84

CHAPTER 4

Figure 1. Location figure with surficial debris avalanche deposits.....	95
Figure 2. Summary stratigraphic column for Montserrat.....	98
Figure 3. Correlative stratigraphic logs.....	102

Figure 4. Grain size and componentry of JR123-3.....	105
Figure 5. Photomicrographs and SEM images of the two units.....	106
Figure 6. Grain size and componentry of JR123-2 and JR123-46.....	107
Figure 7. Geochemical discriminant diagram for both units.....	110

CHAPTER 5

Figure 1. Location and bathymetry map.....	129
Figure 2. Summary stratigraphic column of Montserrat.....	132
Figure 3. Chronology figure.....	141
Figure 4. Proximal core correlations.....	147
Figure 5. Component analysis figure.....	150
Figure 6. X-radiography, magnetic susceptibility, grain size and colour spectrophotometry figure.....	153
Figure 7. XRF core scanning figure.....	155
Figure 8. Photomicrographs and SEM images of primary versus reworked volcaniclastic deposits.....	162
Figure 9. Summary stratigraphic log.....	167

LIST OF TABLES

CHAPTER 4

Table 1. Radiocarbon dates.....	104
Table 2. Geochemical analyses of the two units.....	109

CHAPTER 5

Table 1. Radiocarbon dates.....	140
Table 2. Summary of tephra detection methods.....	156
Table 3. Potential cryptotephra.....	158
Table 4. Visible tephra-primary or reworked.....	160
Table 5. Cryptotephra-primary or reworked.....	161

Declaration of Authorship

I, *Michael Cassidy* declare that this thesis entitled *the evolution of volcanism on Montserrat* and the work presented in it, are my own and has been generated by me as the result of my own original research.

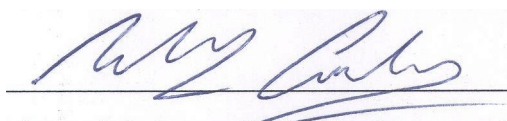
I confirm that:

- This work was done wholly or mainly while in candidature for a research degree at this University;
- Where any part of this thesis has previously been submitted for a degree or any other qualification at this University or any other institution, this has been clearly stated;
- Where I have consulted the published work of others, this is always clearly attributed;
- Where I have quoted from the work of others, the source is always given. With the exception of such quotations, this thesis is entirely my own work;
- I have acknowledged all main sources of help;
- Where the thesis is based on work done by myself jointly with others, I have made clear exactly what was done by others and what I have contributed myself;
- Parts of this work have been published as:

Cassidy, M., Taylor, R.N., Palmer, M.R, Cooper, R., Stenlake C., Trofimovs, J., (2012)
Tracking the magmatic evolution of an island arc volcano: Insights from a high-precision
Pb isotope record of Montserrat, Lesser Antilles. *Geochem. Geophys. Geosyst.* 13,
doi:10.1029/2012GC004064 (in press)

Cassidy, M., Trofimovs, J., Watt, S.F.L., Palmer, M.R., Taylor, R.N., Gernon, T.M., Talling, P.J.,
Le Friant, A. 'Multi-stage collapse events in the South Soufrière Hills, Montserrat, as
recorded in marine sediment cores', *In: Wadge, G., Robertson, R., Voight, B., (eds) The
eruption of Soufrière Hills volcano, Montserrat from 2000 to 2010*, Memoir of the
Geological Society, London (in press)

Signed:

A handwritten signature in blue ink, appearing to read 'Michael Cassidy', is written over a horizontal line.

Date: 25/04/12

ACKNOWLEDGEMENTS

First and foremost I would like thank my three supervisors Jessica Trofimovs, Martin Palmer and Rex Taylor for their excellent supervision and continued enthusiasm in my research. Jess, you've always been totally committed to my supervision and progression, despite going through so much in the time I've been here, such as giving birth to Finley and moving to Australia just to name a few, yet you have been ever present, always encouraging me and installing belief in my research abilities. Martin, you have been fundamental in helping me to develop my ideas and confidence, thanks for encouraging me to take up different scientific opportunities alongside my PhD and being so supportive in my search to find post-doctoral positions. Rex, I have especially enjoyed our hour-long chats in your office about geochemistry, volcanology and Liverpool FC, these causal chats have probably inspired many an idea that went into this project. I have learnt so much from you from lab techniques to subduction zone geochemical processes. All my supervisors have gone beyond the call of duty in many circumstances reading over countless manuscripts versions and giving constructive feedback. I'm ever grateful to NERC for funding this studentship and the Graduate School at NOCS (GSNOCS) for giving me this wonderful opportunity.

Special thanks also go to Tom Gernon for coming out to Montserrat to assist with fieldwork, you've been so supportive and enthusiastic since you've arrived, and it has been great to chat about volcanology and my research (often in a Caribbean accent). Thanks to Pete Talling for financial assistance, and for inspiring to think about the big picture. Other collaborators have significantly improved my research in this thesis by providing more data and ideas, especially Sebastian Watt, Will Symons, Rob Cooper, Chris Stenlake and Anne Le Friant. Thanks to Rachel James for acting as my panel chair and ensuring that I progressed well throughout my PhD. Many thanks go to Paul Cole, Rod Stewart, Adam Sinton, Thomas Christopher plus all the staff at the MVO and also to Bill Tonge from the Montserrat Water Authority for support, advice and access to the field localities.

Laboratory assistance was provided by Agnes Michalik, Matt Cooper, Andy Milton, Bob & John, Suzanne Maclaren, Guy Rothwell, Ian Croudace, Mike Bolshaw and Dave Spanner, you have been essential in making so much of the science at NOCS a success.

Thanks to Sue Mahony, Sam Engwell and Steve Sparks at the University of Bristol for interesting chats about tephra layers in marine sediment cores and to Steve for providing the JCR123 cores. Thanks also to Jodie Fisher at the University of Plymouth, who I asked many a question about oxygen isotope stratigraphy and other paleo things. Thanks to reviewers and editors of manuscripts, such as John Gamble, Tim Elliot, Matthijs van Soest, Alan Smith, Georges Boudon and Geoff Wadge for significantly improving Chapters 2 and 3.

I have Mr Dempsey to thank for inspiring the first bit of confidence in my scientific abilities and perhaps being the saving grace of that school. My obsession with volcanoes and geology began whilst doing an A-level in Geology with Keith Oak, your excellent teaching and encouraging approach inspired my geological career, I have a lot to thank you for! Thanks to all of my lecturers and friends at Bristol University for giving me a great grounding in Geology. Thanks also go to John Stevenson, Nick Varley and Dmitri Rouwet for giving me the opportunity to help study volcanoes in Mexico, my first taste of volcanological research. Staff and friends are thanked from Lancaster University where I completed my MSc, in particular my supervisor Harry Pinkerton, without his enthusiasm and support I would not be here.

Thanks to all my friends at NOCS, you have made my life here in Southampton so much richer - Ed, Anna, Dave, Debbie, Majid, Alex, Joe, Michael, Jimbo, Mark and countless more, we've enjoyed some great times and you have always been there for me, especially Gemma you've been my rock throughout the most difficult parts of my PhD, I can't quite imagine what it would have been like without you. To my family Mum, Dad, Rachel, Naomi, Tim and Nana, who've loved and supported me unconditionally my whole life, you've been the most encouraging and kind people I've ever known.

CHAPTER 1

1. INTRODUCTION

1.1 Executive Summary and Project Rationale

The recent eruptions of the Soufrière Hills volcano (1995-present) have had a devastating effect on the local population living on Montserrat, West Indies. Nineteen people lost their lives, the capital city has been destroyed and over 8,000 of the original 13,000 inhabitants have since emigrated. Detailed knowledge of the past history of an active volcano is crucial for the prediction of future eruptive phenomena, assessment of the long-term probability of occurrence and identification of potentially affected areas. Consequently, this research uses geochemical and sedimentological analyses of volcanic deposits from both the submarine and subaerial realms to understand how volcanism on Montserrat has evolved throughout its history. This will be achieved by: (1) constraining an accurate record of activity by examining the marine sediment record in the ocean around Montserrat, (2) gaining a large geochemical dataset from samples throughout the volcanic evolution of Montserrat to further elucidate the magmatic processes occurring beneath the island, and (3) reconstructing the deposits from large landslides that have shaped the island by their passage into the sea.

Understanding past deposits from a volcano is the key to forecasting future behaviour. This project aims to deliver detailed submarine stratigraphic architecture, that, coupled with subaerial data, will greatly improve our knowledge of the eruption sequence on Montserrat. This will help elucidate future patterns of eruptive activity.

1.2 Geological background of Montserrat

The Lesser Antilles island Arc is a 750 km long arc chain formed by the westward dipping subduction of the North American plate beneath the Caribbean plate (DeMets et al., 2000). The North American plate subducts at a slightly oblique angle (Feuilliet 2000) and a relatively low convergence rate of about 2 cm/yr (Wadge, 1984; Demets et al., 2000). The Caribbean plate is thought to have moved eastwards to its present site from an original location in the

Pacific, where it may have been generated over the Galapagos hotspot 100-75 Ma ago (Pindell and Barrett, 1990). It was then inserted between the North American and South American plates sometime between the Late Campanian and Late Eocene (Pindell and Barrett, 1990). A subduction zone developed, and active volcanism began 40 Ma ago leading to the production of a volcanic island arc (Briden et al., 1979; Bouysse and Westercamp, 1989). The Wadati-Benioff zone dips $\sim 45^\circ$ westward beneath the northern part of the arc (Wadge and Shepherd, 1984). The crustal thickness is estimated at $\sim 30 \pm 4$ km for the northern part of the arc (Wadge, 1984; Sevilla, 2010) and seismic studies indicate that the subducted oceanic slab is segmented into three main parts with differing dips and slip vectors (Wadge and Shepherd, 1984).

To the north of Martinique, the arc divides into two chains of islands (Figure 1a). This is thought to have occurred as a buoyant ridge reached the trench and obstructed subduction in the northern part of the Lesser Antilles, leading to slab break-off (Bouysse and Westercamp, 1989). The eastern chain is older with thick carbonate platforms covering a volcanic basement, and termed the Limestone Caribbees (Wadge 1984). The west chain consists of volcanic rocks younger than 20 Ma (Volcanic Caribbees; Wadge 1984) and includes all the active volcanoes (Bouysse and Westercamp, 1989). The southern Volcanic Caribbees extend from Martinique to Grenada Islands and commonly display Pliocene and Quaternary volcanic rocks superimposed over pre-Miocene volcanic rocks and sedimentary deposits (Maury et al., 1990). Major components of deep water sediment in this region include volcanoclastic silt and clay, redeposited shallow-water carbonate detritus, pelagic carbonate sediment accumulations, and windblown dust from Africa (Reid et al., 1996). It has been estimated that 527 km^3 of volcanic material (285 km^3 D.R.E) has been erupted from volcanoes in the Lesser Antilles in the last 100 ka (Sigurdsson et al., 1980). An estimated 84% of this material has been transported into adjacent marine basins and deposited as volcanogenic sediments (Sigurdsson et al., 1980).

Montserrat is a volcanic island, situated in the northern part of the Lesser Antilles island arc (Figure 1a). The island is 16 km long (north - south), 10 km wide (east - west) and is made up almost exclusively of volcanic rocks. Volcanism has persisted for at least 2.6 Ma erupting from four distinct volcanic centres. These volcanic centres have been separated into three different regions based on Ar-Ar geochronology by Harford et al. (2002). The oldest volcanic centre can be found in the north of the island, the Silver Hills, which dates from 2600-1200 ka. The Centre Hills just south of the Silver Hills was active from 950 ka to 550 ka and the South-Soufrière Hills - Soufrière Hills complex has been active since 174 ka and the Soufrière Hills volcano is active at present (Figure 1b). Harford et al. (2002) document that the volcanic centres age northwards, and they attributed this to a stationary magmatic source

feeding the volcanic output as the plate migrated. The migration of volcanism away from the trench has been interpreted to relate to variation in the subducting slab due to the growth of the accretionary prism (Wadge 1984).

Whilst the majority of deposits on Montserrat are andesitic in composition, the South Soufrière Hills region comprises basalts and basaltic andesites (Rea, 1974; Harford et al., 2002). Mafic inclusions (known as enclaves) are also present within the andesites of the Silver Hills, Centre Hills and Soufrière Hills (Rea 1974, Zellmer et al., 2003). These mafic enclaves are thought to represent a magma recharge system, as hotter mafic magmas injected into the host andesite heat the host magma and load it with volatiles. The resultant build up of pressure is commonly enough to overcome the lithostatic pressure, thus triggering a volcanic eruption (Sparks et al., 1977; Murphy et al., 1998, 2000; Devine et al., 1998). The petrological and geochemical characteristics of the magmas change with age in the South Soufrière Hills–Soufrière Hills complex. Samples older than 150 ka are dominated by two pyroxene andesites, whereas, all samples younger than 110 ka are hornblende-hypersthene andesites (Harford et al., 2002). This composition change coincides with ages for volcanism at South Soufrière Hills (~130 ka). The mineralogical transition therefore appears to have happened after an interlude of mafic volcanism (Harford et al., 2002).

The major deposits on Montserrat are remnants of andesitic lava domes, dome talus breccias, dome-collapse pyroclastic flow deposits, lahar and debris avalanche deposits, with thin tephra-fall deposits (Harford et al., 2002). The Soufrière Hills volcanic complex comprises five andesitic lava domes; Gages Mountain, Chances Peak, Galways Mountain, Perches Mountain and the site of new lava eruptions that is superimposed on an older dome, Castle Peak (Fig. 1b). Garabaldi Hill, Roche's Bluff, Richmond Hill and St Georges Hill are all thought to be uplifted sections from older volcanic deposits, however it is uncertain as to which volcanic centre these uplifted sections belong (Harford et al., 2002). The Soufrière Hills volcano, occupies the site currently active (1995 - present) and is characterised by andesitic dome growth and collapse events, which produce block-and-ash pyroclastic flows and Vulcanian eruptions (Young et al., 1998; Robertson et al., 2000). From 1995 to 2012, the Soufrière Hills has had 5 phases of extrusion: Phase 1, 1995-1998, Phase 2, 1999-2003, Phase 3, 2005-2007, Phase 4, 2008 and Phase 5, 2009-2010 (Source: Montserrat Volcano Observatory - <http://www.mvo.ms>).

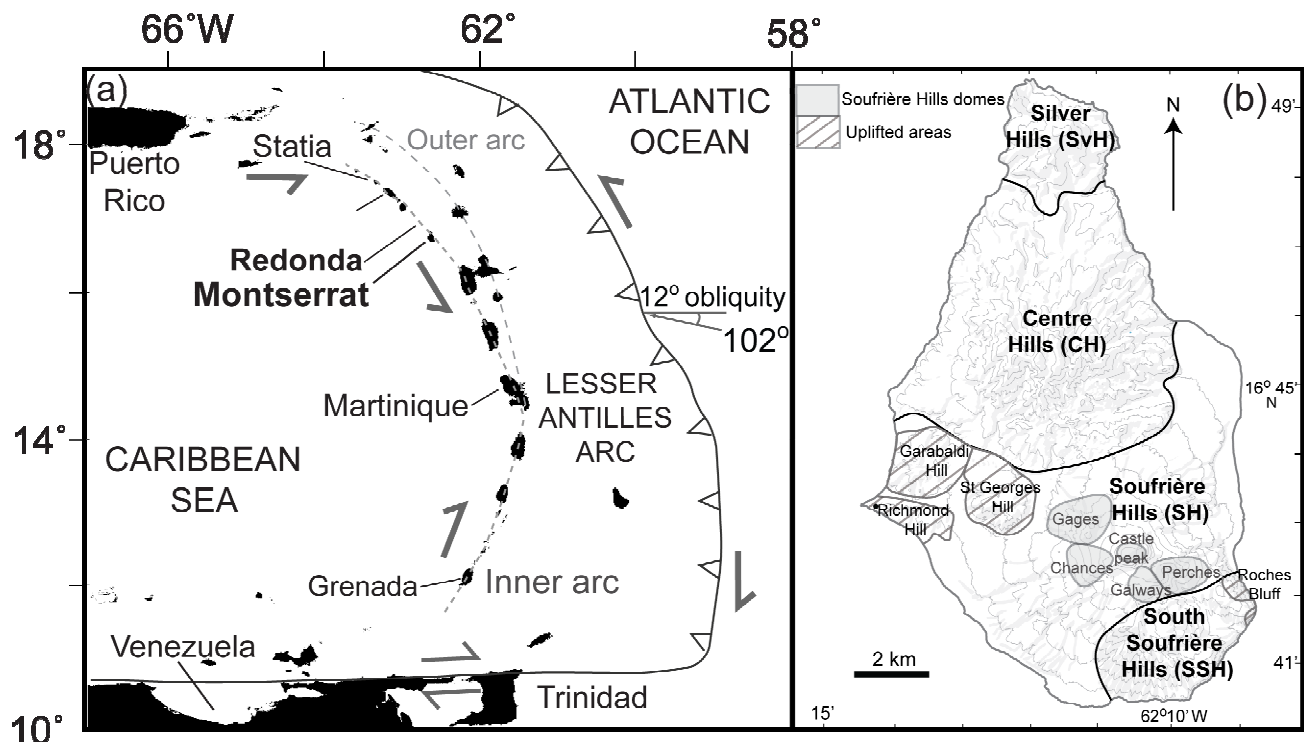


Figure 1 (a) The Lesser Antilles island arc, showing the island of Montserrat which is located in the northern part of the arc. The active (inner) western arc is shown together with the outer-eastern arc, which possesses the older volcanic islands. (b) Shows the volcanic centres on Montserrat, the domes on the Soufrière Hills complex and uplifted areas after Harford et al. (2002).

1.3 Overview of magma genesis at Lesser Antilles and Montserrat

The Lesser Antilles islands display a wide range in isotopic and chemical compositions (White and Dupre, 1986; Davidson 1987, 1996; Thirwall et al., 1996; Macdonald et al., 2000; Van Soest et al., 2002; Lindsay et al., 2005; Toothill et al., 2007; Carpentier et al., 2008; Dufrane et al., 2009; Labanieh et al., 2010; Davidson and Wilson 2011). The primary magmas are thought to have been derived from normal mid-ocean ridge basalts (N-MORB) type mantle which has been modified by the addition of a fluid component derived mainly from subducted basaltic crust and a component derived from partial melting of subducted sediment (Macdonald et al., 2000). It has been noted by various authors, that there is an along-arc chemical gradient, with more radiogenic Pb and Sr isotope ratios and lower Nd ratios in the south relative to the north (Hawkesworth and Powell, 1980; White and Dupre, 1986; Davidson 1987; Turner et al., 1996). These observations have led to the suggestion that the proportion of sediment component increased relative to that of the hydrous fluids towards the south. There is evidence to suggest that this occurs both from crustal assimilation and from subducted slab-derived sediment (White and Dupre, 1986; Davidson 1987; Davidson and Harmon, 1989; Thirwall et al., 1996; Turner et al., 1996). The amount of contamination may be related to volumetric volcanic output (Macdonald et al.,

2000). Dufrane et al. (2009) and Labanieh et al. (2010) recently suggested that partial melt of sediments could explain the large isotopic range for the arc, however the different volcanic islands, and different centres within individual islands, can also show different fractionation histories (Thirlwall et al., 1996; Heath et al., 1998). This indicates that the factors that control magma compositions (such as water concentrations in the source rocks, magmatic sources and magma ascent rates) may vary on the scale of tens of kilometres (Macdonald et al., 2000).

On Montserrat, the most recently active volcanic centres, Soufrière Hills and South Soufrière Hills, were investigated by Zellmer et al. (2003), using major, trace and U, Th and O isotopes. The authors concluded that the source magmas of these volcanic centres were enriched by slab fluid and small amounts (~1.2 %) of sediment. Some geochemical distinctions were noted between the Soufrière Hills and South Soufrière Hills, which the authors attributed to differing degrees and styles of fractionation. The SSH was thought to be derived from an open system, in which the magmatic system was constantly replenished, whereas Soufrière Hills volcano was thought to be dominated by a closed magmatic system, wherein more extensive magmatic fractionation could occur (Zellmer et al. 2003).

1.4 Eruptive history of Montserrat overview

The volcanic history of the Soufrière Hills and SSH volcanic centres has been studied subaerially (Rea, 1974; Roobol and Smith, 1997; Harford et al., 2002; Smith et al., 2007) and subaqueously (Le Friant et al., 2008; Trofimovs et al., 2010). Stratigraphic observation, volume estimations, and geochronology, imply that the periods of volcanic extrusion from the Soufrière Hills and South Soufrière Hills regions are spatially and temporally interspersed (Harford et al., 2002; Smith et al., 2007; Le Friant et al., 2008). The subaerial stratigraphy of the Soufrière Hills – South Soufrière Hills volcanic complex was documented by Roobol and Smith (1998) and later revised (Smith et al., 2007). They subdivided the eruptive history into seven episodes (Figure 2). This activity comprised a combination of Plinian, Pelean and basaltic fire fountaining eruptions. Periods of activity are historically short-lived on Montserrat and normally followed by long periods of dormancy (Harford et al., 2002; Smith et al., 2007, Le Friant et al. 2008).

Recent studies estimate that >80% of volcanic material erupted from subaerial volcanic activity is deposited in the ocean surrounding the island (Trofimovs et al. 2008; Le Friant et al. 2009). Therefore, the marine stratigraphy potentially provides a more complete and comprehensive record of volcanic activity. On this premise, Le Friant *et al.* (2008) analysed one core (Carmon 2) situated 55 km SW of Montserrat, interpreting the occurrence and nature the volcanic episodes by separating volcanoclastic clasts from background

hemipelagic sediment accumulations and point counting. Micropaleontology and $\delta^{18}\text{O}$ isotope analyses were used to date the hemipelagic sediment accumulations between the identified volcanic horizons. The tephra layers in the marine record aid in reconstructing the volcanic history of Montserrat to ca 250 ka (Le Friant et al., 2008). During this period of time, the authors identified eight layers relating to dome eruptions, five of which can be directly correlated to dated domes or related pyroclastic flow sequences on land, and six significant explosive eruptions, which do not correspond with any documented eruptive subaerial deposits.

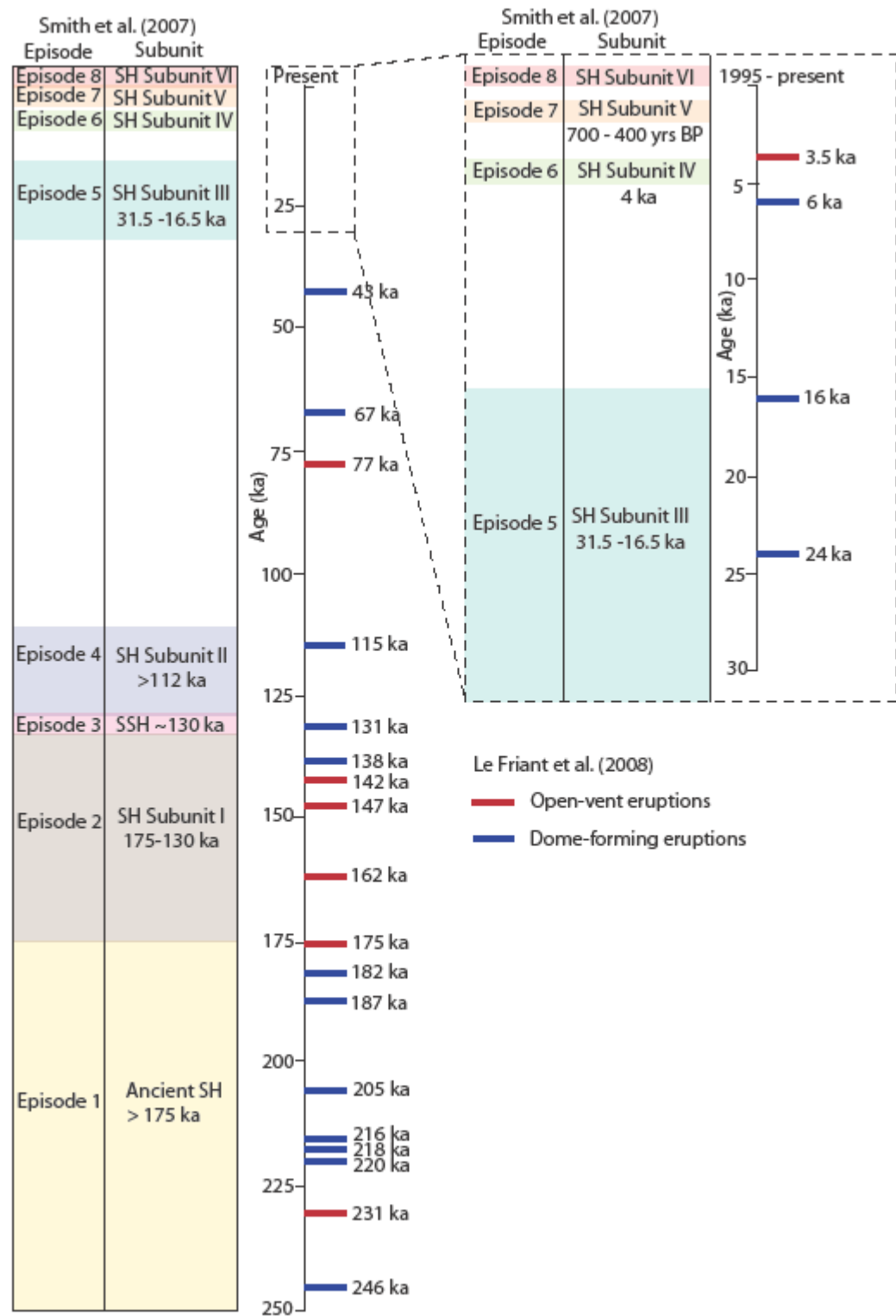


Figure 2. Summary stratigraphic column of the Soufriere Hills-South Soufriere Hills complex, combining the subaerial record of Smith et al. (2007) and submarine tephrochronology of Le Friant et al. (2008).

1.5 Geomorphology and mass movement events

The geomorphology of Montserrat and its surrounding submarine apron has been shaped by prolonged terrestrial and coastal erosion, as well as catastrophic, geologically rapid events such as dome collapse, flank/sector collapse and submarine slope failures (Le Friant et al., 2004; Figure 3). Mass movement poses significant hazards to lives and infrastructure and can change the morphology of the landscape considerably. For example, submarine slope failures have produced some of the largest mass flows in the world and are one of the main agents through which sediments are transferred from the continental slope to the deep ocean (Masson et al. 2006). However large subaerial landslides such as those from ocean island flanks have been identified as the most dangerous of all landslide hazards (Masson et al. 2006) because of their tsunamigenic potential as they enter the ocean (e.g. Ward and Day, 2001; Lovholt et al., 2008).

Subaerial and submarine mapping has shown that large landslides are a common occurrence along the Lesser Antilles arc. At least 40 flank-collapse events have been identified, of which about 15 occurred in the last 12,000 years on active volcanoes (Deplus et al., 2001; Boudon et al., 2007). Such an event occurred ~4 ka at Montserrat, where the eastern part of the Soufrière Hills subsided into the sea, forming English's crater (Boudon et al., 2007).

Bathymetric and geophysical surveys have been undertaken around Montserrat, identifying at least seven submarine landslide deposits (Le Friant et al. 2004; Lebas et al., 2011; Watt et al., 2012). The largest of these deposits has a volume of ~20 km³, with an area (277 km²) far exceeding that of the entire island (~100 km²) (Lebas et al., 2011). These deposits will be a focus of the scientific drilling scheduled for 2012.

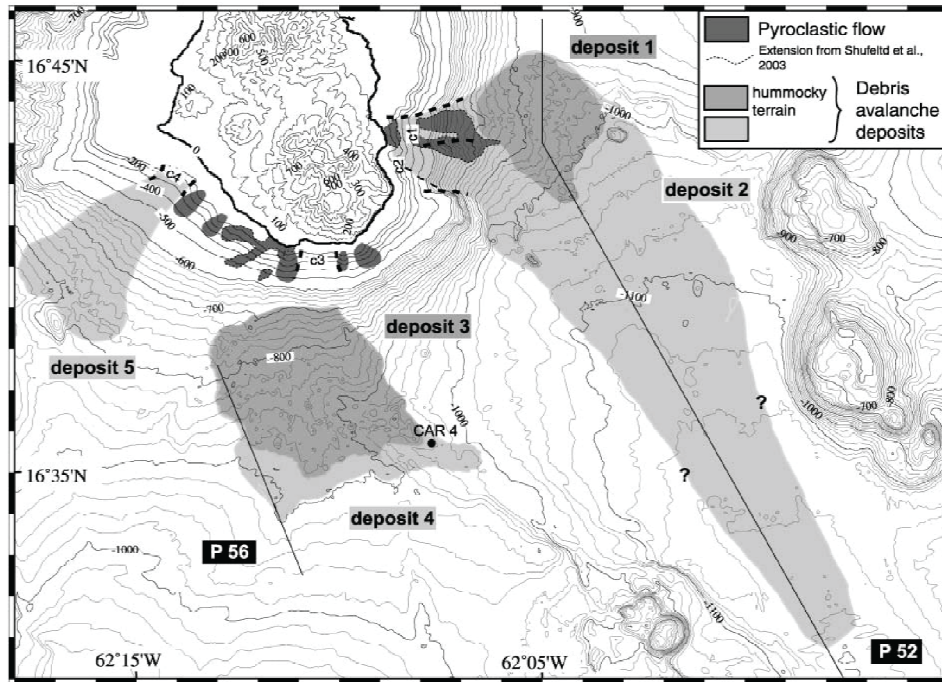


Figure 3 Map showing submarine gravity flow deposits around Montserrat. Dark grey area shows extent of submarine pyroclastic flow deposits; mid-grey area shows extent of debris avalanche deposits with hummocky terrain identified on the bathymetry; light grey area shows debris avalanche deposits identified with 3.5 kHz and seismic data (Figure from Le Friant et al., 2004).

Thesis overview

The overarching aim of this thesis is to investigate how volcanism on Montserrat has evolved. Chapter 2 details a comprehensive isotopic stratigraphy for Montserrat, which aids in understanding how magmas have been generated at Montserrat over time. In Chapters 3 and 4 the emphasis is on understanding the volcanic history by reconstructing individual, yet significant, mass movement events, such as subaerial and submarine flank failures, together with dome collapses to better understand how these occur and behave once in they enter the submarine setting. Chapter 5 addresses the advancement of volcanic record interpretation from marine sediment cores. This chapter reviews different tephrostratigraphy methods using the Montserrat case study. Chapters 2 to 5 of this thesis have been prepared as independent papers for publication. Thus, to avoid repetition, these chapters are only briefly described below with a full abstract given at the start of each chapter. Another consequence of this formatting style is that relevant methods are described in each chapter rather than in a separate and self-contained 'Methods' chapter.

Chapter 2 - Tracking the magmatic evolution of an island arc volcano: Insights from a high-precision Pb isotope record of Montserrat, Lesser Antilles

A study into the sources and processes of magma production at Montserrat and how has this evolved over 2.5 Myrs of volcanism. The work identifies the components that control the composition of the source magmas. Key questions addressed:

(Q2.1) Have the composition of magmas beneath Montserrat been consistent throughout its history?

(Q2.2) What implications does this geochemical study on Montserrat have on the factors controlling the composition magmas at other volcanoes in the Lesser Antilles?

This paper has been accepted by the journal *Geochemistry, Geophysics, Geosystems* cubed and is currently in press, available online at doi:10.1029/2012GC004064

Chapter 3 - Multi-stage collapse events in the South Soufrière Hills, Montserrat, as recorded in marine sediment cores

This chapter is a multi-disciplinary study of the South Soufrière Hills, examining the volcanic and geochemical evolution of the centre and detailing the failure of part of the edifice into the ocean. Key questions addressed:

(Q3.1) What was the chronostratigraphic evolution of the South Soufrière Hills volcanic complex?

(Q3.2) How did such flank collapse(s) and resulting sediment flow(s) behave?

At the time of thesis completion this chapter has been accepted for publication in the *In: Wadge, G., Robertson, R., Voight, B., (eds) The eruption of Soufrière Hills volcano, Montserrat from 2000 to 2010*, Memoir of the Geological Society, London.

Chapter 4 - A new lava dome collapse into the ocean at the Soufrière Hills volcano, Montserrat, West Indies at ca 8 ka: how submarine stratigraphy can complement subaerial eruption histories

Chapter 4 documents a previously unrecognised primary volcanic eruption from the Soufrière Hills volcano at ca 8 ka. These primary pyroclastic deposits overlie deposits from a volcanic flank collapse that occurred between 8 and 35 ka. Both deposits have only been recognised in the submarine sediment record. Key questions addressed:

(Q4.1) Where do the 8 ka Andesitic Volcaniclastic Unit and the Mafic Bioclastic-rich Unit originate from?

(Q4.2) What are the processes that led to the emplacement of these submarine deposits?

This chapter forms the basis of a manuscript in preparation to be submitted to the *Journal of Volcanology and Geothermal Research* (in 2012).

Chapter 5 - Advances in the construction of volcanic records from marine sediment cores: A review and case study (Montserrat, West Indies).

This chapter highlights and resolves common problems that occur when developing a tephrochronological record. This work suggests protocols for the recognition of cryptotephra in marine sediment, determining whether the marine volcanoclastic deposits are primary or secondary and useful methods for dating marine deposits. A tephrochronological record from the marine sediments south and southwest of Montserrat is presented and compared with the literature. Key questions addressed:

(Q5.1) What is the best way of constructing a volcanic record from marine sediment cores?

(Q5.2) Were the volcanic centres on Montserrat more or less volcanically active than previously recognised?

This chapter forms the basis of a manuscript in preparation (to be submitted 2012).

References

- Boudon, G., A. Le Friant, J.C. Komorowski, C. Deplus and M.P. Semet (2007) "Volcano flank instability in the lesser Antilles arc: diversity of scale, processes, and temporal recurrence" Journal of Geophysical Research-Part B-Solid Earth B08205-1-28
- Bouysse, P. and D. Westercamp (1990) "Subduction of atlantic aseismic ridges and late cenozoic evolution of the Lesser Antilles island-arc" Tectonophysics **175** 349-&
- Briden, J.C., D.C. Rex, A.M. Faller and J.F. Tomblin (1979) "K-Ar geochronology and paleomagnetism of volcanic-rocks in the Lesser Antilles arc" Geophysical Journal of the Royal Astronomical Society **57** 272-272
- Carpentier, M., C. Chauvel and N. Mattielli (2008) "Pb-Nd isotopic constraints on sedimentary input into the Lesser Antilles arc system" Earth and Planetary Science Letters **272** 199-211
- Cassidy, M., Trofimovs, J., Palmer, M.R., Taylor, R.N. Moreton, S. (in prep) "A new lava dome collapse into the ocean at the Soufriere Hills volcano, Montserrat, West Indies at ca 8 ka: how submarine stratigraphy can complement subaerial eruption histories"
- Cassidy, M., Trofimovs, J., Watt, S.F.L., Palmer, M.R., Taylor, R.N., Gernon, T.M., Talling, P.J., Le Friant, A. (in press) "Multi-stage collapse events in the South Soufrière Hills, Montserrat, as recorded in marine sediment cores" In G. Wadge, Robertson, R., Voight, B., (eds) *The eruption of Soufrière Hills volcano, Montserrat from 2000 to 2010* Memoir of the Geological Society, London

Cassidy, M.T., R.N., Palmer, M.R, Cooper, R., Stenlake C., Trofimovs, J. (2012) "Tracking the magmatic evolution of island arc volcanism: Insights from a high-precision Pb isotope record of Montserrat, Lesser Antilles" Geochemistry Geophysics Geosystems

Davidson, J. and M. Wilson (2011) "Differentiation and Source Processes at Mt Pelee and the Quill; Active Volcanoes in the Lesser Antilles Arc" Journal of Petrology **52** 1493-1531

Davidson, J.P. (1987) "Crustal contamination versus subduction zone enrichment - Examples from the Lesser Antilles and implications for mantle source compositions of island-arc volcanic-rocks" Geochimica Et Cosmochimica Acta **51** 2185-2198

Davidson, J.P. (1996) "Deciphering mantle and crustal signatures in subduction zone magmatism" Geophys. Monogr. American geophysical union **96** 251-262

Davidson, J.P. and R.S. Harmon (1989) "Oxygen isotope constraints on the petrogenesis of volcanic arc magmas from Martinique, Lesser Antilles" Earth and Planetary Science Letters **95** 255-270

DeMets, C., P.E. Jansma, G.S. Mattioli, T.H. Dixon, F. Farina, R. Bilham, E. Calais and P. Mann (2000) "GPS geodetic constraints on Caribbean-North America plate motion" Geophysical Research Letters **27** 437-440

Deplus, C., A. Le Friant, G. Boudon, J.C. Komorowski, B. Villemant, C. Harford, J. Segoufin and J.L. Cheminee (2001) "Submarine evidence for large-scale debris avalanches in the Lesser Antilles Arc" Earth and Planetary Science Letters **192** 145-157

Devine, J.D., M.D. Murphy, M.J. Rutherford, J. Barclay, R.S.J. Sparks, M.R. Carroll, S.R. Young and J.E. Gardner (1998) "Petrologic evidence for pre-eruptive pressure-temperature conditions, and recent reheating, of andesitic magma erupting at the Soufriere Hills Volcano, Montserrat, WI" Geophysical Research Letters **25** 3669-3672

DuFrane, S.A., S. Turner, A. Dosseto and M. van Soest (2009) "Reappraisal of fluid and sediment contributions to Lesser Antilles magmas" Chemical Geology **265** 272-278

Feuillet, N. (2000) "Sismotectonique des Petites Antilles, liason entre activite sismique et volcanique = Sismotectonics of Lesser Antilles, relationship between seismic activity and volcanism." Rene Diderot University PhD Thesis 283 pp

Harford, C.L., Pringle, M.S., Sparks, R.S.J., Young S.R. (2002) "The volcanic evolution of Montserrat using $^{40}\text{Ar}/^{39}\text{Ar}$ geochronology." In T. H. Druitt, Kokelaar, B.P. (eds) *The eruption*

of Soufrière Hills Volcano, Montserrat, from 1995 to 1999 Geological Society of London Memoirs **21** 93-113

Hawkesworth, C.J. and M. Powell (1980) "Magma genesis in the Lesser Antilles island-arc" Earth and Planetary Science Letters **51** 297-308

Heath, E., R. MacDonald, H. Belkin, C. Hawkesworth and H. Sigurdsson (1998) "Magma genesis at Soufriere Volcano, St Vincent, Lesser Antilles arc" Journal of Petrology **39** 1721-1764

Labanieh, S., C. Chauvel, A. Germa, X. Quidelleur and E. Lewin (2010) "Isotopic hyperbolas constrain sources and processes under the Lesser Antilles arc" Earth and Planetary Science Letters **298** 35-46

Le Friant, A., C. Deplus, G. Boudon, R.S.J. Sparks, J. Trofimovs and P. Talling (2009) "Submarine deposition of volcaniclastic material from the 1995-2005 eruptions of Soufriere Hills volcano, Montserrat" Journal of the Geological Society **166** 171-182

Le Friant, A., C.L. Harford, C. Deplus, G. Boudon, R.S.J. Sparks, R.A. Herd and J.C. Komorowski (2004) "Geomorphological evolution of Montserrat (West Indies): importance of flank collapse and erosional processes" Journal of the Geological Society **161** 147-160

Le Friant, A., E.J. Lock, M.B. Hart, G. Boudon, R.S.J. Sparks, M.J. Leng, C.W. Smart, J.C. Komorowski, C. Deplus and J.K. Fisher (2008) "Late Pleistocene tephrochronology of marine sediments adjacent to Montserrat, Lesser Antilles volcanic arc" Journal of the Geological Society **165** 279-289

Lebas, E., A. Le Friant, G. Boudon, S.F.L. Watt, P.J. Talling, N. Feuillet, C. Deplus, C. Berndt and M.E. Vardy (2011) "Multiple widespread landslides during the long-term evolution of a volcanic island: Insights from high-resolution seismic data, Montserrat, Lesser Antilles" Geochemistry Geophysics Geosystems **12**

Lindsay, J.M., R.B. Trumbull and W. Siebel (2005) "Geochemistry and petrogenesis of late Pleistocene to recent volcanism in Southern Dominica, Lesser Antilles" Journal of Volcanology and Geothermal Research **148** 253-294

Lovholt, F., G. Pedersen and G. Gisler (2008) "Oceanic propagation of a potential tsunami from the La Palma Island" Journal of Geophysical Research-Oceans **113** 21

Macdonald, R., C.J. Hawkesworth and E. Heath (2000) "The Lesser Antilles volcanic chain: a study in arc magmatism" Earth-Science Reviews **49** 1-76

Masson, D.G., C.B. Harbitz, R.B. Wynn, G. Pedersen and F. Lovholt (2006) "Submarine landslides: processes, triggers and hazard prediction" Philosophical Transactions of the Royal Society a-Mathematical Physical and Engineering Sciences **364** 2009-2039

Maury, R.C., Westbrook, G.K., Baker, P.E., Bouysse, P., Westercamp, D. (1990) "Geology of the Lesser Antilles" The Geology of North America H-The caribbean region 141-166

Murphy, M.D., R.S.J. Sparks, J. Barclay, M.R. Carroll and T.S. Brewer (2000) "Remobilization of andesite magma by intrusion of mafic magma at the Soufriere Hills Volcano, Montserrat, West Indies" Journal of Petrology **41** 21-42

Murphy, M.D., R.S.J. Sparks, J. Barclay, M.R. Carroll, A.M. Lejeune, T.S. Brewer, R. Macdonald, S. Black and S. Young (1998) "The role of magma mixing in triggering the current eruption at the Soufriere Hills volcano, Montserrat, West Indies" Geophysical Research Letters **25** 3433-3436

Pindell, J., & Barrett, S. (1990) "Geological evolution of the Caribbean region; a Plate tectonic perspective" Geological Society of America The Geology of North America 405-432 pp

Rea, J.W. (1974) "The volcanic geology and petrology of Montserrat, West Indies" J. Geol. Soc. Lond. **130** 341-366

Reid, R.P., S.N. Carey and D.R. Ross (1996) "Late quaternary sedimentation in the Lesser Antilles island arc" Geological Society of America Bulletin **108** 78-100

Robertson, R.E.A., W.P. Aspinall, R.A. Herd, G.E. Norton, R.S.J. Sparks and S.R. Young (2000) "The 1995-1998 eruption of the Soufriere Hills volcano, Montserrat, WI" Philosophical Transactions of the Royal Society of London Series a-Mathematical Physical and Engineering Sciences **358** 1619-1637

Roobol, M.J. and A.L. Smith (1998) "Pyroclastic stratigraphy of the Soufriere Hills volcano, Montserrat - Implications for the present eruption" Geophysical Research Letters **25** 3393-3396

Sevilla, W.I., C.J. Ammon, B. Voight and S. De Angelis (2010) "Crustal structure beneath the Montserrat region of the Lesser Antilles island arc" Geochemistry Geophysics Geosystems **11** 13

Sigurdsson, H., R.S.J. Sparks, S.N. Carey and T.C. Huang (1980) "Volcanogenic sedimentation in the Lesser Antilles arc" Journal of Geology **88** 523-540

Smith, A.L.R., M.J. Schellekens, J.H. & Mattioli, G.S. (2007) "Prehistoric stratigraphy of the Soufriere Hills–South Soufriere Hills volcanic complex, Montserrat, West Indies" Journal of Geology **115** 115-127

Sparks, R.S.J., H. Sigurdsson and L. Wilson (1977) "Magma mixing: a mechanism for triggering acid explosive eruptions" Nature **267** 315-8

Thirlwall, M.F., A.M. Graham, R.J. Arculus, R.S. Harmon and C.G. Macpherson (1996) "Resolution of the effects of crustal assimilation, sediment subduction, and fluid transport in island arc magmas: Pb-Sr-Nd-O isotope geochemistry of Grenada, Lesser Antilles" Geochimica Et Cosmochimica Acta **60** 4785-4810

Toothill, J., C.A. Williams, R. Macdonald, S.P. Turner, N.W. Rogers, C.J. Hawkesworth, D.A. Jerram, C.J. Ottley and A.G. Tindle (2007) "A complex petrogenesis for an arc magmatic suite, St Kitts, Lesser Antilles" Journal of Petrology **48** 3-42

Trofimovs, J., J.K. Fisher, H.A. MacDonald, P.J. Talling, R.S.J. Sparks, M.B. Hart, C.W. Smart, G. Boudon, C. Deplus, J.C. Komorowski, A. Le Friant, S.G. Moreton and M.J. Leng (2010) "Evidence for carbonate platform failure during rapid sea-level rise; ca 14 000 year old bioclastic flow deposits in the Lesser Antilles" Sedimentology **57** 735-759

Trofimovs, J., R.S.J. Sparks and P.J. Talling (2008) "Anatomy of a submarine pyroclastic flow and associated turbidity current: July 2003 dome collapse, Soufriere Hills volcano, Montserrat, West Indies" Sedimentology **55** 617-634

Turner, S., C. Hawkesworth, P. vanCalsteren, E. Heath, R. Macdonald and S. Black (1996) "U-series isotopes and destructive plate margin magma genesis in the Lesser Antilles" Earth and Planetary Science Letters **142** 191-207

Van Soest, M.C., D.R. Hilton, C.G. Macpherson and D.P. Mattey (2002) "Resolving sediment subduction and crustal contamination in the Lesser Antilles island Arc: A combined He-O-Sr isotope approach" Journal of Petrology **43** 143-170

Wadge, G. (1984) "Comparison of volcanic production-rates and subduction rates in the Lesser Antilles and Central America" Geology **12** 555-558

Wadge, G. and J.B. Shepherd (1984) "Segmentation of the Lesser Antilles subduction zone" Earth and Planetary Science Letters **71** 297-304

Ward, S.N. and S. Day (2001) "Cumbre Vieja Volcano - Potential collapse and tsunami at La Palma, Canary Islands" Geophysical Research Letters **28** 3397-3400

Watt, S.F.L., Talling, P.J., Vardy, M.E., Heller, V., Huhnerbach, V., Urlaub, Morelia, Sarkar, Sudipta, Masson, D.G., Henstock, T.J., Minshull, T.A., Paulatto, M., Le Friant, A, Lebas, E, Berndt, C., Crutchley, G, Karstens, J, Stinton, A and Maeno, F (2012) "Combinations of volcanic-flank and seafloor-sediment failure offshore Montserrat, and their implications for tsunami generation" Earth and Planetary Science Letters **319-320** 228-240

White, W.M. and B. Dupre (1986) "Sediment subduction and magma genesis in the lesser antilles - isotopic and trace-element constraints" Journal of Geophysical Research-Solid Earth and Planets **91** 5927-5941

Young, S.R., R.S.J. Sparks, W.P. Aspinall, L.L. Lynch, A.D. Miller, R.E.A. Robertson and J.B. Shepherd (1998) "Overview of the eruption of Soufriere Hills volcano, Montserrat, 18 July 1995 to December 1997" Geophysical Research Letters **25** 3389-3392

Zellmer, G.F., C.J. Hawkesworth, R.S.J. Sparks, L.E. Thomas, C.L. Harford, T.S. Brewer and S.C. Loughlin (2003) "Geochemical evolution of the Soufriere Hills volcano, Montserrat, Lesser Antilles volcanic arc" Journal of Petrology **44** 1349-1374

CHAPTER 2

TRACKING THE MAGMATIC EVOLUTION OF ISLAND ARC VOLCANISM: INSIGHTS FROM A HIGH-PRECISION Pb ISOTOPE RECORD OF MONTSERRAT, LESSER ANTILLES

This chapter is a reproduction of an article published in *Geochemistry, Geophysics, Geosystems*: Cassidy, M., Taylor, R.N., Palmer, M.R, Cooper, R., Stenlake C., Trofimovs, J., (2012) Tracking the magmatic evolution of an island arc volcano: Insights from a high-precision Pb isotope record of Montserrat, Lesser Antilles. *Geochem. Geophys. Geosyst.* doi:10.1029/2012GC004064, in press

Written by M Cassidy, but I received feedback from Taylor, Palmer and Trofimovs. Cooper and Stenlake did ~20% of the analyses in this chapter as part of their MGeol projects.

Abstract

The volcanic succession on Montserrat provides an opportunity to examine the magmatic evolution of island arc volcanism over a ~2.5 Ma period, extending from the andesites of the Silver Hills centre, to the currently active Soufrière Hills volcano (February 2010). Here we present high-precision double-spike Pb isotope data, combined with trace element and Sr-Nd isotope data throughout this period of Montserrat's volcanic evolution. We demonstrate that each volcanic centre; South Soufrière Hills, Soufrière Hills, Centre Hills and Silver Hills, can be clearly discriminated using trace element and isotopic parameters. Variations in these parameters suggest there have been systematic and episodic changes in the subduction input. The SSH centre, in particular, has a greater slab fluid signature, as indicated by low Ce/Pb, but less sediment addition than the other volcanic centres, which have higher Th/Ce. Pb isotope data from Montserrat fall along two trends, the Silver Hills, Centre Hills and Soufrière Hills lie on a general trend of the Lesser Antilles volcanics, whereas SSH volcanics define a separate trend. The Soufrière Hills and SSH volcanic centres were erupted at approximately the same time, but retain distinctive isotopic signatures, suggesting that the SSH magmas have a different source to the other volcanic centres. We hypothesize that this rapid magmatic source change is controlled by the regional transtensional regime, which allowed the SSH magma to be extracted from a shallower source. The Pb isotopes indicate an interplay

between subduction derived components and a MORB-like mantle wedge influenced by a Galapagos plume-like source.

1.1 Introduction

The main components which control the composition of volcanic rocks in island arc settings are the mantle wedge composition, subducted sediment and altered oceanic crust, with fluids derived from the dehydrating subducting slab causing melting of the mantle wedge and generation of arc magmas [Gill 1981]. These magmas may then be modified by interaction with the lithologies within the island arc crust [e.g. Davidson, 1987, 1996; Thirlwall *et al.*, 1996; Davidson and Wilson, 2011]. Hence, while analyses of volcanic rocks can provide constraints on the composition of the mantle that underlies the arc system, the addition of material from the slab (either due to dehydration fluids or partial melting), or from the crust, can obscure the mantle signature. Pb isotopes are generally considered to be highly sensitive tracers of the involvement of oceanic crust and subducted sediment, hence they have been widely used to study the addition of components to arc volcanic rocks [Miller *et al.*, 1994; Woodhead, 1989]. There is also recent evidence, however, that mantle heterogeneities are more clearly expressed in the Pb isotope composition of arc rocks than has been heretofore recognised [Ishizuka *et al.*, 2003, 2006, 2011; Straub *et al.*, 2009].

The Lesser Antilles islands are an ideal setting in which to study these processes as the arc volcanic rocks display a wide range in isotopic and chemical compositions [White and Dupre, 1986; Davidson, 1986, 1987, 1996; Carpentier *et al.*, 2008; Dufrane *et al.*, 2009; Labanieh *et al.*, 2010]. In particular, there is an along-arc chemical gradient, with more radiogenic Pb and Sr isotope ratios and lower Nd ratios in the south relative to the north. These observations have been used to infer a greater influence of the sediment component relative to that of hydrous fluids towards the south [Hawkesworth and Powell, 1980; White and Dupre, 1986; Davidson, 1987; Turner *et al.*, 1996], but whether this is added as a crustal assimilant or sediment from the slab can vary from island to island. For example, Dufrane *et al.* [2009] and Labanieh *et al.*, [2010] recently invoked partial melt of sediments as a mechanism to explain the isotopic range for the arc, but the different volcanic islands, and different centres within individual islands, also show different fractionation histories [Thirlwall *et al.*, 1996; Heath *et al.*, 1998], indicating that the factors that control magma compositions (such as water concentrations in the source rocks and magma ascent rates) vary on the scale of tens of kilometres [Macdonald *et al.*, 2000]. Thus, while variations in magmatic sources have been observed within individual arc volcanic centres [Thirlwall *et al.*, 1996; Ishizuka *et al.*, 2006], the mechanism by which they are generated remains enigmatic.

In this study we have sought to address this problem by examining the geochemical and isotopic evolution of volcanic activity on the island of Montserrat, in the northern part of the Lesser Antilles arc. In particular, this study aims to determine whether or not volcanic regions on Montserrat be discriminated by their chemical composition. If so, is there an evolutionary trend of the magmas over time, and what implications does this have for our understanding of the current eruptions on Montserrat? Further, do the processes on Montserrat reveal information about the wider controls over the composition of arc volcanism in the Lesser Antilles?

To this end, we present new trace element, Sr, Nd and high-precision double spike Pb isotope data extending from the ~2 Ma andesites of the Silver Hills Complex through to the youngest dome collapse of the Soufrière Hills volcano (February 2010). In addition to subaerial exposures, we have collected volcanogenic samples from marine sediment cores, as significant volumes of pyroclastic material have been transported offshore Montserrat [*Le Friant et al.*, 2009].

1.2 Geological setting

The 750 km long Lesser Antilles island arc (Fig. 1a) was formed by the westward-dipping, slightly oblique, subduction of the North American plate beneath the Caribbean plate, with a convergence rate of ~2 cm/yr [*Wadge*, 1984; *Demets et al.*, 2000; *Feuillet*, 2000]. The Caribbean plate is thought to have moved eastwards to its present site from an original location in the Pacific, where it may have been generated over the Galapagos hotspot 100-75 Ma ago [*Pindell and Barrett*, 1990]. It was then inserted between the North American and South American plates sometime between the Late Campanian and Late Eocene [*Pindell and Barrett*, 1990]. A subduction zone developed at its leading edge, with arc volcanism initiating at ~40 Ma [*Briden et al.*, 1979; *Bouysse and Westercamp*, 1990]. To the north of Martinique, the arc is divided into two chains of islands (Fig. 1). The eastern, inactive, chain is older, with thick carbonate platforms covering a volcanic basement. Tectonic adjustments during the Mid-Miocene modified the orientation of the northern subducting slab, causing migration of the volcanic front to the west and the initiation of a new active arc [*Bouysse and Westercamp*, 1990]. This western chain consists of volcanic rocks younger than 20 Ma (Volcanic Caribbees) and includes all the active volcanoes [*Bouysse and Westercamp* 1990]. The southern part of the active arc extends from Martinique to Grenada, and commonly contains Pliocene and Quaternary volcanic units superimposed over pre-Miocene volcanics and sedimentary units [*Maury et al.*, 1990]. The Benioff zone dips ~45° westward beneath the northern part of the arc [*Wadge and Shepherd*, 1984] and the hypocentres of earthquakes and receiver function

analysis suggest a crustal thickness of $\sim 30 \pm 4$ km for the northern part of the arc [Wadge, 1984; Sevilla et al., 2010]. Seismic studies indicate that the subducted oceanic slab is segmented into three main parts with differing dips and slip vectors [Wadge and Shepherd, 1984].

Montserrat is located on the northern section of the Lesser Antilles arc, overlying crust that is no more than 30 km thick, and an asthenospheric mantle wedge that extends to 130 km depth [Wadge and Shepherd, 1984]. The subaerial part of Montserrat is ~ 160 km² and is made up almost exclusively of volcanic rocks (Figure 1b). Harford et al. [2002] divided Montserrat into three different regions based on Ar-Ar geochronology: Silver Hills (2600-1200 ka), Centre Hills (950-550 ka) and the South-Soufrière Hills (SSH)-Soufrière Hills complex (174 ka to the present) (Figure 1b). They noted a pattern of ageing northwards suggesting a stationary magmatic source and migration of the plate. This migration away from the trench has been interpreted to be related to response of the down-going slab to growth of the accretionary prism [Wadge, 1984]. The majority of volcanics on Montserrat are andesitic, but the SSH volcanic centre comprises basalts and basaltic andesites [Harford et al., 2002]. Mafic lavas are also found as inclusions within the andesites of the Silver Hills, Centre Hills and Soufrière Hills [Rea, 1974; Zellmer et al., 2003].

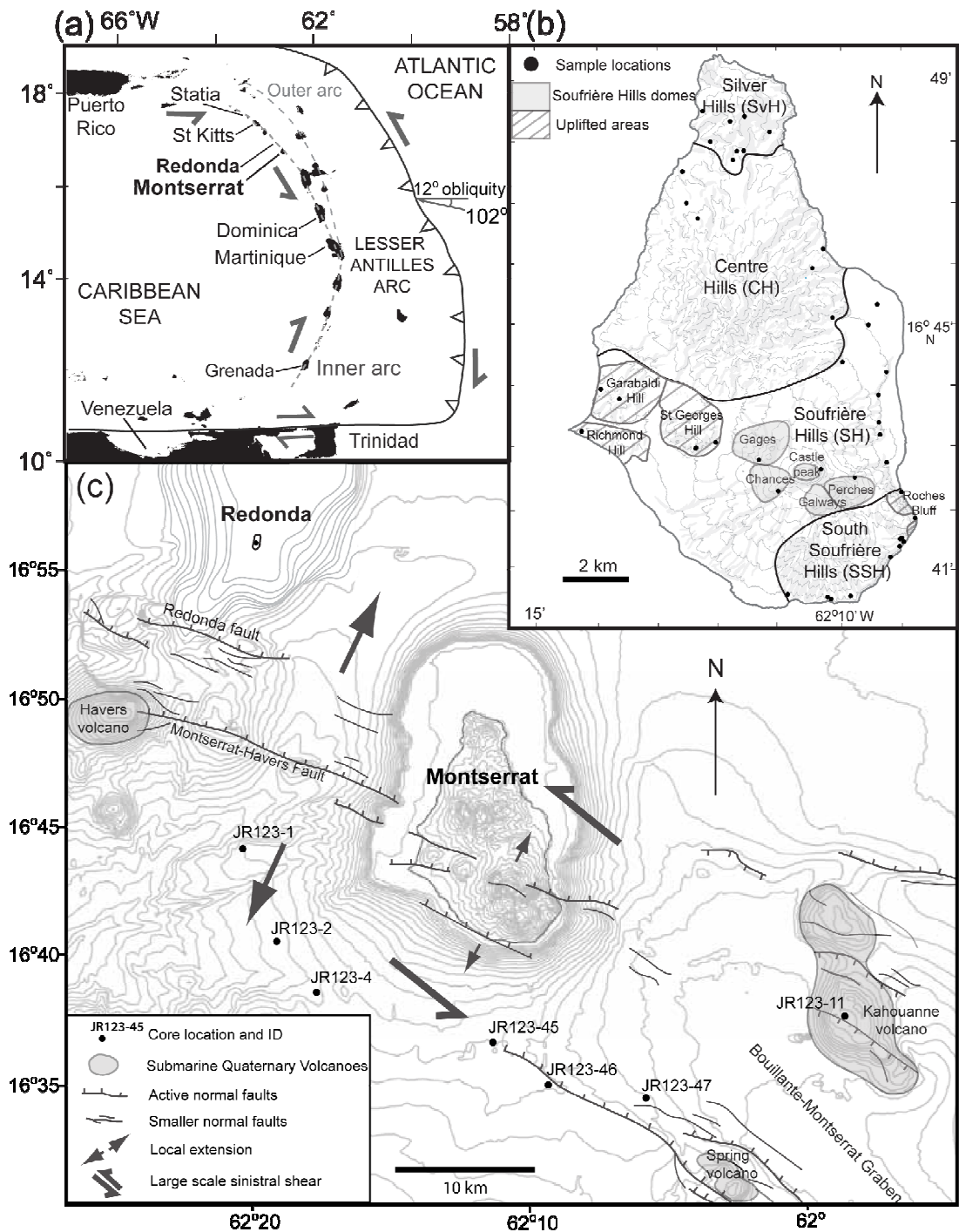


Figure 1. (a) Insert shows the regional context of the Lesser Antilles arc. (b) Map showing the volcanic centres on Montserrat and subaerial sample locations (c) Subaerial and marine contoured map showing local structural features offshore Montserrat and Redonda adapted from Feuillet *et al.* [2010; 2011] with marine sediment cores located.

The most recently active volcanic centres, Soufrière Hills and South Soufrière Hills, were the focus of the study by Zellmer *et al.* [2003], who concluded that the source magmas of the volcanic centres were enriched by slab fluid and small amounts (~1.2 %) of sediment, based on major and trace elements and U, Th and O isotopes. Differing degrees of fractionation have been suggested as a cause of some of the chemical variance between the two volcanic centres,

with SSH thought to be derived from an open system, in which the magmatic system is constantly replenished, whereas Soufrière Hills volcano is thought to be dominated by closed system, more extensive, magmatic fractionation [Zellmer *et al.* 2003]. The petrological and geochemical characteristics of the magmas also change with age in the SSH-Soufrière Hills complex. Samples older than 150 ka are dominated by two-pyroxene andesites, whereas, all samples younger than 110 ka are hornblende-hypersthene andesites. This compositional change coincides with the age of SSH volcanism (~130 ka), hence the mineralogical transition appears to have followed an interlude of mafic volcanism [Harford *et al.*, 2002].

Active volcanism is concentrated at the Soufrière Hills volcano (1995 - present) and is characterised by andesitic dome growth and collapse events, producing pyroclastic flows and vulcanian eruptions [Young *et al.*, 1998; Robertson *et al.*, 2000]. The current period of activity (1995-2010) has consisted of 5 phases of extrusion: Phase 1, 1995-1998, Phase 2, 1999-2003, Phase 3, 2005-2007, Phase 4, 2008 and Phase 5, 2009-2010 [Source: Montserrat Volcano Observatory - <http://www.mvo.ms>]. The flanks of the Soufrière Hills volcano are composed of pyroclastic deposits and its core is formed of five andesitic lava domes; Gages Mountain, Chances Peak, Galways Mountain, Perches Mountain and the site of new lava eruptions that is superimposed on an older dome, Castle Peak (Fig. 1b). Uplifted areas include Garabaldi Hill, Roche's bluff, Richmond Hill and St Georges Hill, but it is uncertain as to which volcanic centres these uplifted sections belong.

2. Methods

2.1 Sample acquisition

A research cruise of the *RRS James Clark Ross* (May 2005 – P.I. RSJ Sparks) sampled submarine volcanic deposits using a vibrocore system developed by the British Geological Survey. The vibrocores used in this study were taken to the south and west of Montserrat, ~8-13 km from shore (Fig. 1c) JR123-11 sampled material from the crater of the Kahouanne submarine volcano. Subaerial samples taken from the four volcanic centres by Harford *et al.*, [2002] study were also analysed, together with supplementary samples taken during fieldwork on Montserrat. Samples from the Montserrat Volcano Observatory (MVO) database were used for analysis, they included rocks recovered from Redonda island and samples from the recent eruptions (1995 to present).

2.2 Analytical techniques

Major elements were analysed in the subaerial samples by X-ray Fluorescence (XRF) analysis of glass beads prepared by fusion of a mixture of subsamples of 0.5 g and lithium tetraborate in a ratio of 1:10. Analysis was undertaken using Philips Magix Pro WD-XRF at the

National Oceanography Centre (NOC), Southampton, UK. Error and external accuracy was generally <2% (Table 1).

Samples for trace element and isotopic analysis were prepared in a clean laboratory suite at NOC. Submarine core samples were cleaned using 18M Ω ultrapure H₂O, sonicated for ten minutes and then dried overnight in an oven at 70°C. The submarine samples were then passed through Teflon sieves (500 μ m), and handpicked under a binocular microscope. The picked samples were then pulverized using an agate mortar. REE, Rb, Sr, Y, Zr, Nb, Cs, Ba, Hf, Pb, Th and U concentrations were determined by ICP-MS at the NOC on a VG Plasmaquad PQ2+ instrument. Reproducibility is better than $\pm 4\%$ (RSD.) for the REE, Rb and Nb, and better than $\pm 6\%$ (RSD) for other elements. The precision of the elemental ratios is better than $\pm 1\%$ (RSD).

Nd, Sr and Pb isotopic compositions were determined on 200 mg of hand-picked rock chips with a grain size of 0.5-1 mm. The rock chips were leached in 4ml of 6 M HCl at 140°C in sealed Teflon pots for 1-2 hours prior to dissolution in HF-HNO₃ for 24 hours on a hot plate at 130°C. The samples were evaporated until dry, before adding a further 0.5 ml of concentrated HCl and 0.5 ml of concentrated HNO₃ to the samples and evaporating until dry after each addition. For Pb analysis, 1.5 ml of hydrobromic (HBr) was added to the residue, the Teflon pot lid was replaced and the vessels placed on a hotplate for 1 hour. The contents were then centrifuged for 5 minutes to produce a supernatant suitable for column chemistry. Isolation of Pb from the matrix was performed using AG1-X8 200-400 mesh anion exchange resin. The procedural blanks measured with the samples contained <50 pg of Pb. Pb isotope analyses were conducted on a VG Sector 54 thermal ionisation mass spectrometer and MC-ICPMS (Neptune and GV IsoProbe) at NOC. Both TIMS and MC-ICPMS techniques utilized the double spike technique to correct instrumental bias using a method outlined by Ishizuka et al. [2003]. Pb standard NBS 981 gave results, 16.9404 ± 32 (2SD) for ²⁰⁶Pb/²⁰⁴Pb, 15.4982 ± 30 for ²⁰⁷Pb/²⁰⁴Pb and 36.7225 ± 85 for ²⁰⁸Pb/²⁰⁴Pb for TIMS and 16.9403 ± 27 for ²⁰⁶Pb/²⁰⁴Pb, 15.4973 ± 21 for ²⁰⁷Pb/²⁰⁴Pb and 36.7169 ± 66 for ²⁰⁸Pb/²⁰⁴Pb for MC-ICP-MS.

For Sr analysis, the Pb residue was evaporated and dissolved in 3M HNO₃. The Sr was isolated using Sr resin (Eichrom Industries, Illinois, USA). For Nd isotopic analysis, the REE were initially separated by cation exchange, before isolating Nd on Ln resin (Eichrom Industries, Illinois, USA) columns. Sr and Nd isotope ratios were measured on a nine-collector VG Sector 54 mass spectrometer, as the average of 150 ratios. Reported values are the average of 150 ratios obtained by measuring ion intensities in multidynamic collection mode normalized to ⁸⁶Sr/⁸⁸Sr = 0.1194 and ¹⁴⁶Nd/¹⁴⁴Nd = 0.7219. Measured values for NBS SRM-987 and JNdi-1 were ⁸⁷Sr/⁸⁶Sr = 0.710297 ± 19 (2 SD, n =58) and ¹⁴³Nd/¹⁴⁴Nd = 0.512096 ± 7 (2 SD, n = 64) during the measurement period. The Sr and Nd isotopic data

presented here have been normalized to NBS SRM-987 (0.710248) and JNdi (0.512110). All the data used in this study are presented in Tables 1 and 2.

3. Results

3.1 Provenance of Montserrat volcanics

The elemental and isotopic indices used to discriminate between the volcanic centres on Montserrat are illustrated in Figure 2 and listed in Tables 1 and 2. Despite covering ~2 Myr of volcanic development, the Silver Hills and Centre Hills centres are essentially indistinguishable in trace element space, but have lower Ba/La compared to the Soufrière Hills magmas (Fig. 2b). The SSH samples can be clearly differentiated from the other centres as they are displaced to lower Th/La and Zr/Er and higher Ba/La and Sr/La (Figs. 2a and 2b). Additionally, the SSH can be further separated into Suite A and Suite B, with the former having higher Zr/Er and lower Ba/La and Sr/La (Figs. 2a and 2b). The submarine samples can be confirmed as originating from the SSH volcanic centre, as their lithological and geochemical characteristics exactly match the sub-aerial material [Cassidy *et al.*, *in press*]. On chondrite-normalised REE plots (Fig. 2 c) the Silver Hills and Centre Hills samples have the highest REE abundances, but display similar LREE enrichments to the Soufrière Hills samples. The Silver Hills and Centre Hills samples are also marked by the presence of both positive and negative Eu anomalies that are not so well-developed in samples from Soufrière Hills and SSH. The SSH samples tend to have lower REE concentrations than the other volcanic centres, with the Suite B samples showing the lowest concentrations. In general, the SSH samples are less LREE enriched than the Silver Hills, Centre Hills and Soufrière Hills samples, with the Suite B samples showing the flattest REE patterns.

In Pb isotope space the Silver Hills and Centre Hills volcanics form a tight grouping with the highest $^{206}\text{Pb}/^{204}\text{Pb}$ (Figs. 2c and 2d). All Soufrière Hills samples have lower $^{206}\text{Pb}/^{204}\text{Pb}$ (<19.03) than the Silver Hills and Centre Hills and higher $^{206}\text{Pb}/^{204}\text{Pb}$ than the SSH samples, which have the lowest $^{206}\text{Pb}/^{204}\text{Pb}$ of all the volcanic centres. Again, the SSH samples can be clearly separated into Suites A and B in these Pb isotope plots, with Suite B having a less radiogenic signature and lower $\Delta 7/4\text{Pb}$ and $\Delta 8/4\text{Pb}$ than Suite A. Two samples from the island of Redonda (which lies ~30 km NW of Montserrat; Fig. 1) have been measured for Pb isotopes: sample RED1 from this study and sample R8202 from Thirlwall [2000]. These samples have a Pb composition that is identical to SSH Suite B. Kahouanne volcano, a submarine volcanic edifice located 25 km south east of Montserrat, plots among the SSH Suite A samples (Fig. 2).

The Pb isotope plots also show that the different volcanic centres fall on two distinct vectors. The Soufrière Hills, Centre Hills and Silver Hills samples lie on the general trend defined by the Lesser Antilles volcanics, whereas the SSH Suites A and B define a separate vector (SSH trend). In both $\Delta 7/4\text{Pb}$ and $\Delta 8/4\text{Pb}$ versus $^{206}\text{Pb}/^{204}\text{Pb}$ plots, the SSH suites have sharply increasing $\Delta 7/4\text{Pb}$ and $\Delta 8/4\text{Pb}$ with higher $^{206}\text{Pb}/^{204}\text{Pb}$. In contrast, the Silver Hills, Centre Hills and Soufrière Hills volcanics lie on a vector that has a shallower slope of $\Delta 7/4\text{Pb}$ and $\Delta 8/4\text{Pb}$ relative to $^{206}\text{Pb}/^{204}\text{Pb}$.

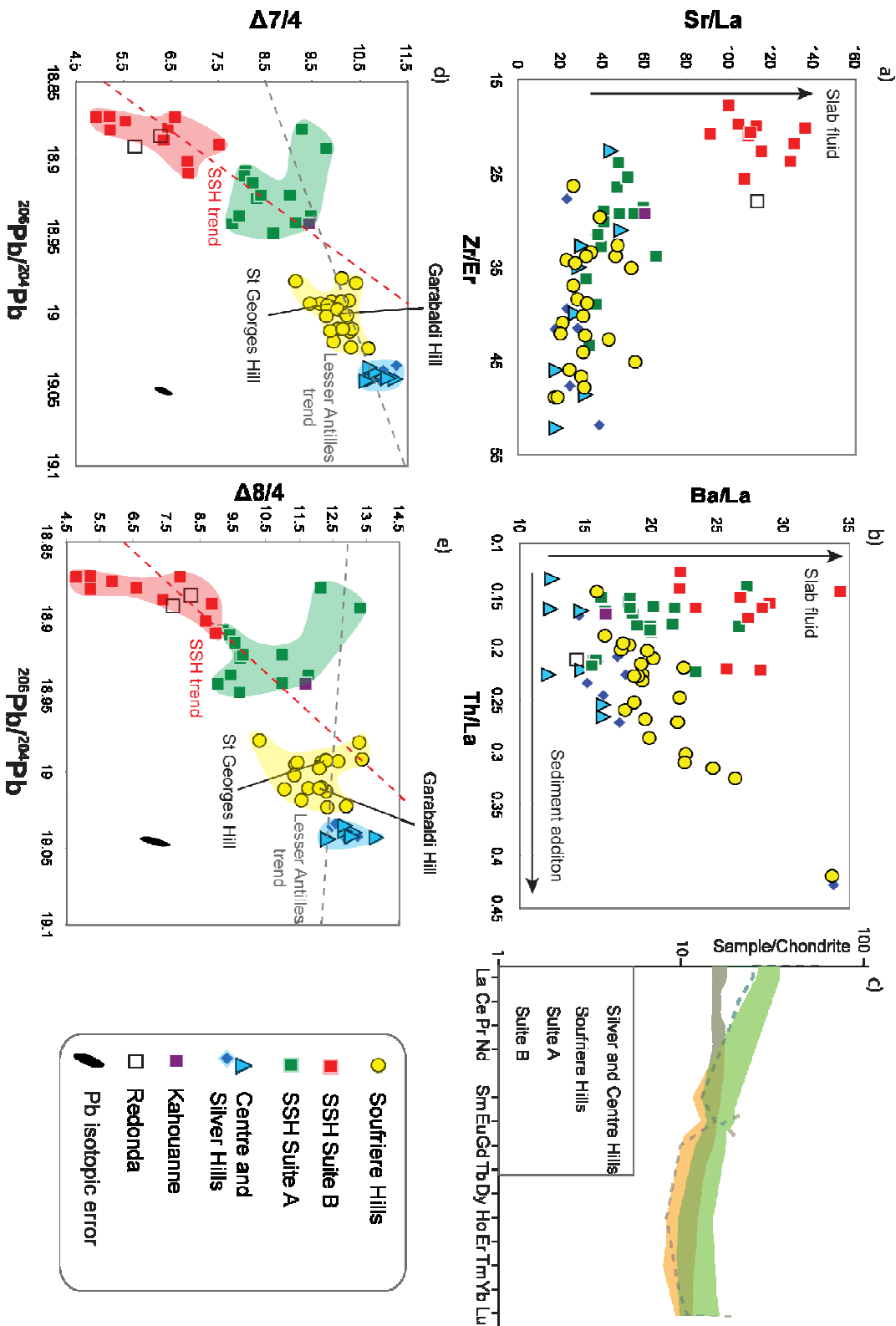


Figure 2. Geochemical variation diagrams, used to distinguish the different volcanic centres. a) and b) use trace elements c) REE trends for the different volcanic centres normalised to chondrite (Sun and McDonough, 1989) d) and e) Pb-Pb plots with trends labelled and fitted by linear regression. One of the Redonda samples (R8202) was measured by Thirlwall, [2000]. The Lesser Antilles trend is drawn from Pb isotope data from analyses from the central and northern islands [Labanih et al., 2010; Davidson and Wilson, 2011], [Toothill et al., 2007] [Lindsay et al., 2005]. All trends are drawn by linear regression of the data. $\Delta 7/4$ and $\Delta 8/4$ are $207Pb/204$ and $208Pb/204Pb$ values calculated relative to the NHR. [Hart, 1984].

3.2 Geochemical time series

Many of the samples used in this study have been dated by the $^{40}\text{Ar}/^{39}\text{Ar}$ method [Hartford *et al.*, 2002], but for the other samples dates are relative, having been assigned according to stratigraphic relationships. The relative ages of the volcanic centres determined by Hartford *et al.*, [2002] shows Silver Hills to be the oldest volcanic centre, followed by Centre Hills, then Soufrière Hills with an interlude of the SSH at ~ 130 ka. The pre-SSH Soufrière Hills samples considered in this study either pre-date the SSH period of volcanism (128 ± 27 ka to 131 ± 7 ka) defined by Ar-Ar dating [Hartford *et al.*, 2002], or have been sampled from sites where the Soufrière Hills units are stratigraphically overlain by the SSH volcanics. As noted above, we have identified two suites within the SSH, with the Suite B overlying Suite A in the stratigraphy, making Suite A the oldest SSH unit. The rest of the Soufrière Hills samples post-date the SSH volcanics and include the five phases of the current period of activity (1995-2010).

3.2.1 Trace elements

Fluid mobile/REE ratios such as Ba/La show a gradual increase from the lower ratios in Silver Hills and Centre Hills samples to the highest ratios in Suite B in SSH (Fig. 3). The Soufrière Hills volcanics have generally lower Ba/La than the SSH volcanics. These trends are mirrored by Ce/Pb ratios, which show that the SSH has the lowest ratios, relative to the other volcanic centres. LREE/MREE ratios such as $(\text{La}/\text{Sm})_{\text{N}}$ are generally highest in the Soufrière Hills samples, with SSH exhibiting the least REE fractionation. This pattern is similar to Th/Ce ratio variations, where the SSH samples generally have the lowest Th/Ce in comparison to the other volcanic centres. In contrast, High Field Strength Element (HFSE) ratios such as Nb/Zr remain relatively constant with time, with slightly lower but variable values for the SSH and then increasing values in the post-SSH Soufrière Hills samples, which exhibit the highest Nb/Zr ratios of the volcanic centres.

Samples from the each of 5 most recent eruptive phases of the 1995-2010 activity period have also been analysed, including a mafic enclave and andesite sampled from the eruption on 11th February 2010, and are included together with data from Zellmer *et al.*, [2003] (Fig. 3). There are no clear trends in the Ba/La, Ce/Pb, $(\text{La}/\text{Sm})_{\text{N}}$ and Nb/Zr ratios over this 15 year time series, but the mafic enclaves have generally lower and less variable Ba/La, Ce/Pb and $(\text{La}/\text{Sm})_{\text{N}}$ ratios compared to the whole rock andesites. The whole rock andesites exhibit a slight decrease in Th/Ce ratios from Phase 1 (1995-1998) to Phase 5 (2009-2010), a trend that draws their composition similar to the Th/Ce ratios of the mafic enclaves, but these

trends are based on a limited data set, so it is difficult to discern the significance of this observation.

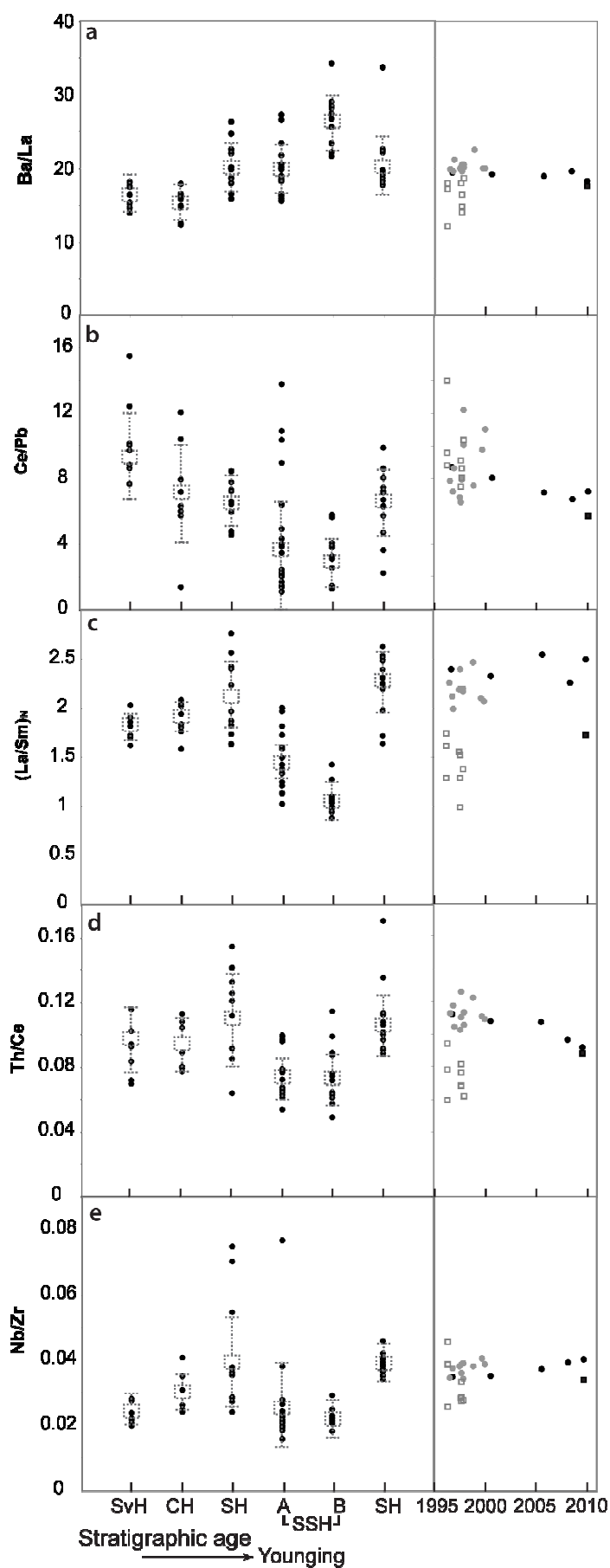
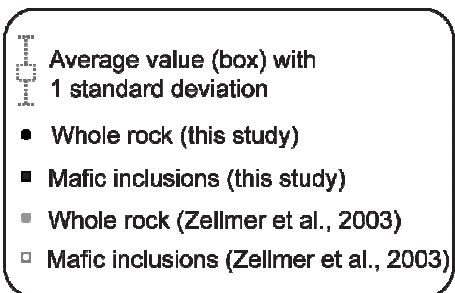


Figure 3. Trace element trends covering the 4 volcanic centres showing the trends over time. SvH= Silver Hills, CH= Centre Hills, SH= Soufriere Hills, SSH= South Soufriere Hills with Suites A & B. Note that Soufrière Hills was active before and after the SSH. Add-on graphs show an expanded trends of the 5 phases from the current period of activity (1995- 2010)



3.2.2 Isotopic time series

Sr, Nd and Pb isotopes are reported in Table 2 and plotted in Figures 4 to 7, to examine how the isotopic composition changes through time. The Pb isotope parameters have a consistent evolution throughout the volcanic history of Montserrat (Fig. 4). $^{206}\text{Pb}/^{204}\text{Pb}$, $\Delta 7/4\text{Pb}$ and $\Delta 8/4\text{Pb}$ are highest in the Silver Hills and Centre Hills, which decrease in the Soufrière Hills with a further decrease in SSH Suite A samples, to the lowest ratios in SSH Suite B. The Pb isotope ratios shift back to higher values in the post-SSH and Soufrière Hills samples.

In contrast, the Sr isotope data (Figure 4e) do not show any clear evolutionary trends and display a limited range in $^{87}\text{Sr}/^{86}\text{Sr}$ ratios (0.70354-0.70368) (Fig. 4). The Nd isotope data do not show such clear trends as the Pb data, possibly because fewer samples were analysed, but they mirror the Pb isotopes data to some extent (Fig. 4). The Silver Hills have high $^{143}\text{Nd}/^{144}\text{Nd}$, which decreases with time to the Centre Hills. The pre-SSH Soufrière Hills samples have higher Nd isotopic values than Centre Hills and this increasing trend continues to the SSH, with Suite B having the highest Nd isotope ratios of all the volcanic centres. The $^{143}\text{Nd}/^{144}\text{Nd}$ ratios then drop again in the post-SSH, Soufrière Hills volcanics. The isotope data for samples from the most recent phases of eruptive activity (1995-2010) show a relatively limited range in all isotope ratios (Fig. 4).

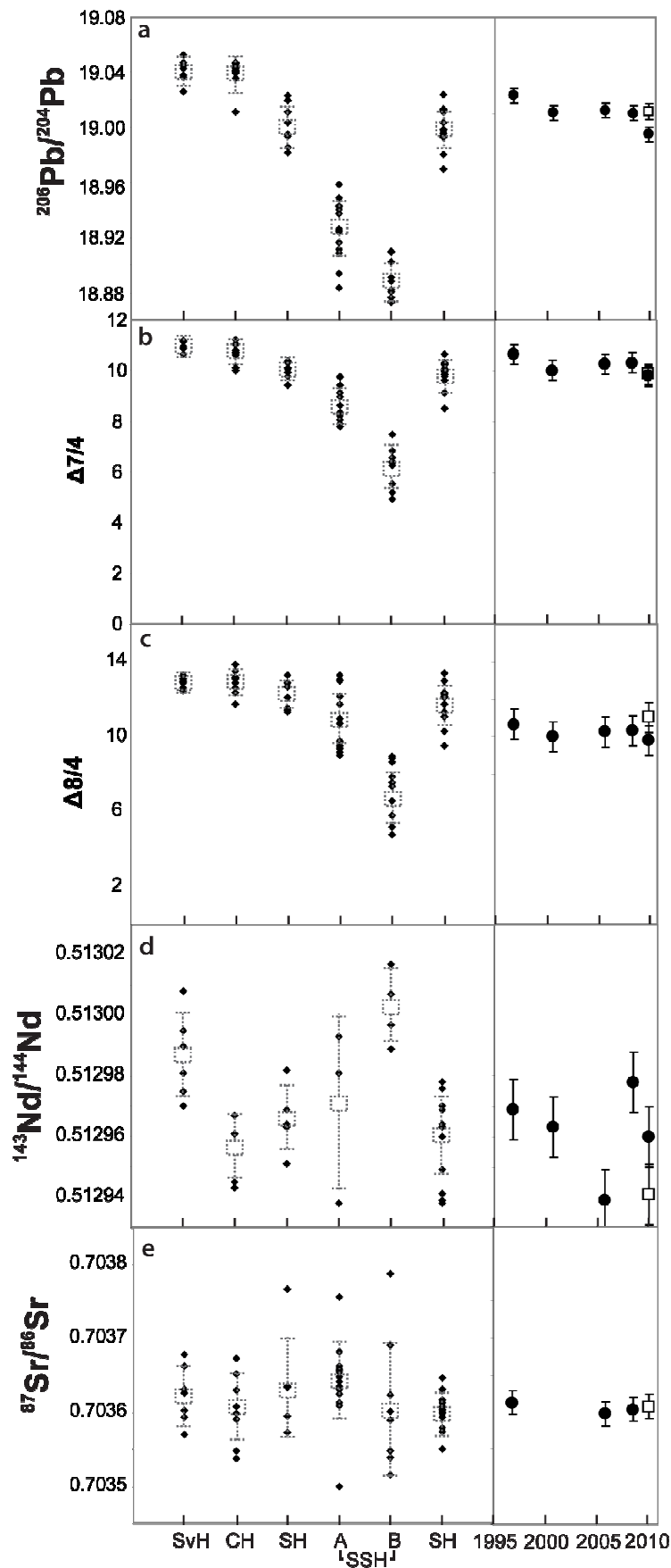


Figure 4. Isotopic trends covering the 4 volcanic centres showing the trends over time. SvH= Silver Hills, CH= Centre Hills, SH= Soufriere Hills, SSH= South Soufriere Hills with Suites A & B. Note that Soufrière Hills was active before and after the SSH. Add-on graphs show an expanded trends of the 5 phases from the current period of activity (1995-2010). Note that Soufrière Hills was active before and after the SSH.

- Average value (box) with 1SD bars
- Mafic inclusions with error bars (this study)
- Whole rock with error bars (this study)

4. Discussion

4.1 Montserrat and shallow level contamination

The Montserrat volcanics show no obvious correlation between their Pb isotope ratios and SiO₂ concentrations, hence the variations in Pb isotope compositions are unlikely to be controlled by shallow level crustal contamination during crystallisation (Fig. 5). Indeed, the SSH samples, which have the least radiogenic Pb ratios, comprise basalts, andesites and dacites. In addition, Sr and Nd isotopes do not show any relationship with SiO₂ (Fig. 5). Again, this implies that crustal contamination is not a significant factor influencing the isotopic composition of magmatic rocks at Montserrat. This appears to contrast with the southern and central islands of the Lesser Antilles such as Martinique, which clearly show evidence for open-system differentiation as evidenced by strong correlations between SiO₂ and Sr, Nd and Pb isotopes [Davidson and Wilson, 2011]. Additionally, most of the rocks chosen for this study have <65 wt% SiO₂ (Table 1) and so would be less likely to exhibit signs of crustal assimilation [e.g. Davidson, 1996]. Indeed, He-O-Sr isotope analyses of Lesser Antilles arc suggest that while crustal contamination is common in southern islands such as Grenada, it is far more limited in more northerly locations such as Montserrat [Van Soest *et al.*, 2002]. The rocks used in this study are not direct melts from the mantle, with MgO values generally <5% (Table 1), suggesting that small amounts of differentiation have occurred. In addition, some degree of assimilation must have occurred during magma evolution. However, the contribution of assimilation to the rock compositions used in this study is minor, and does not appear to disturb the isotopic relationships.

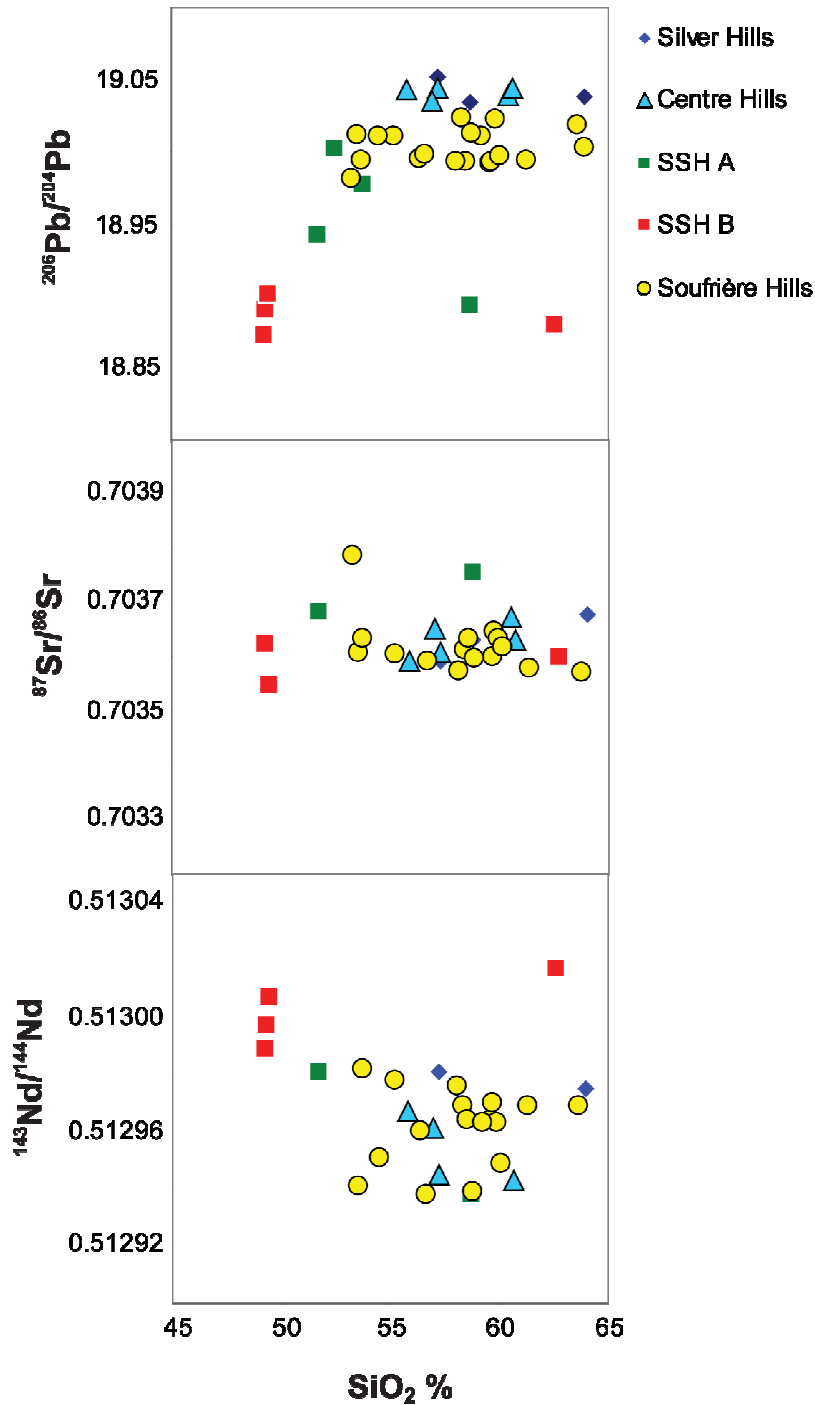


Figure 5. SiO_2 plotted against $^{206}\text{Pb}/^{204}\text{Pb}$, $^{87}\text{Sr}/^{86}\text{Sr}$ and $^{143}\text{Nd}/^{144}\text{Nd}$. Isotopic errors are the same as plotted in Figure 4.

4.2 Age relations of the volcanic centres

As is apparent from the discussion above, Pb isotopes are the most sensitive tool for discriminating between the geochemical compositions of the volcanic centres on Montserrat. A closer examination of these data show that although most samples exposed at the SSH and dated between 128 ± 27 ka to 131 ± 7 ka [Harford *et al.* 2002] belong to Suite A and B of the

SSH, one sample found at the SSH (MVO 136) and dated at $\sim 130 \pm 5$ ka, falls within the field defined by the Soufrière Hills centre. Subsequent field sampling and stratigraphic analysis in this study have demonstrated that the basal volcanic units exposed at the SSH belong to the Soufrière Hills isotopic field, suggesting that the Soufrière Hills and SSH volcanic centres were active at the same time.

Pb isotopic analyses also show that samples from Roche's Bluff and Richmond Hill fall within the field defined by the Silver Hills and Centre Hills province, whereas those from Garabaldi Hill and St Georges Hill clearly belong to the Soufrière Hills geochemical province (Table 2, Fig. 2). This observation suggests that samples from Garabaldi Hill dated at 282 ± 8 ka [Harford *et al.* 2002] may be the oldest rocks associated with the Soufrière Hills volcanic centre, and extends the lower age limit of the Soufrière Hills volcanic period from 174 ka to 282 ka. The Pb isotope analyses also confirm that the mafic enclaves present within the Soufrière Hills lavas – and often claimed to be a trigger for eruptions [Devine *et al.*, 1998; Murphy *et al.*, 1998, 2000], match the Soufrière Hills isotopic signature and differ from that of the SSH volcanic centre.

4.3 Geochemical evolution of Montserrat

The REE trends for Silver Hills, Centre Hills and Soufrière Hills are typified by LREE enrichment and both positive and negative Eu anomalies (Fig. 2c). These features indicate that both amphibole and plagioclase were present in the mineral fractionation assemblage [Bottazzi *et al.*, 1999; Blundy and Wood, 2003]. The LREE enrichment may reflect sediment addition to the mantle wedge, which is supported by a negative correlation between $(\text{La/Sm})_N$ and $^{143}\text{Nd}/^{144}\text{Nd}$ (Fig. 6) and is consistent with the bulk Lesser Antilles sediment composition, which has low $^{143}\text{Nd}/^{144}\text{Nd}$ values [Plank and Langmuir, 1998; Carpentier *et al.*, 2008]. Smaller degrees of melting would also increase the more incompatible LREE concentrations, but would not vary the $^{143}\text{Nd}/^{144}\text{Nd}$ values. The relative lack of MREE to HREE trough-shaped patterns in the SSH magmas suggests amphibole did not play a significant role in any fractional crystallisation evolution of the magmas and is supported by petrological observations [Harford *et al.*, 2002; Zellmer *et al.*, 2003]. Additionally, the lack of pronounced Eu anomalies within the SSH samples suggests that olivine and pyroxene played a more important role in the fractional crystallisation evolution of these magmas relative to role played by plagioclase in the other Montserrat centres.

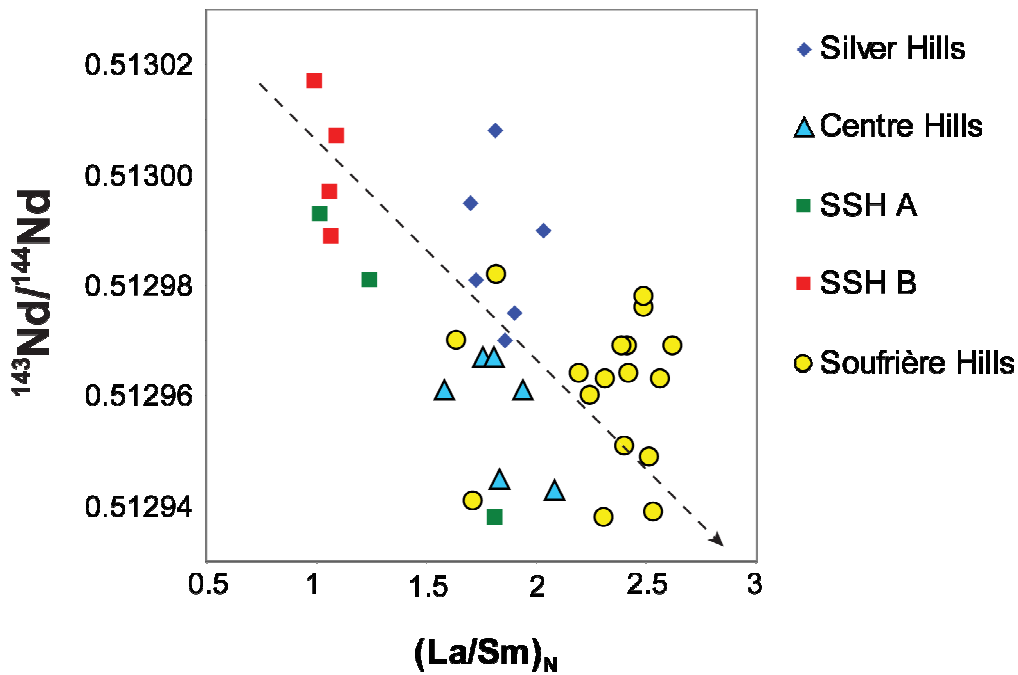


Figure 6. $(\text{La}/\text{Sm})_N$ plotted against Nd isotope.

Fluid mobile elements ratios such as Ba/La and Ce/Pb have been used to infer the presence of an altered oceanic slab fluid contribution to the magma source [Brenan, 1995a, 1995b]. Ba/La ratios are elevated and Ce/Pb ratios are slightly depleted in the SSH suites (Figures 3a and 3b), suggesting that there was a higher slab-fluid contribution to the SSH magma source region compared to the other volcanic centres. This hypothesis accords with observations by Zellmer *et al.* [2003] based on variations in U/Th ratios. The relatively high Ba/La ratios and low Ce/Pb in the SSH samples is, however, also a reflection of the lower LREE enrichment in these samples relative to the other volcanic centres. Indeed, the Soufrière Hills samples generally have higher Ba concentrations than the SSH (Table 1), which suggests that their source regions were also influenced by a slab-fluid contribution.

Th and Ce are not strongly partitioned in the subduction fluid, but are likely to be selectively introduced to the mantle wedge by sediment or sediment melt addition. In particular, Th/Ce ratios elevated above typical sedimentary values may reflect sediment melt leaving the subducting slab [Brenan *et al.*, 1995b; Hawkesworth *et al.*, 1997; Elliott *et al.*, 1997; Plank, 2005]. The higher Th/Ce found in the Silver Hills, Centre Hills and Soufrière Hills centres (Fig. 3d) suggests a greater sediment component in their source compared to the SSH samples, which have generally lower Th/Ce values.

HFSE ratios, such as Nb/Zr, are considered to be the elements least affected by sediment addition [Woodhead *et al.*, 1993], and these elements are not readily transported in fluids [Tatsumi *et al.*, 1986], hence they should be less affected by the slab fluid component and sediment addition. The HFSE compositions should, therefore, provide some constraints on

depletion of the mantle wedge. The observations that Nb/Zr shows no significant variation between the volcanic centres and over time (Fig. 3e) reaffirms that this ratio is not affected by slab components. Furthermore, it implies that the mantle wedge below Montserrat has remained relatively constant in composition over time.

The geochemical time series of the current period of Soufrière Hills activity (1995-2010) shows that the Pb isotope compositions have been stable over this time period (Figs. 4a, 4b & 4c), which suggests that these volcanic products have a similar petrogenesis through this time (including stable sediment and slab fluid contributions). Somewhat wider variations in Nd isotope ratios (Fig. 4d) may reflect mixing between the andesitic magmas and mafic enclaves. Indeed, *Barclay et al.* [2010] note that there is an increase in the proportion of mafic enclaves from Phase 1 (1995-1998) to Phase 3 (2005-2007) and the Phase 3 samples have the lowest Nd isotope values and are similar to the mafic enclaves.

The Silver Hills, Centre Hills and Soufrière Hills volcanic centres have a limited range of isotopic compositions, suggesting that the magma source region to these volcanic centres remained relatively constant for ~2 Myr. Alternatively, the magma plumbing beneath these centres may have efficiently homogenised any incoming heterogeneities. However, the interlude at ~130 ka of dominantly basaltic and basaltic andesite erupted from the SSH volcanic centre shows a distinct deviation to less radiogenic Pb isotope compositions (Fig 4a). This trend is mirrored to a lesser extent in the Nd isotope ratios, which show high $^{143}\text{Nd}/^{144}\text{Nd}$ in Suite B samples (Fig. 4d). These observations suggest that either the composition of the magma source region significantly changed over a short time scale or that a particular source heterogeneity escaped the blending effect of the main Montserrat reservoir in this period. SSH Suites A and B lie along the same isotopic trend, and this trend does not pass through the other three groups (Figs. 2 and 8). Consequently, mixing or assimilation of material from the Soufrière Hills centre with SSH magmas does not appear to have occurred. Rather, we propose that SSH represents a distinct magmatic episode. Within this period Suite A, with the more radiogenic Pb isotope ratios, marks an initial phase with a higher subducted sediment contribution relative to slab fluid than is observed in the later Suite B, which has generally higher Ba/La values (Fig. 2b).

4.4 Slab and sediment contributions

The evidence above indicates there are clear trace element and isotopic differences between the SSH samples and those from the other volcanic centres on Montserrat; particularly apparent in the Pb-Pb plots (Fig. 2 and 7). The isotope systematics support the

hypothesis that Montserrat magmas, and in particular the SSH magmas, are generated by mixing an enriched mantle source, supplemented by subducted sediment addition (Fig. 7).

The Lesser Antilles and SSH trends highlighted in Fig 2 are plotted with the Pb isotope data from other islands on the Lesser Antilles (Fig. 7). Whilst the Silver, Centre and Soufrière Hills volcanic centres are effectively co-linear with these other islands, the SSH trend deviates markedly, particularly in $^{206}\text{Pb}/^{204}\text{Pb}-\Delta 8/4\text{Pb}$ (Fig. 7 b). In both Pb plots (Fig 8a and 8b) the SSH trend marks a projection between the average Lesser Antilles sediment compositions and an enriched mantle source that is not seen in the combined grouping of the other Montserrat suites and the other central and northern Lesser Antilles (Fig. 7). The two alignments may, therefore, be the result of variable amounts of sediment and slab fluid addition, as evidenced by the trace-element trends (Fig. 3). In this hypothesis, the Soufrière Hills, Centre Hills and Silver Hills lie on a trend reflecting more sediment addition from the slab, perhaps in the form of a partial melt, compared to the SSH magmas. This higher sediment component draws the Silver Hills, Centre Hills and Soufrière Hills magmas to more radiogenic Pb isotope compositions, and is supported by the higher Th/Ce ratios and LREE enrichments observed for these volcanic centres relative to the SSH.

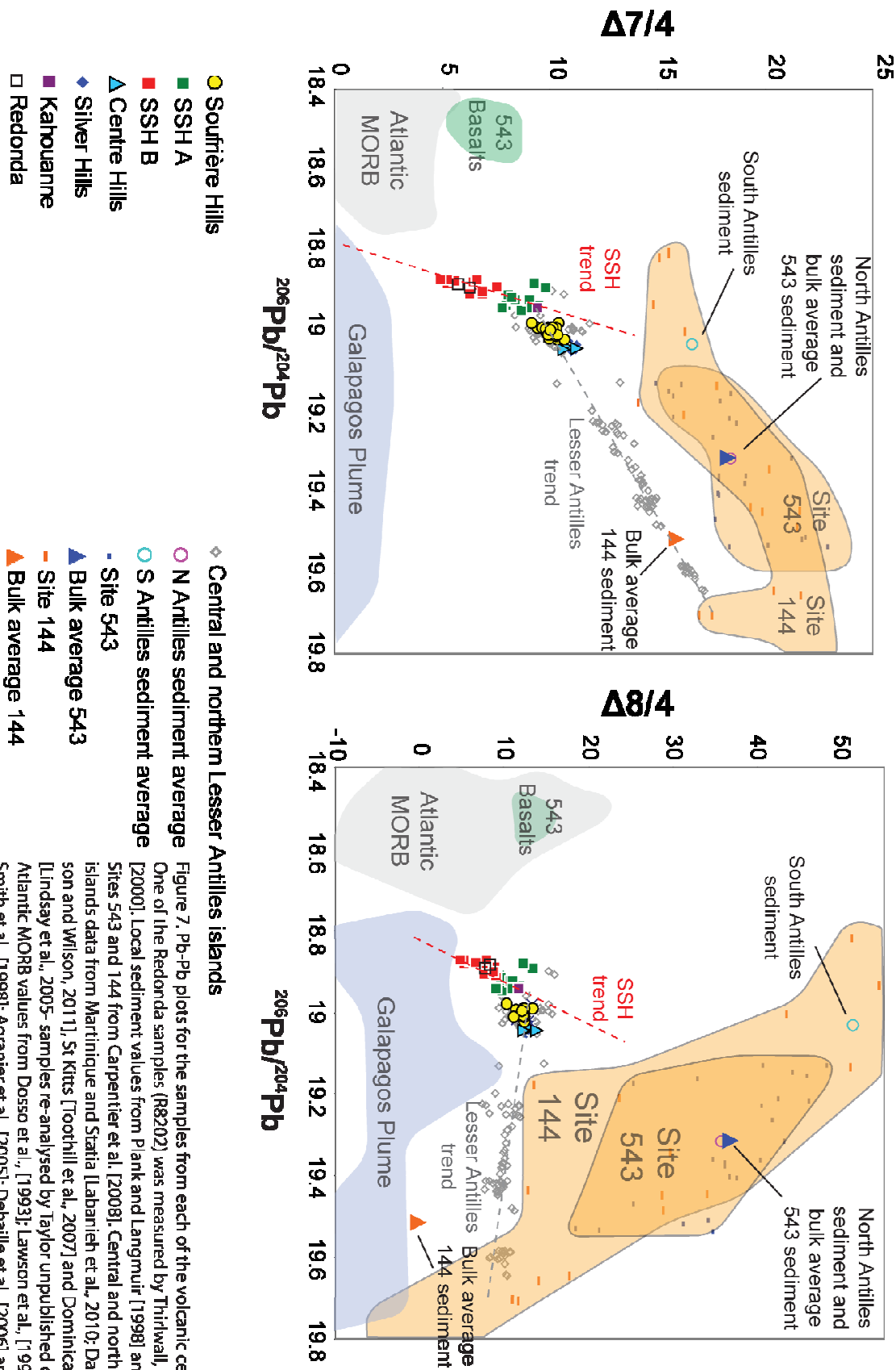


Figure 7. Pb-Pb plots for the samples from each of the volcanic centres. One of the Redonda samples (R8202) was measured by Thirlwall, [2000]. Local sediment values from Plank and Langmuir [1998] and Sites 543 and 144 from Carpenter et al. [2008]. Central and northern islands data from Martinique and Statia [Labanih et al., 2010; Davidson and Wilson, 2011], St Kitts [Toothill et al., 2007] and Dominica [Lindsay et al., 2005- samples re-analysed by Taylor unpublished data]. Atlantic MORB values from Dosso et al., [1993]; Lawson et al., [1996]; Smith et al., [1998]; Agrinier et al., [2005]; Debaille et al., [2006] and Galapagos plume values from Kurtz and Geist, [1999]; Saal et al., [2007].

In Fig. 8 we use end member components from *Dufrane et al.* [2009] and trace element - isotope plots to assess the likely components involved with the generation of

magmas at Montserrat. In a plot of Th/Nd versus $^{143}\text{Nd}/^{144}\text{Nd}$ (Fig. 8a), the SSH samples lie closer to the Galapagos mantle source than the other Montserrat volcanics, and show a slight negative correlation, suggesting mixing of enriched mantle and small amounts of sediment. Montserrat volcanics form a shallower gradient than the SSH, suggesting mixing with a source with higher Th/Nd than bulk sediment. This is potentially consistent with partial melting of subducted sediment which would raise the more incompatible Th relative to Nd. In addition, the Th/Nd against $^{207}\text{Pb}/^{204}\text{Pb}$ plot (Fig. 8b) shows Montserrat samples projecting towards a sediment melt component. By modelling mixing between fluid, melt and mantle components (Figure 8a and 8b), it seems highly likely that partial melt of North Antilles sediment is providing the high Th/Nd values in the Montserrat magmas. 5-10% of bulk sediment addition or 60% of altered oceanic crust fluid is required to re-produce the high Th/Nd values found in the Soufrière Hills samples. Instead only 1-3% of partial melted sediment is required to replicate the high Th/Nd samples, which is in good agreement with Zellmer *et al.* [2003] who estimated a $\sim 1.2\%$ sediment enrichment as a partial melt. Less sediment addition is required for the SSH magmas ($\sim 0.5\%$). Along the length of the Lesser Antilles, partial melting of sediments has been suggested to explain the wide isotopic variations, particularly with respect to the southern and central islands [Dufrane *et al.*, 2009; Labanieh *et al.*, 2010].

As discussed previously, the SSH suites are thought to comprise a greater slab fluid component, this is supported by the Ce/Pb vs. $^{207}\text{Pb}/^{204}\text{Pb}$ plot (Fig. 8c) where SSH magmas lie closer to the oceanic crust fluid end member than the rest of the Montserrat volcanics. Most of the Montserrat samples (including SSH) sit between slab fluid and bulk sediment addition, although some samples, particularly in the Silver Hills, Centre Hills and Soufrière Hills volcanic centres have elevated $^{207}\text{Pb}/^{204}\text{Pb}$ values, which may represent higher amounts of partially melted sediment. This highlights that the main difference between the SSH and the other volcanic centres is primarily controlled by variable sediment input and the manner with which it has been added (i.e. bulk sediment addition or partial melting of sediments). The SSH magmas are less enriched by sediment addition and have a greater slab fluid signature than the rest of the volcanic centres. However as the models show, the Montserrat and SSH magmas do not follow two component mixing lines, and are likely to reflect successive interaction between at least three components. For instance, an altered oceanic crust component may be required to reproduce the lower $^{207}\text{Pb}/^{204}\text{Pb}$ and higher $^{143}\text{Nd}/^{144}\text{Nd}$ observed at Montserrat relative to other islands of the Lesser Antilles (Figures 8a, 8b and 8c).

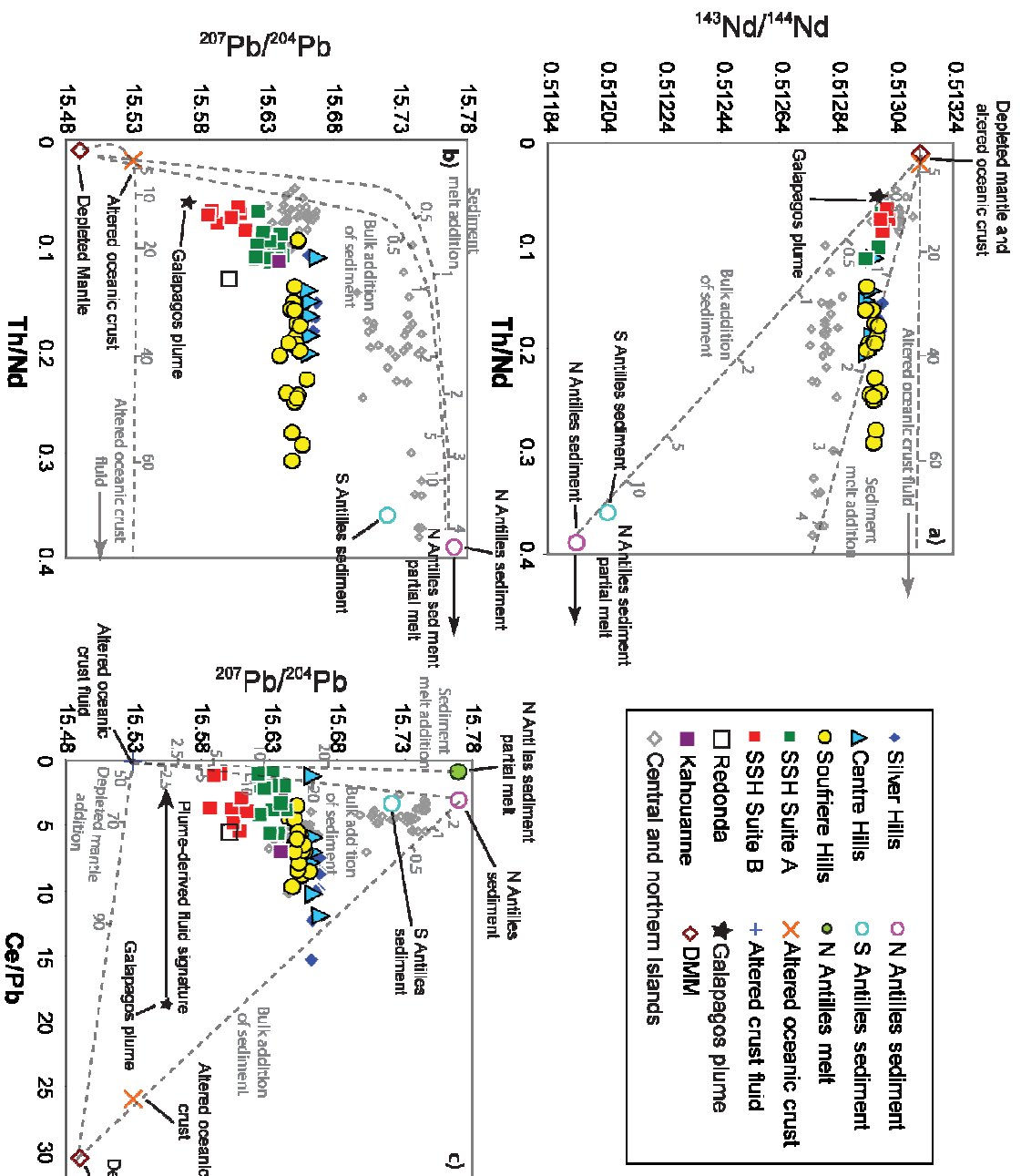


Figure 8. a) Th/Nd versus $^{143}\text{Nd}/^{144}\text{Nd}$ for Montserrat volcanics. Mixing lines between average Depleted MORB Mantle (DMM) and bulk Northern Antilles sediment, sediment melts and altered oceanic crust fluid are shown. Sediment values are from Plank and Langmuir [1998], DMM from Workman and Hart [2005], and Altered oceanic crust from Kelley et al. [2003]; Bach et al. [2003]; Hauff et al. [2003]. Continued below

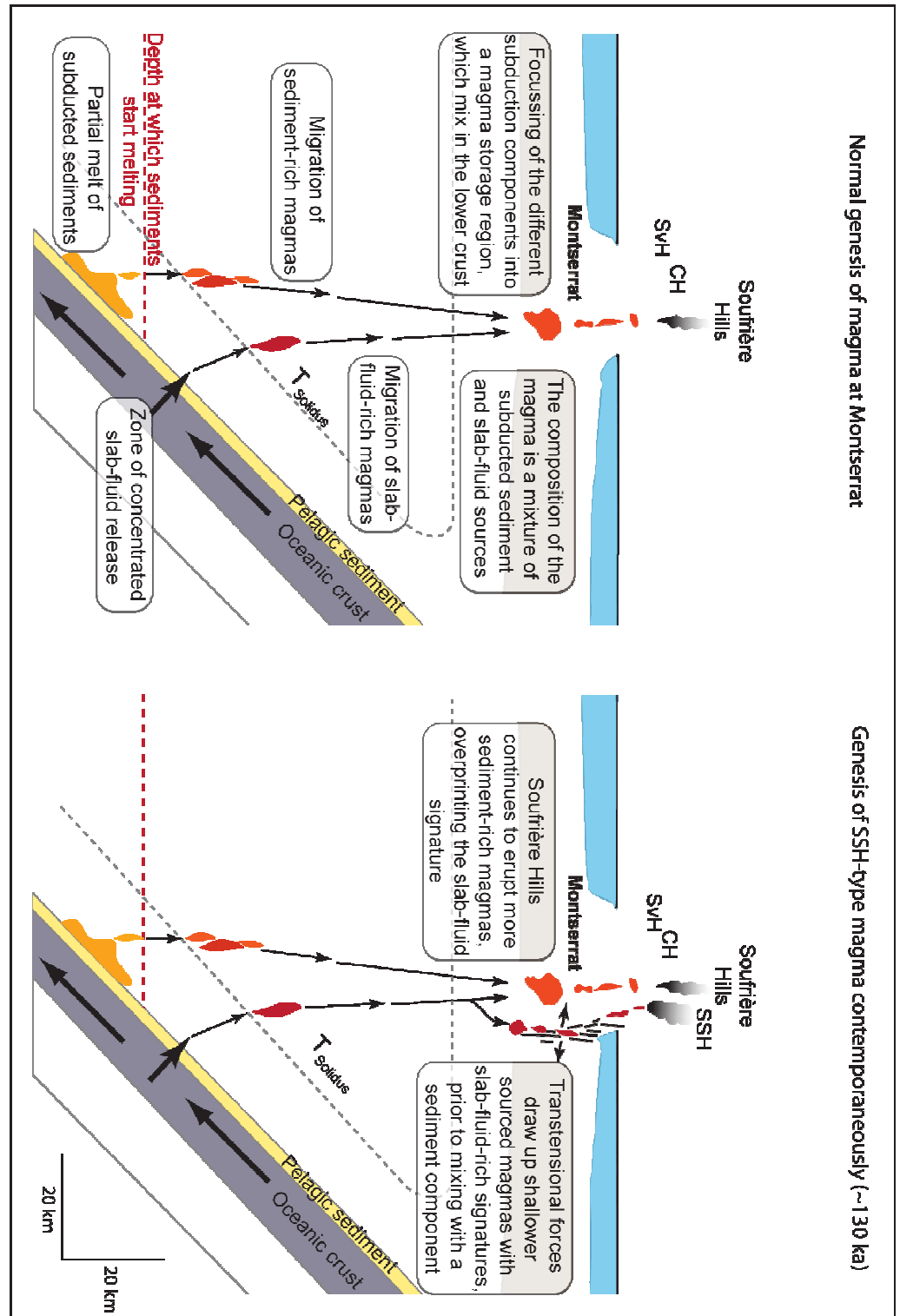
Average Galapagos values are from Kurtz and Geist, [1999]; Saal et al., [2007]. Altered oceanic crust fluid component was derived from Dufrene et al. [2009], using a Rayleigh distillation calculation using an average altered oceanic crust component from Kelley et al. [2003], assuming a 2% fluid release from an eclogitic residue and fluid/mineral partition co-efficients from Brenan et al. [1995b]. North Antilles sediment composition was partially melted (20%) using the 800 °C bulk partition coefficients from Johnson and Plank [1999] and the batch melting equation from Shaw [1970]. The mixing lines between DMM and the bulk sediment, partially melted sediment and altered oceanic crust fluid are labelled in percentages of addition. b) Th/Nd versus $^{206}\text{Pb}/^{204}\text{Pb}$ for Montserrat magmas, the same mixing lines as for Figure 8a are plotted. c) Ce/Pb versus $^{206}\text{Pb}/^{204}\text{Pb}$. Modelled mixing lines between altered oceanic crust fluid and bulk sediment, and between DMM and partial melted sediment/bulk addition of sediment are shown. The northern and central Lesser Antilles islands (St. Kitts, St. Lucia, St. Vincent, St. John, St. Kitts, Dominica and Martinique) are plotted (references listed in the caption to Figure 7)

4.5 Co-existence of two magmatic sources for Montserrat at ~130 ka

The differences between the Pb isotope and other geochemical characteristics of the SSH and rest of volcanic centres on Montserrat suggests they were generated from sources with distinct compositions arising from variations in the relative contribution of sediment and fluid components derived from the subducted slab. It is likely, therefore, that the SSH magmas and the other Montserrat magmas were generated from different depths. The Silver Hills, Centre Hills and Soufrière Hills magmas require a sediment partial melt component, so they may be sourced from deeper (i.e. hotter) depths (ca. >100 km) [Syracuse and Abers, 2006], above the solidus for sediments; ca. >700°C [Hermann and Spandler, 2008], whereas the SSH magmas may be derived from shallower depths where temperatures are too low to melt sediment. In this case, slab-fluid dehydration is the dominant component being added to the mantle wedge (Fig. 9).

The nature of the mechanism responsible for changes in melting depth is uncertain at this time, but there is evidence that this process is not confined to Montserrat as shown by the Pb isotope composition of Redonda and Kahouanne volcanoes, which plot within the fields and trend defined by the SSH Suite B and SSH Suite A respectively. Although Redonda and Kahouanne are located >30 km and >20 km respectively from the SSH, with no visual fault network connecting them [Feuillet *et al.*, 2010; Fig. 1], their similar Pb isotope systematics to SSH may be a reflection of a more regional pathway for SSH magmas in the area. The northern part of the Lesser Antilles arc is influenced by transtensional forces, leading to internal deformation caused by the oblique subduction of the North American plate (Fig.1); [Feuillet, 2000; Feuillet *et al.*, 2010]. Due increased shear stresses in the north, slip rates along the inner arc faults are higher and large to moderate earthquakes are more frequent [Feuillet *et al.*, 2011]. An example of these forces is provided by the Montserrat-Bouillante graben (Fig. 1c), which is the expression of a sinistral transtensional fault striking at 140-160°, that links Montserrat and Guadeloupe [Feuillet *et al.*, 2010]. Structures parallel to this fault are observed in the bathymetric data (Fig. 1c) and in seismic traces of magma movements at Basse Terre volcano, Guadeloupe, that are thought to be influenced by this fault system [Mathieu *et al.*, 2011]. Faults such as these likely extend down into the lower crust and upper mantle as a result of slip partitioning [Bowman *et al.*, 2003; Feuillet *et al.*, 2011]. We hypothesize that local extension forces may draw up slab-fluid-rich magmas from shallower portions of the mantle wedge which have not been so heavily influenced by sediment addition or mantle depletion, and thus yield the geochemical features observed in the SSH, Redonda and Kahouanne samples (Fig 9). Trace element and isotopic heterogeneities on the scale of kilometres have been observed within and across other arcs [Taylor and Nesbitt,

1998; *Ishizuka et al.*, 2003, 2006; *Marske et al.*, 2011], illustrating that different subduction derived components can be individually sampled from subadjacent volcanic centres <10km apart. This may be facilitated by transport of slab-derived components to the mantle wedge by discrete channelized flows [*Herbert et al.*, 2009]. It may also be that there were phases of SSH-type volcanism earlier in the history of Montserrat, but that these volcanic products have been buried beneath subsequent eruptions, or have been eroded away. This hypothesis may be tested by further high precision and high temporal-spatial resolution isotopic work on other volcanic islands in the Lesser Antilles that have volcanic centres that lie along these transtensional faults.



4.6 Mantle enrichment

The SSH Pb isotope trend does not point to an Atlantic MORB source, but one that is slightly more radiogenic (Fig. 7). One possible origin for the enriched mantle source may be

the palaeo-Galapagos hotspot. *Duncan and Hargraves* [1984] suggested that the mantle beneath the Lesser Antilles arc was affected (i.e., enriched) by the Galapagos mantle plume during the Late Cretaceous when the Caribbean oceanic plateau was formed, and that this influenced the early stage of formation of the Lesser Antilles arc [*Duncan and Hargraves*, 1984; *Pindell and Barret*, 1990; *Pindell and Kinmann*, 2009 and references therein]. *Thirlwall et al.* [1996] sought to test this hypothesis and noted that while Sr-Nd isotope ratios in exposed sections of the Caribbean plateau crust are similar to Atlantic MORB values, Pb isotopes are substantially more radiogenic. However, they were unable to apply this model to the Pb isotopic compositions of Grenada rocks because of the high degree of shallow crustal assimilation. Montserrat volcanics are, however, less affected by crustal assimilation than Grenada and the SSH magmas in particular lack a strong sediment component, and may thus preserve an enriched mantle signature. Hence, we propose that the Galapagos plume is the source for the enriched Pb isotopic end member, likely captured by slab fluids as they chemically interacted with the enriched mantle on ascension. As a consequence of this interaction, the Pb isotopes in the fluid would take on a Galapagos signature while retaining low Ce/Pb values (Fig. 8c),

5. Summary and conclusions

The different volcanic centres on Montserrat; the Silver Hills, Centre Hills, Soufrière Hills and 2 suites of the South Soufrière Hills can be distinguished by selected geochemical parameters, of which high-precision Pb analyses are the most effective. These results show that the SSH was active at the same time as Soufrière Hills, Garabaldi Hill may represent the earliest stage of volcanism (282 ± 8 ka) at the current Soufrière Hills volcanic centre and that mafic enclaves from the current period of Soufrière Hills activity are sourced from the Soufrière Hills volcanic centre.

For a period of ~ 2 Myr Montserrat has experienced highly consistent isotopic compositions which was interrupted by a rapid shift in trace element, Pb and Nd isotopic compositions during the formation of SSH Suites A and B at ~ 130 ka, possibly corresponding to regional transtensional tectonics which may have extracted magma from a shallower source. Subsequent volcanism returned to more consistent isotopic compositions in the currently active, Soufrière Hills volcano. The composition of magma sources to the current phases of activity at Soufrière Hills on Montserrat during the last 15 years has remained fairly stable.

With the use of high-precision Pb isotopes we have shown that Montserrat (and the Lesser Antilles arc) is not a simple two component system, but is affected by bulk sediment

addition, sediment melt, slab fluids, altered oceanic crust and Galapagos plume components. The SSH suite on Montserrat has the least radiogenic Pb isotopes reported from the Lesser Antilles, and represents a distinct composition within this volcanic arc. This SSH component, together with Redonda and Kahouanne, has a higher slab-fluid signature than the other volcanic centres, and lacks a sediment melt component. As such it more closely preserves the mantle wedge composition, which has been enriched by a Galapagos plume component.

References:

- Agranier, A., J. Blichert-Toft, D. Graham, V. Debaille, P. Schiano and F. Albarede (2005) "The spectra of isotopic heterogeneities along the mid-Atlantic Ridge" Earth and Planetary Science Letters **238** 96-109
- Bach, W., B. Peucker-Ehrenbrink, S.R. Hart and J.S. Blusztajn (2003) "Geochemistry of hydrothermally altered oceanic crust: DSDP/ODP Hole 504B - Implications for seawater-crust exchange budgets and Sr- and Pb-isotopic evolution of the mantle" Geochemistry Geophysics Geosystems **4**
- Barclay, J., R.A. Herd, B.R. Edwards, T. Christopher, E.J. Kiddle, M. Plail and A. Donovan (2010) "Caught in the act: Implications for the increasing abundance of mafic enclaves during the recent eruptive episodes of the Soufriere Hills Volcano, Montserrat" Geophysical Research Letters **37**
- Blundy, J. and B. Wood (2003) "Partitioning of trace elements between crystals and melts" Earth and Planetary Science Letters **210** 383-397
- Bottazzi, P., M. Tiepolo, R. Vannucci, A. Zanetti, R. Brumm, S.F. Foley and R. Oberti (1999) "Distinct site preferences for heavy and light REE in amphibole and the prediction of D-Amph/L(REE)" Contributions to Mineralogy and Petrology **137** 36-45
- Bouysse, P. and D. Westercamp (1990) "Subduction of atlantic aseismic ridges and late cenozoic evolution of the Lesser Antilles island-arc" Tectonophysics **175** 349-&
- Bowman, D., G. King and P. Tapponnier (2003) "Slip partitioning by elastoplastic propagation of oblique slip at depth" Science **300** 1121-1123
- Brenan, J.M., H.F. Shaw and F.J. Ryerson (1995) "Experimental- evidence for the origin of lead enrichment in convergent-margin magmas " Nature **378** 54-56

- Brenan, J.M., H.F. Shaw, F.J. Ryerson and D.L. Phinney (1995) "Mineral-aqueous fluid partitioning of trace-elements at 900-degrees-C and 2.0 GPA - Constraints on the trace-element chemistry of mantle and deep-crustal fluids" Geochimica Et Cosmochimica Acta **59** 3331-3350
- Briden, J.C., D.C. Rex, A.M. Faller and J.F. Tomblin (1979) "K-Ar geochronolgy and paleomagnetism of volcanic-rocks in the Lesser Antilles arc" Geophysical Journal of the Royal Astronomical Society **57** 272-272
- Carpentier, M., C. Chauvel and N. Mattielli (2008) "Pb-Nd isotopic constraints on sedimentary input into the Lesser Antilles arc system" Earth and Planetary Science Letters **272** 199-211
- Cassidy, M., Trofimovs, J., Watt, S.F.L., Palmer, M.R., Taylor, R.N., Gernon, T.M., Talling, P.J., Le Friant, A. (in press) "Multi-stage collapse events in the South Soufrière Hills, Montserrat, as recorded in marine sediment cores" In G. Wadge, Robertson, R., Voight, B., (eds) *The eruption of Soufrière Hills volcano, Montserrat from 2000 to 2010* Memoir of the Geological Society, London
- Davidson, J. and M. Wilson (2011) "Differentiation and Source Processes at Mt Pelee and the Quill; Active Volcanoes in the Lesser Antilles Arc" Journal of Petrology **52** 1493-1531
- Davidson, J.P. (1987) "Crustal contamination versus subduction zone enrichment - Examples from the Lesser Antilles and implications for mantle source compositions of island-arc volcanic-rocks" Geochimica Et Cosmochimica Acta **51** 2185-2198
- Davidson, J.P. (1996) "Deciphering mantle and crustal signatures in subduction zone magmatism" Geophys. Monogr. American geophysical union **96** 251-262
- Debaille, V., J. Blichert-Toft, A. Agranier, R. Doucelance, P. Schiano and F. Albarede (2006) "Geochemical component relationships in MORB from the Mid-Atlantic Ridge, 22-35 degrees N" Earth and Planetary Science Letters **241** 844-862
- DeMets, C., P.E. Jansma, G.S. Mattioli, T.H. Dixon, F. Farina, R. Bilham, E. Calais and P. Mann (2000) "GPS geodetic constraints on Caribbean-North America plate motion" Geophysical Research Letters **27** 437-440
- Devine, J.D., M.D. Murphy, M.J. Rutherford, J. Barclay, R.S.J. Sparks, M.R. Carroll, S.R. Young and J.E. Gardner (1998) "Petrologic evidence for pre-eruptive pressure-temperature conditions,

and recent reheating, of andesitic magma erupting at the Soufriere Hills Volcano, Montserrat, WI" Geophysical Research Letters **25** 3669-3672

Dosso, L., H. Bougault and J.L. Joron (1993) "Geochemical morphology of the North Mid-Atlantic Ridge, 10°–24°N: Trace element-isotope complementarity" Earth and Planetary Science Letters **120** 443-462

DuFrane, S.A., S. Turner, A. Dosseto and M. van Soest (2009) "Reappraisal of fluid and sediment contributions to Lesser Antilles magmas" Chemical Geology **265** 272-278

Duncan, R.A. and R.B. Hargraves (1984) "Plate tectonic evolution of the caribbean region in the mantle reference frame" Geological Society of America Memoirs **162** 81-93

Elliott, T., T. Plank, A. Zindler, W. White and B. Bourdon (1997) "Element transport from slab to volcanic front at the Mariana arc" Journal of Geophysical Research-Solid Earth **102** 14991-15019

Feuillet, N. (2000) "Sismotectonique des Petites Antilles, liason entre activite sismique et volcanique = Sismotectonics of Lesser Antilles, relationship between seismic activity and volcanism." Rene Diderot University PhD Thesis 283 pp

Feuillet, N., Beauducel, F., Tapponnier, P (2011) "Tectonic context of moderate to large historical earthquakes in the Lesser Antilles and mechanical coupling with volcanoes" Journal of Geophysical Research **116**

Feuillet, N., F. Leclerc, P. Tapponnier, F. Beauducel, G. Boudon, A. Le Friant, C. Deplus, J.F. Lebrun, A. Nercessian, J.M. Saurel and V. Clement (2010) "Active faulting induced by slip partitioning in Montserrat and link with volcanic activity: New insights from the 2009 GWADASEIS marine cruise data" Geophysical Research Letters **37** 6

Gill, J.B. (1981) "Orogenic andesites and plate tectonics" Orogenic andesites and plate tectonics xiv+385

Harford, C.L., Pringle, M.S., Sparks, R.S.J., Young S.R. (2002) "The volcanic evolution of Montserrat using $^{40}\text{Ar}/^{39}\text{Ar}$ geochronology." In T. H. Druitt, Kokelaar, B.P. (eds) *The eruption of Soufrière Hills Volcano, Montserrat, from 1995 to 1999* Geological Society of London Memoirs **21** 93-113

Hart, S.R. (1984) "A large-scale isotope anomaly in the southern-hemisphere mantle" Nature **309** 753-757

Hauff, F., K. Hoernle and A. Schmidt (2003) "Sr-Nd-Pb composition of Mesozoic Pacific oceanic crust (Site 1149 and 801, ODP Leg 185): Implications for alteration of ocean crust and the input into the Izu-Bonin-Mariana subduction system" Geochemistry Geophysics Geosystems **4**

Hawkesworth, C.J. and M. Powell (1980) "Magma genesis in the Lesser Antilles island-arc" Earth and Planetary Science Letters **51** 297-308

Hawkesworth, C.J., S.P. Turner, F. McDermott, D.W. Peate and P. vanCalsteren (1997) "U-Th isotopes in arc magmas: Implications for element transfer from the subducted crust" Science **276** 551-555

Heath, E., R. MacDonald, H. Belkin, C. Hawkesworth and H. Sigurdsson (1998) "Magma genesis at Soufriere Volcano, St Vincent, Lesser Antilles arc" Journal of Petrology **39** 1721-1764

Hebert, L.B., P. Antoshechkina, P. Asimow and M. Gurnis (2009) "Emergence of a low-viscosity channel in subduction zones through the coupling of mantle flow and thermodynamics" Earth and Planetary Science Letters **278** 243-256

Hermann, J. and C.J. Spandler (2008) "Sediment melts at sub-arc depths: An experimental study" Journal of Petrology **49** 717-740

Ishizuka, O., R.N. Taylor, J.A. Milton and R.W. Nesbitt (2003) "Fluid-mantle interaction in an intra-oceanic arc: constraints from high-precision Pb isotopes" Earth and Planetary Science Letters **211** 221-236

Ishizuka, O., R.N. Taylor, J.A. Milton, R.W. Nesbitt, M. Yuasa and I. Sakamoto (2006) "Variation in the mantle sources of the northern Izu arc with time and space - Constraints from high-precision Pb isotopes" Journal of Volcanology and Geothermal Research **156** 266-290

Ishizuka, O., R.N. Taylor, M. Yuasa and Y. Ohara (2011) "Making and breaking an island arc: A new perspective from the Oligocene Kyushu-Palau arc, Philippine Sea" Geochemistry Geophysics Geosystems **12** 40

Johnson, M.C., and Plank, T., (1999) "Dehydration and Melting Experiments Constrain the Fate of Subducted Sediments" Geochemistry Geophysics Geosystems **1** 1007

Kelley, K.A., T. Plank, J. Ludden and H. Staudigel (2003) "Composition of altered oceanic crust at ODP Sites 801 and 1149" Geochemistry Geophysics Geosystems **4**

- Kurz, M.D. and D. Geist (1999) "Dynamics of the Galapagos hotspot from helium isotope geochemistry" Geochimica Et Cosmochimica Acta **63** 4139-4156
- Labanieh, S., C. Chauvel, A. Germa, X. Quidelleur and E. Lewin (2010) "Isotopic hyperbolas constrain sources and processes under the Lesser Antilles arc" Earth and Planetary Science Letters **298** 35-46
- Lawson, K., Searle, R.C., Pearce, J.A., Browning, P., Kempton P. (1996) "Detailed volcanic geology of the MARNOK area, Mid-Atlantic Ridge north of Kane transform" Geology society special publication **118** 61-102
- Le Friant, A., C. Deplus, G. Boudon, R.S.J. Sparks, J. Trofimovs and P. Talling (2009) "Submarine deposition of volcanoclastic material from the 1995-2005 eruptions of Soufriere Hills volcano, Montserrat" Journal of the Geological Society **166** 171-182
- Le Friant, A., C.L. Harford, C. Deplus, G. Boudon, R.S.J. Sparks, R.A. Herd and J.C. Komorowski (2004) "Geomorphological evolution of Montserrat (West Indies): importance of flank collapse and erosional processes" Journal of the Geological Society **161** 147-160
- Lindsay, J.M., R.B. Trumbull and W. Siebel (2005) "Geochemistry and petrogenesis of late Pleistocene to recent volcanism in Southern Dominica, Lesser Antilles" Journal of Volcanology and Geothermal Research **148** 253-294
- Macdonald, R., C.J. Hawkesworth and E. Heath (2000) "The Lesser Antilles volcanic chain: a study in are magmatism" Earth-Science Reviews **49** 1-76
- Marske, J.P., A.J. Pietruszka, F.A. Trusdell and M.O. Garcia (2011) "Geochemistry of southern Pagan Island lavas, Mariana arc: the role of subduction zone processes" Contributions to Mineralogy and Petrology **162** 231-252
- Mathieu, L., B.v.W. de Vries, M. Pilato and V.R. Troll (2011) "The interaction between volcanoes and strike-slip, transtensional and transpressional fault zones: Analogue models and natural examples" Journal of Structural Geology **33** 898-906
- Maury, R.C., Westbrook, G.K., Baker, P.E., Bouysse, P., Westercamp, D. (1990) "Geology of the Lesser Antilles" The Geology of North America H-The caribbean region 141-166
- Miller, D.M., S.L. Goldstein and C.H. Langmuir (1994) "Cerium lead and lead-isotope ratios in arc magmas and the enrichment of lead in the continents" Nature **368** 514-520

- Pindell, J., & Barrett, S. (1990) "Geological evolution of the Caribbean region; a Plate tectonic perspective" Geological Society of America **The Geology of North America** 405-432 pp
- Pindell, J.L. and L. Kennan (2009) "Tectonic evolution of the Gulf of Mexico, Caribbean and northern South America in the mantle reference frame: an update" In K. H. L. M. A. P. J. L. James (eds) *Origin and Evolution of the Caribbean Plate* **328** 1-55
- Plank, T. (2005) "Constraints from thorium/lanthanum on sediment recycling at subduction zones and the evolution of the continents" Journal of Petrology **46** 921-944
- Plank, T. and C.H. Langmuir (1998) "The chemical composition of subducting sediment and its consequences for the crust and mantle" Chemical Geology **145** 325-394
- Rea, J.W. (1974) "The volcanic geology and petrology of Montserrat, West Indies" J. Geol. Soc. Lond. **130** 341-366
- Robertson, R.E.A., W.P. Aspinall, R.A. Herd, G.E. Norton, R.S.J. Sparks and S.R. Young (2000) "The 1995-1998 eruption of the Soufriere Hills volcano, Montserrat, WI" Philosophical Transactions of the Royal Society of London Series a-Mathematical Physical and Engineering Sciences **358** 1619-1637
- Saal, A.E., M.D. Kurz, S.R. Hart, J.S. Blusztajn, J. Blichert-Toft, Y. Liang and D.J. Geist (2007) "The role of lithospheric gabbros on the composition of Galapagos lavas" Earth and Planetary Science Letters **257** 391-406
- Sevilla, W.I., C.J. Ammon, B. Voight and S. De Angelis (2010) "Crustal structure beneath the Montserrat region of the Lesser Antilles island arc" Geochemistry Geophysics Geosystems **11** 13
- Shaw, D.M. (1970) "Trace element fractionation during anatexis" Geochimica Et Cosmochimica Acta **34** 237-&
- Smith, S.E., J.F. Casey, W.B. Bryan, L. Dmitriev, S. Silantyev and R. Magakyan (1998) "Geochemistry of basalts from the Hayes Transform region of the Mid-Atlantic Ridge" Journal of Geophysical Research-Solid Earth **103** 5305-5329
- Straub, S.M., S.L. Goldstein, C. Class and A. Schmidt (2009) "Mid-ocean-ridge basalt of Indian type in the northwest Pacific Ocean basin" Nature Geoscience **2** 286-289

- Sun, S., McDonough, W.F. (1989) "Chemical and isotopic systematics of ocean basalts: implications for mantle composition and processes" Geological Society Special Publication **42** 313-345
- Syracuse, E.M. and G.A. Abers (2006) "Global compilation of variations in slab depth beneath arc volcanoes and implications" Geochemistry Geophysics Geosystems **7**
- Tatsumi, Y., D.L. Hamilton and R.W. Nesbitt (1986) "Chemical characteristics of fluid phase released from a subducted lithosphere and origin of arc magmas - Evidence from high-pressure experiments and natural rocks" Journal of Volcanology and Geothermal Research **29** 293-309
- Taylor, R.N. and R.W. Nesbitt (1998) "Isotopic characteristics of subduction fluids in an intra-oceanic setting, Izu-Bonin Arc, Japan" Earth and Planetary Science Letters **164** 79-98
- Thirlwall, M.F. (2000) "Inter-laboratory and other errors in Pb isotope analyses investigated using a ^{207}Pb – ^{204}Pb double spike" Chemical Geology **163** 299-322
- Toothill, J., C.A. Williams, R. Macdonald, S.P. Turner, N.W. Rogers, C.J. Hawkesworth, D.A. Jerram, C.J. Ottley and A.G. Tindle (2007) "A complex petrogenesis for an arc magmatic suite, St Kitts, Lesser Antilles" Journal of Petrology **48** 3-42
- Turner, S., C. Hawkesworth, P. vanCalsteren, E. Heath, R. Macdonald and S. Black (1996) "U-series isotopes and destructive plate margin magma genesis in the Lesser Antilles" Earth and Planetary Science Letters **142** 191-207
- Van Soest, M.C., D.R. Hilton, C.G. Macpherson and D.P. Matthey (2002) "Resolving sediment subduction and crustal contamination in the Lesser Antilles island Arc: A combined He-O-Sr isotope approach" Journal of Petrology **43** 143-170
- Wadge, G. (1984) "Comparison of volcanic production-rates and subduction rates in the Lesser Antilles and Central America" Geology **12** 555-558
- Wadge, G. and J.B. Shepherd (1984) "Segmentation of the Lesser Antilles subduction zone" Earth and Planetary Science Letters **71** 297-304
- White, W.M. and B. Dupre (1986) "Sediment subduction and magma genesis in the lesser antilles - isotopic and trace-element constraints" Journal of Geophysical Research-Solid Earth and Planets **91** 5927-5941

Woodhead, J., S. Eggins and J. Gamble (1993) "High-field strength and transition element systematics in island-arc and back-arc basin basalts - Evidence for multiphase melt extraction and a depleted mantle wedge" Earth and Planetary Science Letters **114** 491-504

Woodhead, J.D. (1989) "Geochemistry of the Mariana arc (western Pacific) - source composition and processes " Chemical Geology **76** 1-24

Workman, R.K. and S.R. Hart (2005) "Major and trace element composition of the depleted MORB mantle (DMM)" Earth and Planetary Science Letters **231** 53-72

Young, S.R., R.S.J. Sparks, W.P. Aspinall, L.L. Lynch, A.D. Miller, R.E.A. Robertson and J.B. Shepherd (1998) "Overview of the eruption of Soufriere Hills volcano, Montserrat, 18 July 1995 to December 1997" Geophysical Research Letters **25** 3389-3392

Zellmer, G.F., C.J. Hawkesworth, R.S.J. Sparks, L.E. Thomas, C.L. Harford, T.S. Brewer and S.C. Loughlin (2003) "Geochemical evolution of the Soufriere Hills volcano, Montserrat, Lesser Antilles volcanic arc" Journal of Petrology **44** 1349-1374

CHAPTER 3

MULTI-STAGE COLLAPSE EVENTS IN THE SOUTH SOUFRIÈRE HILLS, MONTSERRAT AS RECORDED IN MARINE SEDIMENT CORES

This chapter is a reproduction of an article published in the Memoir of the Geological Society of London:

Cassidy, M., J. Trofimovs, S.F.L. Watt, M.R. Palmer, R.N. Taylor, T.M. Gernon, P.J. Talling, A. Le Friant. 'Multi-stage collapse events in the South Soufrière Hills, Montserrat, as recorded in marine sediment cores', *In: Wadge, G., Robertson, R., Voight, B., (eds) The eruption of Soufrière Hills volcano, Montserrat from 2000 to 2010*, Memoir of the Geological Society, London.

Written by M Cassidy, but I received feedback from all the authors, Trofimovs especially helped with the guidance of this chapter. Watt provided Figure 5 and some thought on sections 2.2 and 3.2. Palmer and Gernon helped with fieldwork in the SSH, Talling helped with feedback and financial assistance, Le Friant was added as she provided the submarine and subaerial DEM data files which I used to make Figures 1 and 6.

Abstract:

We present new evidence for sector collapses of the South Soufrière Hills (SSH) edifice, Montserrat during the mid-Pleistocene. High-resolution geophysical data provides evidence for sector collapse, producing a $\sim 1 \text{ km}^3$ submarine collapse deposit to the south of SSH. Sedimentological and geochemical analyses of submarine deposits sampled by sediment cores suggest that they were formed by large multi-stage flank failures of the subaerial SSH edifice into the sea. This work identifies two distinct geochemical suites within the SSH succession on the basis of trace element and Pb isotope compositions. Volcaniclastic turbidites in the cores preserve these chemically heterogeneous rock suites. However, the subaerial chemostratigraphy is reversed within the submarine sediment cores. Sedimentological analysis suggests that the edifice failures produced high concentration turbidites and that the collapses occurred in multiple stages, with an interval of at least ~ 2 kyr between the first and second failure. Detailed field and petrographic observations coupled with SEM image analysis shows that the SSH volcanic products preserve a complex record of magmatic activity. This activity consisted of episodic explosive eruptions of

andesitic pumice, likely triggered by mafic magmatic pulses and followed by eruptions of poorly vesiculated basaltic scoria and dacitic and basaltic lava flows.

1. Introduction

Large scale slope failures pose a major potential hazard and they can significantly alter the morphology of volcanic islands (Moore *et al.* 1989, 1994; Watts & Masson 1995; Masson 1996; Ollier *et al.* 1998; Masson *et al.* 2002). For example, volcanic island slope failures have produced some of the largest volume mass flows on Earth and are one of the main agents through which sediment is transferred from the volcanic islands to the deep ocean (Masson *et al.*, 2002). Large subaerial landslides from ocean island flanks have been identified as one of the most dangerous of all landslide hazards because of their tsunamigenic potential (Masson *et al.*, 2006; Lovholt *et al.* 2008).

Subaerial and submarine mapping have identified at least 47 flank-collapse landslides within the Lesser Antilles Arc (Boudon *et al.*, 2007), located between the Atlantic Ocean and the Caribbean Sea (Figure 1), with 15 of these occurring in the last 12,000 years on active volcanoes (Boudon *et al.* 2007). Le Friant *et al.* (2004) and Lebas *et al.* (2011) identified at least seven submarine debris avalanche deposits (Figure 1) derived from the flanks of Montserrat. The geomorphology of Montserrat and its surrounding submarine apron has been shaped by subaerial lava dome collapse, island flank collapse and submarine slope failure events (Le Friant *et al.* 2004; Herd *et al.* 2005; Trofimovs *et al.* 2008; 2010; Lebas *et al.* 2011; Watt *et al.*, 2012). Research is needed to understand the failure dynamics of flank and dome collapses and the risk they pose to inhabitants of small volcanic islands, such as Montserrat, through landslide and tsunami hazards.

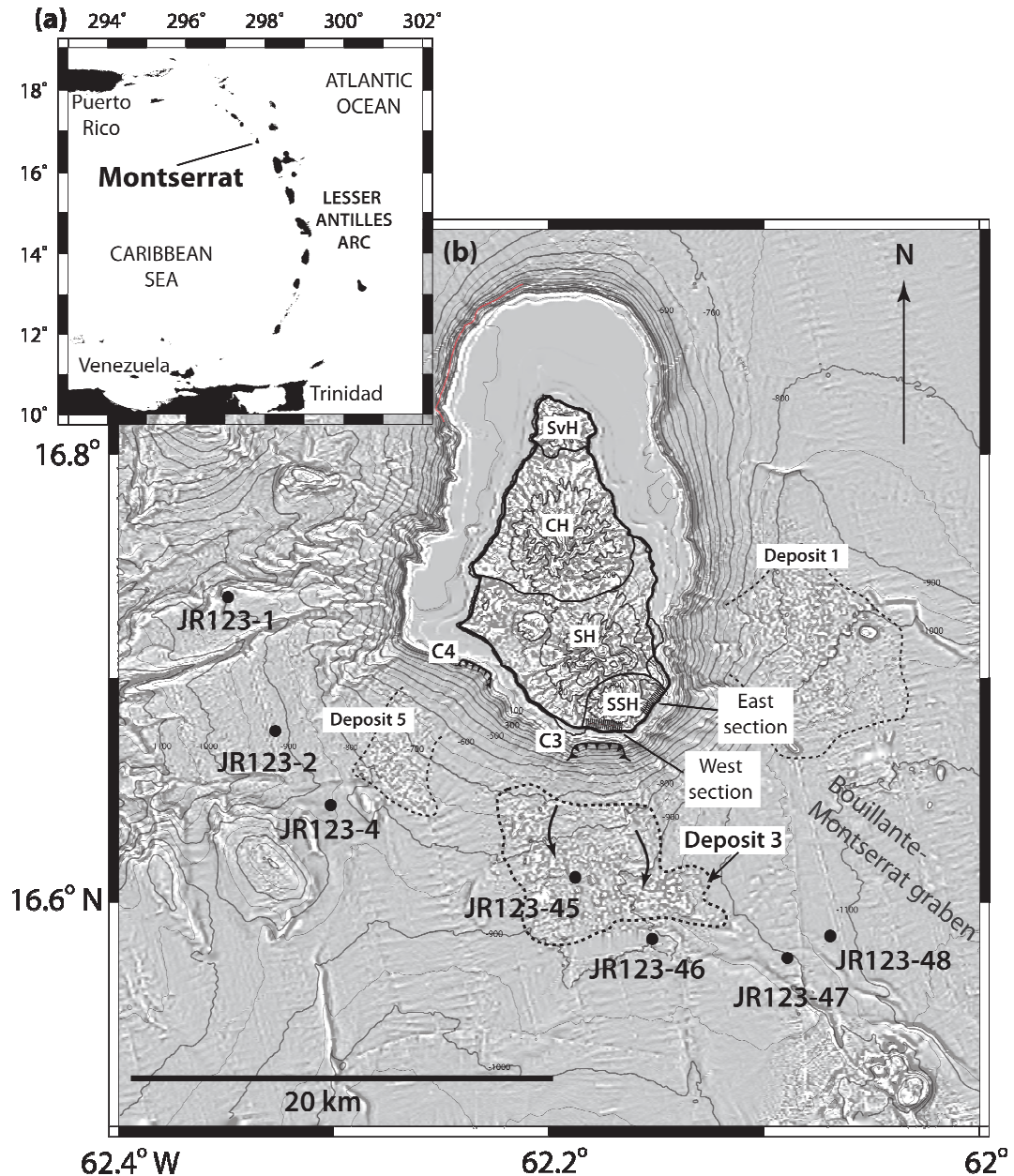


Figure 1. (a) Insert of Lesser Antilles island arc. (b) Curvature map of Montserrat and surrounding bathymetry. It highlights the surficial debris avalanche deposits (dotted lines) and submarine embayment (C3) identified by Le Friant et al. (2004); Lebas et al. (2011). Core locations and east and west subaerial field sections are annotated. SvH= Silver Hills, CH=Centre Hills SH= Soufrière Hills and SSH= South Soufrière Hills. Swath-bathymetry was attained during the Aguadamor cruise (1999) and Caraval cruise (2002) and on the R.V. L'Atalante as described by Le Friant et al. (2004). Subaerial topography was digitised from topographic maps provided by G.Wadge.

This paper documents the evolution of the South Soufrière Hills (SSH) volcanic complex, including episodes of edifice collapse into the sea, using new proximal (8-13 km from shore) submarine sediment cores, subaerial mapping, and offshore geophysical data. This contribution aims to answer the following questions: what types of volcanism have occurred within the SSH? What evidence is there in both the subaerial and submarine record

to suggest that the SSH has experienced mass wasting events? How did such flank collapse(s) and resulting sediment flow(s) behave?

1.1 Geological background

Montserrat is located in the Lesser Antilles island arc (Figure 1), a 750 km long volcanic chain formed by 2 cm/yr westward subduction of the North American plate beneath the Caribbean plate (Wadge, 1984; Demets *et al.*, 2000). Montserrat is situated in the northern part of this arc. The island is 16 km long (from north to south), 10 km wide (from east to west) and is composed almost entirely of volcanic rocks (Harford *et al.*, 2002).

Ar-Ar geochronology has been used to divide Montserrat into four separate volcanic regions. These are the Silver Hills (2600 – 1200 ka), Centre Hills (950 – 550 ka), Soufrière Hills complex (174 ka to present) and the South Soufrière Hills (131 – 128 ka) (Harford *et al.*, 2002) (Figure 1). The majority of the deposits on Montserrat are andesitic in composition. However, the SSH region also comprises basalts and basaltic andesites (Harford *et al.*, 2002). The older volcanic centres have been exposed to much terrestrial and coastal erosion. As a result, a wide (1 to 3 km), flat, and shallow (60 to 100 m depth) submarine shelf has formed around the northern part of the island. This shelf is much narrower in the south where the volcanic centres are younger, and have not been subject to significant erosion. The shelf around southern Montserrat, adjacent to the Soufrière Hills and SSH volcanic complexes, extends 0.5 km from the coast.

Activity of the SSH volcano is constrained by a few ^{40}Ar – ^{39}Ar ages from terrestrial sections, suggesting that the volcanic centre was erupted over a relatively short period of time (between $131 \text{ ka} \pm 7$ to $128 \pm 27 \text{ ka}$; Harford *et al.*, 2002). However, Le Friant *et al.* (2008) contend that the SSH was active for a longer period based on tephrochronology of marine sediments (147 – 124 ka). Rea (1974) documents a stratigraphy for the SSH consisting of basalt lava flows and basalt and basaltic andesitic fall deposits. More recently Smith *et al.* (2007) logged a repeated sequence of basaltic and andesitic fall deposits. These authors also noted ash flow and scoriaceous surge deposits, and a minor proportion of block and ash flow and surges, pumiceous lapilli, ash flow and mudflow deposits. Evidence for Vulcanian eruptions on the SSH at 147 – 142 ka is also thought to have been preserved by glass shards in a distal marine sediment core (55 km offshore Montserrat) (Le Friant *et al.* 2008).

2. Methods

2.1 Marine core sampling, logging and fieldwork

A research cruise onboard the *RRS James Clark Ross* (May 2005 – P.I. Prof. R.S.J. Sparks) sampled submarine volcanic deposits using a vibrocore system that was developed by the British Geological Survey. The vibrocore was capable of sampling up to six metres of unconsolidated marine sediment in water depths of less than 2000 m. The vibrocores discussed in this contribution are located south and west of Montserrat, 8 to 13 km offshore (Figure 1). Cores were sedimentologically logged, detailing grain size, sedimentary structure and appearance. The SSH volcanoclastics were sub-sampled from the cores and sieved over nested sieve sets for grain size analysis. The grain size measured was -1.5ϕ to 4ϕ (2.8 - 0.063 mm) at half-Phi (0.5 ϕ) intervals.

Field mapping and stratigraphic logging was conducted on coastal exposures along the east and west coasts of the SSH volcanic complex (Figure 1). The generally poor on-land exposure and access difficulties due to the current volcanic exclusion zone limits meant the SSH field study was confined to these two coastal sections. Samples were collected for petrological and geochemical analysis.

2.2 Morphological and geophysical data

The seafloor south of Montserrat has been previously described from swath bathymetry and seismic profiles collected during several marine geophysical surveys (Deplus *et al.*, 2001; Le Friant *et al.*, 2004; Lebas *et al.*, 2011; Watt *et al.*, 2012). These surveys have defined the sequence and dimensions of multiple large landslide deposits interbedded with the marine sedimentary stratigraphy south and east of Montserrat. A near-surface blocky landslide deposit, named Deposit 3 by Le Friant *et al.* (2004), is prominent in the study area south of SSH (Figure 1).

Here, we use two-dimensional seismic profiles (generator-injector air-gun source; 60 channel streamer; 50-150 Hz source bandwidth; <5 m vertical resolution) and swath bathymetry (Kongsberg Simrad EM 120; processed at a 20 m bin size) collected on the JC45/46 research cruise on RRS James Cook in 2010, to provide high resolution imagery of landslide deposits south of Montserrat.

2.3 Geochemistry

Major elements were analysed in the subaerial samples by X-ray Fluorescence (XRF) analysis of glass beads prepared by fusion of a mixture of subsamples of 0.5 g and lithium tetraborate in a ratio of 1:10, and measured using Philips Magix Pro WD-XRF at the National

Oceanography Centre (NOC), Southampton, UK. Error and external accuracy was generally <2% (Table 1).

Samples for trace element and isotopic analysis were prepared in a clean laboratory suite at NOC. Submarine core samples were cleaned using 18M Ω ultrapure H₂O, sonicated for ten minutes and then dried overnight in an oven at 70°C. The submarine samples were then passed through Teflon sieves (500 μ m), and handpicked under a binocular microscope. Plagioclase phenocrysts, dark groundmass matrix fragments and pale porphyritic, vesicular fragments were separated to assess the potential geochemical variability within the deposit. The picked samples were then pulverized using an agate mortar. The Rare Earth Elements (REE), Rb, Sr, Y, Zr, Nb, Cs, Ba, Hf, Pb, Th and U concentrations of the picked submarine samples and subaerial volcanics were analysed by the ICP-MS at the NOC on a VG Plasmaquad PQ2+ instrument. Reproducibility is better than 4% (Relative standard deviation - RSD) for the REE, Rb and Nb, and better than 6% (RSD) for other elements. Precision when using elemental ratios is better than 1% (RSD).

Pb isotopic compositions were determined on 200 mg of hand-picked rock chips with a grain size of 0.5– 1 mm. The rock chips were leached in 4ml of 6 M HCl at 140 °C in sealed Teflon pots for 2 to 5 hours prior to dissolution in HF–HNO₃ for 24 hours on a hot plate at 130°C. The samples were evaporated until dry, before adding a further 0.5 ml of concentrated HCl and 0.5 ml of concentrated HNO₃ and evaporating until dry after each addition. Finally, 1.5 ml of hydrobromic (HBr) was added to the residue, the Teflon pot lid was replaced and the vessels were placed on a hotplate for 1 hour. The contents were then centrifuged for 5 minutes to produce a supernate suitable for column chemistry. Isolation of Pb from the matrix was performed using AG1-X8 200-400 mesh anion exchange resin. The procedural blanks measured with the samples contained <50 pg/g of Pb. Pb isotope analyses were conducted on a VG Sector 54 thermal ionization mass spectrometer at NOC and MC-ICPMS (Neptune) micromass/GV IsoProbe. Both mass spectrometers utilized the double spike technique to correct instrumental bias using a method outlined by Ishizuka *et al.* (2003). Pb standard NBS 981 gave results, 16.9404 \pm 32 (2SD- 2 Standard Deviations) for ^{206/204}Pb, 15.4982 \pm 30 for ^{207/204}Pb and 36.7225 \pm 85 for ^{208/204}Pb for TIMS and 16.9403 \pm 27 for ^{206/204}Pb, 15.4973 \pm 21 for ^{207/204}Pb and 36.7169 \pm 66 for ^{208/204}Pb for MC-ICP-MS.

3. Results

3.1 Subaerial stratigraphy of the SSH volcanic complex

Subaerial field observations and measurements were made on two sections along the coast (termed the east section and west section; Figure 1). A cliff sequence of volcanics occurs

on the east side of the SSH (Figure 2). This succession is laterally continuous for at least 1 km. The stratigraphy dips away from the sea, as does the surface at the top of this succession. A thick (10-15 m) dacitic lava flow (Lower Dacite) occurs at the base of the sequence, which is heavily fractured, exhibiting vertical columnar jointing. The Lower Dacite comprises 50% phenocrysts and 50% groundmass. The phenocrysts have a seriate size distribution and comprise 50% plagioclase feldspar, 25% orthopyroxene, 20% hornblende and 5% clinopyroxene. Abundant dark-coloured inclusions of mafic material (54% SiO₂) ranging from 1 to 30 cm in size are observed (Figures 3a & 3b). Within the dacite, most of these inclusions appear smooth-sided and well rounded; sometimes deformed in the direction of flow (Figure 3a). Bright green xenoliths were also found, comprising equigranular orthopyroxene-plagioclase and minor magnetite similar to those described in Kiddle *et al.* (2010).

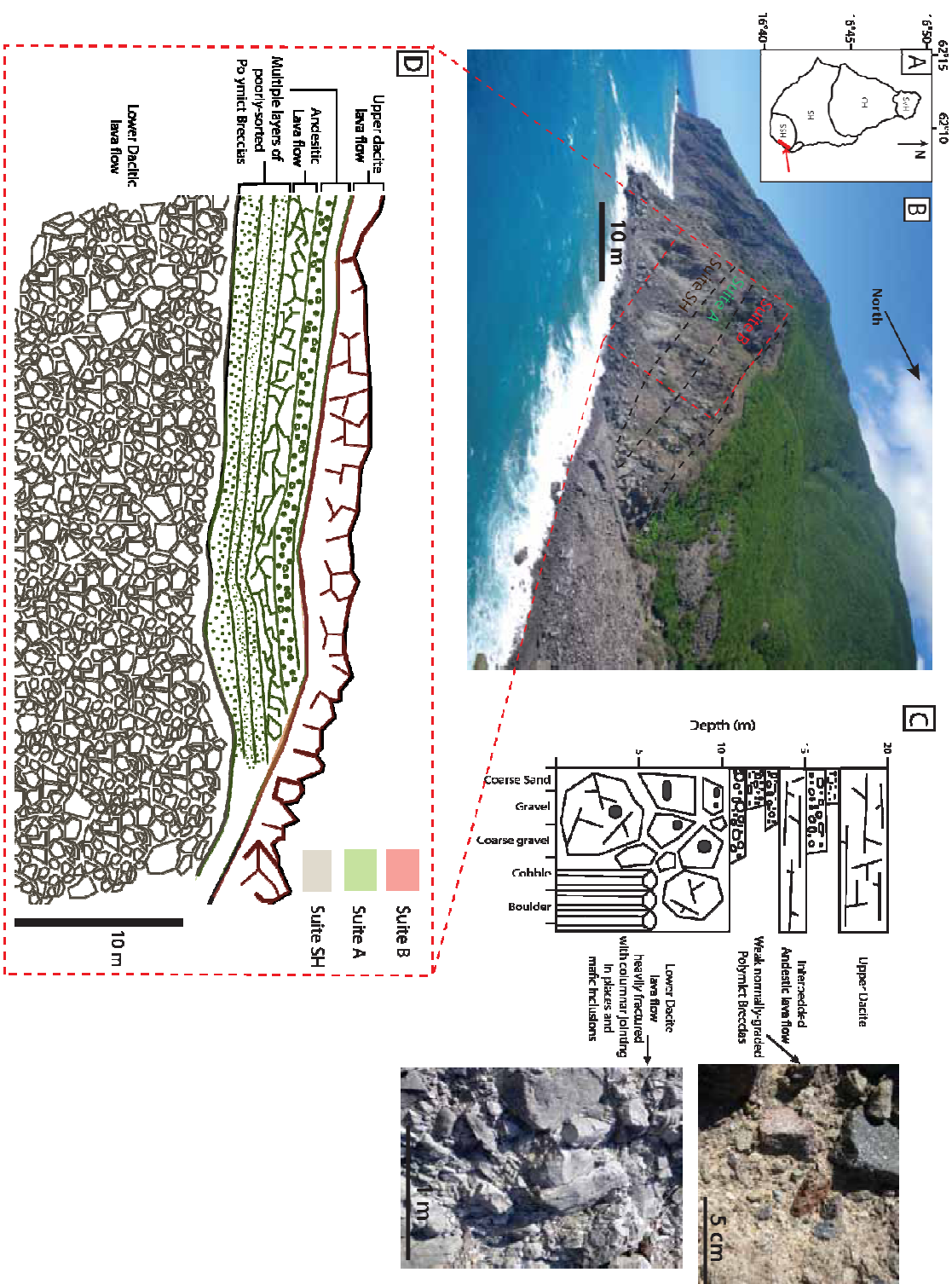


Figure 2. (a) Map insert of Montserrat with field location in red. The red arrow shows the angle that image b was taken from. (b) Cliff section comprising the east section, with beds dipping away from the sea as does the upper surface of the sequence, showing structures, grain size distributions and images of the rock units. (c) Graphic log through the sequence, showing SSH cliff section, displaying the full range of chemical suites.

Overlying the Lower Dacite are 5 beds of polymict breccia, each with a thickness of ~ 1 m. This amounts to 4-5 metres in total, although bed thickness is laterally variable across

the section. These polymict breccia deposits have clast sizes from 0.5 cm to 8 cm and comprise coarse-grained equigranular felsic rocks (30%), basaltic andesite pumice (25%), oxidised basaltic scoria clasts (25%), angular mafic clasts (15%), magma-mingled clasts of andesite and basalt (3%) (Figures 3c & 3d) and sulphur-rich hydrothermally altered clasts (2%). Interbedded with these deposits is a 2 m thick andesitic lava flow, which contains abundant zoned plagioclase (55%), orthopyroxene (30%), clinopyroxene (10%) and hornblende (5%). At the top of the sequence is another dacitic lava flow ~7 m thick (Upper Dacite). The Upper Dacite is darker in colour than the Lower Dacite and has a blocky appearance, with irregular cooling fractures. The Upper Dacite comprises 65% phenocrysts to 35% groundmass. The phenocrysts comprise 60% plagioclase, 25% clinopyroxene and 15% orthopyroxene.

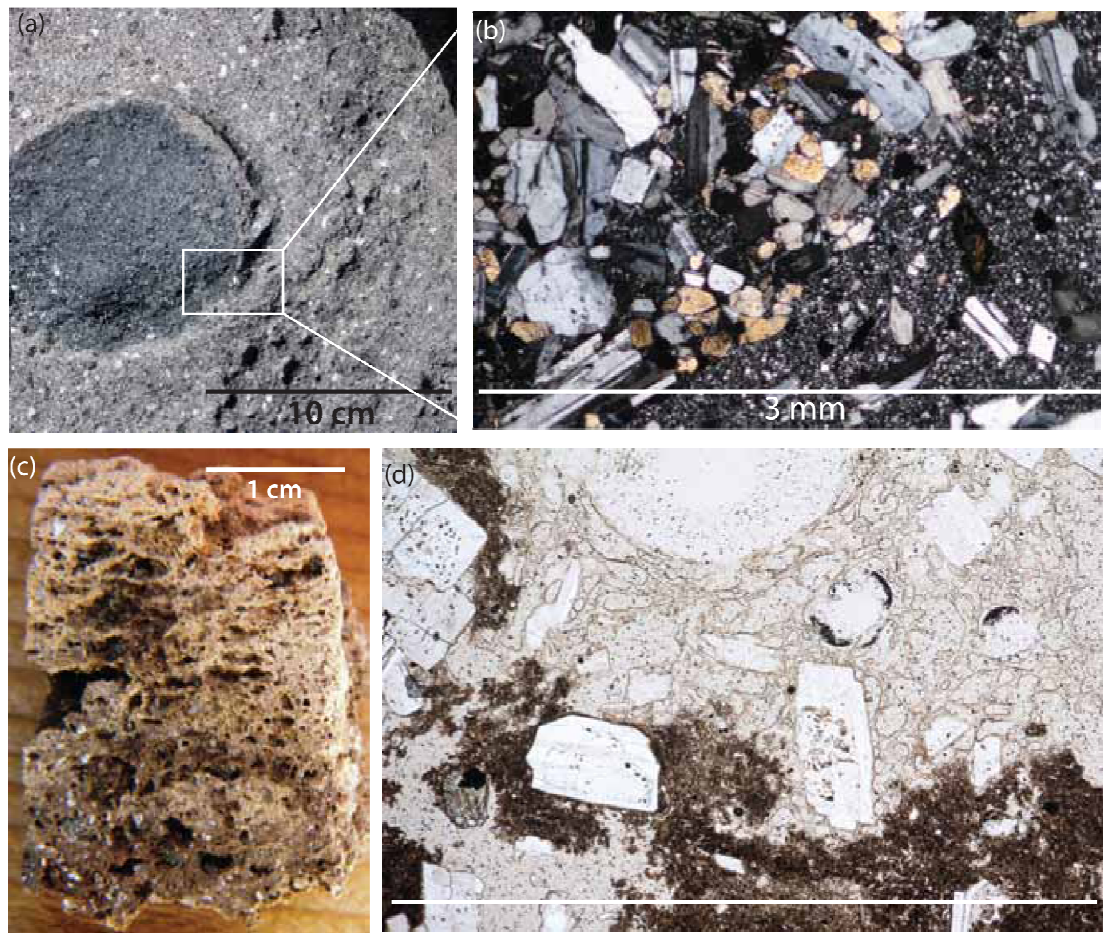


Figure 3. (a) Example of rounded mafic inclusions as seen the in the Lower Dacite. (b) Cross polar image of the coarser grained mafic inclusion next to the Lower Dacite. (c) An example of magma mingling exhibited in a specimen from the polymict breccia. (d) Thin section of magma mingling texture in plane polarised light.

In the west coastal section (Figure 4), at least 3 basaltic lava flows are present, with locally variable dip directions. The flows are typically 3-4 m thick, some containing large (1 cm diameter) phenocrysts of plagioclase. The basaltic flows comprise 55% phenocrysts of which 65% are plagioclase, 30% orthopyroxene and 5% clinopyroxene. Above the lava flows

are thinner beds (~2 m) of coarse grained (0.5 to 10 cm), poorly-sorted polymict breccias. To the east of this western section, a basaltic scoria-rich sequence consisting of multiple monomict layers (1-2 m thick) of ballistic scoria and lava blocks is preserved (Figure 4). The monomict layers are inversely graded, although the grading is crude, and the deposit is poorly sorted overall. Intact breadcrust bombs and large vesicular clasts (25-100 cm) were observed throughout the scoriaceous sequence. The basaltic scoria-rich deposits are found interbedded with 2 – 3 m thick lava flows of similar composition to the basalt lava flows described further west in this section (Figure 4).

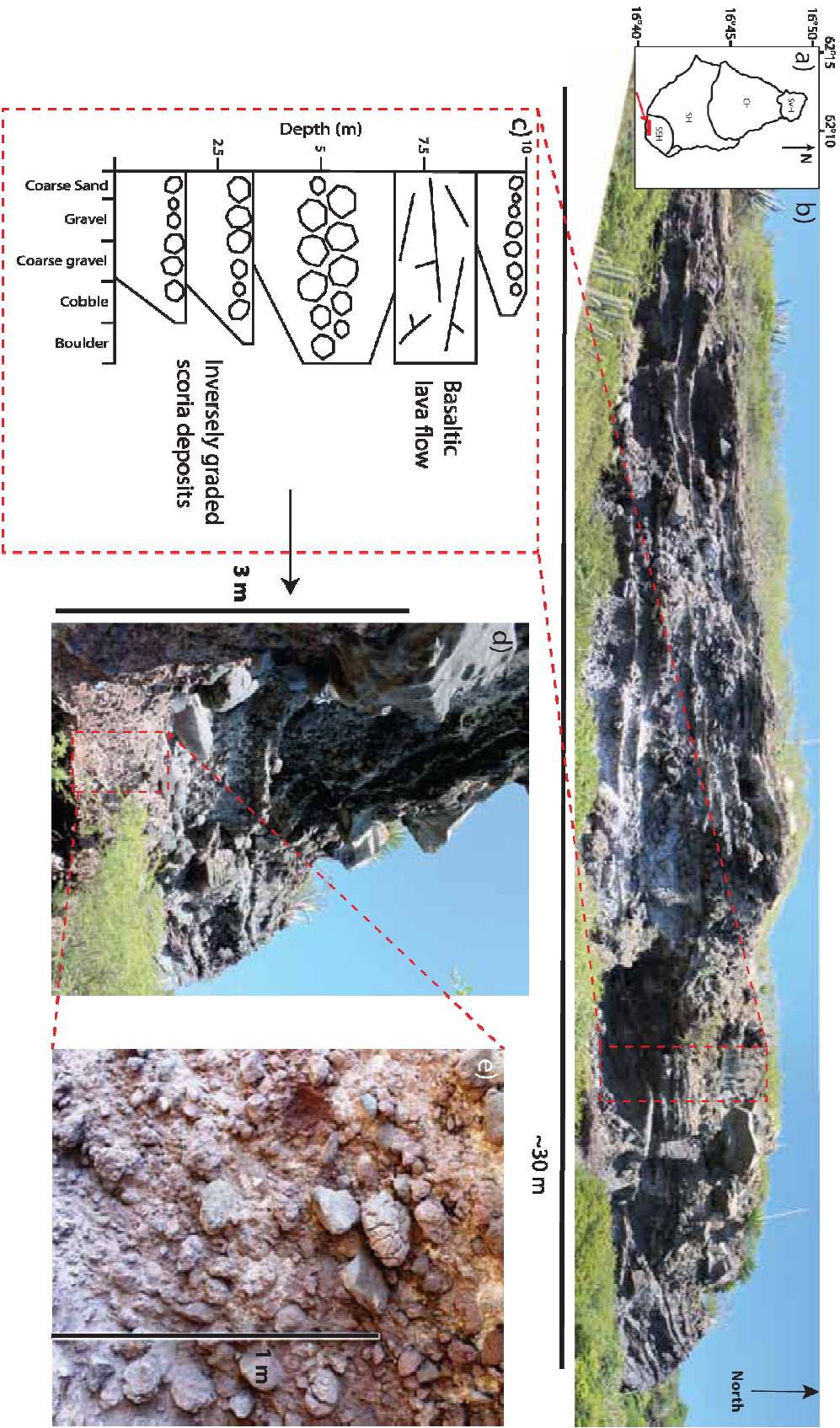


Figure 4. (a) Map insert showing the western field section of the SSH. (b) Panoramic view of a section through basaltic scoria deposits. (c) Graphic log through the section highlighting structures, clast and bedding size. (d) Image of the inversely graded monogenetic beds of proximal scoria and breadcrust bombs as depicted in the graphic log. (e) Close-up image of breadcrust bombs and the poorly-sorted scoria deposit.

3.2 Submarine morphology and geophysical data offshore from the SSH volcanic complex

There are two main submarine depressions offshore Montserrat (Figure 1), where water depths exceed 1000 m. These are the Bouillante-Montserrat graben to the south-east, and a series of submarine canyons and basins to the west, which extend SW to the Grenada Basin (Le Friant *et al.*, 2004; Feuillet *et al.*, 2010). South of Montserrat, the island flank is constructed on a shallower platform, at a depth of ~700 m, which gradually deepens southwards. There are several areas of hummocky morphology on the sea floor south of Montserrat, interpreted as debris avalanche deposits (Le Friant *et al.*, 2004): Deposit 1 in the east (Le Friant *et al.* 2004), Deposit 5 in the south east, thought to be derived from a submarine shelf embayment (C4 in Le Friant *et al.*, 2004), and Deposit 3 to the south of the SSH. Deposit 3 (as originally described by Le Friant *et al.* 2004) lies at the base of the southern flank of Montserrat and has a surface of scattered, angular blocks and an overall sub-circular morphology (Figures 1 & 5). These characteristics are typical of volcanic debris avalanche deposits observed widely in both subaerial and submarine settings (Siebert, 1984; Urgeles *et al.* 1997; Deplus *et al.*, 2001).

The area and volume of Deposit 3 were estimated by Lebas *et al.* (2011) as 59 km² and 1.2 km³ respectively. JC45/46 swath bathymetry shows that the largest blocks in Deposit 3 are 300 m across and stand up to 50 m above the surrounding seafloor. Bathymetric profiles and the outline of the blocky field are shown in Figure 5. The southern margin of Deposit 3 terminates on seafloor slopes of ~1°. Within the deposit, there is a rough scattering of the largest blocks towards the deposit edges, with blocks in the centre generally having smaller dimensions. An eastern lobe of the deposit, which encountered steepening slopes at the faulted margin of the Bouillante-Montserrat graben, extends into the graben and has formed a cluster of large blocks at the base of the slope (Figure 5). JC45/46 seismic profiles suggest that Deposit 3 is relatively thin (Figure 5) in comparison with a morphologically similar deposit to the east of Montserrat (Deposit 1, Watt *et al.*, 2012). The chaotic deposit matrix, between the large blocks, has a maximum thickness of ~25 m (for a seismic velocity of 2000 m/s).

The bulk of Deposit 3 lies below ~800 m water depth, and the deposit cannot be traced more proximally onto the steep island flanks. No sedimentary drape over Deposit 3 can be resolved from our seismic profiles, suggesting that post-depositional sediment accumulation is 5-10 m, or even less. This implies a stratigraphic depth for Deposit 3 that is potentially consistent with the SSH Lower Unit identified in the JR123 submarine sediment cores (discussed below in section 3.3.).

Approximately 50 m beneath Deposit 3, irregular and discontinuous reflections indicate a much larger landslide deposit (Deposit 4; Le Friant *et al.*, 2004; Lebas *et al.*, 2011; Watt *et al.*, 2012), which shows evidence of large blocks within its central part. The chaotic seismic facies of Deposit 4 contrasts with the well-bedded seafloor sediments observed further to the west and below the deposit (Figure 5).

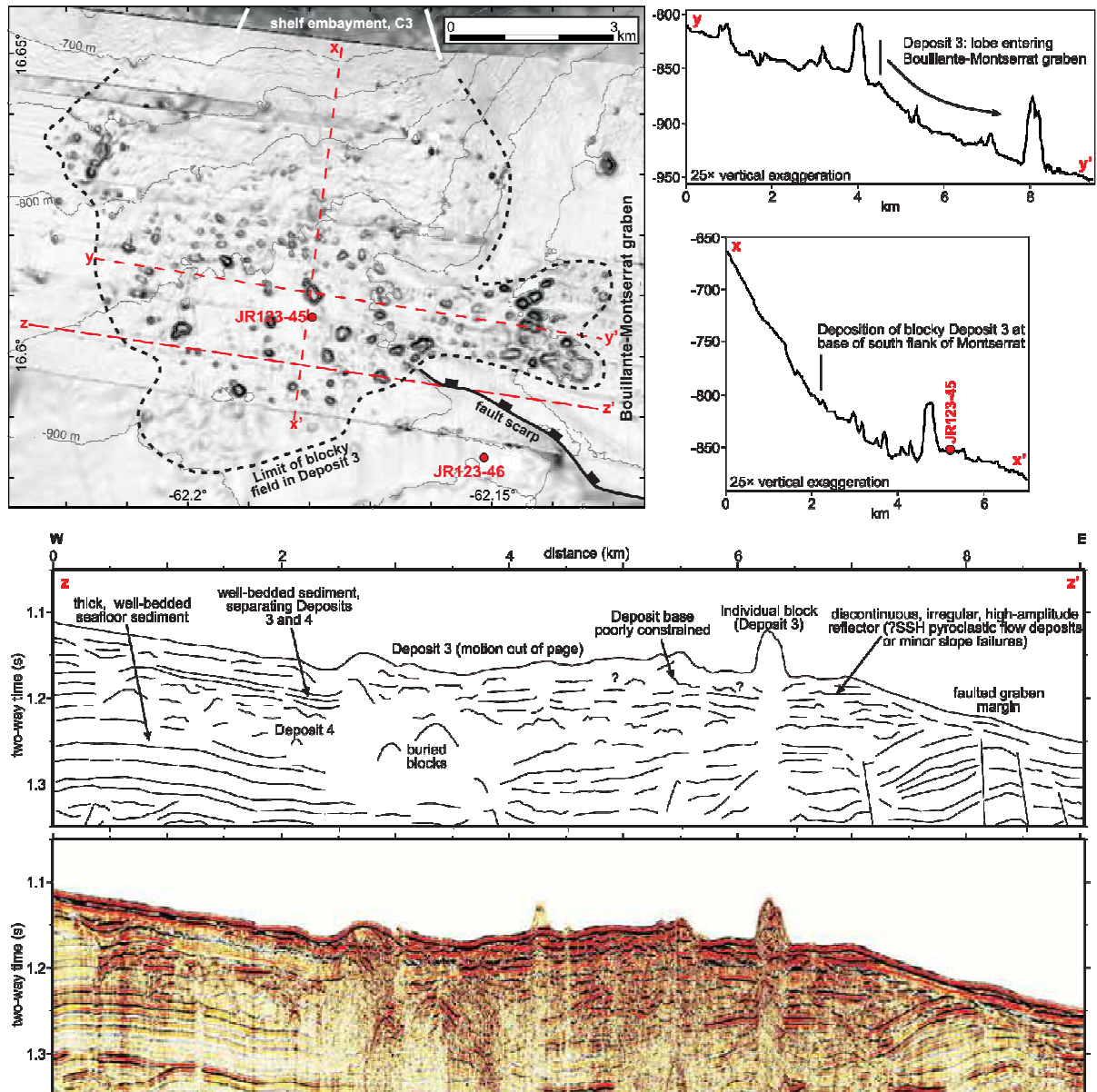
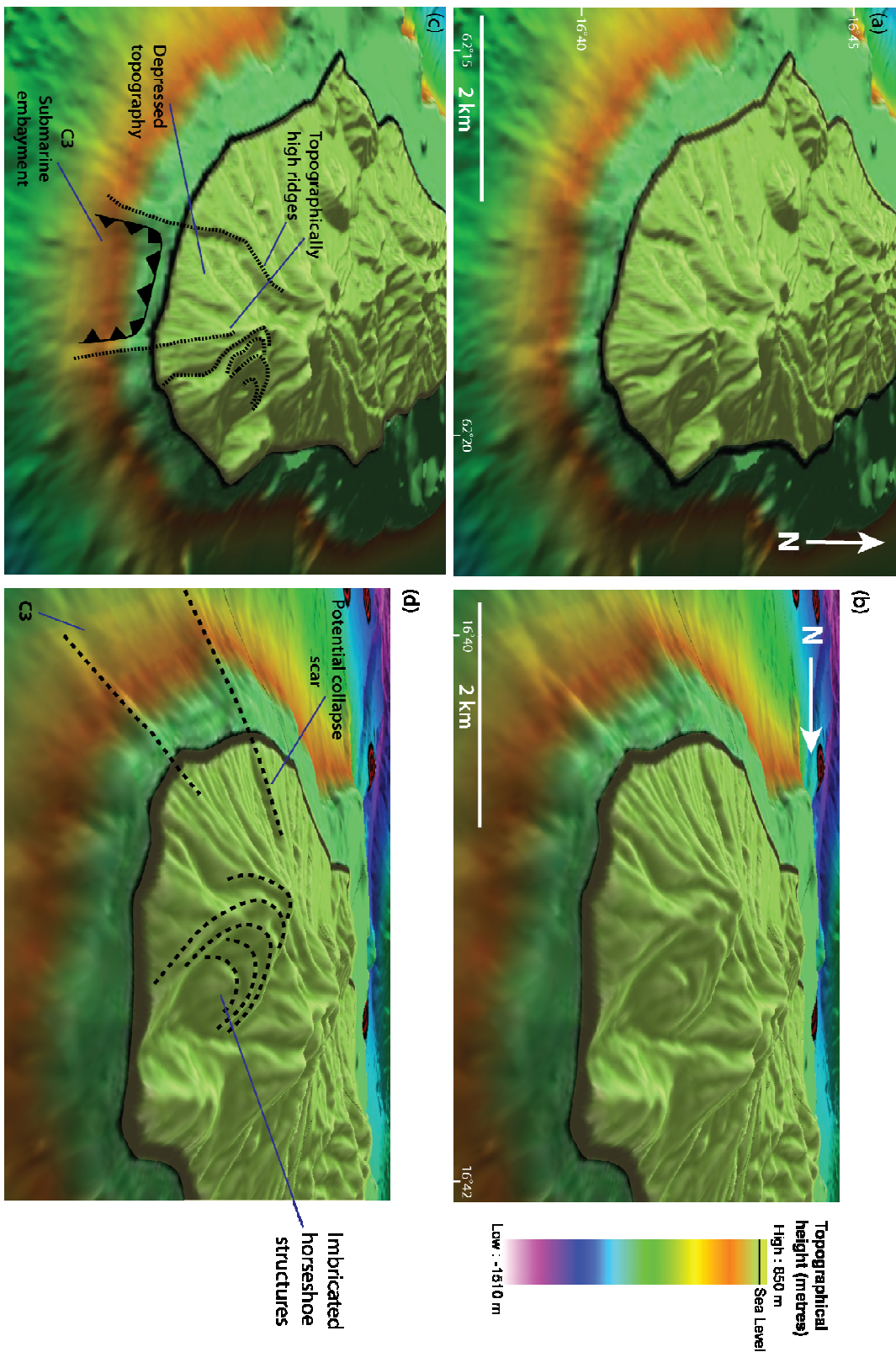


Figure 5. Top left: gradient shaded swath bathymetry south of Montserrat (see Figure 1 for location). Core locations (JR123-45 and 46) are shown as red dots. Contours drawn at 50 m intervals, with interpreted features labelled. Top right: seafloor topographic profiles across Deposit 3. Bottom: Interpreted JC45/46 seismic profile showing the upper part of the sedimentary stratigraphy south of Montserrat. Line locations shown on the bathymetry map.

Deposit 3 has been linked with an embayment on the submerged southern flank of Montserrat (C3; Le Friant *et al.*, 2004). This embayment can be traced onshore to some extent (Figure 6), where it forms a deeply incised valley with topographically prominent bounding

levees. Other large-scale topographic features, interpreted from the subaerial morphology (Figure 6) and thought to be associated with the SSH volcanic system, are imbricated horseshoe-shaped depressions open to the east (Harford *et al.*, 2002).

Figure 6. (a) & (b) Topographically coloured 3D images of the SSH edifice, combining swath bathymetry and the DEM of Montserrat. (c) & (d) Interpretive images highlighting C3, a submarine embayment identified by Le Friant *et al.* (2004). Dotted lines identify morphological features around the SSH.



3.3 Submarine stratigraphy and deposit characteristics

The marine sediment cores sampled to the south and east of Montserrat comprise intercalated volcanic, bioclastic and hemipelagic deposits. The SSH volcanoclastic deposits are found in the deeper sections of the cores, and are identified by their predominant basaltic with subordinate andesite lithology and geochemical characteristics. The geochemistry of the clasts within the deposit are almost identical to those exposed on the SSH (discussed in section 3.4); no Soufrière Hills like compositions were found in the analysed marine sediments.

The SSH marine core deposits can be separated into three distinct units, based on their sedimentological characteristics: SSH Lower Unit, SSH Hemipelagic-rich Unit and SSH Upper Unit (Figure 7b). The consistent 13 cm of hemipelagic material (SSH Hemipelagic-rich Unit), with pod-like sand sized material from the SSH Lower Unit sits between the two basaltic-rich units, helps identify the SSH Upper and Lower Units. Additionally, the differing sedimentological characteristics in the two basaltic-rich units, (for example the presence of a reversely graded base in the SSH Upper Unit and multiple stacked graded beds) help correlate these units from core to core. The detailed lithofacies for each of the units are described below.

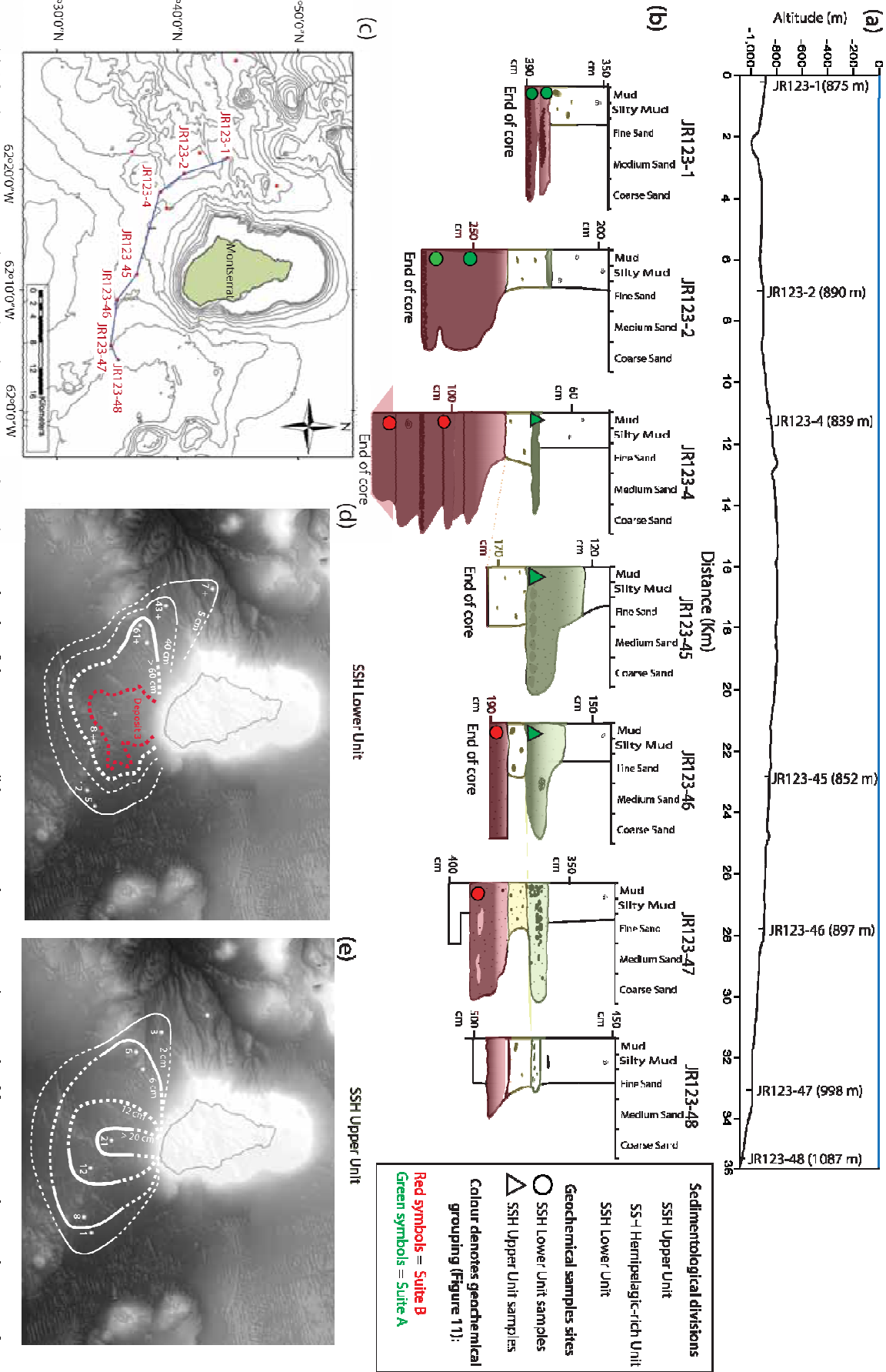


Figure 7. (a) A bathymetric section showing the relative topography and water depths of the core sites. (b) A stratigraphic transect showing the SSH marine sediment deposits. The geochemical suites have been assigned by Pb isotopes, discussed in section 3.4. Note that the SSH Lower Unit comprises clasts from Suites B and A, whilst the SSH Upper Unit only contains clasts from Suite A. (c) Location map showing the marine sediment cores and a transect through the marine stratigraphy shown in 7b. (d) & (e) Isopach maps of SSH Lower Unit and SSH Upper Unit respectively. The red dotted line defines the limit of the debris avalanche deposit (Deposit 3). The numbers next to the core locations denote the thickness of the deposit in cm, dotted lines are used where core coverage is lacking.

3.3.1 SSH Lower Unit

Correlating the SSH Lower Unit between the cores (Figure 7b) shows that the SSH Lower Unit is thickest in the south western cores, (e.g. >61 cm in JR123- 4). In JR123- 4 and JR123-2, multiple normally graded beds are stacked on top of each other (Figure 8). Sorting within the beds is moderate to poor and the deposits contain little material in the silt-clay size fraction (<20%), with the mean grain size ranging from very coarse sand to coarse sand - 0.17ϕ (1.22 mm) to 0.92ϕ (0.55 mm). The bottom subunit is finer (mean, 0.48ϕ , 0.7 mm) than the bed above (mean, -0.17ϕ , 1.1 mm). Most samples from the SSH Lower Unit in the south west are skewed towards the coarse grained material and the distribution is predominantly unimodal. In the south eastern cores (JR123-46, JR123-47 & JR123-48), the SSH Lower Unit is thinner, has an erosional base and consists of a single graded unit which contains medium gravel-sized grains (-3 to -4ϕ , 8-16 mm). In core JR123-46, the SSH Lower Unit is poorly to very poorly sorted and it is crudely graded with a very coarse sand graded base (mean: 0.03ϕ , 0.97 mm) and coarse sand top (mean of 0.48ϕ , 0.7 mm). The deposit is skewed towards the coarse component, but has more (~30%) of a fine grained component than in core JR123-2 (Figure 8).

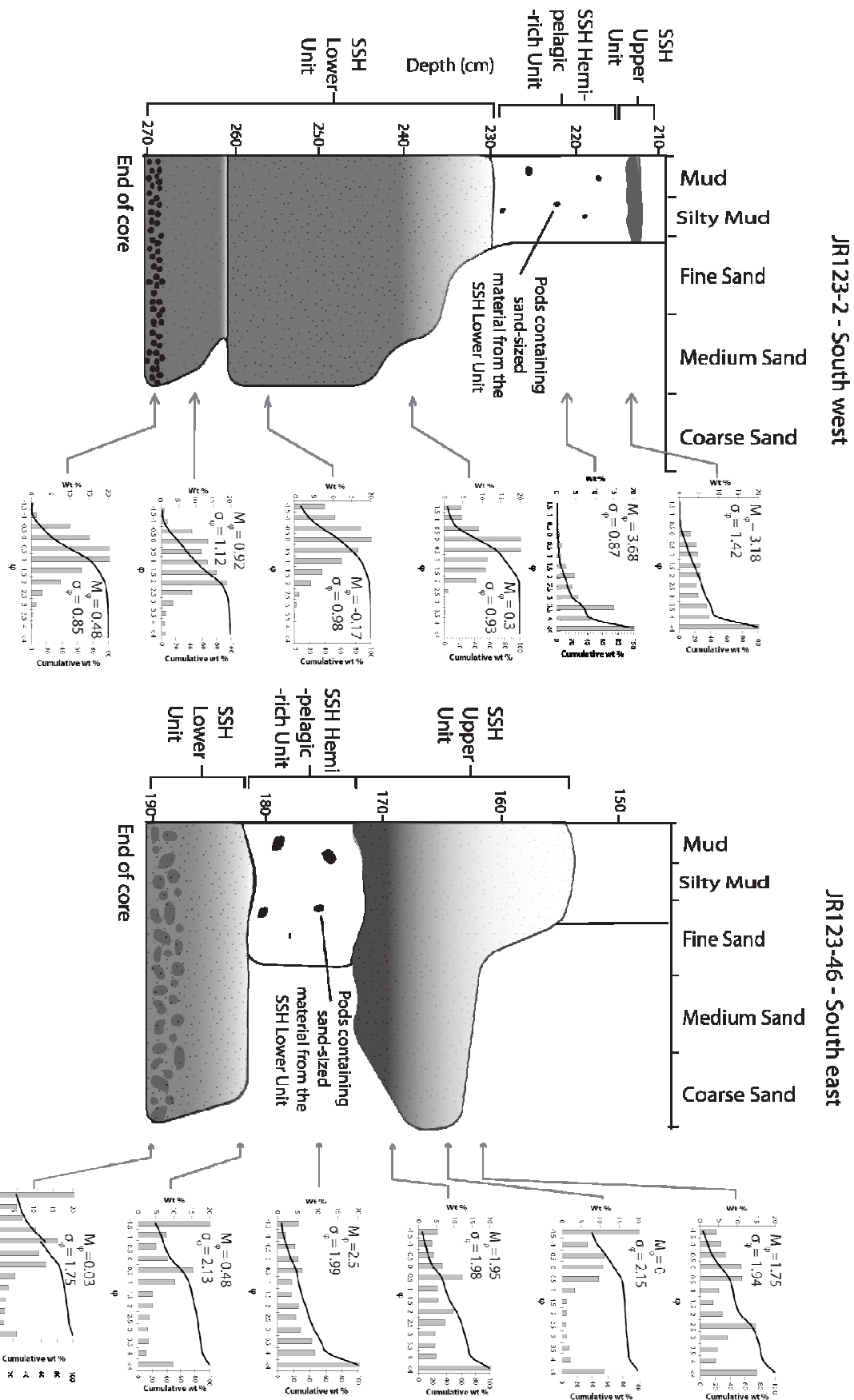


Figure 8. Grain size statistics from two cores, one located south west of Montserrat, JR123-2 and one to the south east, JR123-46. The arrows shown on logs denote where samples were taken for grain size analysis. The histograms also show cumulative frequency, using the Folk and Ward (1957) method. M ϕ denotes Mean and sigma (σ) denotes the amount of variance or sorting. All values are given in the ϕ scale.

The volcanic components of the SSH Lower Unit have sub-rounded clasts and comprise a variety of volcanogenic components including basaltic clasts (40%), feldspar

crystals (25%), pyroxene crystals (10%), and pale-coloured andesitic pumice clasts (25%) (Figure 9). The basaltic clasts and andesitic pumice differ in appearance and exhibit two different vesiculation histories (Figure 9). The andesite clasts are highly vesiculated with thin vesicle walls, whereas the basalt clasts have small, irregularly shaped vesicles (Figure 9). The basaltic samples contain 30-40% phenocrysts ($>350\text{ }\mu\text{m}$ in size) and 50-60% microlites (2 - 15 μm), with the rest consisting of groundmass glass (Figure 9d). The dominant phenocryst phases are plagioclase (55%), clinopyroxene (15%), orthopyroxene (15%), olivine (10%), and minor opaque minerals (5%). The andesitic clasts contain a very fine groundmass glass (60%), 30-40% phenocrysts and few microlites ($\sim 2\%$). The major phenocrysts in the andesite are plagioclase (65%), clinopyroxene (15%), orthopyroxene (15%), and magnetite (5%). The feldspars and pyroxenes commonly display oscillatory zoning, clino/orthopyroxene overgrowths and micrographic textures.

Several clasts within the submarine deposits in the marine cores show andesite and basalt mingled together (Figure 9e). In Figure 9e both the basalt and the pale coloured, highly-vesiculated andesite are petrologically similar to the descriptions above and appear to have been mingled with each other.

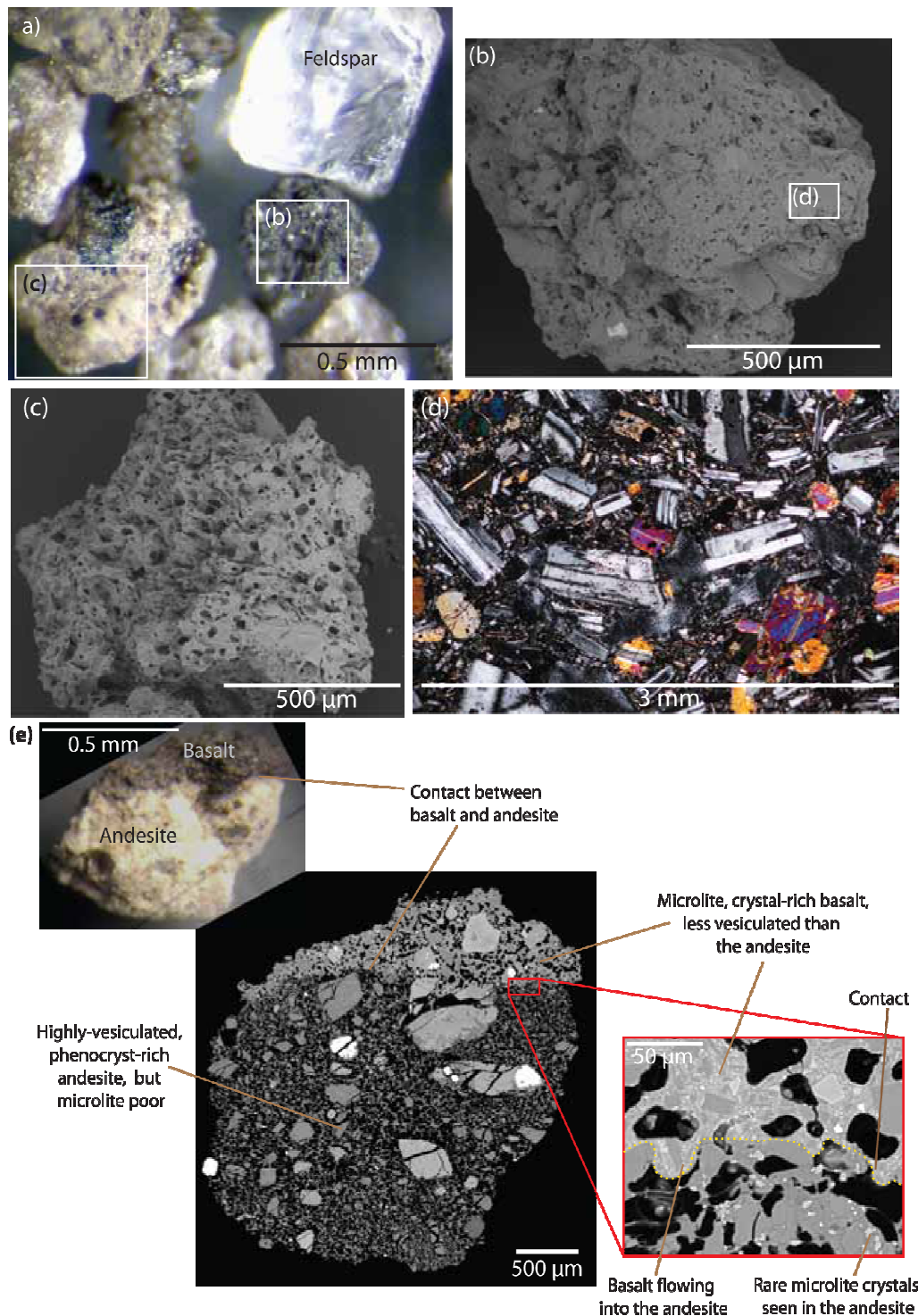


Figure 9. (a) Photomicrograph showing the range of clasts found in the submarine deposits from SSH. (b) SEM image of a poorly vesiculated basalt clast, designated as b in Figure 8a. (c) SEM image of highly vesiculated andesite clast, designated as c in Figure 8a. (d) Cross-polarised thin section (X5 magnification) of basaltic clast, showing phenocrysts of plagioclase, clinopyroxene and orthopyroxene, designated as d in Figure 8b. (e) Photograph of a clast found in the submarine deposits. First image shows a photomicrograph of a basaltic scoria clast bound with the pale andesitic pumice. Backscattered SEM images show the relationship of this contact at greater magnification; note the variation in vesicularity and crystallinity between the two phases.

3.3.2 SSH Hemipelagic-rich Unit

The SSH Hemipelagic-rich Unit is located between the two basalt-rich units (SSH Lower Unit and SSH Upper Unit). It contains a large proportion of hemipelagic material (~80-90%), with some volcanic-rich 'pods' ~1 cm in scale containing sand-sized grains from the SSH Lower Unit (Figure 8). This almost structureless deposit has a thickness of 13 cm, which is relatively consistent from core to core. The grain size ranges from -1.5ϕ to $<4 \phi$ (granule to coarse silt size, 2.75- 0.063 mm), it is therefore generally very poorly sorted. The mean grain-sizes are fine sand (2.1ϕ and 2.5ϕ , 0.22 - 0.177 mm) for core JR123-46 and polymodal peaks are visible on the grain size histograms (Figure 8). The SSH Hemipelagic-rich Unit in core JR123-2 is moderately sorted, with a large range in grain-size, 0ϕ to $<4 \phi$ (very coarse sand to coarse silt, 1 – 0.063 mm), it is heavily skewed to the fine grained material; the mean grain size in core JR123-2 is 3.68ϕ (very fine sand, 0.080 mm) (Figure 8).

3.3.3 SSH Upper Unit

The SSH Upper Unit is thickest and coarsest in the south and south eastern cores (Figure 7c). The SSH Upper Unit in core JR123-46 is a poorly-to very-poorly sorted deposit and is inversely graded at the bottom, with a scoured erosional base and has a normally graded top. Within this unit there is a medium sand base (mean: 1.98ϕ , 0.26 mm), a heavily skewed very coarse sand middle (mean of 0ϕ , 1 mm) and a finer medium sand grain size top, with a mean of 1.75ϕ (0.30 mm). This unit is fines-rich (>60%) and shows a polymodal grain size distribution, from -1.5ϕ to $<4 \phi$ (2.75- 0.063 mm) (Figure 8), the SSH Upper Unit in core JR123-2 preserves a 1 cm thick bed. The deposit thins and pinches out in the western cores (Figure 7c). In JR123-2 the SSH Upper Unit is poorly sorted, comprising a large range in grain size, from -0.5ϕ to $<4 \phi$ (very coarse sand to coarse silt), the median lies in the $<4 \phi$ (coarse silt) range and the mean grain size is very fine, 3.18ϕ (0.11 mm). The components seen in the SSH Upper Unit are the same as observed for the SSH Lower Unit facies description.

The thickness distribution of the SSH Lower Unit and SSH Upper Unit is depicted in isopach maps (Figures 7d & 7e), which have been determined based on the thicknesses of the deposits within a cored transect around the southern end of Montserrat (Figure 7c). The SSH Lower Unit is generally thicker than the SSH Upper Unit in the isopach maps and has been emplaced toward the south and south west. The SSH Upper Unit is thickest in the south and thins towards the south west. In cores JR123-1, 2, 4, 45 and 46, the basal contact of the SSH Lower Unit is not intersected, therefore the maps show a minimum deposit thickness.

3.4 Chemostratigraphy

The Montserrat volcanics are sub-alkaline and occupy a range of compositions from basalt to dacite (Figure 10). Most of the SSH volcanics are composed of basalt (49% SiO₂) and basaltic andesite, but they also contain more differentiated rocks such as andesite and dacite (62% SiO₂) (Figure 10 & Supplementary Table 2). Rocks from the other volcanic centres on Montserrat exhibit a range of silica values from basaltic andesite to dacite, but with a much larger concentration of these being andesites.

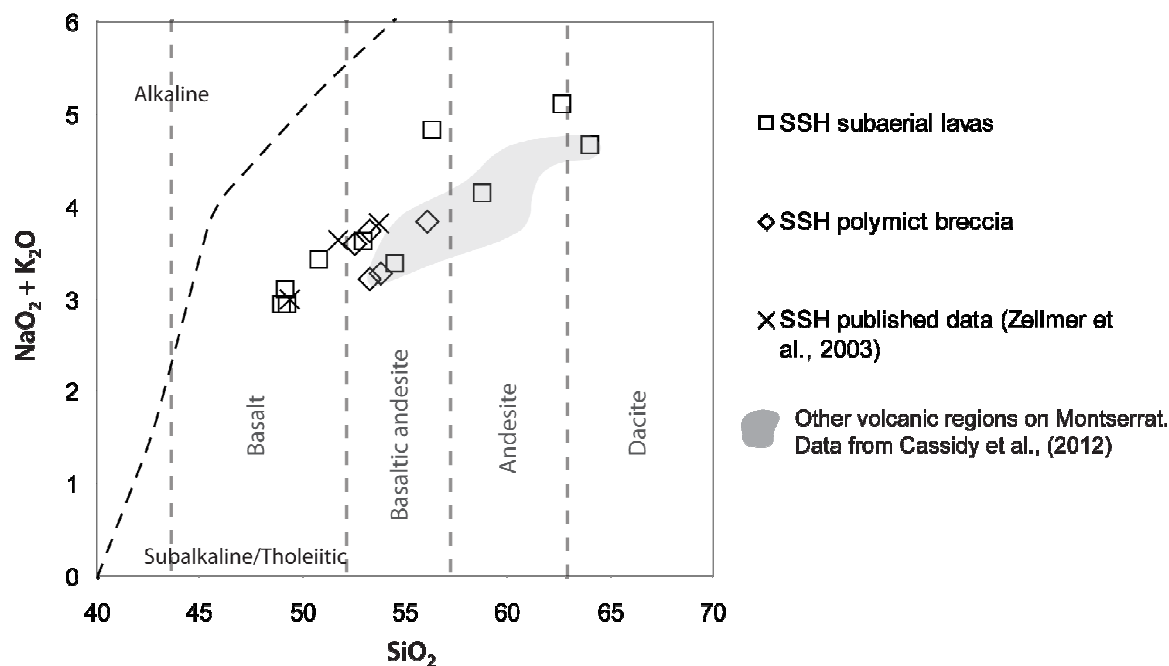


Figure 10. Subaerial samples from the SSH, along with volcanics from the other volcanic regions on Montserrat plotted on a silica versus total alkali diagram (after Le Bas *et al.*, 1986). The SSH samples occupy a range from basalt to dacite.

The volcanic centres on Montserrat can be discriminated from one another using trace elements and high-precision, Pb isotope ratios (Cassidy *et al.*, in review). The SSH volcanics have trace element and isotopic compositions that clearly distinguish it from the other volcanic centres in the rest of the island. Some examples of this type of discrimination are shown in Figure 11. As well as discrimination of the SSH from Soufrière Hills, SSH can be subdivided on the basis of stratigraphy (Suites A and B, Figure 2). This division carries through to a geochemical distinction in Pb isotopes (Figure 11).

Suite SH has a Pb isotopic composition that suggests it is derived from the Soufrière Hills volcano (Cassidy *et al.*, 2012) rather than the SSH eruptive centre. In the Pb isotopic discriminant diagrams (Figures 11c & 11d), Suite SH has more radiogenic Pb isotopic ratios than the SSH. In the trace element variation diagrams (Figures 11a & 11b) Suite SH overlaps significantly with Suite A, but Suite B can be discriminated from the rest of the centres. In Figure 11a, the Soufrière Hills samples are shifted to lower Sr/La ratios and higher Zr/Er ratios than Suite B. Suite SH occupies the region with low Sm/Zr ratios and higher Ce/Sr ratios relative to Suite B (Figure 11b). Suite A plots in the middle between Suite B and Suite

SH for both trace elements and isotopic composition (Figure 11). Although Suite A overlaps with Suite SH in the trace element plots (Figure 11a & 11b), Suite A can be easily discriminated in Pb isotope plots (11c & 11d).

Suite B has the least radiogenic Pb isotopic ratios relative to Suites A and Soufrière Hills (Figure 11). Suite B has the highest Sr/La values (100-180) and lowest Zr/Er values (17-22) relative to Suites A and SH (Figure 11a). Suite B is shifted to high Sm/Zr (0.048 to 0.065) and low Ce/Sr (0.02 to 0.034) (Figure 11b).

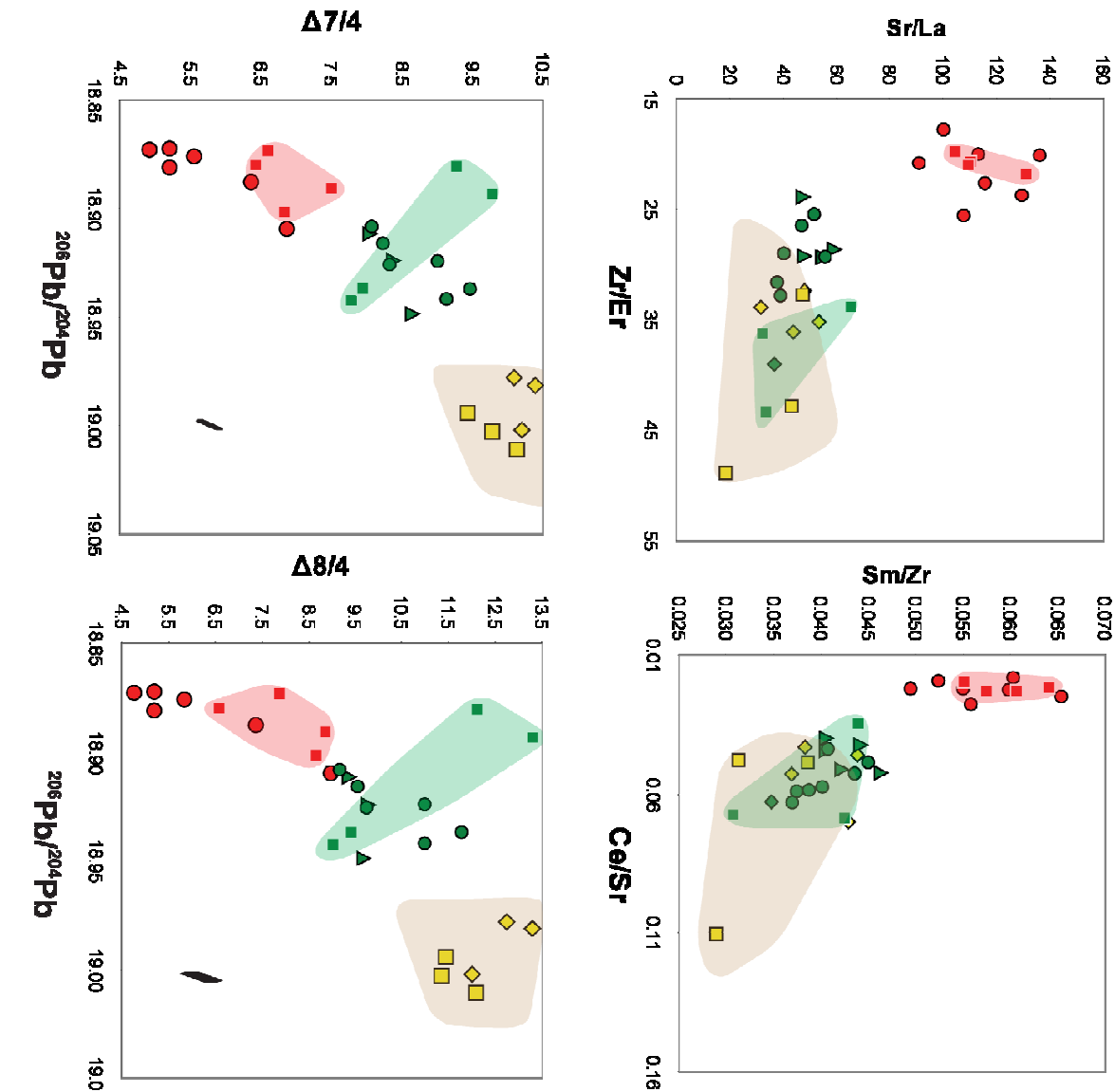


Figure 11. Geochemical variation diagrams, used to discriminate the SSH samples into three geochemical suites (A, B & SH) (a) & (b) use trace and rare earth elemental concentrations and ratios and (c) & (d) use Pb isotopic ratios. Symbol shapes relate to stratigraphic position and colour denotes their geochemical suite. The geochemical suites have been defined by Pb isotope differences of the subaerial samples (Cassidy et al., 2012). Note that the SSH Lower Unit comprises both Suite A and Suite B material, whilst the SSH Upper Unit contains only Suite A material. No Suite SH material was found in the submarine deposits.

A range of rocks from the east cliff succession in the SSH volcanic complex (Figure 2), displays all of the above geochemical suites. Suite SH is found at the base of the sequence

(Lower Dacite). The polymict breccias units that lie above the Lower Dacite contain clasts from both a Suite A and Suite SH source. The interbedded andesitic lava flow has a Suite A composition and Suite B is found at the top of succession (Upper Dacite). Other subaerial samples found on the west field section help define the chemical ranges described above (Supplementary Tables 1, 2 & 3).

The submarine deposits fall within similar ranges defined by the subaerial rocks (Figure 11), hence we have assigned the submarine SSH samples to Suites A, B and Soufrière Hills based on the parameters identified in Figure 11. The multiple stacked beds or subunits of the submarine SSH Lower Unit represent separate sedimentological events and record a progression from Suite B at the bottom to Suite A and Suite B, which are found within the upper subunits of the SSH Lower Unit (Figure 7b). This chemostratigraphy is a simplified succession based on the combination of SSH Lower Unit deposits from a number of cores. The SSH Upper Unit contains clasts solely of Suite A composition, but no samples belonging to the SH region were identified in the submarine deposits.

Discussion

4.1 Emplacement of the subaerial SSH deposits

The subaerial SSH deposits comprise a range of volcanic units from basaltic to dacitic lava flows, scoria and pumice deposits and volcanoclastic breccias. Within the Lower Dacite, which originated from the Soufrière Hills volcano (Suite SH), the abundance and characteristics of the xenoliths suggests that there has been assimilation of equigranular mafic cumulates as the magma ascended (Zellmer *et al.*, 2003; Kiddle *et al.*, 2010). In addition the flow may have incorporated loose talus as it flowed over the volcanic terrain, as indicated by the rounding of some of the more mafic xenoliths found within it (Blake and Fink, 2000). Lavas from the Soufrière Hills are exposed at the bottom of the succession found in the SSH, hence the SSH edifice was built on top of older Soufrière Hills deposits.

The east succession (Figure 2), which dips away from the sea, may have been rotated. This succession is unlikely to be emplaced on pre-existing tilted topography as the deposits within this sequence, such as thick mass wasting breccias, are sourced from the SSH and Soufrière Hills volcanic centres. Additionally, the succession sits at the base of the horseshoe slumping structures observed by Harford *et al.* (2002) (Figure 6), so it is conceivable that the rotated sequence could be related to this slumping episode.

A sample found in the SSH (MVO136) and dated at 130 ka using Ar-Ar geochronology (Harford *et al.*, 2002), falls within the Soufrière Hills suite (Suite SH) in terms of its Pb isotopic composition (Figures 12c & 12d). However, other subaerial samples taken from the

SSH that are also dated at 128-131 ka (MVO830, MVO1099 and MVO791) (Harford *et al.*, 2002), have a Pb isotopic composition defined by the SSH centre (Suites A & B). This is an important observation as it implies that the Soufrière Hills and SSH volcanoes were both active at closely overlapping intervals.

The widespread presence of epiclastic, coarse-grained and poorly-sorted breccias found in both the east and west sections of the SSH suggests that there were a series of short-lived, high-energy episodes of mass wasting of volcanoclastic material (c.f. Koster and Steel, 1984). The widespread and voluminous nature of these epiclastic deposits suggests that they might be caused by multiple episodes of gravitational collapse. The reworked deposits comprise a range of clast compositions (and vesicularities), ranging from basalt lava flows to andesitic pumice. The clasts that make up the breccias were sourced from both the Soufrière Hills and younger (Suite A) SSH deposits. Between the episodes of mass wasting events, volcanic activity on the SSH persisted, as indicated by the presence of lava flows which are both interbedded with and overlying the breccias.

The west section comprises more mafic volcanic deposits, such as porphyritic lava flows and mafic scoria fall deposits than are found in the east. One basaltic scoria-rich sequence (Figure 4) consists of multiple layers of monomict ballistic scoria, lava blocks and breadcrust bombs, with lava flows interbedded within the deposits. This sequence suggests a proximal source, based on the angular, intact clasts of monomictic composition. The monomict layers of inversely graded beds are thought to represent small mass-flow deposits formed syn-eruptively as the scoriaceous clasts landed on steep topography, possibly a small scoria cone, and flowed a short distance down slope. This would have occurred when the volcano was still active, as inferred by the presence of interbedded lava flows.

Volcanism on the SSH was dominantly effusive, as indicated by the many basaltic and more evolved lava flows. The presence of andesitic pumice within the breccias suggests that viscous gas-rich magmas may have caused explosive volcanism (Mangan *et al.*, 1993; Cashman and Mangan, 1994). The evidence for magma mingling found in both the subaerial and submarine settling indicates that basaltic and andesitic magma interacted with each other at depth. This mechanism is widely reported in the Soufrière Hills volcano as a possible triggering mechanism for explosive andesitic eruptions (Murphy *et al.*, 1998; 2000; Devine *et al.*, 1998). It is likely that the action of super heating the andesite and/or increasing the volatile content, by addition of basaltic melt would have increased the fluid pressure of the country rock and may have triggered explosive eruptions from the SSH (c.f., Sparks *et al.*, 1977, Huppert *et al.*, 1982).

4.2 Emplacement of the submarine SSH deposits

Sedimentological analysis of the SSH Upper Unit and SSH Lower Unit allows for reconstruction of events that occurred during emplacement of the submarine SSH deposits. The deposits are normally graded, and some have inversely graded bottoms with scoured bases. These are composed of coarse grains (>5 cm in some cases) with some planar bedding but no cross bedding structures, suggesting that they are deposits from high-concentration erosive turbidity currents (Lowe *et al.*, 1982, Mutti *et al.*, 1992, Mulder and Alexander 2001). It is well established that high-concentration turbidites inhibit particle freedom and allow some finer-grained material to be retained within the deposit, accounting for the poorly-sorted deposits in this study. The remaining fine fraction, i.e. muds and silt, often forms a capping layer within classic turbidite sequences (Division E in Bouma, 1962). However, in the SSH volcanoclastic turbidites there is an abrupt grain-size discontinuity above the turbidites, separating it from the overlying fine-grained hemipelagic sedimentation. Hence, the fine fraction most likely bypassed the study area and was deposited more distally (Amy *et al.* 2005).

The coarse grain size, heterogeneous volcanic clasts, variable bed thickness and deposit distribution can be explained by flank collapses of the SSH edifice. Further support for this hypothesis comes from the fact that the deposits are too widespread and voluminous to have been produced by river floods, or reworking of shelf sediments by ocean currents (Masson *et al.*, 2006). The presence of multiple-stacked, normally graded beds suggests that there were a number of flank collapses, or pulses in the depositing flow. Flow reflection can be ruled out, based on the fact that the upper subunit in JR123-2 is coarser than the bed below it (Figure 8) (c.f. Garcia, 1996; Wynn and Masson, 2003). The SSH Lower Unit comprises multiple sub-units that are tens of centimetres in thickness, separated by erosive bases and grain-size breaks. These sub-units are not separated by hemipelagic sediment, suggesting that they were emplaced within a short period of time or that significant basal erosion removed all trace of any intervening background sediment accumulations.

The SSH Hemipelagic-rich Unit has a consistent thickness throughout the cores (~13 cm). The deposit is dominated by fine-grained hemipelagic material, is poorly sorted in places and has reworked 'pods' containing sand-sized volcanoclastic clasts that originated from the SSH. The SSH Hemipelagic-rich Unit is inferred as a time gap, wherein background sedimentation occurred and intermittent SSH clasts were emplaced as the previous SSH turbidite material was reworked and bioturbated. Sedimentation rates of hemipelagic accumulations vary in proximity to Montserrat; a sedimentation rate of 1-3 cm ka⁻¹, as calculated by Le Friant *et al.* (2008) from the CAR-MON 2 core, located 55 km from

Montserrat is likely too low for the proximal cores used in this study. However, Trofimovs *et al.* (2010) calculated a sedimentation rate of 6.9 cm ka⁻¹ from proximal cores south east of Montserrat for the time period 90 - 130 ka. Using this estimate, the 13 cm of hemipelagic sediment would amount to a time period of ~2 kyr. The SSH may have been active over a relatively short timescale (cf. Harford *et al.* 2002), but may have continued to erode and transport material offshore for several thousands of years after volcanic activity ceased.

The SSH Upper Unit comprises a normally graded turbidite with a reversely graded base. This could either have resulted from kinetic sieving along the bottom of the turbidity current, allowing the small, dense volcanic clasts to fall through openings between the larger particles and therefore accumulate at the base of the deposit (Gray & Hutter, 1997; Schwarzkopf *et al.*, 2005). Alternatively it could represent a variable energy in the source as the turbidity current waxed and waned, allowing different size fractions to deposit at different times. The latter is more likely as turbidites are thought to progressively aggrade, and therefore record temporal changes in flow structure (Mulder and Alexander, 2001; Kneller and McCaffery, 2003).

From the cored turbidite thickness, the SSH Lower Unit appears to have been more voluminous and spread over a larger area than the SSH Upper Unit. The SSH Upper Unit represents a smaller deposit that was predominantly confined to the south. The thickness of the turbidites, however, does not reflect the overall size of the collapse as it does not include the debris avalanche component, or the finer-grained component that would have spread distally beyond the area cored within this study.

4.3 Source of the submarine deposits, the geophysical evidence

The hummocky submarine debris avalanche deposit, Deposit 3, was related to the submarine embayment, C3 (Figure 6), by Le Friant *et al.* (2004). The larger landslide deposit buried beneath Deposit 3 (Figure 5) also appears to be derived from a similar position on the flanks of Montserrat. Between these deposits, the intervening sediment is marked by high-amplitude, discontinuous reflections, which may comprise smaller mass-flow deposits, and represent a period of slope wasting and volcanoclastic accumulation off the south flank of Montserrat, potentially associated with the construction of the SSH edifice.

We have indicated in Figure 6 that C3 can be traced onshore, with the western edge of the scar being especially clear and observed to follow a line to the west of SSH, towards Soufrière Hills. It is not clear whether the C3 structure (including both its subaerial and submarine features) formed during the Deposit 3 landslide, but it may represent a composite failure structure associated with Deposit 3 and/or the underlying mass-flow deposits. If, as

the 2D seismic lines suggest, Deposit 3 was sourced from a flank collapse that incised into the SSH edifice, the outline of this scar may have been obscured both by erosion and later volcanic activity.

The turbidites identified in marine cores have been linked to the subaerial SSH complex by geochemical provenance (Section 3.4). The spatial distribution of these turbidites suggests they come from a region south of Montserrat (Figures 7d and 7e), and this region has a submarine embayment (C3) that can be traced onshore (Figure 6). The multi-channel seismic line that imaged the area most likely to host the proximal part of the turbidites, discovered a blocky avalanche deposit (Deposit 3). It is therefore conceivable that Deposit 3 is the source of the SSH turbidite units identified in the sediment cores and that both were sourced by a failure of SSH edifice. This agrees with the lack of sedimentary drape over Deposit 3 (Figure 5) suggesting that the debris avalanche lies within the top 5-10 metres of sediment. The one core site that lies within the debris avalanche deposit (JR123-45) did not recover any of the SSH Lower Unit, but bottomed-out within the SSH Hemipelagic-rich Unit. If Deposit 3 is the proximal equivalent of SSH Lower Unit then the absence of SSH Lower Unit in this cores would be expected due to coarse and heterogeneous nature of the debris avalanche, which would make it difficult for a core to penetrate. This supports the hypothesis of Deposit 3 and the SSH Lower Unit representing the same landslide event.

4.4 Chemostratigraphic interpretations

The SSH deposits have been divided into 2 geochemical suites (Figure 11), based on trace element and Pb isotopic compositions (Suites A & B). This geochemical variability is independent of major element fractionation trends. The subaerial chemostratigraphy separates the SSH volcanic complex into two magmatic stages (Suite A and B), which likely reflects the manner in which the magmas were generated, representing injections of magma of differing trace element and isotopic compositions (Cassidy et al., in review).

Suite SH lava and clastics were emplaced at the base of the subaerial SSH stratigraphy and were then successively overlain by polymict breccias and the interbedded lava flow from Suite A, with Suite B erupting dacitic lava flows followed by basaltic scoria. In the submarine turbidite deposits, this succession has been reversed. The first turbidite to be emplaced (SSH Lower Unit) contains clasts predominantly from the younger Suite B source, although the upper subunits of the SSH Lower Unit also contain Suite A clasts (Figure 7). Overlying this is the SSH Upper Unit, which contains clasts solely from the older Suite A source. At the east section of the SSH (Figure 2), the basal lithology belongs to the Soufrière Hills geochemical

suite. This is not recorded in the cores, suggesting that the flank collapses recorded offshore did not incise into these rocks.

4.5. Collapse model

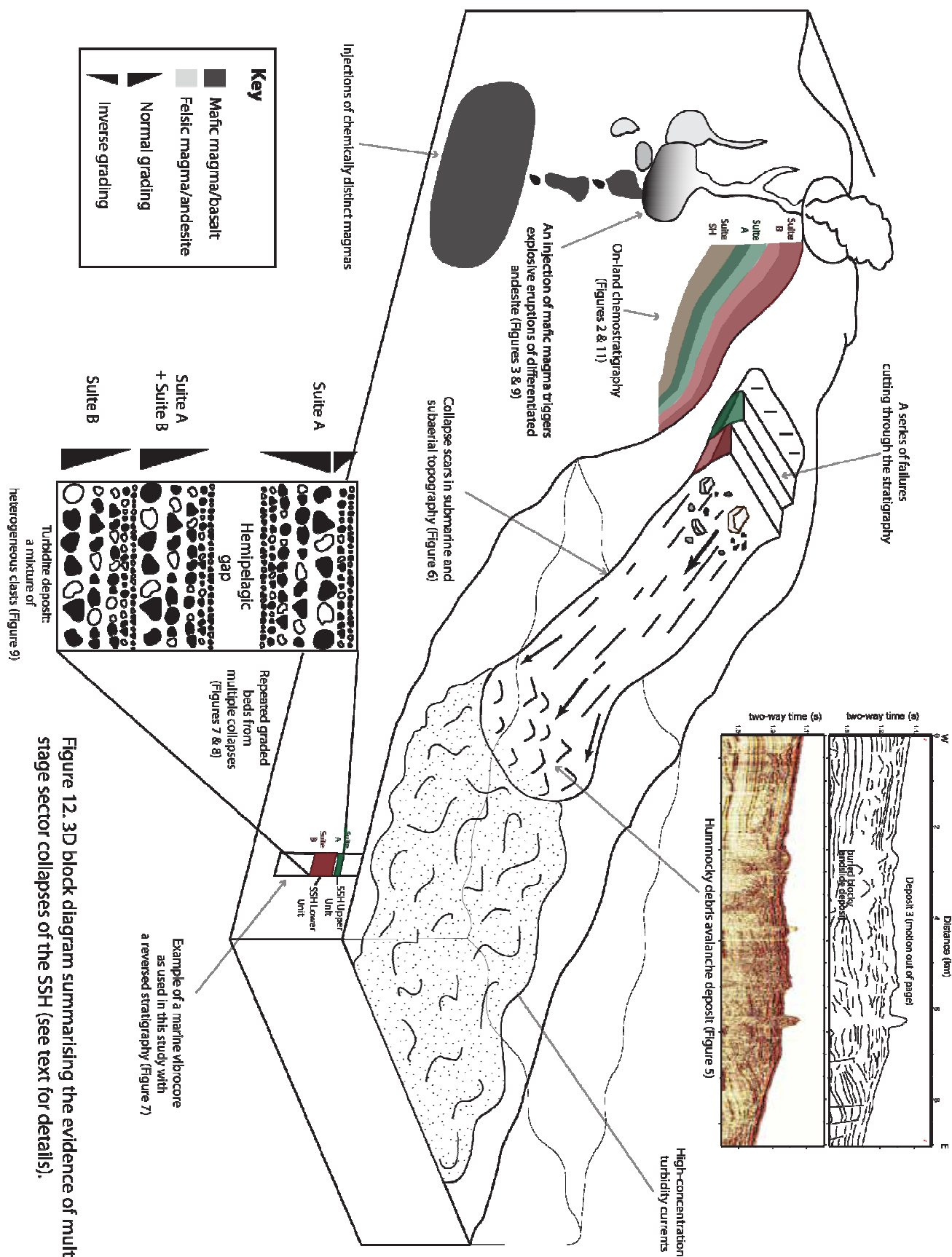
The geophysical, morphological and subaerial field observations provide evidence of several flank collapses originating from the SSH volcanic complex (Figure 12). Examination of the sedimentology and geochemistry of the submarine deposits sourced from the SSH has been key in ascertaining the detailed collapse dynamics. Figure 12 summarises the main insights gained from this study.

The SSH sector collapses left a scoured embayment (C3) as it eroded the steep submarine slopes of the island (Figures 1 & 6). At the break of slope at the base of the submarine volcanic flanks, the largest collapse lost energy, emplacing large blocks of material and forming a $\sim 1 \text{ km}^3$ debris avalanche deposit (Deposit 3) (Figures 1 & 5). The turbidites sampled in this study were formed upon disintegration and water entrainment of the debris avalanche (c.f. Mulder & Cochonat 1996; Ilstad *et al.* 2004; Bryn *et al.* 2005). The SSH Lower Unit turbidity currents flowed toward the south and south west, efficiently combining the subaerially sourced stratigraphic units from the SSH (e.g. basalt and andesite pumice deposits) into compositionally immature graded beds. Multiple stages of this collapse led to the development of stacked graded beds.

The SSH Hemipelagic-rich Unit represents a $\sim 2 \text{ ka}$ period of quiescence. Following this, the second turbidite (SSH Upper Unit) was then emplaced. This collapse appears to have been smaller in volume than the SSH Lower Unit.

The chemostratigraphy of the subaerial SSH volcanic succession of: 1) Suite SH, 2) Suite A, with 3) Suite B, has been reversed in the submarine stratigraphy (Figure 12) due to multiple collapses sampling older stratigraphy respectively within the SSH edifice. The SSH Lower Unit primarily removed Suite B stratigraphy from the top of the subaerial sequence. The failure then successively cut back through the chemostratigraphic succession sampling Suite A in the upper deposits of the SSH Lower Unit. After a $\sim 13\text{-}30 \text{ ka}$ time gap, the second turbidite, the SSH Upper Unit, was emplaced (Figure 12). This second collapse sampled solely Suite A material. The multi-stage failures do not appear to have reached the stratigraphic depth containing the Suite SH (Figure 11).

The multi-stage nature of the SSH Lower Unit suggests that the likelihood of it generating a large tsunami is low, when compared to the scenario of the entire volume being emplaced in a single stage failure.



5. Conclusions

This study highlights the potential geohazards associated with small volcanic islands, such as Montserrat, and provides further insight into how Montserrat has evolved geomorphologically through episodic sector collapses. Volcanism at SSH has also been shown to be more complex than was previously thought. As well as explosive andesitic volcanism related to this centre, there have been effusive and more voluminous eruptions of poorly vesiculated basalt. The occurrence of magma mingling between these two different magmas clearly shows that basalt magma flowed into the andesite, and suggests that the explosive andesitic eruptions may have been triggered by pulses of mafic magma disturbing a differentiated magma chamber. This study reveals that the SSH and the Soufrière Hills volcanoes were active at closely overlapping intervals.

Geochemical analyses have been used to assign the provenance of clasts to different volcanic sources on Montserrat and to confirm the stratigraphic correlations of both the subaerial and submarine SSH deposits. The chemostratigraphy has also been used to discern how the collapse occurred. These data show that the subaerial stratigraphy has been reversed in the marine turbidites, as the multi-stage collapses successively cut back into older, chemically distinct deposits.

This study demonstrates that a reconstruction of the volcanic history of SSH recorded solely from the subaerial record would omit some key past volcanic events, as the collapses have transported large amounts of erupted material to the ocean.

References

- Amy, L. A., A. J. Hogg, J. Peakall and P. J. Talling (2005). "Abrupt transitions in gravity currents." Journal of Geophysical Research-Earth Surface **110**(F3).
- Blake, S. and J. H. Fink (2000). "On the deformation and freezing of enclaves during magma mixing." Journal of Volcanology and Geothermal Research **95**(1-4): 1-8.
- Boudon, G., A. Le Friant, J. C. Komorowski, C. Deplus and M. P. Semet (2007). "Volcano flank instability in the lesser Antilles arc: diversity of scale, processes, and temporal recurrence." Journal of Geophysical Research-Part B-Solid Earth: B08205-1-28.
- Bouma, A. H. (1962). Sedimentology of Some Flysch Deposits: A Graphic Approach to Facies Interpretation. Amsterdam, Elsevier.

Bryn, P., K. Berg, C. F. Forsberg, A. Solheim and T. J. Kvalstad (2005). "Explaining the Storegga Slide." Marine and Petroleum Geology **22**(1-2): 11-19.

Cashman, K. V. and M. T. Mangan (1994). "Physical aspects of magmatic degassing 2. Constraints on vesiculation processes from textural studies of eruptive products." Volatiles in Magmas **30**: 447-478.

Cassidy, M. Taylor, R.N., Palmer, M.R, Cooper, R., Stenlake C., Trofimovs, J., (2012) "Tracking the magmatic evolution of island arc volcanism: Insights from a high-precision Pb isotope record of Montserrat, Lesser Antilles" Geochemistry, Geophysics, Geosystems, in press

Deplus, C., A. Le Friant, G. Boudon, J. C. Komorowski, B. Villemant, C. Harford, J. Segoufin and J. L. Cheminee (2001). "Submarine evidence for large-scale debris avalanches in the Lesser Antilles Arc." Earth and Planetary Science Letters **192**(2): 145-157.

DeMets, C., P. E. Jansma, G. S. Mattioli, T. H. Dixon, F. Farina, R. Bilham, E. Calais and P. Mann (2000). "GPS geodetic constraints on Caribbean-North America plate motion." Geophysical Research Letters **27**(3): 437-440.

Devine, J. D., M. D. Murphy, M. J. Rutherford, J. Barclay, R. S. J. Sparks, M. R. Carroll, S. R. Young and J. E. Gardner (1998). "Petrologic evidence for pre-eruptive pressure-temperature conditions, and recent reheating, of andesitic magma erupting at the Soufrière Hills Volcano, Montserrat, WI." Geophysical Research Letters **25**(19): 3669-3672.

Feuillet, N., F. Leclerc, P. Tapponnier, F. Beauducel, G. Boudon, A. Le Friant, C. Deplus, J. F. Lebrun, A. Nercessian, J. M. Saurel and V. Clement "Active faulting induced by slip partitioning in Montserrat and link with volcanic activity: New insights from the 2009 GWADASEIS marine cruise data." Geophysical Research Letters **37**: 6.

Folk, R. L., and W.C. Ward (1957), Brazos River bar: A studying the significance of grain-size parameters, *Journal of Sedimentary Petrology*, **27**, 3-26.

Garcia, M. O., Ed. (1996). Turbidites from slope failure on Hawaiian volcanoes. Volcano instability on the Earth and other planets, Geological Society London Special Publication.

Gray, J. and K. Hutter (1997). "Pattern formation in granular avalanches." Continuum Mechanics and Thermodynamics **9**(6): 341-345.

Harford, C. L., Pringle, M.S., Sparks, R.S.J., & Young S.R. (Ed.) (2002), The volcanic evolution of Montserrat using $^{40}\text{Ar}/^{39}\text{Ar}$ geochronology. In: Druitt, T.H. & Kokelaar, B.P. (eds) *The eruption of Soufrière Hills volcano, Montserrat from 1995 to 1999*. Geological Society, London, Memoirs, **21**, 93-113 pp.

Herd, R. A., M. Edmonds and V. A. Bass (2005). "Catastrophic lava dome failure at Soufrière Hills Volcano, Montserrat, 12-13 July 2003." Journal of Volcanology and Geothermal Research **148**(3-4): 234-252.

Huppert, H. E., R.S.J. Sparks and J.S. Turner (1982), Effects of volatiles on mixing in calc-alkaline magma systems *Nature*, 297, 554-557.

Ilstad, T., A. Elverhoi, D. Issler and J. G. Marr (2004). "Subaqueous debris flow behaviour and its dependence on the sand/clay ratio: a laboratory study using particle tracking." Marine Geology **213**(1-4): 415-438.

Ishizuka, O., R. N. Taylor, J. A. Milton and R. W. Nesbitt (2003). "Fluid-mantle interaction in an intra-oceanic arc: constraints from high-precision Pb isotopes." Earth and Planetary Science Letters **211**(3-4): 221-236.

Kiddle, E. J., B. R. Edwards, S. C. Loughlin, M. Pettersen, R. S. J. Sparks and B. Voight (2010). "Crustal structure beneath Montserrat, Lesser Antilles, constrained by xenoliths, seismic velocity structure and petrology." Geophysical Research Letters **37**: 6.

Kneller, B. C. and W. D. McCaffrey (2003). "The interpretation of vertical sequences in turbidite beds: The influence of longitudinal flow structure." Journal of Sedimentary Research **73**(5): 706-713.

Koster, E. H. and Steel, R.H. (1984). "Sedimentology of gravels and conglomerates." Canadian Society of Petroleum Geologists Mem. **10**: 441.

Lebas, M. J., R. W. Lemaitre, A. Streckeisen and B. Zanettin (1986). "A chemical classification of volcanic-rocks based on the total alkali silica diagram." Journal of Petrology **27**(3): 745-750.

Lebas, E., A. Le Friant, G. Boudon, S.F.L. Watt, P.J. Talling, N. Feuillet, C. Deplus, C. Berndt, and M.E. Vardy (2011) Multiple widespread landslides during the long-term evolution of a volcanic island: Insights from high-resolution seismic data, Montserrat, Lesser Antilles. Geochem. Geophys. Geosyst., **12** Q05006 **Doi:** 0.1029/2010GC003451

Le Friant, A., C. L. Harford, C. Deplus, G. Boudon, R. S. J. Sparks, R. A. Herd and J. C. Komorowski (2004). "Geomorphological evolution of Montserrat (West Indies): importance of flank collapse and erosional processes." Journal of the Geological Society **161**: 147-160.

Le Friant, A., E. J. Lock, M. B. Hart, G. Boudon, R. S. J. Sparks, M. J. Leng, C. W. Smart, J. C. Komorowski, C. Deplus and J. K. Fisher (2008). "Late Pleistocene tephrochronology of marine sediments adjacent to Montserrat, Lesser Antilles volcanic arc." Journal of the Geological Society **165**: 279-289.

Lovholt, F., G. Pedersen and G. Gisler (2008). "Oceanic propagation of a potential tsunami from the La Palma Island." Journal of Geophysical Research-Oceans **113**(C9): 21.

Lowe, D. R. (1982). "Sediment gravity flows 2. Depositional models with special reference to the deposits of high-density turbidity currents." Journal of Sedimentary Petrology **52**(1): 279-298.

Mangan, M. T., K. V. Cashman and S. Newman (1993). "Vesiculation of basaltic magma during eruption." Geology **21**(2): 157-160.

Masson, D. G. (1996). "Catastrophic collapse of the volcanic island of Hierro 15 ka ago and the history of landslides in the Canary Islands." Geology **24**(3): 231-234.

Masson, D. G., A. B. Watts, M. J. R. Gee, R. Urgeles, N. C. Mitchell, T. P. Le Bas and M. Canals (2002). "Slope failures on the flanks of the western Canary Islands." Earth-Science Reviews **57**(1-2): 1-35.

Masson, D. G., C. B. Harbitz, R. B. Wynn, G. Pedersen and F. Lovholt (2006). "Submarine landslides: processes, triggers and hazard prediction." Philosophical Transactions of the Royal Society a-Mathematical Physical and Engineering Sciences **364**(1845): 2009-2039.

Moore, J. G., D. A. Clague, R. T. Holcomb, P. W. Lipman, W. R. Normark and M. E. Torresan (1989). "Prodigious submarine landslides on the Hawaiian Ridge." Journal of Geophysical Research-Solid Earth and Planets **94**(B12): 17465-17484.

Moore, J. G., W. R. Normark and R. T. Holcomb (1994). "Giant Hawaiian landslides." Annual Review of Earth and Planetary Sciences **22**: 119-144.

Mulder, T. and P. Cochonat (1996). "Classification of offshore mass movements." Journal of Sedimentary Research **66**(1): 43-57.

Mulder, T. and J. Alexander (2001). "The physical character of subaqueous sedimentary density flows and their deposits." Sedimentology **48**(2): 269-299.

Murphy, M. D., R. S. J. Sparks, J. Barclay, M. R. Carroll, A. M. Lejeune, T. S. Brewer, R. Macdonald, S. Black and S. Young (1998). "The role of magma mixing in triggering the current eruption at the Soufrière Hills volcano, Montserrat, West Indies." Geophysical Research Letters **25**(18): 3433-3436.

Murphy, M. D., R. S. J. Sparks, J. Barclay, M. R. Carroll and T. S. Brewer (2000). "Remobilization of andesite magma by intrusion of mafic magma at the Soufrière Hills Volcano, Montserrat, West Indies." Journal of Petrology **41**(1): 21-42.

Mutti, E. (1992). Turbidite Sandstones, AGIP. 275 pp.

Ollier, G., P. Cochonat, J. F. Lenat and P. Labazuy (1998). "Deep-sea volcanoclastic sedimentary systems: an example from La Fournaise volcano, Reunion Island, Indian Ocean." Sedimentology **45**(2): 293-330.

Rea, J. W. (1974), The volcanic geology and petrology of Montserrat, West Indies, *Journal of the Geological Society London.*, **130**, 341-366.

Schwarzkopf, L. M., H. U. Schmincke and S. J. Cronin (2005). "A conceptual model for block-and-ash flow basal avalanche transport and deposition, based on deposit architecture of 1998 and 1994 Merapi flows." Journal of Volcanology and Geothermal Research **139**(1-2): 117-134.

- Siebert, L., 1984. Large volcanic debris avalanches: characteristics of source areas, deposits, and associated eruptions. *Journal of Volcanology and Geothermal Research* 22, 163–197.
- Smith, A. L. R., M.J. Schellekens, J.H. & Mattioli, G.S. (2007), Prehistoric stratigraphy of the Soufrière Hills –South Soufrière Hills volcanic complex, Montserrat, West Indies, *Journal of Geology*, 115, 115-127.
- Sparks, R. S. J., H. Sigurdsson and L. Wilson (1977), Magma mixing: a mechanism for triggering acid explosive eruptions, *Nature*, 267, 315-318.
- Trofimovs, J., R. S. J. Sparks and P. J. Talling (2008). "Anatomy of a submarine pyroclastic flow and associated turbidity current: July 2003 dome collapse, Soufrière Hills volcano, Montserrat, West Indies." *Sedimentology* 55(3): 617-634.
- Trofimovs, J., J. K. Fisher, H. A. MacDonald, P. J. Talling, R. S. J. Sparks, M. B. Hart, C. W. Smart, G. Boudon, C. Deplus, J. C. Komorowski, A. Le Friant, S. G. Moreton and M. J. Leng (2010) "Evidence for carbonate platform failure during rapid sea-level rise; ca 14 000 year old bioclastic flow deposits in the Lesser Antilles." *Sedimentology* 57(3): 735-759.
- Urgeles, R., M. Canals, J. Baraza, B. Alonso and D. Masson (1997). "The most recent megalandslides of the Canary Islands: El Golfo debris avalanche and Canary debris flow, west El Hierro island." *Journal of Geophysical Research-Solid Earth* 102(B9): 20305-20323.
- Wadge, G. (1984), Comparison of volcanic production-rates and subduction rates in the Lesser Antilles and Central America, *Geology*, 12(9), 555-558.
- Watt, S. F. L., P. J. Talling, M. E. Vardy, V. Heller, V. Hühnerbach, M. Urlaub, S. Sarkar, D. G. Masson, T. J. Henstock, T. A. Minshull, M. Paulatto, A. Le Friant, E. Lebas, C. Berndt, G. J. Crutchley, J. Karstens, A. J. Stinton, F. Maeno (2012). "Combinations of volcanic-flank and seafloor-sediment failure offshore Montserrat, and their implications for tsunami generation." *Earth and Planetary Science Letters* 319–320: 228–240.
- Watts, A. B. and D. G. Masson (1995). "A giant landslide on the north flank of Tenerife, Canary Islands." *Journal of Geophysical Research-Solid Earth* 100(B12): 24487-24498.

Wynn, R. B. and Masson, D. G., Ed. (2003). Canary island landslides and tsunami generation: can we use turbidite deposits to interpret landslide processes. Submarine mass movements and their consequences. Dordrecht, Netherlands, Kluwer Academic Publishers.

Zellmer, G. F., C. J. Hawkesworth, R. S. J. Sparks, L. E. Thomas, C. L. Harford, T. S. Brewer and S. C. Loughlin (2003). "Geochemical evolution of the Soufrière Hills volcano, Montserrat, Lesser Antilles volcanic arc." Journal of Petrology **44**(8): 1349-1374.

CHAPTER 4

A NEW LAVA DOME COLLAPSE INTO THE OCEAN AT THE SOUFRIÈRE HILLS VOLCANO, MONTSERRAT, WEST INDIES AT CA 8 KA: HOW SUBMARINE STRATIGRAPHY CAN COMPLEMENT SUBAERIAL ERUPTION HISTORIES

This chapter forms the basis of a manuscript in preparation with the following authors: Cassidy, M., Trofimovs, J., Palmer, M.R., Taylor, R.N. Moreton, S. (to be submitted 2012).

Written by M Cassidy, but I received feedback from Trofimovs and Palmer. Morton carried out the AMS radiocarbon analyses in the NERC radiocarbon facility (Environment), from a successful funded application by Cassidy and Trofimovs to NERC for 13 AMS radiocarbon dates.

Abstract

The eruption record of volcanic islands is constantly being improved through marine studies, such as geophysical surveys and analysis of marine sediment cores. This chapter details two voluminous mass movement deposits, offshore southern Montserrat, West Indies. The deposits, which were emplaced in the last 35 ka have not previously been recognised in the subaerial or distal submarine records. Age constraints, provided by AMS (Accelerated Mass Spectrometry) radiocarbon dating, show that a primary volcanic eruption occurred at ca 8 ka succeeding a large re-worked bioclastic and volcanoclastic flow event which deposited turbidites between 8 and 35 ka. Through the correlation of marine sediment cores, component and geochemical analysis we discuss the origin of these deposits; the 8 ka primary volcanic event was likely derived from a pyroclastic flow that entered the ocean and mixed with the water column forming a water-supported density current. The origin of the bioclastic flow event is consistent with a shallow marine shelf collapse offshore the south west coast of Montserrat.

The recognition of these two previously undiscovered volcanoclastic deposits highlights the importance of obtaining an accurate marine record of events offshore from volcanic islands and incorporating such data into eruption history reconstructions. Previous stratigraphic and magma production studies suggested that there was a magmatic hiatus

from the Soufrière Hills volcano between 16 and 6 ka. The ca 8 ka event suggests that there was less magmatic repose between eruptions than previously recognised.

1. Introduction

The marine record of explosive eruptions on island volcanoes is typically more complete than that preserved on land because subaerial deposits are prone to vegetative cover, erosion and (or) burial by subsequent eruptions. Large volumes of eruptive products are commonly transported into the ocean, particularly from smaller islands, wherein they form stacked volcanoclastic eruption sequences (Trofimovs et al., 2006; Masson et al., 2006). These sequences are often separated by background hemipelagic material, the foraminifera within which can be dated using radiocarbon measurements or stable isotope profiles. Therefore accurately dated and more complete eruption histories can potentially be derived from marine sediment cores.

The Soufrière Hills volcano, Montserrat, West Indies (Figure 1), provides an excellent natural laboratory for understanding the potentially hazardous, often catastrophic, and poorly understood events that transport sediment into the marine environment surrounding andesitic volcanoes. Since 1995 the volcano has extruded 1 km³ of magma, 75% of which has been transported into the ocean, largely by the direct entrance of pyroclastic flows and ash fallout into seawater (Trofimovs et al., 2006; Le Friant et al., 2009). The subaerial eruption sequence of the Soufrière Hills volcano including the current eruption (1995-present), has been monitored and documented in unprecedented detail (e.g. Druitt and Kokelaar, 2002; Voight et al., 2006). These on-land observations have now been supplemented by recent research cruises to the area that have taken advantage of advances in coring techniques to generate a more complete marine sediment record (Trofimovs et al., 2006, 2008, 2010, 2012; Le Friant et al., 2008; Cassidy et al., in press).

This chapter describes a previously unrecognised volcanic flank collapse off the southern coast of Montserrat, together with a primary volcanic eruption from the Soufrière Hills volcano that is preserved in proximal marine sediment cores 7 - 14 km from shore. The deposits from this new primary eruption have not been recognised in the onshore stratigraphy (Roobol and Smith 1997; Harford et al., 2002; Smith et al 2008). Sedimentological logging of the marine deposits, grain size and component analyses, together with SEM imagery and geochemical provenance analysis are used to determine the origin of these events and aid in reconstructing their emplacement mechanisms. In addition, AMS radiocarbon dates are used constrain the age of the events and to constrain their position within the established subaerial volcanic record of Montserrat.

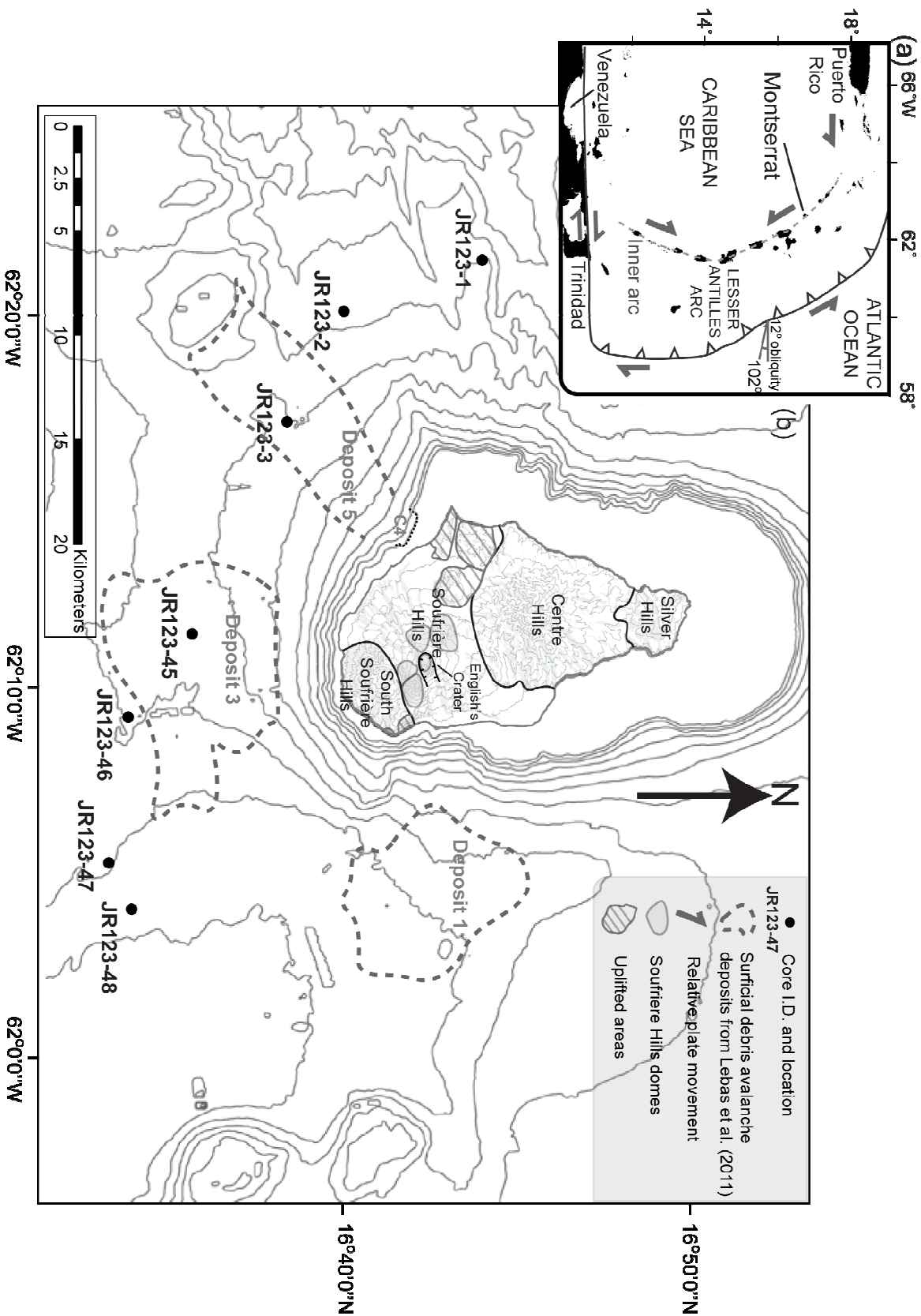


Figure 1. (a) Insert of the Lesser Antilles volcanic arc. (b) Contoured map of the submarine bathymetry and core locations offshore Montserrat, surficial debris avalanche deposits are highlighted from Le Friant et al. (2004) and Lebas et al. (2011).

1.1 Geological setting

Montserrat is located in the northern part of the Lesser Antilles Island Arc, a 750 km long island chain created by the subduction of the North American plate underneath the Caribbean plate (Wadge, 1984; Demets et al., 2000). Montserrat has dimensions of 16 km (north- south) and 10 km (east – west) and is comprised primarily of volcanoclastic rocks (Harford et al., 2002). Most of the volcanic deposits on the island are andesitic, however mafic enclaves are found within deposits from the Soufrière Hills volcanic centre and the South Soufrière Hills dominantly comprises basaltic rocks (Figure 1) (Harford et al., 2002; Smith et al., 2007; Cassidy et al., in press).

There are four volcanic centres on Montserrat dated by Ar-Ar by Harford et al. (2002), namely the Silver Hills (2600 -1200 ka), Centre Hills (950 - 550 ka) Soufrière Hills (282 ka - present) and South Soufrière Hills (128- 131 ka). Each centre can be geochemically distinguished by isotopic and trace element parameters (Cassidy et al., 2012).

Stratigraphic observation, volume estimates, and geochronology, imply that the periods of volcanic extrusion from the Soufrière Hills and South Soufrière Hills regions are spatially and temporally interspersed (Harford et al., 2002; Smith et al., 2007; Le Friant et al., 2008). The subaerial eruptive record for the intercalated Soufrière Hills and South Soufrière Hills volcanic complexes has been investigated by Roobol and Smith (1998) and later revised by Smith et al. (2007), who proposed seven episodes of volcanism (Figure 2). Episode 1 represents the ‘Ancient’ Soufrière Hills stage exposed on Garabaldi Hill (>200 ka). Episode 2 formed the Soufrière Hills Subunit I (<175 ka), and is characterised by Peléan activity (andesite lava dome growth and collapse to form pyroclastic flows) and a Plinian eruption, as evidenced by the presence of ignimbrites. Episode 3 is represented by basaltic effusive eruptions from the South Soufrière Hills volcanic centre at 128 - 131 ka. Episodes 4, 5, 6 & 7 (112,000 - 400 yrs BP), correspond to Soufrière Hills Subunits II-V when the eruptions returned to more characteristic andesitic Peléan activity. In the last 30 ka there have been several documented periods of volcanic activity on land (Figure 2). These include the emplacement of Soufrière Hills Subunit III, which dates from 31.5 to 16.9 ka comprising dominantly block and ash flow deposits. Subsequent to this there was a period of repose until 4 ka when the Soufrière Hills Subunit IV was emplaced, consisting of dense andesite ash flow deposits (Smith et al., 2007). Two large volcanic flank collapses within Soufrière Hills Subunit IV (Episode 6) are thought to have produced a large collapse scar on the eastern flank of the Soufrière Hills volcano, called English’s Crater (Figure 1), and are dated at 3.9 ka (Roobol and Smith, 1998) and 1.9 ka (Boudon et al., 2007). The current eruption (Subunit VI; 1995-present) marks the 8th eruptive episode in Montserrat’s volcanic history (Smith et al., 2007).

A submarine tephrochronological record was constructed for the Soufrière Hills volcano by Le Friant *et al.* (2008) using a distal marine sediment core taken 55 km south west of Montserrat. Micropaleontology and $\delta^{18}\text{O}$ isotope analyses were used to date the hemipelagic sediment accumulations between volcanic horizons, and produce an eruption history for the last 250 ka (Figure 2). The authors found eight layers relating to dome eruptions, five of which can be directly correlated to dated domes or related pyroclastic flow sequences on land. They also dated the marker sequence of basaltic tephra layers at 124 - 147 ka, which corresponds to the eruptions from the South Soufrière Hills. Le Friant *et al.* (2008) suggested the presence of six more significant explosive eruptions, on the basis of increased abundance of pumiceous glassy ash, that do not correspond with any documented eruptive deposits on land. Hemipelagic sediment accumulations with low abundances of volcanic material were interpreted to result from long periods (10 ka) of dormancy or low activity. In the last 30 ka they also recorded Peléan style eruptions at 24 ka, 16 ka, 6 ka and 3.5 ka, with periods of quiescence in between.

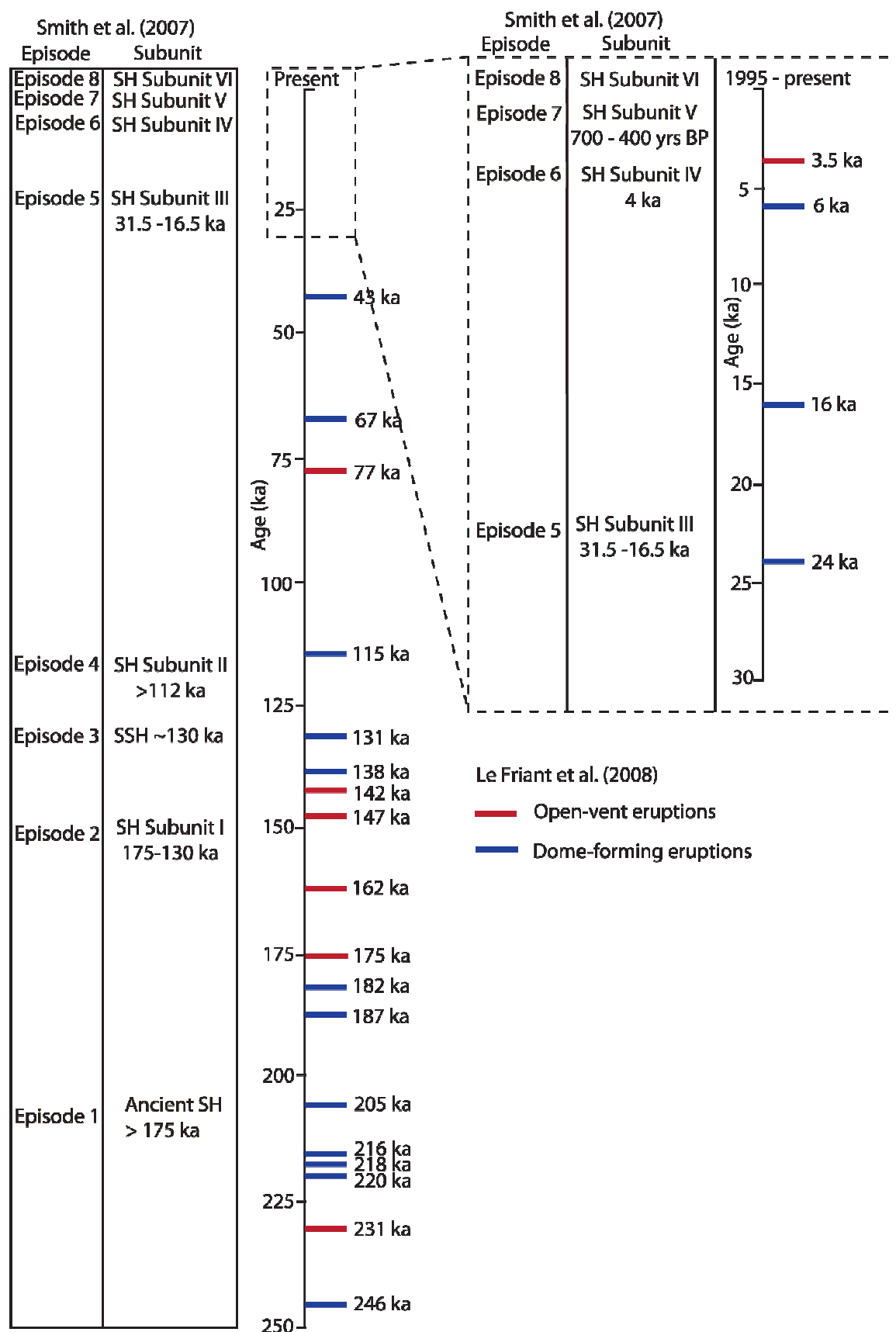


Figure 2. Summary stratigraphic column of the Soufriere Hills-South Soufriere Hills complex, combining the subaerial record of Smith et al. (2007) and submarine tephrochronology of Le Friant et al. (2008).

2. Methods

2.1 Marine core sampling

A research voyage in May 2005 onboard the RRS James Clark Ross (P.I. Prof. R.S.J. Sparks) sampled submarine volcanoclastic deposits offshore Montserrat using a vibrocore system developed by the British Geological Survey. The vibrocores discussed in this chapter are located south and west of Montserrat, 8 to 15 km offshore (Figure 1). The cores were sedimentologically logged; visually detailing grain size, structure and appearance. Approximately 1 cm³ samples were taken from targeted volcanoclastic horizons for quantitative grain size and component analysis. The coarse-grained nature of the volcanoclastic samples, necessitated the use of nested sieve sets to provide grain size measurements. Half Phi intervals were measured between -1.5 ϕ to 4 ϕ (2.8 - 0.063 mm). Bulk point counting a minimum of 300 grains for each sample was used to classify the grain populations under a binocular microscope.

2.2 AMS radiocarbon dating

Samples were taken for Accelerator Mass Spectrometry (AMS) ¹⁴C dating, in order to date the hemipelagic sediment immediately above and below the studied volcanoclastic horizon, to provide maximum and minimum age estimates for the deposit. We take the dates from the hemipelagic sediment directly above the volcanoclastic horizon as the closest estimate for depositional timing, as this represents the cessation of volcanoclastic deposition and a return to background hemipelagic sedimentation conditions. Dates below the targeted unit may provide evidence of the amount of erosion of the underlying substrate.

The samples were disaggregated in deionized water and washed through a 63 μ m sieve. They were then dried and sieved to collect the >150 μ m size fraction. An assemblage of around 1000 planktonic foraminifera tests (>150 μ m) was picked to provide a 14-16 mg sample. Specimens showing any signs of reworking or diagenesis were avoided. The foraminifera specimens exhibit remarkable preservation, and delicate, yet intact pteropods indicate good preservation.

Weighed samples of cleaned, dried sample material were hydrolysed to CO₂ using 85% orthophosphoric acid. The gas was cryogenically isolated and a subsample of CO₂ was analysed on a dual inlet stable isotope mass spectrometer (VG OPTIMA) to determine ¹³C/¹²C ratios, which were used to normalize ¹⁴C values to -25‰ $\delta^{13}\text{C}_{\text{VPDB}}$. The remaining sample CO₂ was converted to graphite by iron/zinc reduction (Slota et al., 1987) and ¹⁴C activity determined by accelerator mass spectrometry at the Scottish Universities Environmental Research Centre (SUERC) AMS Laboratory using either a NEC 5 MV AMS (Xu et al., 2004) or a NEC 250 kV single stage AMS (Freeman et al. 2008). In addition to the samples measured at SUERC, three AMS radiocarbon dates of foraminifera samples were measured commercially

by Beta Analytic Inc. (Florida, USA) using their in-house protocols. Details of the technique used can be obtained from the company web site (www.radiocarbon.com). The results are reported as conventional radiocarbon years BP (relative to AD 1950) and % modern ^{14}C , with both expressed at the $\pm 1\sigma$ confidence level. The dates were calibrated against the Marine09 dataset using CALIB 6.0.0 Radiocarbon Calibration software. The Marine09 dataset calibrates ages between 0 and 46.743 ka to 95% probability (2σ).

2.3 Geochemical analyses

Samples of the studied volcanoclastic units were taken for major, trace and rare earth element abundance. These samples were prepared in a clean laboratory suite at the National Oceanography Centre, Southampton (NOC). Submarine core samples were cleaned using 18M Ω ultrapure H_2O , sonicated for ten minutes and then dried overnight in an oven at 70°C. The samples were then passed through Teflon sieves (500 μm) and handpicked under a binocular microscope. Dense and poorly vesiculated juvenile clasts, mafic clasts and pale porphyritic, vesicular fragments were separated to assess the potential geochemical variability within the deposit. The hand-picked samples were then pulverized using an agate mortar. The Rare Earth Elements (REE), Rb, Sr, Y, Zr, Nb, Cs, Ba, Hf, Pb, Th and U concentrations were analysed by the ICP-MS at the NOC on a VG Plasmaquad PQ2+ instrument. Reproducibility is better than $\pm 4\%$ (RSD) for the REE, Rb and Nb, and better than $\pm 6\%$ (RSD) for other elements. Precision when using elemental ratios is better than 1% (RSD).

3. Results

3.1 Sea floor morphology and submarine facies architecture

The submarine shelf offshore of Montserrat varies in its shape and extent (Figure 1). North of the island, adjacent to the extinct volcanic centres, the shelf is wide (1-3 km) and shallow (60 to 100 m water depth), as the result of long term terrestrial and coastal erosion. The submarine shelf towards the south is narrower as these relatively young volcanic centres have not been subject to extensive erosion (Le Friant et al., 2004).

Offshore Montserrat there are two main submarine depressions exceeding 1000 metres water depth; the Bouillante-Montserrat graben located south east from Montserrat and extending towards Guadeloupe, and a series of submarine canyons to the west, which extend south west to the Grenada Basin (Le Friant et al. 2004; Feuillet et al. 2010). Seamounts are present along the margins of the Bouillante-Montserrat graben and towards the south west of Montserrat (Figure 1). Shallow acoustic and bathymetric surveys have identified areas of hummocky morphology on the ocean floor surrounding Montserrat (Figure 1), that

are thought to be debris avalanche deposits, sourced from subaerial and submarine failures (Le Friant et al. 2004; Lebas et al., 2011; Watt et al., 2012; Cassidy et al., in press).

The submarine sediment cores used in this study are located in 852 to 1057 metres of water, and form a south west to south east transect 7.3 km to 14.5 km from the Montserrat shore (Figure 1). The slopes upon which the marine sediment cores were sampled are dominantly shallow ($< 2^\circ$) and exhibit flat local topography. The marine stratigraphy offshore Montserrat preserves volcanoclastic and bioclastic deposits intercalated with hemipelagic sediment accumulations (Figure 3). Hemipelagic sedimentation rates have been shown to vary around Montserrat. Le Friant et al. (2008) use a single core to the south west of Montserrat to estimate rates of 1 to 3 cm kyr⁻¹, with an average of 2.3 cm kyr⁻¹, whereas Trofimovs et al. (2010) record a range of 3.7 to 6.88 cm kyr⁻¹ from a core proximal to the east of Montserrat. This is similar to Reid et al. (1996), who show variation from 1 to 3 cm kyr⁻¹ in the Lesser Antilles backarc region, to 5 to 10 cm kyr⁻¹ in the magmatic arc platform, with lower sedimentation rates observed during interglacial periods.

This chapter details two volcanoclastic deposits that are preserved in the marine sediment cores below the deposits from the most recent activity of the Soufrière Hills volcano (1995-present) (Figure 3). The two deposits, the Upper Andesitic Volcanoclastic Unit and the underlying Lower Mafic and Bioclastic-rich Unit, have been identified and correlated between cores using geochronology, geochemistry and characterisation of their distinct lithofacies, as described below.

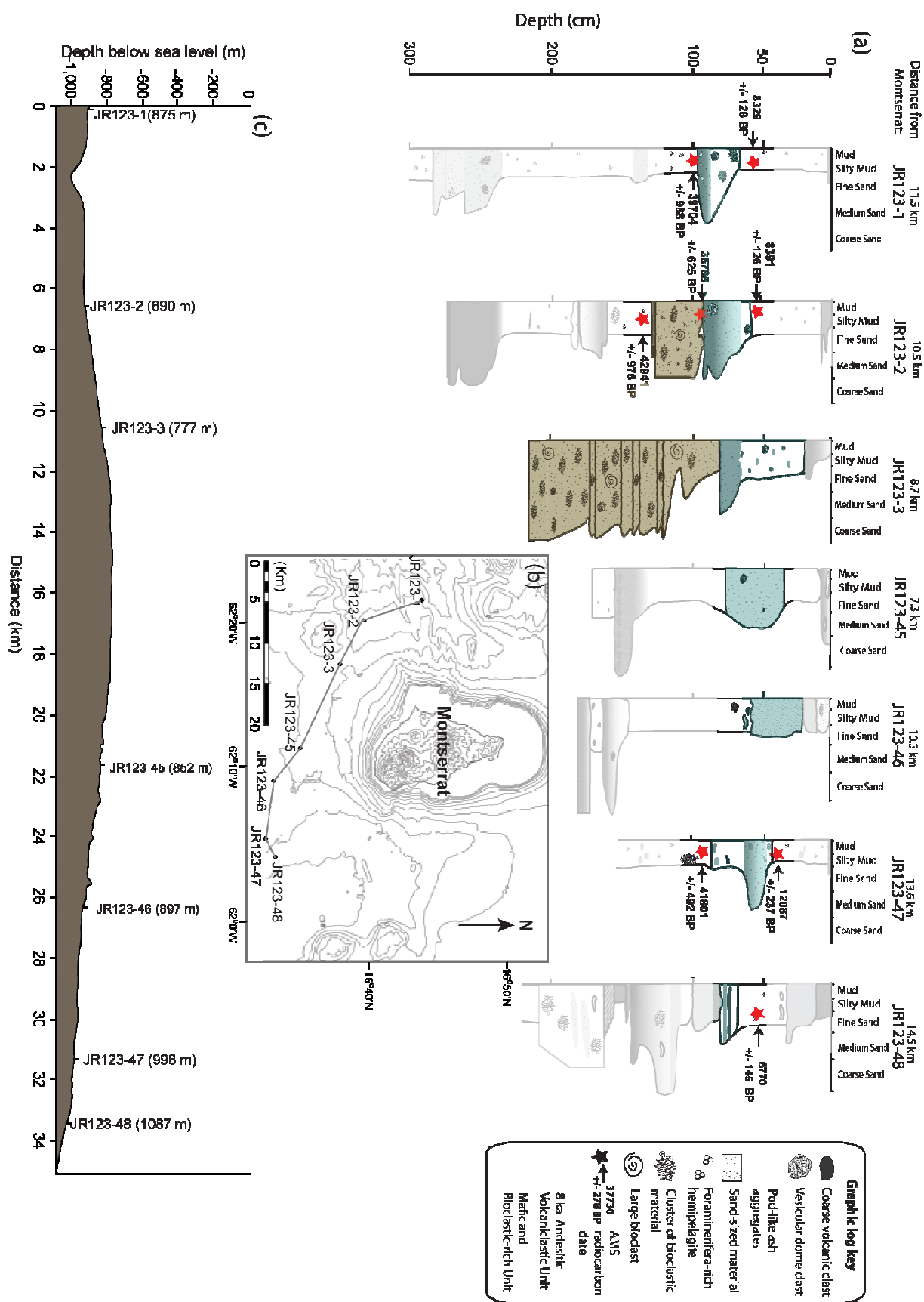


Figure 3. (a) Correlative stratigraphic logs showing the proximal submarine stratigraphic sequence from south west to south east. Radiocarbon dates are annotated and marine topography drawn. (b) Location map showing the transect from south west to south east. (c) Topographic profile of the submarine transect

3.2 Radiocarbon (AMS) dating constraints

The stratigraphic correlations in Figure 3 are supported by radiocarbon dates from the hemipelagic sediment overlying the Upper Andesitic Volcaniclastic Unit. A range of dates from 6.8 ka \pm 0.2 BP to 12.1 ka \pm 0.2 BP was obtained, providing an average age of 8.9 ka (Figure 3; Table 1). The sample that produced the oldest date of 12.1 ka BP was taken from hemipelagic sediment directly adjacent to the top of the Upper Andesitic Volcaniclastic Unit. This sample was chosen as it was believed to come from the hemipelagic sediment deposited on top of the targeted unit, however, the anomalously older ^{14}C age suggests that this sample may have been contaminated with reworked older sediment from within the Upper Andesitic Volcaniclastic Unit itself. Hence we believe that this older date is erroneous and the true end of volcaniclastic deposition and return to background hemipelagic sediment likely occurred closer to 8 ka. When the Upper Andesitic Volcaniclastic Unit is preserved in cores without the Lower Mafic and Bioclastic-rich Unit, dates below the Upper Unit range from 39.7 ka \pm 1.0 BP to 41.8 \pm 0.5 ka BP, implying significant erosion (\sim 31.4 kyr) at the base of the deposit. This equates to the removal of \sim 8.5 cm hemipelagic sediment, using the sedimentation rate of 3.7 cm kyr $^{-1}$ from Trofimovs et al. (2010) calculated from proximal cores from around 30 ka.

In the two cores where both units are found together (cores JR123-2 and JR123-3; Figure 3), the Upper Andesitic Volcaniclastic Unit lies directly on top of the Lower Mafic and Bioclastic-rich Unit. There is no discernable hemipelagic material between the two deposits. It is therefore impossible to obtain an accurate radiocarbon date from the top of the underlying unit which would ascertain its timing of emplacement. However, the Lower Mafic and Bioclastic-Rich Unit contains hemipelagic rip up clasts preserved in core JR123-2. An AMS radiocarbon date from one of these clasts provides an age of 35.8 ka \pm 0.7 BP. Together with the age below the Lower Mafic and Bioclastic-rich Unit in this core is 42.9 ka \pm 1.0 BP, this suggests that the Lower Mafic and Bioclastic-rich Unit eroded at least \sim 1.9 cm of the underlying hemipelagic sediment. We therefore suggest that the age of the Upper Andesitic Volcaniclastic Unit is 8.4 ka \pm 0.1 BP, whilst the Lower Mafic and Bioclastic-rich Unit is dated at between 8.4 ka \pm 0.2 and 35.8 ka \pm 0.7. Both units exhibit significant erosion at their base.

Table 1. Radiocarbon dates from the submarine stratigraphy offshore south west Montserrat

Publication code	Core I.D.	Sample depth (cm)	$\delta^{13}\text{C}_{\text{VPDB}}$ ‰ ± 0.1	Conventional Radiocarbon Age (years BP)	+/- 1 σ (radiocarbon yrs BP)	Calibrated age mid-point	Calibrated age ± 1 σ	2 σ Calibrate Error	Calibrate Error
SUERC-33137	JCR123-2	132	1.4	38880	617	Too old for calibration			
SUERC-33138	JCR123-1	63	4.1	7880	35	8651	55	7985	185
SUERC-33139	JCR123-1	101	1.4	35014	387	Too old for calibration			
SUERC-33140	JCR123-47	49	1.4	10688	39	12630	44	11440	278
SUERC-25163	JR123-2	53		7911	35	8021	92	8011	185
Beta - 306878	JCR123-48	64	-0.7	6700	40	7225	55	7245	105
Beta - 306877	JCR123-47	92		37730	300	Too old for calibration			
Beta - 313875	JCR123-2	88		31700	200			35785	625

3.3 Facies characteristics of the Mafic and Bioclastic-rich Unit

The (Lower) Mafic and Bioclastic-rich Unit is preserved in two marine cores south west of Montserrat, JR123-2 and JR123-3, located 10.5 and 8.7 km from shore respectively (Figure 1). The deposit ranges in thickness from 38 cm in core JR123-2 to >101 cm in core JR123-3, as the base is not intersected by the core (Figure 3). Variation in grain size and sorting is seen throughout the Mafic and Bioclastic-rich Unit in the form of stacked, normally graded beds. The deposits contain very coarse-grained subunits (e.g. -0.45 ϕ , 1.35 mm) including a moderately well-sorted (0.517 σ_{ϕ}), coarse sand deposit (0.85 ϕ , 0.6 mm), intercalated with very poorly to poorly-sorted subunits. Weak vertical grading is present within core JR123-3, however, the deposit is generally poorly to very poorly sorted, with an average sorting of 1.30 σ_{ϕ} and a very coarse sand mean grain size (0.99 ϕ 0.5 mm) (Figure 4). The Mafic and Bioclastic-rich Unit appears yellow and black in the exposed core and comprises abundant crystal fragments of feldspar, pyroxene and amphiboles (35-56%), mafic clasts (7-10%), dense and poorly vesiculated andesitic clasts (20-30%), bioclastic material such as broken coral and shells (6-20%), altered andesite lava clasts (4-9%), and vesicular juvenile andesitic clasts (2-10%) (Figure 4).

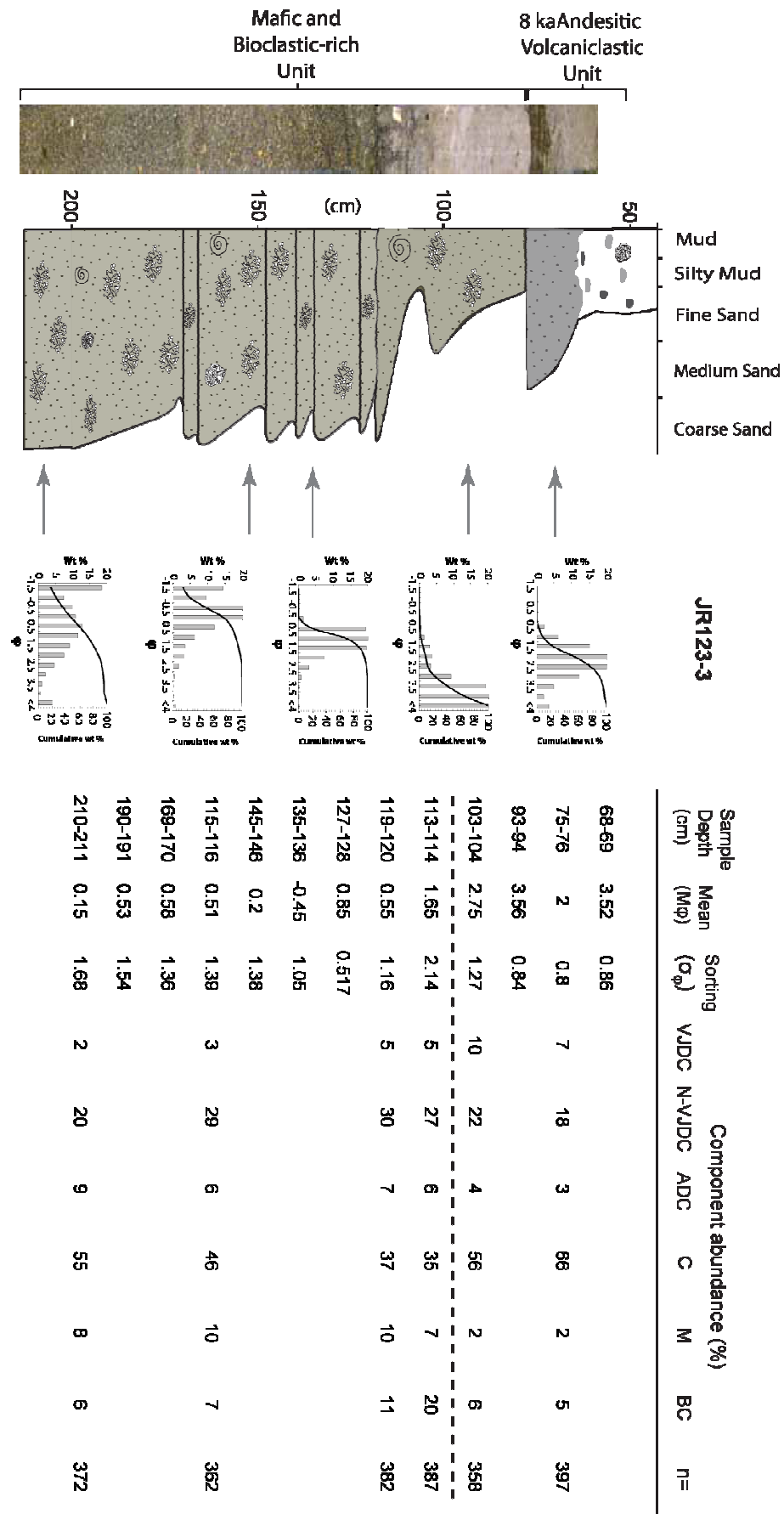


Figure 4. Core photograph, graphic log, grain size and component analysis data for JR123-3. VJDC=Vesicular Juvenile Dome Clasts, N-VJDC=Non-Vesicular Juvenile Dome Clasts, ADC=Altered Dome Clasts, C=Crystals, M=Mafic Clasts, BC=Biogenic Clasts, n=total number of clasts counted.

The volcanoclastic clasts exhibit a sub-rounded and sub-spherical morphology. The bioclastic material appears broken and angular (Figure 5).

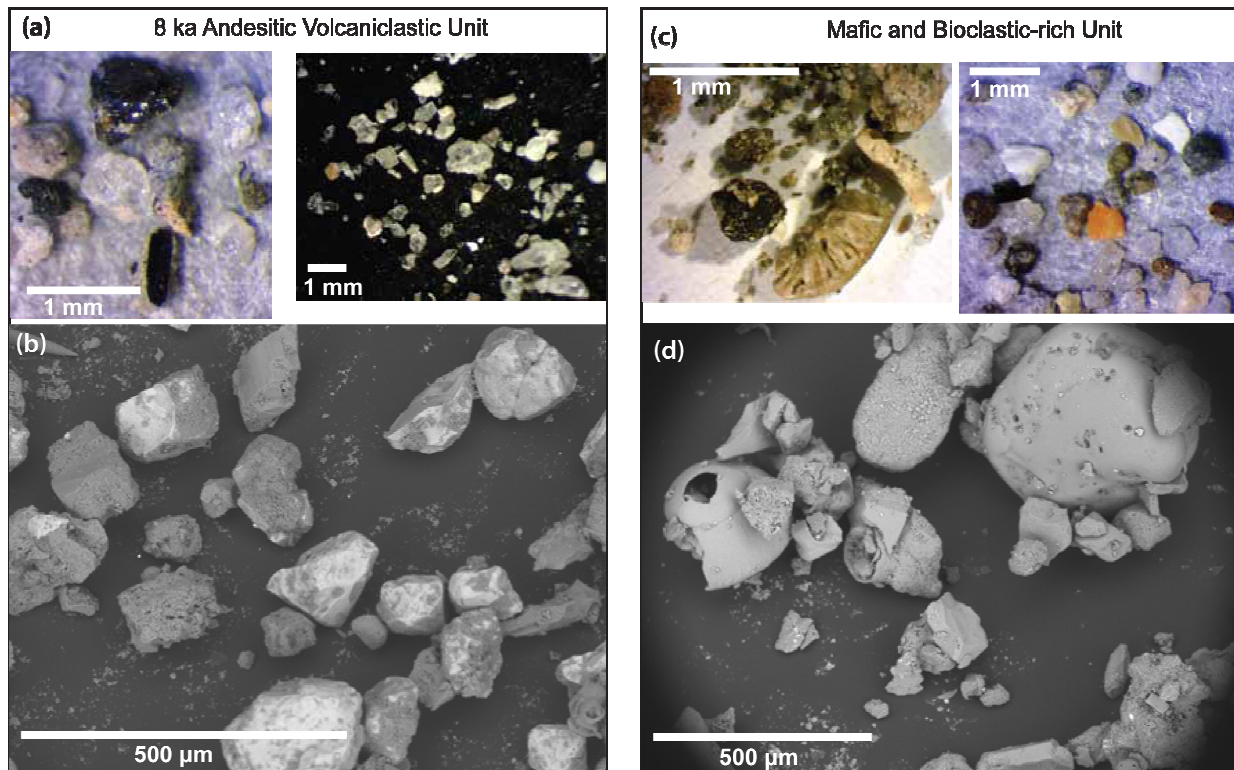


Figure 5. (a) Two images of the 8ka Andesitic Volcanoclastic Unit taken down a microscope, showing an abundance of angular crystal fragments and poorly vesiculated andesitic clasts. (b) SEM image of the 8ka Andesitic Volcanoclastic Unit showing the angular volcanic components. (c) Two photomicrographs of the Mafic and Bioclastic-rich Unit, showing fragmented bioclastic material and reworked volcanic clasts (d) SEM image of the Mafic and Bioclastic-rich Unit, showing the rounded volcanic clasts and poorly preserved bioclasts.

The bulk of the deposit is fines-poor ($\sim 10\% < 63\mu\text{m}$), however, the top of the deposit contains finer grain sizes (3.56ϕ , 0.088 mm), and shows poor to moderate sorting ($0.84\sigma_\phi$). The predominantly very fine sand top of the deposit also contains larger clasts of low density material such as, coarse vesicular dome clasts, scoria and heavily porous coral fragments up to 3 cm in diameter.

In core JR123-2 the Mafic and Bioclastic-rich Unit is 38 cm thick, generally poorly-sorted (average of $1.41 \sigma_\phi$) and a mean grain size of 1.56ϕ (0.35 mm) (Figure 6). At the base of the deposit is a thin (2.5 cm), fine-grained (3.01ϕ , 0.125 mm) and moderately-sorted deposit ($0.79 \sigma_\phi$), with fine planar stratification. Above this layer are thick bedded, massive deposits with varying coarse grain sizes, from 1.03ϕ (0.48 mm) to 1.46ϕ (0.32 mm). The Mafic and Bioclastic-rich Unit in this core comprises crystal fragments (44-46%), mafic clasts (12-15%), dense and poorly andesite vesiculated clasts (10-15%), bioclastic material such as broken coral and shells (16-19%), altered lava clasts (8-10%), and vesicular juvenile andesite clasts (2-4%) (Figure 6). The top of the Mafic and Bioclastic-rich Unit preserves rip-up clasts of hemipelagic sediment similar in character to the hemipelagic material directly below the deposit.

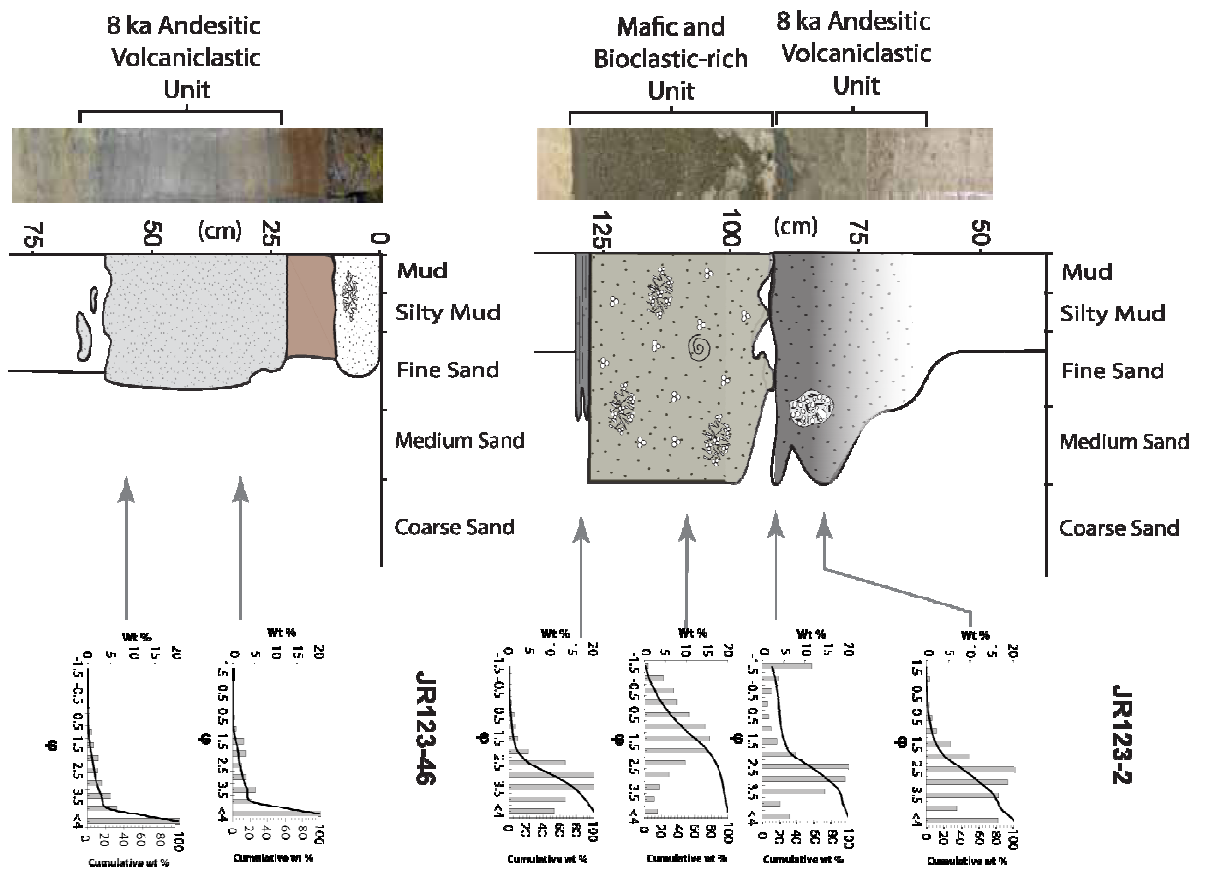


Figure 6. Core photograph, graphic log, grain size and component analysis data for JR123-2 and JR123-46

The volcanic centres on Montserrat can be discriminated from one another using trace-element and high-precision Pb isotopes (Cassidy et al., 2012). In particular Suite B of the South Soufrière Hills (SSH) volcanic centre has a distinctly different geochemical character, making it easy to distinguish from the other volcanic centres. This difference is highlighted by a Zr/Er versus Sr/La discriminant diagram (Figure 7) (Cassidy et al., 2012). Three samples were analysed for trace element concentrations from the Mafic and Bioclastic-rich Unit (MC14G, MC16G, MC16A) and two samples from the (Upper) 8 ka Andesitic Volcaniclastic Unit (MC13A, MC15A), these are plotted on Figure 7 (Table 2). Samples MC14G and MC16G from the Mafic and Bioclastic-rich Unit plot close together within the field defined by SSH Suite B (Cassidy et al. 2012). SSH Suite B is one of two geochemical suites that geochemically define the South Soufrière Hills volcanic centre. The South Soufrière Hills volcanic centre characteristically exhibits higher Sr/La values in comparison with the geochemical signature of the other volcanic centres on Montserrat (Cassidy et al., 2012). The other sample from the Mafic and Bioclastic-rich unit (MC16A) falls within the non-SSH group, it has lower Sr/La and higher Zr/Er values compared with the SSH and derives from the Soufrière Hills volcanic suite (Cassidy et al., 2012). Therefore the Mafic and Bioclastic-rich unit preserves evidence of a mixed provenance.

Table 2. Trace-element data for 4 picked samples from marine sediment core deposits

Latitude			16.6761	16.651	16.651	16.6761	16.651
Longitude			62.3272	62.2794	62.2794	62.3272	62.2794
Submarine core I.D.			JR123-2	JR123-3	JR123-3	JR123-2	JR123-3
Sample depth interval (cm)			113-114	133-134	133-134	88-89	75-76
			<i>Mafic and Bioclastic-rich Unit</i>			<i>Andesitic and Crystal-rich Unit</i>	
Trace elements	JA-2	% RSD	MC14G	MC16G	MC16A	MC13A	MC15A
<i>Li</i>	30.19	2.42	6.56	7.11	11.50	14.35	15.04
<i>Sc</i>	18.22	0.68	36.10	32.43	15.95	12.59	12.01
<i>Rb</i>	77.24	5.68	7.98	8.66	19.69	18.46	19.04
<i>Sr</i>	245.80	1.19	423.90	400.22	295.01	285.98	288.22
<i>Y</i>	17.68	1.66	18.90	16.45	18.16	23.23	22.15
<i>Zr</i>	120.70	5.06	53.28	52.01	80.82	83.51	87.80
<i>Nb</i>	8.93	0.59	1.47	1.50	2.82	3.36	3.31
<i>Cs</i>	5.17	3.58	0.20	0.27	0.63	0.56	0.61
<i>Ba</i>	319.20	0.92	118.85	115.07	223.40	242.64	244.47
<i>La</i>	16.00	0.44	5.01	4.95	9.98	11.00	11.49
<i>Ce</i>	33.28	0.88	12.21	11.52	20.85	24.25	24.71
<i>Pr</i>	3.81	1.94	1.80	1.63	2.64	3.16	3.82
<i>Nd</i>	14.47	1.30	8.56	7.49	10.72	13.23	13.86
<i>Sm</i>	3.11	0.25	2.46	2.09	2.49	3.17	2.97
<i>Eu</i>	0.90	0.92	0.90	0.81	0.94	1.06	1.01
<i>Gd</i>	3.02	0.34	2.95	2.48	2.67	3.43	3.58
<i>Tb</i>	0.48	0.43	0.48	0.41	0.43	0.55	0.52
<i>Dy</i>	2.90	0.12	3.08	2.63	2.75	3.49	3.58
<i>Ho</i>	0.59	1.98	0.65	0.56	0.59	0.74	0.72
<i>Er</i>	1.71	0.20	1.89	1.65	1.79	2.25	2.45
<i>Tm</i>	0.25	1.63	0.28	0.25	0.28	0.36	0.31
<i>Yb</i>	1.70	0.61	1.86	1.68	2.00	2.52	2.83
<i>Lu</i>	0.26	1.33	0.28	0.26	0.32	0.40	0.41
<i>Hf</i>	2.91	0.41	1.49	1.44	2.13	2.28	2.34
<i>Pb</i>	22.10	8.83	6.75	6.47	8.26	10.94	9.41
<i>Th</i>	4.85	2.17	0.92	1.07	2.38	2.73	2.86
<i>U</i>	2.26	1.76	0.37	0.38	0.75	0.85	0.88

Samples with the Suffix A =Andesite, G=Basaltic groundmass

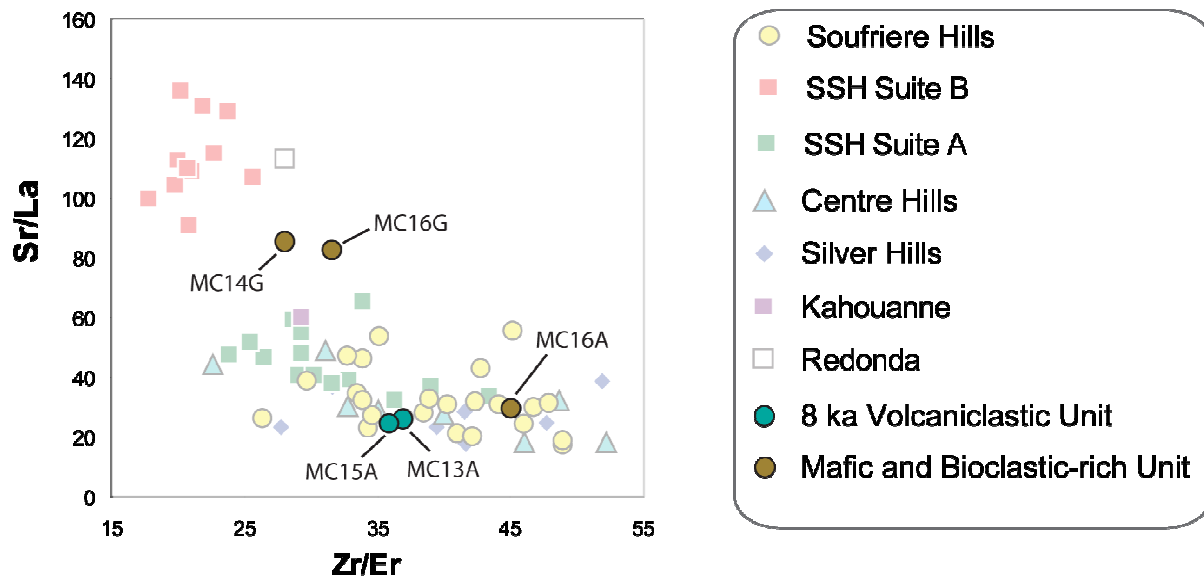


Figure 7. Discriminant diagram from Cassidy et al., (2012), with new units plotted on top.
Data from Table 2

3.4 Facies characteristics of the 8 ka Andesitic Volcaniclastic Unit

The 8 ka Andesitic Volcaniclastic Unit is widespread and is found in 7 marine cores offshore from the west to the southeast of Montserrat (Figure 3). A similar deposit thicknesses of around 30 cm is observed in most of the cores, but the deposit thins to <10 cm in a single core south east of Montserrat (core JCR123-48; Figure 3). The 8 ka Andesitic Volcaniclastic Unit is typified by weak normal grading, an erosive base and, in general, lacks tractional structures such as planar and cross bedding. The deposit exhibits poor to moderate sorting ($1.91 - 0.8 \sigma_\phi$) (Figures 4 and 6) and the mean grain size varies from silt-clay (4.12ϕ , 0.06 mm) to medium sand (1.51ϕ , 0.355), although rare large clasts (up to 100 mm) are found randomly distributed throughout the unit. The 8 ka Andesitic Volcaniclastic Unit is grey in appearance and comprises an abundance of crystals of feldspar, amphibole and pyroxene (56-66%), grey-coloured dense and poorly vesiculated andesite clasts (18-22%) and vesicular juvenile clasts (6-10%), altered andesite lava fragments, mafic and biogenic clasts are present in smaller proportions (<7%) (Figures 4 & 6). The volcanic clasts found within this unit are sub-angular to angular in shape and dominantly made up of fractured crystals (Figure 5). The andesitic clasts are porphyritic with 0.5 mm sized phenocrysts of pyroxene and feldspar making up 10-15% of the rock. The deposit is compositionally mature, generally lacking bioclastic material, altered dome material or any other clast type (Figures 4 & 6).

In core JCR123-2 (south west of Montserrat; Figure 3), the base of the unit is very poorly sorted ($1.91 \sigma_\phi$), displaying a polymodal grain size distribution, with peaks in the fine gravel $> -1.5 \phi$ (> 2.8 mm) and the fine sand (2.5ϕ to 3.5ϕ , $0.177 - 0.088$ mm) grain size categories, while the mean grain size is medium sand (1.51ϕ , 0.355 mm). The sorting improves towards the top of the unit ($0.8 \sigma_\phi$ in JCR123-3) as the deposit becomes less coarse grading to a fine sand grain size (2.83ϕ , 0.14 mm). In core JR123-46 southeast of Montserrat, the unit is composed of a much finer silt grain size (mean, 4.12ϕ , 0.06 mm) and it is moderately well sorted ($0.55 \sigma_\phi$), with diffuse stratification also present. The geochemical samples analysed from the 8 ka Andesitic Volcaniclastic Unit (MC13A and MC15A) are plotted on a Zr/Er versus Sr/La discriminant diagram in Figure 7 (Table 2), where they lie within the Soufrière Hills volcanic field (c.f. Cassidy et al., 2012).

4. Discussion

4.1 Source of the units

The Mafic and Bioclastic-rich Unit comprises a range of volcanic and biogenic debris. Volcanic clasts erupted from multiple eruptions as evidenced by the petrology, component analysis and the geochemical provenance of the volcanic clasts which show a wide geochemical variation between clasts (figure 7). There is also an abundance (6 – 20 %) of coarse-grained, predominantly shallow marine, biogenic material such as coral and mollusc shell fragments, which suggests the Mafic and Bioclastic-rich Unit originated, at least in part, from a shallow marine source (Trofimovs et al., 2010; Wilkinson and Drummond, 2004). Visual analysis and SEM imagery shows that much of the material found in the Mafic and Bioclastic-rich Unit is either sub-rounded volcanic clasts or fragmented angular biogenic material (Figure 5). The submarine shelf surrounding Montserrat hosts live coral reef systems (www.montserratreefproject.com), together with fragmented bioclastic sediment accumulations produced by storm and wave erosion of the coral. The shallow shelf also preserves deposits from pyroclastic flows into the ocean from the Soufrière Hills volcanic complex and reworked volcaniclastic material produced by the gradual erosion of the volcanic edifices (Le Friant et al., 2004). These account for all the components observed within the Mafic and Bioclastic-rich Unit as seen in the marine cores. We envisage a collapse of the shallow marine shelf around Montserrat as the source of the Mafic and Bioclastic-rich unit, similar to those documented in the Canary Islands (Masson et al., 2002; and references therein), although much smaller in scale.

The Mafic and Bioclastic-rich Unit's confined location and limited exposure (only in JCR123-2 and JCR123-3 cores) is consistent with the distribution of the very shallow, and

relatively small (0.3 km³) submarine debris avalanche deposit imaged in bathymetric surveys and seismic lines offshore the south east coast of Montserrat (Deposit 5 of Le Friant et al. 2004; Lebas et al. 2011; Figure 1). Deposit 5 is characterised by hummocky morphology on the sea floor and extends 9 km from the shore until it terminates at the base of a small submarine bathymetric high (Figure 1). Le Friant et al. (2004) suggest that Deposit 5 was sourced from a submarine embayment (C4; Figure 1), on the shallow marine shelf of Montserrat (Le Friant et al., 2004; their Figure 8a). This inferred source region correlates well with the cored geographic extent of the Mafic and Bioclastic unit and the components observed within the deposit.

The 8 ka Andesitic Volcaniclastic Unit appears to have originated from the south west of Montserrat, as the marine deposits found in the south west cores are generally thicker with coarser grain sizes, in comparison with the cores to the south and southeast. Provenance analysis of the 8 ka Andesitic Volcaniclastic Unit deposit did not detect significant geochemical heterogeneity. The deposit is compositionally mature with lithologically similar, sub-angular, porphyritic andesite lava clasts and crystal fragments (Figure 5). Consequently, we hypothesise that this deposit resulted from a primary volcanic event. The lack of intensely vesiculated clasts (>40%), suggests this was unlikely to have been a highly explosive eruption (Cashman and Managan, 1994), instead the abundance of dense and poorly vesiculated material suggests that the eruption was similar in character to the current style of eruptions of the Soufrière Hills volcano; such as dome collapse, pyroclastic flows and Vulcanian eruptions (c.f. Young et al. 1998; Cole et al., 2002). The minor mafic and bioclastic component of the deposit may be explained by small amounts of erosion and entrainment of material from the shelf, given that the radiocarbon dating has shown that 8.5 cm of underlying seafloor strata was eroded beneath the 8 ka Andesitic Volcaniclastic Unit in core JR123-1. The presence of mafic clasts may also be explained by the inclusion of mafic enclaves, which are commonly erupted with the andesites from the Soufrière Hills volcano (Devine et al., 1998; Murphy et al., 1998, 2000).

4.2 Reconstructing the emplacement mechanisms

The sedimentological characteristics of both the 8 ka Andesitic Volcaniclastic Unit and the Mafic and Bioclastic-rich Unit can be used to reconstruct the processes that led to their submarine emplacement. The units are normally-graded, but generally poorly-sorted, with coarse clasts (>50 mm) found throughout. Additionally, they generally lack structures such as cross-bedding and planar laminae. This suggests that both the 8 ka Andesitic Volcaniclastic

Unit and the Mafic and Bioclastic-rich Unit were emplaced by high sediment-concentration turbidity currents (Lowe, 1982). These turbulent gravity-driven flows are essentially defined by their structureless nature, as the high sediment concentration within the flow hinders the formation of well-defined tractional structures and vertical grading, and traps a proportion of the finer particles within the bulk of the flow due to suppressed sediment fallout rates from hindered settling (Lowe, 1982; Mutti et al., 1992; Mulder and Alexander, 2001).

4.2.1 The Mafic and Bioclastic-rich Unit

The Mafic and Bioclastic-rich Unit was emplaced prior to the 8 ka Andesitic Volcaniclastic unit, between 8 and 35 ka. As observed in core JR123-2 the base of the unit preserves a fine-grained, moderately-sorted, thin turbidite with diffuse laminations, suggesting that the collapse started with a low sediment concentration turbidity current (Mulder and Alexander, 2001). Above this subunit are multiple stacked normally-graded beds of coarse-grained and poorly-sorted turbidites. Some of the subunits within the turbidite are moderately-sorted reflecting a change in the flow regime, showing fluctuation between high and low sediment concentration turbidity currents. The basal grain sizes of the stacked graded turbidites do not become finer up-sequence, which suggests that the individual turbidites are not the result of flow reflection but original turbidity currents from source (Garcia, 1996; Wynn and Masson, 2003). Moreover, the bathymetry lacks discrete flow channels between the south western shelf of Montserrat to the cored locality (Le Friant et al., 2004). Hence it is unlikely that the flow partitioned into multiple flows and followed different pathways, only to be emplaced in the same location. Thus the evidence suggests the collapse involved multiple failures at source. Each stacked bed exhibits normal grain size grading which suggests waning flow energy within each pulse (Branney & Kokelaar 1992; Kneller and Branney, 1995; Mulder and Alexander, 2001; Kneller and McCaffery, 2003).

The uppermost subunit of the Mafic and Bioclastic-rich Unit is finer-grained, poorly to moderately-sorted with porous bioclastic fragments (such as coral) and hemipelagic mud rip-up clasts. This subunit may represent the waning stages of the entire collapse and may also be graded by density, as the high energy turbidity current eroded and entrained hemipelagic mud and coarse bioclastic fragments at the base of the flow upslope from the final deposit, with the less dense clasts migrating to the top of the flow and subsequent deposit during transport.

4.2.2 The 8 ka Andesitic Volcaniclastic Unit

The 8 ka Andesitic Volcaniclastic Unit exposed in the south western cores is coarser grained, structureless and poorly-sorted and thus also exhibits characteristics consistent with

emplacement from a high-concentration turbidity current (Mulder and Alexander, 2001). However, towards the south east, the deposit becomes thinner, better-sorted and finer-grained (Figure 3). The south eastern cores also preserve planar laminations, implying that the turbidity current was less particle rich in this region (Bouma, 1962; Baas et al. 2005). The finer top of the 8 ka Andesitic Volcaniclastic Unit, suggests that the flow waned in energy at the tail end of the flow (Kneller and McCaffery, 2003).

The composition of the 8 ka Andesitic Volcaniclastic Unit gives some clues as to how this primary volcanic event evolved into a high-concentration turbidity current. The 8 ka Andesitic Volcaniclastic Unit is very crystal-rich (56 - 66%) and it is depleted in pumice and shards in comparison to typical subaerial pyroclastic flow deposits (cf. Walker, 1972). The clasts found in the deposit are sub-angular to angular and contain a high proportion of juvenile dome clasts. These characteristics are very similar to facies seen in other settings which have been interpreted as pyroclastic flows entering the water. Such features have also been observed in deposits from other islands in the Lesser Antilles, for example the Roseau eruption in Dominica (Whitham, 1989). Whitham (1989) records an increase in the crystal to lithic ratio in the marine deposits compared to the subaerial pyroclastic units and suggests that this is a product of quench fragmentation. This process produces a high proportion of broken, angular crystals and volcanic clasts (Cole and DeCelles, 1991), similar to those observed in the 8 ka Andesitic Volcaniclastic Unit. The crystal enrichment typically observed in ignimbrites (e.g., Walker, 1972) could be further enhanced by the loss of finer material, such as ash and glass shards, in ash plumes created by littoral explosions as the pyroclastic flow interacted with the ocean at the shoreline. This was observed during the 2003 dome collapse of the Soufrière Hills volcano when dome collapse pyroclastic flows entered the ocean off the east coast of the island (Edmonds and Herd, 2005; Trofimovs et al., 2008). The entrance of the pyroclastic flow into the ocean leads to the generation of subaqueous sediment gravity flows (e.g., Kneller and Branney, 1995) in which fine (shard) and light (pumice) components were effectively separated from the basal subaqueous crystal-rich mass flows.

There are two main theories for how pyroclastic flows behave upon entrance into sub aqueous environment; 1) that the pyroclastic flows can maintain their heat by forming a carapace of gas trapped between the grains, thus keeping the interior of the flow hot and gas supported without mixing with water (Sparks 1980). This is evidenced by high-temperature emplacement and welded submarine features (Mandeville et al., 1994; White and McPhie, 1997; Kokelaar and Königer, 2000), and 2) that the pyroclastic flows ingest significant amounts of water to form cool, water-supported density currents, which evolved into more dilute turbidity currents (Whitham, 1989; Cole & DeCelles, 1991; Freundt, 2003; Trofimovs et

al., 2006, 2008). Although quench fragmentation likely occurred when the 8 ka Andesitic Volcaniclastic Unit first interacted with the water, there is neither textural nor lithofacies evidence to support high-temperature emplacement. Therefore the evidence given in this study suggests that the initially hot pyroclastic flow evolved into a water-supported density current upon entrance into the ocean. This process is analogous to pyroclastic turbidite deposition from the 2003 dome collapse of the Soufrière Hills volcano (Trofimovs et al., 2006; 2008).

4.3 Timing of events

Upon reconstruction of the eruption history of the Soufrière Hills volcano on Montserrat, Smith et al. (2007) record a hiatus of volcanic activity between Subunit III (16 ka) and IV (4 ka). Similarly, Le Friant et al. (2008) record eruptions at 16 ka and 6 ka from their tephrochronological studies of distal submarine core (Figure 2), with a gap between the activity. In contrast, the primary volcanic event reported in this chapter (8 ka Andesitic Volcaniclastic Unit) is dated at ~8.4 ka and therefore represents a new eruption in the history of the volcano. If this hypothesis is correct, then it suggests that the Soufrière Hills volcano was more active in this period than previously recognised.

The Mafic and Bioclastic-rich Unit directly underlies the 8 ka Andesitic Volcaniclastic Unit, without any intervening hemipelagic sedimentation, making the depositional date for this event difficult to constrain. However, a single AMS radiocarbon date obtained from a hemipelagic sediment clast ripped up and incorporated into the flow that deposited the Mafic and Bioclastic-rich Unit provided an age of 35.8 ka \pm 0.7. Hemipelagic sediment below the Mafic and Bioclastic Unit has been dated at 42.9 ka \pm 1.0, suggesting ~7 - 11 cm of erosion of hemipelagic material. When the 8 ka Andesitic Volcaniclastic Unit is present in cores without the Mafic and Bioclastic-rich Unit beneath it, the ages below it range from 39.7 ka \pm 1.0 BP to 41.8 \pm 0.5 ka BP. This illustrates that erosion of hemipelagic sediment is observed both when the two units are found together and when only the 8 ka Andesitic Volcaniclastic Unit is exposed. This may indicate that these events were potentially separated in time by ~27.4 kyr and that the hemipelagic sediment was eroded by the later 8 ka Andesitic Volcaniclastic Unit.

5. Conclusions

In this chapter we describe a bioclastic-rich flow, (the Lower Mafic and Bioclastic-rich Unit), that was likely derived from a shelf collapse in the south west of Montserrat, and a primary pyroclastic volcanic event dated at ~8.4 ka (the Upper 8ka Andesitic Volcaniclastic

Unit), that most likely formed from an andesitic lava dome collapse towards the south west of Montserrat. Both flows were emplaced within the marine environment as high sediment concentration turbidity currents. The proposed shelf collapse deposit closely matches the debris avalanche deposits discovered by seismic acoustic surveys and bathymetry and allows us to constrain the age of this event to between 8.4 and 35.7 ka. The ~8 ka Andesitic Volcaniclastic Unit likely represents a pyroclastic flow which underwent quench fragmentation as the hot flow interacted with the cold seawater. The flow rapidly mixed with the ocean water to become water-supported gravity-driven density flow, which resulted in a crystal-rich volcaniclastic deposit. Identification of this primary volcanic event adds to the eruptive history of Montserrat in a period when the Soufrière Hills volcano was considered quiescent.

References

- Baas, J.H., W.D. McCaffrey, P.D.W. Haughton and C. Choux (2005) "Coupling between suspended sediment distribution and turbulence structure in a laboratory turbidity current" Journal of Geophysical Research-Oceans **110**
- Boudon, G., A. Le Friant, J.C. Komorowski, C. Deplus and M.P. Semet (2007) "Volcano flank instability in the lesser Antilles arc: diversity of scale, processes, and temporal recurrence" Journal of Geophysical Research-Part B-Solid Earth B08205-1-28
- Branney, M.J. and P. Kokelaar (1992) "A reappraisal of ignimbrite emplacement - Progressive aggradation and changes from particulate to nonparticulate flow during emplacement of high-grade ignimbrite" Bulletin of Volcanology **54** 504-520
- Cashman, K.V. and M.T. Mangan (1994) "Physical aspects of magmatic degassing 2. Constraints on vesiculation processes from textural studies of eruptive products" Volatiles in Magmas **30** 447-478
- Cassidy, M., Trofimovs, J., Watt, S.F.L., Palmer, M.R., Taylor, R.N., Gernon, T.M., Talling, P.J., Le Friant, A. (in press) "Multi-stage collapse events in the South Soufrière Hills, Montserrat, as recorded in marine sediment cores" In G. Wadge, Robertson, R., Voight, B., (eds) *The eruption of Soufrière Hills volcano, Montserrat from 2000 to 2010* Memoir of the Geological Society, London

Cassidy, M.T., R.N., Palmer, M.R, Cooper, R., Stenlake C., Trofimovs, J. (2012) "Tracking the magmatic evolution of island arc volcanism: Insights from a high-precision Pb isotope record of Montserrat, Lesser Antilles" Geochemistry Geophysics Geosystems

Cole, P.D., Calder, E.S., Sparks, R.S.J., Clarke, A.B., Druitt, T.H., Young, S.R., Herd, R.A., Harford, C.L. and Norton, G.E (2002) "Deposits from dome-collapse and fountain-collapse pyroclastic flows at Soufrie`re Hills Volcano, Montserrat. In: The Eruption of Soufrie`re Hills Volcano, Montserrat, from 1995 to 1999 (Eds T.H. Druitt and B.P. Kokelaar)" Geol. Soc. London Mem. **21** 231-261

Cole, R.B. and P.G. Decelles (1991) "Subaerial to submarine transitions in early Miocene pyroclastic flow deposits, southern San Joaquin basin, California" Geological Society of America Bulletin **103** 221-235

DeMets, C., P.E. Jansma, G.S. Mattioli, T.H. Dixon, F. Farina, R. Bilham, E. Calais and P. Mann (2000) "GPS geodetic constraints on Caribbean-North America plate motion" Geophysical Research Letters **27** 437-440

Devine, J.D., M.D. Murphy, M.J. Rutherford, J. Barclay, R.S.J. Sparks, M.R. Carroll, S.R. Young and J.E. Gardner (1998) "Petrologic evidence for pre-eruptive pressure-temperature conditions, and recent reheating, of andesitic magma erupting at the Soufriere Hills Volcano, Montserrat, WI" Geophysical Research Letters **25** 3669-3672

Druitt, T.H. and B.P. Kokelaar (2002) "The eruption of the Soufrière Hills Volcano, Montserrat 1995 to 1999" The Geological Society Memoirs, London **21**

Edmonds, M. and R.A. Herd (2005) "Inland-directed base surge generated by the explosive interaction of pyroclastic flows and seawater at Soufriere Hills volcano, Montserrat" Geology **33** 245-248

Feuillet, N., F. Leclerc, P. Tapponnier, F. Beauducel, G. Boudon, A. Le Friant, C. Deplus, J.F. Lebrun, A. Nercessian, J.M. Saurel and V. Clement (2010) "Active faulting induced by slip partitioning in Montserrat and link with volcanic activity: New insights from the 2009 GWADASEIS marine cruise data" Geophysical Research Letters **37** 6

Freeman, S.P.H.T., A. Dougans, L. McHargue, K.M. Wilcken and S. Xu (2008) "Performance of the new single stage accelerator mass spectrometer at the SUERC" Nuclear Instruments & Methods in Physics Research Section B-Beam Interactions with Materials and Atoms **266** 2225-2228

- Freundt, A. (2003) "Entrance of hot pyroclastic flows into the sea: experimental observations" Bulletin of Volcanology **65** 144-164
- Garcia, M.O. (1996) "Turbidites from slope failure on Hawaiian volcanoes" Geological Society London Special Publication **vol. 110** 281-294
- Harford, C.L., Pringle, M.S., Sparks, R.S.J., Young S.R. (2002) "The volcanic evolution of Montserrat using $^{40}\text{Ar}/^{39}\text{Ar}$ geochronology." In T. H. Druitt, Kokelaar, B.P. (eds) *The eruption of Soufrière Hills Volcano, Montserrat, from 1995 to 1999* Geological Society of London Memoirs **21** 93-113
- Kneller, B.C. and M.J. Branney (1995) "Sustained high-density turbidity currents and the deposition of thick massive beds" Sedimentology **42** 607-616
- Kneller, B.C. and W.D. McCaffrey (2003) "The interpretation of vertical sequences in turbidite beds: The influence of longitudinal flow structure" Journal of Sedimentary Research **73** 706-713
- Kokelaar, P. and S. Koniger (2000) "Marine emplacement of welded ignimbrite: the Ordovician Pitts Head Tuff, North Wales" Journal of the Geological Society **157** 517-536
- Le Friant, A., C. Deplus, G. Boudon, R.S.J. Sparks, J. Trofimovs and P. Talling (2009) "Submarine deposition of volcaniclastic material from the 1995-2005 eruptions of Soufrière Hills volcano, Montserrat" Journal of the Geological Society **166** 171-182
- Le Friant, A., C.L. Harford, C. Deplus, G. Boudon, R.S.J. Sparks, R.A. Herd and J.C. Komorowski (2004) "Geomorphological evolution of Montserrat (West Indies): importance of flank collapse and erosional processes" Journal of the Geological Society **161** 147-160
- Le Friant, A., E.J. Lock, M.B. Hart, G. Boudon, R.S.J. Sparks, M.J. Leng, C.W. Smart, J.C. Komorowski, C. Deplus and J.K. Fisher (2008) "Late Pleistocene tephrochronology of marine sediments adjacent to Montserrat, Lesser Antilles volcanic arc" Journal of the Geological Society **165** 279-289
- Lebas, E., A. Le Friant, G. Boudon, S.F.L. Watt, P.J. Talling, N. Feuillet, C. Deplus, C. Berndt and M.E. Vardy (2011) "Multiple widespread landslides during the long-term evolution of a volcanic island: Insights from high-resolution seismic data, Montserrat, Lesser Antilles" Geochemistry Geophysics Geosystems **12**

Lowe, D.R. (1982) "Sediment gravity flows 2. Depositional models with special reference to the deposits of high-density turbidity currents" Journal of Sedimentary Petrology **52** 279-298

Mandeville, C.W., S. Carey and H. Sigurdsson (1996) "Sedimentology of the Krakatau 1883 submarine pyroclastic deposits" Bulletin of Volcanology **57** 512-529

Mulder, T. and J. Alexander (2001) "The physical character of subaqueous sedimentary density flows and their deposits" Sedimentology **48** 269-299

Mutti, E. (1992) "Turbidite Sandstones" AGIP 275 pp.

Reid, R.P., S.N. Carey and D.R. Ross (1996) "Late quaternary sedimentation in the Lesser Antilles island arc" Geological Society of America Bulletin **108** 78-100

Roobol, M.J. and A.L. Smith (1998) "Pyroclastic stratigraphy of the Soufriere Hills volcano, Montserrat - Implications for the present eruption" Geophysical Research Letters **25** 3393-3396

Slota, P.J., A.J.T. Jull, T.W. Linick and L.J. Toolin (1987) "Preparation of small samples for C-14 accelerator targets by catalytic reduction of CO" Radiocarbon **29** 303-306

Smith, A.L.R., M.J. Schellekens, J.H. & Mattioli, G.S. (2007) "Prehistoric stratigraphy of the Soufriere Hills-South Soufriere Hills volcanic complex, Montserrat, West Indies" Journal of Geology **115** 115-127

Sparks, R.S.J., Sigurdsson, H. and Carey, S. (1980) "The entrance of pyroclastic flows into the sea. II. Theoretical considerations on subaqueous emplacement and welding.

" J. Volcanol. Geoth. Res. **7** 97-105

Trofimovs, J., Fisher, J. K., Macdonald, H. A., Talling, P. J., Sparks, R. S J., M. B. Hart, C. W. Smart, G. Boudan, C. Deplus, J.C. Komorowski, A. Le Friant, S. G. Moreton, M. J. Leng (2010) "Evidence for carbonate platform failure during rapid sea-level rise; ca 14 000 year old bioclastic flow deposits in the Lesser Antilles" Sedimentology **57** 735 - 759

Trofimovs, J., L. Amy, G. Boudon, C. Deplus, E. Doyle, N. Fournier, M.B. Hart, J.C. Komorowski, A. Le Friant, E.J. Lock, C. Pudsey, G. Ryan, R.S.J. Sparks and P.J. Talling (2006) "Submarine pyroclastic deposits formed at the Soufriere Hills volcano, Montserrat (1995-2003): What happens when pyroclastic flows enter the ocean?" Geology **34** 549-552

- Trofimovs, J., R.S.J. Sparks and P.J. Talling (2008) "Anatomy of a submarine pyroclastic flow and associated turbidity current: July 2003 dome collapse, Soufriere Hills volcano, Montserrat, West Indies" Sedimentology **55** 617-634
- Wadge, G. (1984) "Comparison of volcanic production-rates and subduction rates in the Lesser Antilles and Central America" Geology **12** 555-558
- Walker, G.P.L. (1972) "Crystal concentration in Ignimbrites" Contributions to Mineralogy and Petrology **36** 135-&
- Watt, S.F.L., Talling, P.J., Vardy, M.E., Heller, V., Huhnerbach, V., Urlaub, Morelia, Sarkar, Sudipta, Masson, D.G., Henstock, T.J., Minshull, T.A., Paulatto, M., Le Friant, A., Lebas, E., Berndt, C., Crutchley, G., Karstens, J., Stinton, A and Maeno, F (2012) "Combinations of volcanic-flank and seafloor-sediment failure offshore Montserrat, and their implications for tsunami generation" Earth and Planetary Science Letters **319-320** 228-240
- White, M.J. and J. McPhie (1997) "A submarine welded ignimbrite crystal-rich sandstone facies association in the Cambrian Tyndall Group, western Tasmania, Australia" Journal of Volcanology and Geothermal Research **76** 277-295
- Whitham, A.G. (1989) "The behaviour of subaerially produced pyroclastic flows in a subaqueous environment: evidence from the Roseau eruption, Dominica, West Indies" Marine Geology **86** 27-40
- Wilkinson, B.H. and C.N. Drummond (2004) "Facies mosaics across the Persian Gulf and around Antigua - Stochastic and deterministic products of shallow-water sediment accumulation" Journal of Sedimentary Research **74** 513-526
- Wynn, R.B.M., D. G. (2003) "Canary island landslides and tsunami generation: can we use turbidite deposits to interpret landslide processes." Kluwer Academic Publishers **325-332**
- Xu, S., R. Anderson, C. Bryant, G.T. Cook, A. Dougans, S. Freeman, P. Naysmith, C. Schnabel and E.M. Scott (2004) "Capabilities of the new suerc 5MV AMS facility for C-14 dating" Radiocarbon **46** 59-64
- Young, S.R., R.S.J. Sparks, W.P. Aspinall, L.L. Lynch, A.D. Miller, R.E.A. Robertson and J.B. Shepherd (1998) "Overview of the eruption of Soufriere Hills volcano, Montserrat, 18 July 1995 to December 1997" Geophysical Research Letters **25** 3389-339

CHAPTER 5

ADVANCES IN THE CONSTRUCTION OF VOLCANIC RECORDS FROM MARINE SEDIMENT CORES: A REVIEW AND CASE STUDY (MONTSERRAT, WEST INDIES)

This chapter forms the basis of a manuscript in preparation with the following authors: Cassidy, M., Trofimovs, J., Palmer, M.R., Symons W., Taylor, R.N. Moreton, S. (to be submitted 2012).

Written by M Cassidy, but I received feedback from Trofimovs and Palmer. Symons carried out the component analysis by point counting clasts within core JC18-19 as part of his MGeol project conceived and supervised Cassidy and Palmer. Moreton undertook the AMS radiocarbon dating at the NERC radiocarbon facility (Environment).

Abstract

In this contribution we test and review techniques for generating volcanic eruption records from marine sediment cores. The data are presented using cores sampled proximally (8-14 km) and distally (55 km) south and south west offshore the volcanic island of Montserrat as a case study. Volcanism on Montserrat has been well-characterised by numerous studies detailing the subaerial and submarine geology, which provides a well-defined platform from which to assess the submarine volcanic products. These cores have been analysed to assess the variety of primary and secondary volcanic facies observed within the sediments; e.g. Pyroclastic ash fall, primary volcanoclastic gravity flows and reworked volcanoclastic deposits. Visible tephra deposits identified by fundamental sedimentological logging were used to test the effectiveness of different tephra detection techniques, such as, point counting component analysis, colour spectrophotometry, grain size measurements, XRF core scanning, magnetic susceptibility and X-radiography. These techniques were assigned an efficiency rating based on their ability to detect the identified visible tephra. The most efficient techniques were then applied to sections of the marine sediment cores where no visible tephra layers were present in order to determine the presence of cryptotephra and thus provide a complete record of visible and non-visible tephra horizons.

Based on these studies we suggest the following protocol for generating volcanic records from submarine sediment cores: (1) visual sedimentological logging visual tephra, (2) the use of time-efficient, non-destructive techniques that are able to detect and locate

potential tephra tephras horizons (e.g., XRF core scanning and magnetic susceptibility), (3) sampling of targeted horizons for component analysis to discriminate between primary and reworked volcanic deposits (this has been achieved here by using specific criteria related to glass shard morphology, compositional maturity, sorting and sedimentological facies indicators), and (4) a robust framework must then be developed to provide absolute dates for the tephrastatigraphy (here, hemipelagic material was dated using AMS radiocarbon on foraminifera when younger than 47 ka and, for older hemipelagic sediment deposits, an oxygen isotope stratigraphy was developed from bulk carbonate material and benthic foraminifera).

The outcome of this tephra chronological study is unprecedented detail of four periods of heightened volcanic activity on Montserrat in the last ~130 ka. More discrete volcanic events have been recognised than previous marine tephrChronological studies in the region. In addition, this work critically evaluates the problems and limitations of generating volcanic records from marine sediments, however we show that good stratigraphic and analytical practices, coupled with good core coverage, can achieve a more complete record of volcanic events than can be obtained from terrestrial studies alone.

1. Introduction

1.1 Rationale and aims

The vast majority of volcanoes are situated close to the sea so a high proportion of volcanic material enters the oceans through a variety of mechanisms. Marine sediment cores are, hence, widely used to reconstruct eruptive records of volcanoes because sub-aerial eruption histories can be hindered by poor preservation of rock exposures due to erosion or burial by later volcanic material. The marine record thus provides a good medium by which to assess the periodicity of eruptions and potential hazards posed by a volcano e.g. the Campanian Ignimbrite eruption (Pyle et al., 2006). Although construction of such volcanic records from marine sediment core is important, they are susceptible to erroneous analysis and variations in interpretation. For example, inadequate tephra detection techniques can overlook thin tephra layers or those invisible to the naked eye (cryptotephras) or, can lead to the interpretation of reworked volcanoclastic deposits as primary volcanic events. These issues can therefore lead to reconstruction of inaccurate records of volcanism and false chronostratigraphic marker horizons.

The methods used to detect, date and characterise volcanic deposits have rapidly advanced in the last few decades (Lowe et al., 2011), particularly as tephras become increasingly recognised as useful isochronous markers for constructing past climatic records.

It is important, however, to identify which of this wealth of new methodologies and improved technology is most effective in developing comprehensive tephrostratigraphy reconstructions. Here, we test and review some of the most widely-used techniques employed to generate volcanic records from marine sediment cores; including, correlating proximal volcanic units, detecting cryptotephra, geochronology and characterising the volcanoclastic deposit origins. These methods are described in detail using a case study of marine sediment cores sampled proximally (7-15 km) and distally (55 km) offshore Montserrat in the West Indies (Figure 1).

Montserrat is an especially useful example, as the submarine system has been well studied from geophysical surveys (Le Friant et al., 2004, 2009; Lebas et al., 2011; Watt et al., 2012) and submarine sediment analysis (Trofimovs et al., 2006, 2008, 2010; Le Friant et al., 2008, 2009, 2010; Cassidy et al., in press, in prep). In addition, the subaerial record of volcanism and igneous geochemistry is particularly well-constrained (Rea, 1974; Roobol and Smith, 1998; Harford et al., 2002; Zellmer et al., 2003; Smith et al., 2007; Cassidy et al., 2012, in press). This study builds on this previous work, on and offshore Montserrat with the aim to understand better the preservation and detection of volcanic sedimentation in the marine environment around volcanic islands. Our review of good tephrochronological practice and techniques has implications for tephrochronological research and marine volcanic studies globally.

1.2 Terminology

Ideally tephrochronological studies are multidisciplinary undertakings. We therefore provide an overview of terminology used herein for reference and note that processes and products from different research backgrounds, e.g. physical volcanology and sedimentology, may be applied across different disciplines.

Volcanology

'Tephra' is a term derived from a Greek word for ash, it is the collective term for all the unconsolidated pyroclastic products of a volcanic eruption, it includes all grain sizes from fine ash (<0.06 mm) to blocks and bombs (>64 mm) (Froggatt and Lowe, 1990; Lowe and Hunt, 2001). 'Pyroclastic' is the collective term for clastic or fragmentary material, welded to non-welded, explosively ejected from a volcanic vent (Froggatt and Lowe, 1990).

'Cryptotephra' are tephra layers that are not visible to the naked eye, often preserved as concentrations of glass shards or crystal fragments (Lowe and Hunt, 2001). 'Volcanoclastic' describes particles formed by the fragmentation of volcanic rocks, reworked or primary that were once sourced from a volcanic eruption (Carey, 2000). 'Primary volcanic' represents an eruption deposit with volcanic origin that has not been eroded and redeposited (Cas and Wright, 1987). 'Reworked volcanoclastic' describes previously erupted material that has been

eroded, transported and redeposited (Cas and Wright, 1987). 'Pyroclastic Airfall' is the rain-out of clasts through the atmosphere from an eruption jet or plume during an explosive eruption (Walker, 1971; Houghton et al., 2000). 'Pyroclastic density currents' are gravity controlled, laterally moving mixture of pyroclasts and gas (Wilson and Houghton, 2000; Branney and Kokelaar, 2002). A high-concentration pyroclastic density current is often referred to as a 'pyroclastic flow', where most of the material and momentum is contained in a basal concentrated particulate dispersion (Wilson and Houghton 2000). A low-concentration pyroclastic density current is often referred to as a pyroclastic surge (Valentine and Fisher 2000). 'Lahars' are mudflows of volcanic material produced as surface water mixes with unconsolidated primary volcanic deposits and may be transported to the ocean (Hampton, 1975, 1979; Iverson, 1997).

Sedimentology

The term 'Turbidity current' refers to a dilute gravity flow, where fluid turbulence is the dominant support mechanism (Kneller and Buckee, 2000; Mulder and Alexander, 2001). Their deposits, known as turbidites, result from progressive aggradation, accumulating clasts in a layer-by-layer fashion (Kuenen, 1966; Walker, 1969; Allen, 1971). This layer-by-layer accumulation leads to vertical grading unless the flow becomes unsteady (Amy and Talling, 2006; Talling et al., 2007). Subaerially erupted pyroclastic flows can become turbidity currents upon entrance into the ocean (Trofimovs et al., 2006; 2008). 'Debris flows' are water-saturated mixtures with large sediment concentrations that move down-slope as a laminar or weakly turbulent flow, where grain to grain interactions dominate particle support (Iverson, 1997; Vallance, 2000; Mulder and Alexander, 2001). 'Debris avalanche' is the product of a large-scale collapse of a sector of a volcanic edifice under water-undersaturated conditions. Debris avalanches are flows of cohesionless blocks, where grain-to-grain interaction is inferred to be the dominant mechanism of fragmentation and particle support (Masson et al., 2006). They are typified by depressional scars at the source and hummocky topographic features (Ui et al., 2000). Compositional maturity is a term used to describe the degree of variance of different components, such as glass shards or mafic clasts. A compositionally mature deposit would comprise a predominance in one or two components which originate from similar source, whereas a compositionally immature deposit contains different clast types derived from several different sources (Hsü, 2004).

1.3 Volcanic sedimentation in oceanic settings

Volcanic material can enter the ocean in a number of ways; 1) airfall from explosive volcanic eruptions, 2) primary volcanic flows, such as lahars or pyroclastic density currents, and 3) reworked volcanic material transported by subaerial and submarine collapses, gradual erosion by rivers and wind, ocean currents and, in colder settings, Ice-Rafted Debris (IRD).

1.3.1 Primary airfall ash deposits

Explosive eruptions, especially phreatomagmatic or Plinian eruptions may transport volcanic material (tephra) large distances (Walker et al. 1971; Wilson and Walker, 1987). The degree of fragmentation of volcanic material (size of the particles), weather conditions, and height and energy of the eruptive plume control the distribution and extent of ash fallout (Sparks et al., 1997). Airfall deposits are most useful for tephrochronology as the tephra can be emplaced within a short timescale and over a wide area in the oceanic setting. Upon reaching the surface of the ocean, both field studies and experiments suggest that tephra sinks up to 1-3 orders of magnitude faster than Stokes Law settling due to the generation of vertical density currents (Carey, 1997; Manville and Wilson, 2004). This is reflected in the tephra deposits themselves, which commonly exhibit sharp bases, with bioturbated or gradational upper contacts and abundances of fresh glass. The rapid sedimentation of tephra deposits in the marine setting also lessens the effect of ash being re-mobilised by ocean currents (Carey, 1997).

1.3.2 Primary Volcaniclastic flow deposits

In settings where the volcanic source is proximal to the ocean, explosive eruptions may produce pyroclastic density currents into the ocean originating from the collapse of vertical ash columns (e.g. Fisher and Heiken, 1982; Sparks et al., 1997). Extrusive lava domes may also collapse to form block-and-ash pyroclastic flows into the ocean (e.g. Montserrat; Young et al. 1998; Cole et al., 2002; Trofimovs et al., 2006). Lahars result from surface water mixing with unconsolidated volcanic deposits and may be transported to the ocean (Iverson 1997). Such mass flow deposits generated by these processes are often preserved as thick volcaniclastic deposits (relative to airfall deposits) within the sedimentological record, especially proximal to the source (Wynn and Masson, 2003). Flow deposits can also be distinguished from primary airfall pyroclastic deposits by the presence of tractional structures, such as cross- and planar-laminae, grading, mud caps, erosive bases and (or) poor sorting (Bouma 1962; Kneller and Buckee, 2000; Mulder and Alexander 2001).

Pyroclastic density current deposits may also preserve a high proportion of crystals relative to lithics, as fragmented crystals and shards form when hot pyroclasts rapidly chill and quench fragment as they contact seawater (Whitham 1989). The pyroclastic density current may remain hot and gas supported as it enters the water as steam forms an insulating carapace around the flow, preventing mixing with the ocean water (Sparks et al., 1980a, b). This can lead to the formation of a welded ash interior and a non-welded basal region (Kokelaar & Königer, 2000; White & McPhie, 1997). Alternatively, the flow may mix rapidly with the water to become a cool, water-supported gravity current, similar in character to

submarine turbidity currents (Witham, 1989; Cole & DeCelles, 1991; Freundt, 2003; Trofimovs et al., 2006, 2008).

Volcaniclastic deposition in the marine environment is strongly controlled by original source conditions and submarine topography (bathymetry). For example, if sediments are sampled on bathymetric highs they are more likely to contain ash fall deposits, whereas sediments sampled in submarine canyons and basins would likely comprise more sediment gravity flow deposits. The analysis of these different types of volcaniclastic deposits has both advantages and limitations when it comes to reconstructing volcanic events. For example, volcaniclastic flow deposits are generally thicker and thus more likely to be preserved, but they can be erosional and therefore underlying substrate may be missing, leading to the generation of an incomplete record. Conversely, airfall deposits are not erosional and can form stacked sequences of readily datable material in the marine realm. However the deposits may be thin and (or) invisible to the naked eye. Such deposits are susceptible to partial or complete bioturbation (e.g. Wetzel 2009) and are therefore hard to recognise in sediment cores.

1.3.3 *Reworked Volcaniclastic deposits*

Volcanic material can be emplaced on the sea floor without a primary eruption occurring. Previously erupted material is commonly transported into the oceans, particularly in volcanically active regions such as the Lesser Antilles, through wind, surface water and wave action that can all gradually erode and remobilise volcanic edifices and islands (Sigurdsson et al., 1980; Carey and Sigurdsson 1984; Fisher and Schminke 1994; Reid et al., 1996; Le Friant et al., 2004). In addition, potentially catastrophic sector collapses can remobilise large volumes of volcaniclastic debris into the sea over a relatively short time (Moore 1994; Masson et al., 2006). The Canary islands, Hawaii, Reunion and Lesser Antilles all have recorded sector collapses, from the subaerial edifice (Moore 1994; Masson 1996, Deplus et al., 2001; Masson et al., 2002; Boudon et al., 2007; Trofimovs et al., 2006, 2008, 2012; Hunt et al., 2011; Cassidy et al., in press) and/or submarine shelf collapses (Moore 1989; Trofimovs et al., 2010, Lebas et al., 2011; Watt et al., 2012; Cassidy et al., in prep). Large landslides of this nature may produce debris avalanches containing large blocks that can be tens of metres in length large enough to be visible in sea floor bathymetric surveys (Siebert 1984; Ui et al., 1986; Le Friant et al., 2004; Lebas et al., 2011). As landslides propagate and lose energy, they deposit their larger blocks at the slope-break at the base of the submarine volcanic flanks. The submarine avalanche can evolve into poorly-sorted, mud-rich debris flows, flowing as a laminar pulse or a weakly turbulent flow, in which grain-to-grain interactions maintain particles in suspension (Iverson, 1997; Mulder and Alexander, 2001). The debris flows can evolve into turbidity currents via flow dilution due to particle

sedimentation and water entrainment (c.f. Mulder & Cochonat 1996; Ilstad *et al.*, 2004; Bryn *et al.*, 2005). The turbidity currents can be very thick (up to 5 m; Rothwell *et al.*, 1992), coarse-grained, far reaching (>1000 km; Rothwell *et al.*, 1992; Piper *et al.*, 1999; Fine *et al.*, 2005) and possess significant erosive capabilities (Garcia 1996; Wynn and Masson 2003; Masson *et al.*, 2006; Hunt *et al.*, 2011). Such sector collapse events may also pose significant tsunamigenic hazards (Ward and Day, 2001; Lovholt *et al.*, 2008).

Ice-rafted debris events, (IRD) are characteristic of modern day polar regions and colder palaeo-climates (Heinrich 1998; Bond *et al.*, 1992). These cold and ice-rich regions may also accumulate volcanic and other terrigenous material over large periods of time from airfall ash events, and transportation of terrigenous material by wind and water erosion that can then become entrained into glaciers. During warming events (Heinrich events), ice may detach from landmasses and drift into warmer waters where it melts, releasing the accumulated material within it and depositing volcanic material in marine environment (Bond *et al.*, 1992).

Volcanic eruptions are geologically short-lived events, only occupying a small amount of geological time when compared to the periods between eruptions. Between eruptions a volcano is subject to erosion, transportation and redeposition of any erupted material. For island arc volcanoes, the percentage of volcanoclastic material available for remobilisation is >90% by volume, compared to <40% for intra plate oceanic islands such as Hawaii, and <10% from mid-ocean ridges (Carey 2000). As a consequence of the widespread remobilisation of volcanic material, it is important that reworked volcanoclastic material is taken into consideration when generating volcanic record, as incorrect interpretation of a reworked volcanoclastic deposit will lead to inaccuracies in eruption history reconstruction.

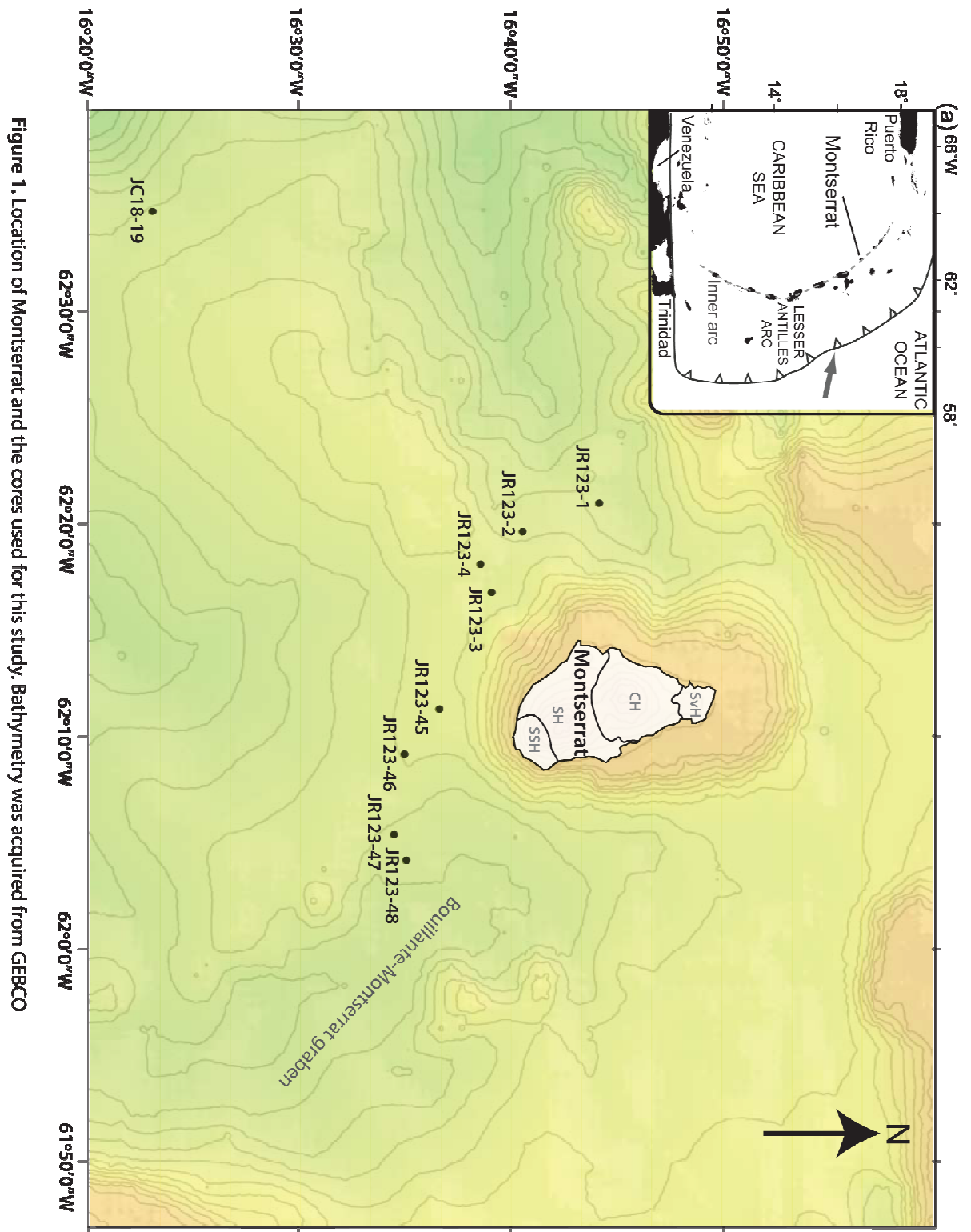
1.4 Cryptotephra

Volcanic ash can be transported over vast distances, for example glass shards from the El Chichón (Mexico) eruption in 1982 were identified in Greenland ice, ~10,000 km from the source (Zielinski *et al.*, 1997). These non-visible tephra horizons are commonly thin, fine-grained, diffuse and composed of transparent glass shards. Cryptotephra are thus notoriously difficult to identify within marine sequences, especially considering that even the most prominent tephra layers are often subject to bioturbation, or reworking by ocean currents. It is hypothesised that more often than not, cryptotephra are not identified within marine sequences, owing to inadequate techniques for detecting ash layers within sediment cores (Stanton *et al.*, 2010) or them not being deemed important to the overall reconstruction. Conventional methods used to detect cryptotephra, such as component analysis (point counting) and systematic grain sizing throughout the cores, is time-consuming and results in the destruction or damage of valuable sediment core material. It is therefore

imperative to refine rapid, non-destructive identification techniques for cryptotephra to promote widespread inclusion of such deposits in marine sediment core reconstructions.

1.5 Montserrat: the natural laboratory

The 750 km long Lesser Antilles island arc was formed by westward subduction of the North American plate beneath the Caribbean plate. This slow (2 cm per year), slightly oblique, subduction has given rise to volcanic islands such as Montserrat, which sits in the northern part of the arc (Wadge 1984; DeMets et al., 2000; Feuillet et al., 2000) (Figure 1). Volcanic activity on the island arc has persisted for 40 Ma (Briden et al., 1979; Bouysse and Westercamp, 1990), but the locus of volcanism to the north of Dominica shifted in the late Miocene, producing a new chain of islands west of the older, now extinct Limestone Caribbees island chain (Bouysse and Westercamp, 1990). This bifurcation of the arc created two sedimentological regimes (Reid et al., 1996). In the northern part of the arc a broad arc platform separates high-relief, active volcanoes (Volcanic Caribbees; Wadge, 1984) from low-relief, extinct volcanoes (Limestone Caribbees; Wadge, 1984) surrounded by wide carbonate shelves. The major components of deep water sediment in this region are volcanoclastic silt and clay, redeposited shallow-water carbonate detritus, pelagic carbonate sediment accumulations, and windblown dust from Africa (Reid et al., 1996). Sigurdsson et al. (1980) estimated that 527 km³ of volcanic material (285 km³ D.R.E) has been erupted from the Lesser Antilles island volcanoes in the last 100 ka. The vast majority of this material (84%) has been transported into adjacent marine basins and deposited as volcanogenic sediments. This illustrates the large contribution volcanism has on marine sedimentation within in the arc.



The island of Montserrat has been active for at least 2.6 Ma and comprises four volcanic regions, the Silver Hills (2600 - 1100), Centre Hills (900 - 500 ka), Soufrière Hills (282 - present) and an interlude of volcanism at the South Soufrière Hills (SSH) (128 - 131 ka) (Harford et al., 2002). The volcanic history of the Soufrière Hills and SSH volcanic centres has been studied from subaerial (Rea, 1974; Roobol and Smith, 1997; Harford et al., 2002; Smith et al., 2007; Cassidy et al., 2012) and submarine deposits (Le Friant et al., 2008; Trofimovs et

al., 2010; Cassidy et al., in press, in prep). Stratigraphic observation, volume estimations, and geochronology, imply that the periods of volcanic extrusion from the Soufrière Hills and South Soufrière Hills regions are spatially and temporally interspersed, with extensive periods of magmatic repose in both complexes (Hartford et al., 2002; Smith et al., 2007; Le Friant et al., 2008). The subaerial eruptive record for the intercalated Soufrière Hills and South Soufrière Hills volcanic complexes was investigated by Roobol and Smith (1998) and later revised by Smith et al. (2007). They proposed seven episodes of volcanism (Figure 2). Episode 1 is represented by the 'Ancient' Soufrière Hills stage exposed on Garabaldi Hill (>200 ka). Episode 2 formed the Soufrière Hills Subunit I (<175 ka), which is characterised by Peléan activity (andesite lava dome growth and collapse to form pyroclastic flows) and a Plinian eruption, as evidenced by the presence of ignimbrites. Episode 3 is represented by basaltic effusive eruptions from the SSH volcanic centre at 128 - 131 ka. Episodes 4, 5, 6 & 7 (112,000 - 400 yrs BP), correspond to Soufrière Hills Subunits II-V where the eruptions returned to more characteristic andesitic Peléan activity. The current eruption (1995 to present) marks the 8th eruptive episode and Soufrière Hills Subunit VI in Montserrat's volcanic history (Smith et al., 2007).

A submarine tephrochronological record was constructed for the Soufrière Hills volcano by Le Friant *et al.* (2008) using a distal marine sediment core, 55 km south west of Montserrat. Eruptive episodes were detected by point counting abundances of different types of clasts (glass shards, dense and poorly vesiculated juvenile clasts, crystals, vesicular juvenile clasts and lithics) at 10 cm intervals, except for tephra-rich zones wherein the core was sampled every 5 cm. A base level of 16% abundance for glass shards was chosen and any counts above this value were deemed to represent an explosive eruption. Similarly, any samples that contained more than the designated base level of 28% for dense and poorly vesiculated clasts, were interpreted as dome eruptions. Using this method, the authors identified eight layers relating to dome eruptions, five of which were directly correlated to dated subaerial domes or related pyroclastic flow sequences on Montserrat, and six significant explosive eruptions, which do not correspond with any documented eruptive deposits in the subaerial record. Micropaleontology-biostratigraphy and $\delta^{18}\text{O}$ isotope analyses of bulk carbonate samples throughout the core were used to date the hemipelagic sediment accumulations between the volcanic horizons, to produce an eruption history for the last 250 ka (Figure 2). Hemipelagic sediment accumulations with low abundances of volcanic material were interpreted to represent long periods (~10 ka) of dormancy or low activity (Le Friant et al., 2008).

The current eruption on Montserrat has provided a unique opportunity for the study of pyroclastic material entering the ocean. The subaerial expression of the eruption has been

monitored in arguably unprecedented detail, with timing, volume and flow dynamic data all recorded for individual pyroclastic flows (Murphy et al., 1998, 2000; Barclay et al., 1998; Sparks et al., 1998, 2000; Young et al., 1998; Cole et al., 1998; Menlik and Sparks, 1999; Voight et al. 1999; Calder et al., 1999; Couch et al., 2001, 2003; Zellmer et al., 2003; Herd et al., 2005; Cassidy et al., 2012). Similarly, the current eruption has acted as a natural laboratory for understanding the submarine emplacement of subaerially erupted pyroclastic material (Trofimovs et al., 2006, 2008, 2012; Le Friant et al., 2009, 2010). This rare opportunity to combine the study of subaerial flow conditions into the ocean with in situ deposit morphology derived from marine sediment cores, has allowed valuable insight into submarine pyroclastic flow emplacement dynamics (Trofimovs et al., 2006, 2008). The excellent marine sediment core coverage around Montserrat and the detailed subaerial eruption history (back to 2.6 Ma) provide a uniquely comprehensive background for the tephrostratigraphy study presented herein.

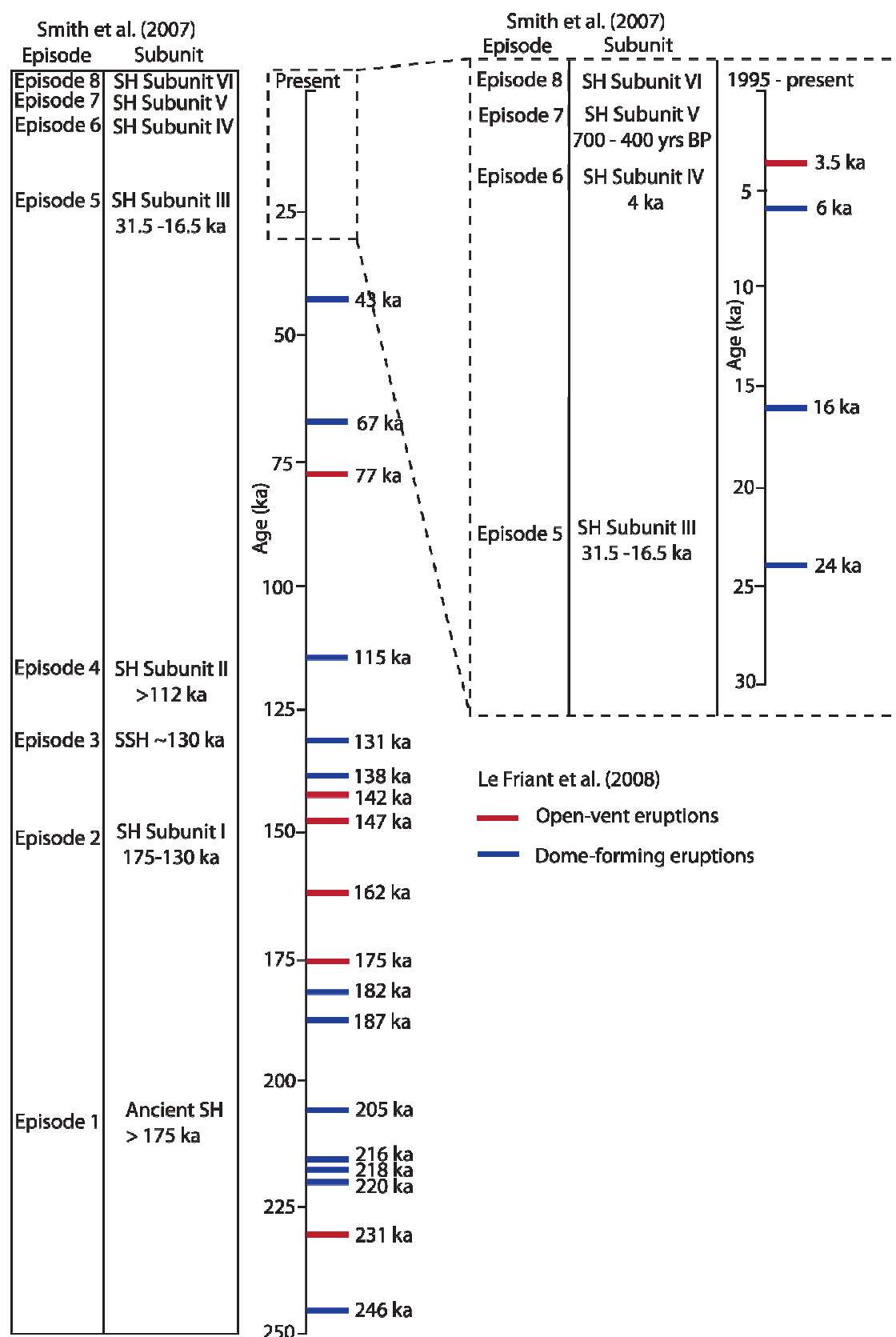


Figure 2. Summary stratigraphic column of the Soufriere Hills-South Soufriere Hills complex, combining the subaerial record of Smith et al. (2007) and submarine tephrochronology of Le Friant et al. (2008).

2. Methods

2.1 Core sampling and sedimentological logging

Two research voyages; the *RRS James Clark Ross* (May 2005 – P.I. Prof. R.S.J. Sparks) and *RRS James Cook* (2007 - P.I. Prof. M.R. Palmer), used a vibrocore system (developed by the British Geological Survey) and gravity corer, respectively to sample marine sediment around Montserrat. The vibrocore system was able to recover a maximum of six metres of unconsolidated marine sediment in water depths of less than 2000 m. The core coverage was spread over the southern and western side of Montserrat ranging from proximal (7 km) to distal locations (55 km) from the island (Figure 1). The vibrocore sampled volcanoclastic material with clast diameters up to and including 10 cm. Real-time, onboard analysis of the vibrocore penetration rate against time allowed the maximum penetration to be achieved in both fine-grained and coarser-grained materials. Visual observation of the sea floor via a video camera mounted on the coring rig aided in the selection of suitable coring sites – i.e., shallow slopes without rough topography. The marine gravity cores utilised a more rudimentary sampling technique wherein the coring system is lowered as fast as possible into the sea floor allowing gravity and inertia to drive the corer barrel into the sediment. This method recovered up to 5 m of predominantly fine-grained (mud, silt and some sand) sediment within core barrels 10 cm wide.

The coring strategy encompassed as wide a geographic range around Montserrat as ship time and method allowed. Core JC18-19 (Figure 1) was sampled for its distal location from source in the prevailing wind direction on a topographic high, in order to exclusively target sample airfall tephra samples (Bonadonna et al., 2002). The eight cores sampled more proximal to source (7-15 km) encompassed topographic highs and, which allowed for an in-depth study of both primary and reworked volcanoclastic flows south and south west offshore Montserrat.

All the cores were housed in refrigerated storage at the British Ocean Sediment Core Facility (BOSCORF), based at the National Oceanography Centre (NOC), Southampton, UK. Cores were sedimentologically logged and photographed to allow for initial identification of visible volcanic units. Grain size, presence or absence of sedimentary structures and general appearance was noted.

2.2 Stable Oxygen isotopes

Samples for bulk oxygen isotope values were taken at 4-5 cm intervals down the core, cleaned over a 63 µm sieve and dried at 50°C. The samples were then homogenized by crushing and weighed for analysis in the stable oxygen lab at the NOC. All stable isotope measurements were performed using a Europa GEO 20-20 mass spectrometer equipped with

an automatic carbonate preparation system (CAPS). Results are reported relative to the Vienna Pee Dee Belemnite (VPDB) standard with an external analytical precision, based on replicate analysis of an in-house standard calibrated to NBS-19, of 0.065‰ for $\delta^{18}\text{O}$ and 0.031‰ for $\delta^{13}\text{C}$ (at 1 σ level).

Benthic stable oxygen isotope data were generated by analysing specimens of well-preserved *Cibicidoides wullesstorfi* and *Cibicidoides mundulus*, hand-picked from the >212 μm sediment fraction of washed samples. Samples were taken at 4 cm intervals within the hemipelagic accumulations. 3 to 8 individual foraminifera were typically analyzed per sample, the $\delta^{18}\text{O}$ difference between the two species was minimal (± 0.11 ‰). The $\delta^{18}\text{O}$ values of the foraminifera ($\delta^{18}\text{O}_{\text{cib}}$) presented in Figure 3 have been adjusted for species-specific offsets by adding +0.64‰ VPDB (Shackleton and Hall, 1984). This latter method provided a more reliable stable isotope curve than bulk sediment oxygen isotopes.

2.3 AMS radiocarbon dating

Samples were also dated by Accelerator Mass Spectrometry (AMS) ^{14}C . Samples for these analyses were taken from hemipelagic sediment immediately above and below the studied volcanoclastic deposit, thus providing the maximum and minimum age estimates. Dates from the hemipelagic sediment directly above the volcanoclastic horizon likely give the closest estimate for emplacement timing, as this material represents the end of volcanoclastic deposition and the return to background hemipelagic sedimentation conditions. Dates obtained from below the targeted units may provide evidence of the amount of erosion of the underlying hemipelagic sediment. Disaggregation of the samples was achieved by washing the samples in deionized water over a 63 μm sieve. They were then dried and sieved to collect the >150 μm size fraction. A 14-16 mg assemblage of planktonic foraminifera tests (~1000 tests) was picked, avoiding any specimens showing signs of reworking or diagenesis. It should be noted, however, that the West Indies foraminifera specimens exhibit remarkable preservation, where the presence of well-preserved pteropods are indicative of the generally good preservation. The dried samples were hydrolysed to CO_2 using 85% orthophosphoric acid. The gas was cryogenically isolated and a subsample analysed in a dual inlet stable isotope mass spectrometer (VG OPTIMA) to determine $^{13}\text{C}/^{12}\text{C}$ ratios, which were used to normalise ^{14}C values to -25‰ $\delta^{13}\text{C}_{\text{VPDB}}$. The remaining CO_2 was converted to graphite by iron/zinc reduction (Slota et al., 1987) and ^{14}C activity determined by accelerator mass spectrometry at the Scottish Universities Environmental Research Centre (SUERC) AMS Laboratory using either a NEC 5 MV AMS (Xu et al., 2004) or a NEC 250 kV single stage AMS (Freeman et al. 2008). In addition to the samples measured at SUERC, four AMS radiocarbon dates of foraminifera samples were measured commercially by Beta Analytic Inc. (Florida,

USA) using their in-house protocols. Details of the technique used can be obtained from their company web site (www.radiocarbon.com). The results are reported as conventional radiocarbon years BP (relative to AD 1950) and % modern ^{14}C , both expressed at the $\pm 1\sigma$ level for overall analytical confidence. The dated samples were calibrated with the Marine09 dataset using CALIB 6.0.0 Radiocarbon Calibration software. The Marine09 dataset calibrates ages between 0 and 46.743 ka to 95% probability (2σ).

2.4 Component analysis

Samples of $\sim 0.5\text{ cm}^3$ were taken throughout the distal JC18-19 core at 4 cm intervals and dried at 60°C . The bioclastic content and preservation condition were then assessed using a binocular microscope, with preservation being assessed by the degree of fragmented bioclasts. An abundance of bioclasts (bioclast maxima), was recorded where coarse bioclasts ($>100\text{ }\mu\text{m}$) made up more than 70% of any one sample, often indicative of bioclastic flow deposits. The samples were then washed with deionised water over a $63\text{ }\mu\text{m}$ sieve to remove the fine-grained hemipelagic component and 2.5 ml of acetic acid (20%) was added to the sample and left for two hours to dissolve the biogenic carbonate. The samples were then washed again over a $63\text{ }\mu\text{m}$ sieve and dried in an oven at 55°C . Aliquots of individual samples were placed on a gridded microscope slide. An average of 400 individual grains were point counted and characterised into six categories according to the classification of Le Friant et al. (2008); 1) Volcanic glass shards, which are fine-grained particles formed by the explosive disruption of magma. 2) Crystal fragments, such as pyroxene, feldspars and amphiboles. 3) Vesicular juvenile andesite lava clasts, for example, unaltered pumice-like material clasts formed by the exsolution of dissolved gases from magma. 4) Non-vesicular juvenile andesite lava clasts that are likely derived as the Soufrière Hills dome is extruded. 5) Altered andesite lava dome clasts, which have been weathered by hydrothermal fluids and gases. 6) Mafic clasts that are darker than andesitic clasts and are low in silica, similar to a basalt. Examples of these subdivisions are provided as photos and SEM images in the Appendix. This technique and clasts subdivisions were chosen to be directly comparable to the tephrostratigraphic study by Le Friant et al. (2008).

2.5 Scanning Electron Microscope (SEM)

The TM1000 tabletop SEM based at the NOC BOSCORF facility was used to take high resolution images of volcanic clasts to assess clast morphology. The advantage of this particular SEM is that minimal preparation is required to take images of 3D clasts, as unlike conventional SEM systems, it does not require carbon-coated thin sections or gold-plated samples.

2.6 Magnetic susceptibility

Magnetic susceptibility is a commonly used tool in tephra studies (e.g. Hodgson et al., 1998; Takemura et al. 2000; Rasmussen et al., 2003; Kutterolf et al., 2007; Vogel et al., 2010), hence the GeoTek™ MSCL-XYZ multi-sensor core logger, based at the NOC BOSCORG facility, was used to provide magnetic susceptibility measurements at 0.5 cm intervals on whole split cores using a Bartington MS2E point sensor. This non-destructive method is capable of sampling at 8 mm resolution (Rothwell and Rack, 2006), but the interval of 0.5 cm was chosen to provide good spatial resolution with slightly overlapping measurements.

2.7 Colour spectrophotometry

Colour spectrophotometry was measured in conjunction with magnetic susceptibility on the Geotek MSCL-XYZ logger at 0.5 cm intervals. Again, this is a non-destructive method, capable of sampling at 3 mm resolution. A Konica Minolta colour spectrophotometer measured reflectance from the very near UV wave lengths through the visible light spectrum and into the very near IR range (wavelengths 360-740nm) in 10-nm spectral bands. The data from this method represent the optical properties of the sediment, where L* and greyscale represent Lightness and reflectance gradients (0- black to 100 – pure white). The actual colour (hue) is expressed as a* (negative values are red, positive is green) and b* (negative for blue and positive for yellow) (Nederbragt et al., 2006). This technique has also been used for several studies of tephra detection in conjunction with other methods (Caseldine et al., 1999; Gehrels et al., 2008). However it was noted that very low concentrations of shards and highly dispersed tephra layers may not be resolvable from background noise.

2.8 Grain size

Core JC18-19 was sampled at 3 cm intervals for laser diffraction grain size analysis. The 1 cm³ samples were added to 25 mL of RO water with a 0.05% sodium hexametaphosphate dispersant and left on a shaking table overnight. The dispersed sediment solutions were analysed using a Malvern (Mastersizer 2000) particle size analyser, which is able to measure 0.02 µm to 2000 µm grain sizes. The particles are kept in suspension using in-built stirrers and the sample is pumped continuously through the Malvern analyser to ensure random orientation of the particles relative to the laser beam. Light obscuration was between 10-20%. Standard materials of mean average 32 µm and 125 µm were used to monitor precision, while three repeat runs for each sample were used to monitor accuracy (reported at <0.5% SD). This method has previously been applied to tephra from North Iceland (Gudmundsdottir et al., 2011).

2.9 XRF-core scanning

The bulk geochemical composition (semi-quantitative) of the sediment was determined by XRF core scanning (ITRAX_{tm} COX Ltd; Croudace et al., 2006) at a spatial resolution of 0.2–1 mm using a molybdenum x-ray tube at the BOSCORF facility at the NOC. The surface of split cores must be carefully flattened in order to reduce effects of surface roughness, and thus improve the signal-to-noise ratio of XRF logging records. Repeated scans of intervals of core JC18-19 within this study have shown that the ITRAX_{tm} XRF core scanner produces highly reproducible results at submillimetre to millimetre scales, generally <10% uncertainty for the reported data for the elements used in this study (Kylander et al., 2012). The results are presented as log ratios as it has been suggested that these provide a reliable record of relative changes in chemical compositions along the length of the sediment core (Weltje and Tjallingii, 2008). Ca and Sr were used as denominator elements as they possessed the highest intensities in the studied marine sediments and showed the highest contrast between the volcanic units and background sedimentation. Mn, Fe, Ti, K, Si were used as proxies for volcanogenic material, as these elements are found in the major minerals (feldspars, pyroxenes, amphiboles, titanite, magnetite) and groundmass that comprise the Montserratian volcanic rocks and generally have very low concentrations in hemipelagic sediments. Of these element ratios, $\ln(\text{Mn}/\text{Sr})$, $\ln(\text{Fe}/\text{Ca})$ were found to be the most efficient at detecting volcanic material from the Soufrière Hills and SSH volcanic complexes.

No direct comparison between grain size and XRF values was noted, suggesting that grain size variations within the core were not substantially affecting the reported chemical ratios. It is important to emphasise, however, that the results from the ITRAX are semi-quantitative and must be validated by direct measurement of elemental contents in discrete samples. These analyses were not undertaken in this study, hence the results are only indicative of the relative changes in geochemistry that result from changes in the relative abundance of volcanic material within background hemipelagic sediments. Nevertheless, this technique has been used successfully in paleoclimatology studies (Palike et al., 2001), as well as in studies of volcanic deposits (Vogel et al. 2009, Brendryen et al. 2010; Kylander et al. 2012).

2.10 X-radiography

This technique provides a digital image of any internal structure and physical property changes within a split core section. Such images were measured by the ITRAX instrument using optical and radiographic line cameras. The X-rays used to irradiate the core

section are generated from a 3 kW Mo target and focused through a flat glass capillary waveguide to allow high-resolution measurement (down to 200 μm step size) (Croudace et al. 2006; Rothwell and Rack, 2006). This method has also been used in other tephra studies (Lowe, 1988, Dugmore and Newton, 1992; Turner et al. 2008) with variable results.

3. Results and Interpretations

3.1 Sea floor morphology

There are two main submarine depressions adjacent to Montserrat where water depths exceed 1000 m. South east of Montserrat, the Bouillante-Montserrat graben extends from the Tar River valley towards Guadeloupe. The graben floor is at approximately 1200 m water depth and is bound by normal faults and seamounts. To the west of Montserrat are a series of submarine canyons and basins, which extend south west to the Grenada Basin (Le Friant *et al.*, 2004; Feuillet *et al.*, 2010). South of Montserrat, the island flank is constructed on a shallower platform, at a depth of ~ 700 m, which gradually deepens southwards. The proximal submarine sediment cores used in this study are located in 852 to 1057 metres of water, and form a south west to south east transect 7.3 km to 14.5 km from the Montserrat shore (Figure 1). The distal core used in this study, JC18-19, was sampled on a topographic high 55 km south west of Montserrat in water depths of 1130 metres (Figure 1). The slopes where the cores were taken are dominantly shallow ($< 2^\circ$) and exhibit flat local topography.

3.2 Core Chronology

The original bulk $\delta^{18}\text{O}$ curve (Figure 3), sampled at 5 cm intervals down core, proved to be difficult to interpret, as the ambiguous signal produced was difficult to match to the marine $\delta^{18}\text{O}$ records commonly used, such as Imbrie (1984). The $\delta^{18}\text{O}$ values from this study are less negative than would be expected in comparison with analogous studies by Reid et al. (1996) and Imbrie (1984). This is likely due to the background volcanic material present within the samples, which has much higher $\delta^{18}\text{O}$ values than uncontaminated hemipelagic sediment (Zellmer et al., 2003). The bulk hemipelagic samples also contained a range of bioclastic material, for example broken foraminifera, pteropod fragments, calcareous nanofossils, calcified dinoflagellates and other aragonitic and calcitic debris. It was therefore decided to attempt to improve this resolution by generating $\delta^{18}\text{O}$ values solely from benthic foraminifera. Benthic foraminifera typically reside in deeper colder waters and produce a more stable $\delta^{18}\text{O}$ signal. They are less affected by vital effects, seasonal and weather changes than bulk carbonate and planktonic oxygen isotope records (Zachos et al., 2001). Consequently an oxygen isotope stratigraphy using two species of benthic foraminifera (*Cibicidoides wullesstorfi* and *Cibicidoides mundulus*) was generated (Figure 3). This provided a

higher resolution curve that more closely matched previous values, such as those in Lisiecki and Raymo (2005) (Figure 3). A disadvantage of this method is the time-consuming nature of picking benthic species. However the better results yielded made it a worthwhile undertaking.

In addition to the oxygen isotope data, six AMS radiocarbon dates were obtained to further improve the chronological accuracy of core JC18-19 (Table 1, Figure 3) and eleven ^{14}C were obtained to date the proximally sampled cores (Table 1, Figure 4). AMS radiocarbon dating is a relatively fast method compared to the time taken to develop an oxygen isotope stratigraphy, and this method provides an accurate absolute age. However the range is limited to <47 ka (using the Marine09 calibration curve).

The agreement of the data with the LR04 benthic stack (Lisiecki and Raymo, 2005) is poor in some sections, particularly between 50 - 150 cm. This likely reflects the re-worked nature of this core, hence marine isotope stages (MIS) were assigned based on the AMS dates and curve comparison. The data become clearer in the deeper parts of the core, and the lowest value (peak) at 265 cm is thought to represent MIS 5.5. The values then increase to 355 cm, coincident with the transition from MIS 5 to MIS 6. This age assignment of this transition is supported by the relative abundance decrease of *G. menardii*, which is abundant in MIS 5 (10 % of all planktonic foraminifera) to MIS 6 (1-2 %), as observed in the studies of Le Friant et al. (2008) and Reid et al. (1996). The peak at 50 - 60 cm is unexpected and may represent hidden ash layers that have contaminated the oxygen isotope signal. Overall, these data suggest that the core reaches down to the MIS 6 boundary (>130 ka), with large erosive events at ~3.7 ka to 37 ka and increased sediment deposition appears to have occurred between 40 – 42 ka, suggesting sedimentation rates were fast during this interval. The sedimentation rates vary significantly down the core, with slow sedimentation accumulation rates between 42 - 123 ka that speed up from 123 - 130 ka. Overall the reworked nature of this distal sediment core results in an imperfect age model, however the results do provide some constraints on the eruptive events from Montserrat.

Table 1- AMS radiocarbon dates

Publication code	Core I.D.	Sample depth (cm)	Sample identifier	$\delta^{13}\text{C}_{\text{VPDB}}\text{‰}$ ± 0.1	Radiocarbon		2σ		Error
					age	Error	Calibrated ages		
SUERC-33137	JCR123-2	60	MCAMS03	1.4	38880	617	42941		975
SUERC-33138	JCR123-1	63	MCAMS04	4.1	7880	35	8328.5		127.5
SUERC-33139	JCR123-1	12	MCAMS05	1.4	35014	387	39703.5		967.5
SUERC-33140	JCR123-47	49	MCAMS07	1.4	10688	39	12087		237
SUERC-33146	JC18-21	90	MCAMS12	1.8	36849	480	41425.5		799.5
SUERC-33149	JC18-21	147	MCAMS15	1.5	27728	161	31495		300
SUERC-25163	JR123_2	53	MCAMS		7911	35	8391		126
Beta - 306878	JCR123-48	64	21	-0.7	6700	40	6770		145
Beta - 306877	JCR123-47	92	MCAMS20	0.8	37730	300	41800.5		491.5
SUERC-33147	JCR123-1	78	MCAMS13	1.1	50393	2566	N/A		N/A
SUERC-33148	JCR123-47	50	MCAMS14	1.4	47283	1747	N/A		N/A
SUERC-33141	JC18-19	120	MCAMS08	1.1	36771	475	41361		807
SUERC-33144	JC18-19	143	MCAMS09	0.9	35172	392	39834		998
SUERC-33145	JC18-19	180	MCAMS10	0.9	37708	536	42070		775
SUERC-33136	JC18-19	65	MCAMS02	1.4	35947	445	40514		1072
Beta - 306875	JC18-19	10	MCAMS16	1.4	3850	30	3291		132
Beta - 306876	JC18-19	35	MCAMS17	-10.6	33820	250	37832		836
Beta - 313875	JCR123-2	88	MCAMS23	1.5	31700	200	35785		625

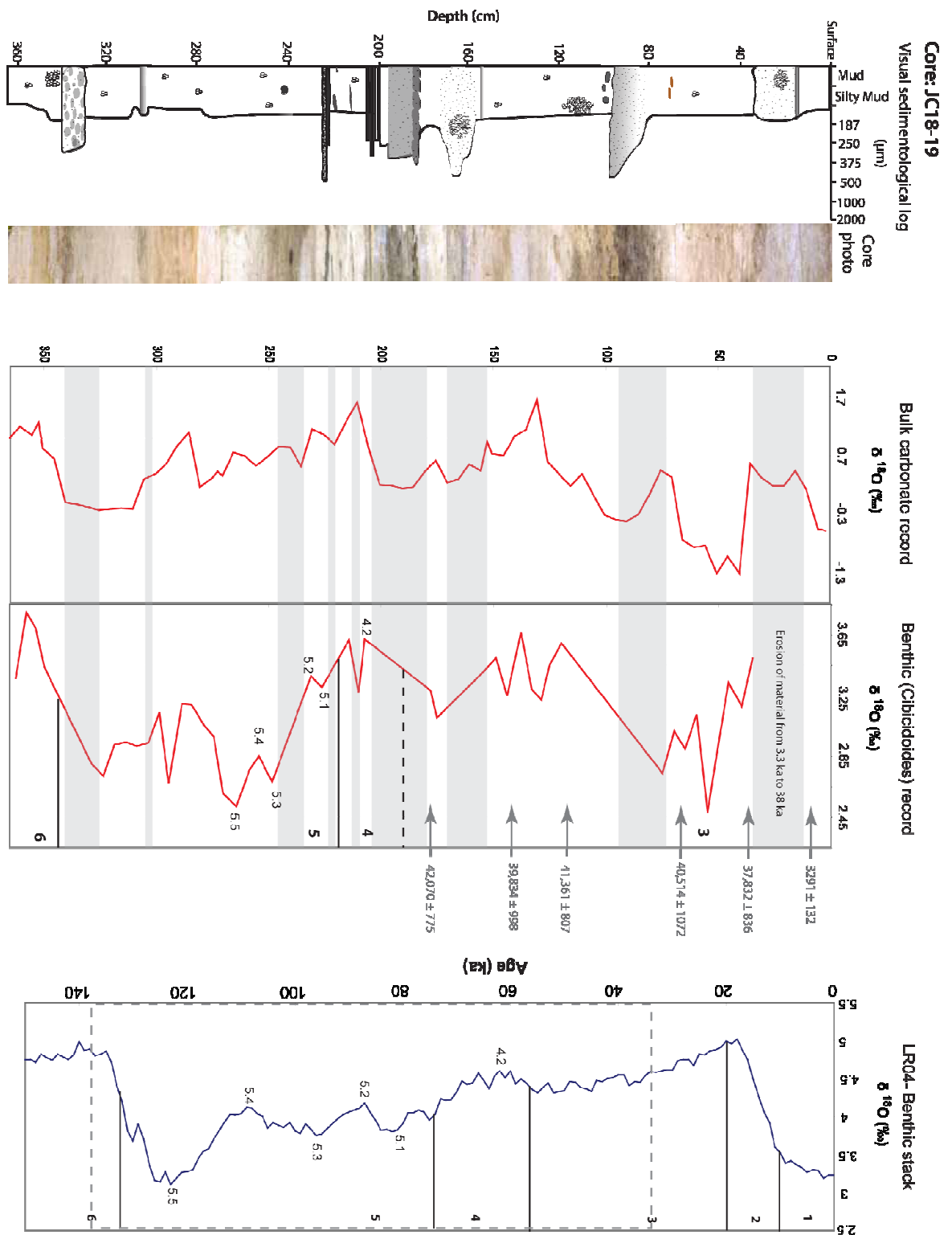


Figure 3. Core chronology of core JC18-19. AMS radiocarbon dates are presented along with the oxygen isotope stratigraphy. Left to right: Visual log, oxygen isotope stratigraphy from bulk carbonate, oxygen isotope stratigraphy from benthic foraminifera, LR04 Benthic stack compiled by from Lisiecki and Raymo (2005). Grey areas indicate the visible volcanic units

3.3 Proximal core correlations south and south west offshore Montserrat

The proximal cores in this study comprise volcanic and bioclastic depositional units intercalated with hemipelagic sediment. The average accumulation rates for hemipelagic sediment within this area range from 3.7-6.8 cm ka⁻¹ (Trofimovs et al., 2010), compared to 1-3 cm ka⁻¹ for more distal regions (Le Friant et al., 2008). Figure 4 shows the proposed correlation between the proximal sediment cores, located offshore ~7-15 km south and south west of Montserrat. The stratigraphy within the Bouillante-Montserrat graben south east of Montserrat has been previously detailed by Trofimovs et al. (2010). Correlations between the volcanoclastic horizons in the cores in this study, are based primarily on sedimentological features; e.g., grain size, appearance, sedimentary structures and stratigraphic relationships (Figure 4). This correlation has been supplemented by stable isotope profiles, AMS radiocarbon dating and geochemical provenance studies, which all help to confirm the proposed correlations (Cassidy et al., 2012, in press; in prep) (Table 1). The presence of hemipelagic material between the volcanoclastic or bioclastic units is attributed to periods where the volcano was inactive or low, or deposition of volcanic material occurred elsewhere. The visible volcanoclastic horizons are described below in ascending stratigraphic order.

3.4 Stratigraphic Architecture

3.4.1 SSH Lower and Upper Units

Observations

The SSH Lower and Upper Units are the deepest and therefore the oldest deposits intersected by the studied cores (Figure 4). They are preserved in all of the cores, except for JR123-3, which bottoms out in younger material. The SSH Lower and Upper Units are thick (up to 60 cm), coarse-grained (up to coarse gravel size), and are very dark in appearance, reflecting their dominant basaltic lithology. The deposits are separated into two distinct units, by ~13 cm of intervening hemipelagic sediment. The SSH Lower Unit is thickest in the south west and is characterised by multiply-stacked, normally-graded beds, and the mean grain size ranges from very-coarse sand -0.17 ϕ (1.22 mm) to coarse sand to 0.92 ϕ (0.55 mm). This unit is moderate to poorly-sorted and contains <20% silt-clay size fraction material. The volcanic components of the SSH Lower Unit have sub-rounded clasts and comprise a variety of volcanogenic components; including, basaltic clasts (40%), feldspar crystals (25%), pyroxene crystals (10%), and pale-coloured andesitic pumice clasts (25%). The SSH Upper Unit is thickest in the south and south east, it is poorly- to very poorly-sorted and is inversely graded at the bottom, with a scoured erosional base and normally graded top. This unit is fines-rich (>60%) and shows a polymodal grain size distribution, from -1.5 ϕ to <4 ϕ (2.75- 0.063 mm). Within this unit there is a medium sand base (mean: 1.98 ϕ , 0.26

mm), a heavily skewed very-coarse sand middle (mean of 0ϕ , 1 mm) and a finer medium sand grain size top, with a mean of 1.75ϕ (0.30 mm). The components observed in both the Upper and Lower SSH Units are identical. These horizons are described in detail by Cassidy et al. (in press).

Interpretations

The submarine deposit originates from the SSH volcanic centre, as distinguished by their lithological and geochemical characteristics, which geochemically match the subaerial SSH strata (Cassidy et al., in press). The distinct chemostratigraphy (trace elements and Pb isotopes) of the subaerial SSH sequence is reversed in the submarine chemostratigraphy, suggesting the deposits were emplaced from multi-stage edifice collapses, successively cutting back into older, chemically distinct deposits. The submarine deposits show characteristics of being emplaced from high-concentration turbidity currents, as they preserve features such as coarse grain size, poor sorting and erosive bases. The SSH Lower turbidity current flowed south west, whereas the SSH Upper turbidity current was directed to south and south east offshore Montserrat. The two units are separated by a ~ 2 ka interval of hemipelagic sediments, based on average sedimentation rates from Trofimovs et al. (2010) (Cassidy et al., in press).

3.4.2 75 ka Glass Shard-rich Unit

Observations

This unit is preserved at the base of the 75ka Stratified Volcaniclastic Unit in core JR123-2. The 75 ka date is an estimate calculated using average hemipelagic sedimentation rate from Trofimovs et al. (2010) and the ^{14}C date below the Mafic and Bioclastic-rich Unit in core JR123-1 (Figure 4). The 75 ka Glass Shard-rich Unit appears grey in the exposed core and is very thin (1 cm), with sharp upper and lower boundaries. Angular glass shards make up 80-90% of the deposit, the remaining 10-20% consists of crystal fragments and vesicular juvenile clasts. The deposit comprises clasts of silt to fine sand size and is well-sorted.

Interpretations

This deposit comprises a dominance of one component type (glass shards), this suggests that it is derived from a single source. These shards are well-sorted and angular, indicating that they have not been subject to extensive weathering or erosion, but the transportation mechanism has effectively sorted the grain sizes before deposition. These evidences, coupled with the preservation of sharp upper and lower boundaries of this thin deposit, suggests it represents an airfall deposit from the Soufrière Hills volcano.

3.4.3 75 ka Stratified Volcaniclastic Unit

Observations

The 75 ka Stratified Volcaniclastic Unit is a localised deposit that is only found in cores JR123-2 and JR123-1, which lie to the south west of Montserrat (Figure 4). This Unit directly overlies the 55ka Glass Shard-rich Unit. The deposit ranges in thickness from 40 cm in core JR123-1 to 35 cm in JR123-2, and is coarser in JR123-2 with grain sizes ranging from fine to medium sand size. The 75 ka Stratified Volcaniclastic Unit, preserved in JR123-1 comprises bioturbated and diffuse silt to fine sand clasts. In JR123-2 the grain size varies over a narrow depth range in the sediment core. The unit is moderately to well-sorted and preserves various sedimentological structures, such as parallel laminations and splay and fade stratification. The deposit has a scoured basal contact and is inversely graded, with sub-rounded to spherical clast morphologies. The deposit is light grey in appearance and comprises crystal fragments of pyroxene, amphibole and feldspar (30%), altered lava dome clasts (20%), glass shards (20%), poorly vesiculated andesitic clasts (10%), mafic clasts (10%) and bioclastic material (10%).

Interpretations

This is a well-sorted unit, yet it is composed of a range of different source components. The well preserved sedimentary structures, fine sand grain size and erosive base suggest it was formed by a low concentration turbidity current (Iverson et al., 1997; Mulder and Alexander, 2001). The turbidity current likely waxed in energy to produce the inversely-graded unit (Mulder and Alexander, 2001; Kneller and MaCaffery, 2003). The source material for this turbidity current is likely previously reworked volcaniclastic material, due to the well-rounded nature of the clasts. Lahar deposits in the Belham River on Montserrat have similar components and clast morphologies (Barclay et al., 2007). Therefore it is possible that the 55ka Stratified Volcaniclastic Unit represents the submarine extension of such deposits.

The 55ka Stratified Volcaniclastic Unit directly overlies the 55ka Glass Shard-rich Unit in the stratigraphy. This may indicate that the reworked volcaniclastic turbidity current may represent lahars following a primary volcanic eruption.

3.4.4 8-35 ka Mafic and Bioclastic-rich Unit

Observations

The Mafic and Bioclastic Unit is a significant, but localised unit, that is found in only two cores (JR123-2 and JR123-3) in the south west offshore Montserrat. It is a thick-bedded deposit, ranging from 38 cm in JR123-2 to more than 101 cm in JR123-3, where the base is not intersected by the core. Variations in grain size and sorting are seen throughout the Mafic and Bioclastic-rich Unit in the form of stacked, normally-graded beds. The deposit contains very coarse-grained subunits (e.g. -0.45ϕ , 1.35 mm) including a moderately well-sorted ($0.517 \sigma_{\phi}$), coarse sand deposit (0.85ϕ , 0.6 mm), intercalated with very poorly- to poorly-

sorted subunits. The Mafic and Bioclastic-rich Unit contains a high percentage of fragmented bioclastic material and reworked volcanic deposits and appears yellow and black in the exposed core. The unit comprises abundant crystal fragments of feldspar, pyroxene and amphiboles (35-56%), dense and poorly vesiculated andesitic clasts (20-30%), mafic clasts (7-10%), bioclastic material such as broken coral and shells (6-20%), altered andesite lava clasts (4-9%), and vesicular juvenile andesitic clasts (2-10%). Geochemical analyses show that it contains volcanic clasts from both the SSH and Soufrière Hills volcanic centres (Cassidy et al., in prep). AMS radiocarbon dates constrain this deposit to 8-35 ka (Table 1).

Interpretations

This deposit was likely derived from a shallow marine source, as indicated by the presence of fragmented coral and other shallow marine bioclasts, potentially from a shelf collapse in the south west offshore Montserrat. This hypothesis is consistent with observation of a shelf-derived debris avalanche imaged by bathymetric surveys (Deposit 5 of Le Friant et al., 2004). The coarse-grained, poorly-sorted nature of this unit, coupled with its lack of structures such as cross-bedding and parallel laminae suggest that it formed from a high-concentration turbidity current (Lowe, 1982). The stacked graded beds suggest the collapse involved multiple failures at source. Each stacked bed exhibits normal grain size grading from a waning flow energy within each pulse (Branney & Kokelaar 1992; Kneller and Branney, 1995; Mulder and Alexander, 2001; Kneller and McCaffery, 2003).

3.4.5 8ka Andesitic Volcaniclastic Unit

Observations

The 8ka Andesitic Volcaniclastic Unit is found in 7 cores off the west to the southeast coast of Montserrat (Figure 4). Most of the cores contain a ~30 cm thickness of this deposit, but it thins to <10 cm in core JCR123-48 to the south east of Montserrat (Figure 4). The 8 ka Andesitic Volcaniclastic Unit is typified by weak, normal grading, an erosive base and a general, lack of tractional structures such as planar or cross bedding. The deposit exhibits poor- to moderate-sorting and the mean grain size varies from silt-clay at the top of the deposit (4.12ϕ , 0.06 mm) to medium sand at the base (1.51ϕ , 0.355). Rare large clasts (up to 100 mm) are found randomly distributed throughout the deposit. The 8 ka Andesitic Volcaniclastic Unit is grey in appearance and comprises predominantly of broken feldspar, amphibole and pyroxene crystals (56-66%), grey-coloured dense and poorly-vesiculated andesite clasts (18-22%) and vesicular juvenile andesite clasts (6-10%). Altered andesite lava fragments; mafic and biogenic clasts are present in small proportions (<10% for all). The majority of the components are sub-angular to angular in shape and dominantly made up of fractured crystals. Two trace element analyses of picked clasts from this deposit show very similar geochemical compositions.

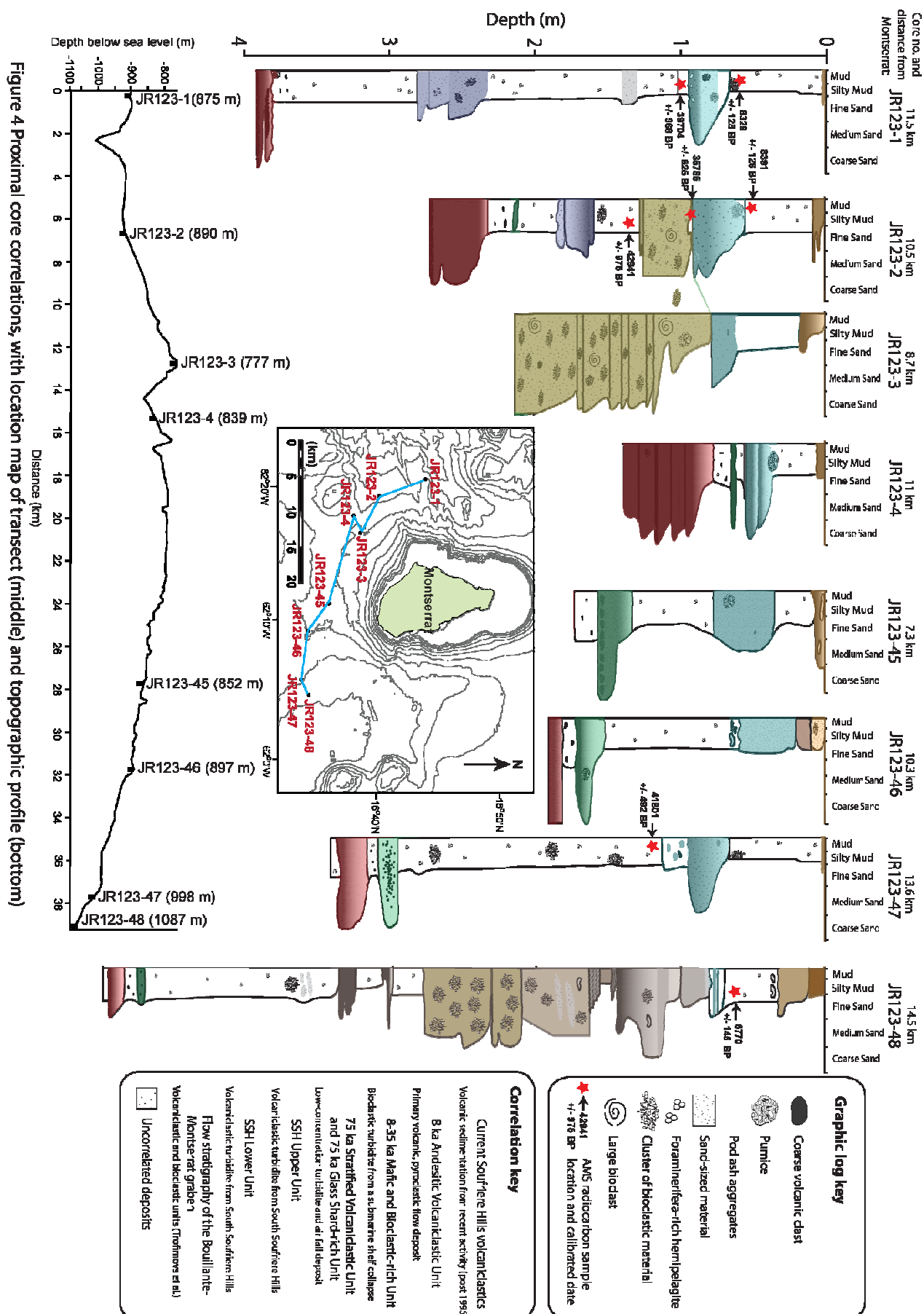
Interpretations

This unit is interpreted to be a primary volcanic deposit, as indicated by the lack of chemical variation in the deposit and the compositional maturity of the clasts, which comprise monogenetic porphyritic andesite lava clasts and crystal fragments. The geochemistry of the deposit defines its origin as the Soufrière Hills volcanic complex (Cassidy et al., in prep). The submarine deposit originates from the south west of Montserrat, where the deposits are thickest and grain size coarse. The crystal-rich nature of this unit, coupled with its primary volcanic origin, suggests it was emplaced by a pyroclastic density current from the Soufrière Hills volcano, when the hot flow quenched rapidly and fragmented into the crystal-rich deposit on contact with the water (Whitham 1989). As the flow entered the sea, it continued to mix rapidly with the water to become a water-supported gravity flow. The coarse-grained nature and lack of tractional features found within the 8ka Andesitic Volcaniclastic Unit suggest it was emplaced from a high-concentration turbidity current. This energetic flow eroded ~8.5 cm of hemipelagic material, which equates to ~31 ka time interval, based on average sedimentation rates (Cassidy et al., in prep). AMS dates constrain the age of this deposit to be 8.4 ka – a period previously thought to be devoid of volcanic activity (Harford et al., 2002; Smith et al., 2007; Le Friant et al. 2008).

3.4.6 Current Soufrière Hills volcano eruptive products

Observations

Recent deposits from the ongoing eruptive activity at the Soufrière Hills volcano (1995-present) are represented at the top of the studied cores. The deposits are preserved as fine grained, red-brown ash and sand dominated units, which are generally coarsest and thickest in the most proximal cores (JR123-45 and JR123-3). Fine planar laminations are preserved. This deposit is identified as resulting from the current Soufrière Hills volcano activity as it is exposed at the very top surface of the cores, where it has been emplaced as ash fall, pyroclastic flows, lahars and turbidity currents observed entering the sea during the current eruption (Druitt and Kokelaar, 2002; Cole et al., 2002). This unit was not studied in detail herein, instead we refer to other papers where the deposits are described in detail (Trofimovs et al. 2006; 2008; 2012).



3.5 Distal core stratigraphy

Core JC18-19 was chosen for distal stratigraphic analysis, due to its location 55 km south west offshore Montserrat, where prevailing winds are known to have distributed ash from recent eruptions of the Soufrière Hills volcano (Bonadonna et al., 2002) and also JC18-19's relative proximity to CARMON2, a sediment core studied by Le Friant et al. (2008). In this core, 9 visual volcanic units were identified using sedimentological logging and digital photography. These units are named VT01 - VT09 and highlighted in grey in Figures 5, 6 & 7, and different techniques (e.g. component analysis, magnetic susceptibility) were tested to assess how many of these visual tephra would have been detected if they were not visible within the core (Table 2). A discussion of the benefits and limitations of each of the techniques based on the collected data from core JC18-19, is given in the following section. The benefits and limitations of each technique are also reviewed here, using the case study from core JC18-19. A preliminary tephra detection rating is used in this study that ranges from 1 to 5 (1 for the least efficient and 5 for the most). This rating is based on each of the techniques advantages, limitations and how many of the visually identified tephra they are able to detect (Table 2).

3.5.1 Component analysis by point counting

Samples were taken throughout the core at 4 cm intervals, after dissolution of carbonate material and cleaning the samples over a sieve, they were observed under a microscope. Different components were subdivided into glass shards, crystal fragments, vesicular juvenile clasts, non-vesicular juvenile clasts, altered dome clasts and mafic clasts and were point counted for their percentage abundance (Figure 5). Component analysis by individual point counting was able to detect five out of the nine visual tephra in core JC18-19 (Figure 5). This method is limited by its sampling resolution, because sufficient sample must be taken to provide enough grains to yield statistically significant data, and a sufficient number of samples must be taken to capture all the volcanic events. In practice, it is not feasible or desirable to point count the entire core. In this study, samples were taken every 4 cm, so thin ash layers could be missed from the record. Even if the resolution was increased, this technique is both destructive and very time-consuming. Additional problems include a dilution effect when presenting the point counting results as percentages (c.f. Le Friant et al., 2008). For example if there is a lack of glass shards in a sample will increase the relative concentrations of the other components, e.g. dome clasts, which produces a false peak in these subdivisions. Furthermore, placing a background percentage level for normal hemipelagic sedimentation after dissolution of the actual carbonate material is subjective.

This technique does offer some benefits however, as it proves to be very helpful in characterising the deposits types. Also thorough inspection of the clasts within the sample can help determine if the deposit is of primary or reworked origin. Component analysis was given a rating of 2 because the signal was noisy and it was only able to identify five of the nine visible tephras (Table 2).

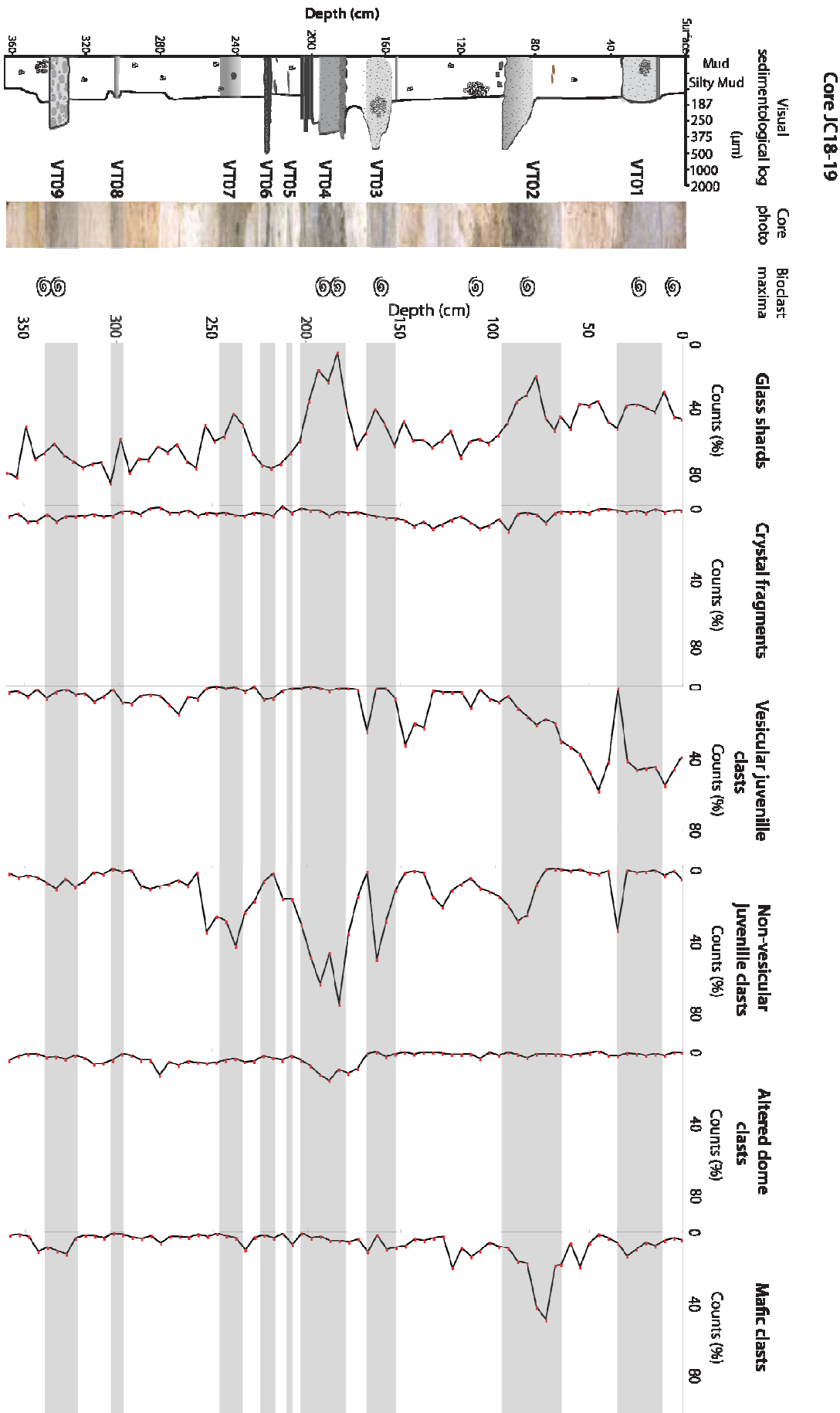


Figure 5. Sedimentological log of core JC18-19 (left), with visible tephras highlighted and extrapolated in grey. This figure shows the component analysis throughout the core by point counting. Shell symbols adjacent to the profiles indicate depths where coarse bioclastic material was abundant (>70%) (Bioclast maxima).

3.5.2 *Magnetic susceptibility*

This is a fast, cost effective and non-destructive technique (Figure 6). The sampling resolution is good (0.5 cm). While a higher resolution would be advantageous, this is limited by the type of point sensor employed. During this study, this technique was only able to detect thick volcanoclastic units and failed to identify some of the thinner tephra layers or cryptotephra. Such layers are commonly diffusely dispersed within the hemipelagic sediment, and thus do not provide a strong magnetic signal. Magnetic susceptibility reflects the volume of magnetic minerals (Blum, 1997), therefore if only glass shards are preserved in a cryptotephra (as is often the case) they can go undetected using this technique. This method was able to detect eight out of the nine visual tephra and so was given a detection rating of 4 (Table 2).

3.5.3 *Colour spectrophotometry*

Colour spectrophotometric measurements were performed at the same time as magnetic susceptibility analyses. Hence it is also fast, cost-effective and non-destructive. By using a combination of grey-scale, lightness, and both a^* and b^* colour hue it is possible to recognize eight of the nine visual tephra, but the signal is noisy, and identification of some of the tephra layers (particularly VT-01) is somewhat ambiguous and subjective (Figure 6). The efficiency of this technique could be improved by extending the measurements to higher wavelengths (that are capable of yielding specific mineral reflectance spectra; Clark, 1999), but this would increase the time required for the measurement and would require a more powerful light source. Hence, this technique was given a detection rating of 3 in the configuration used in this study (Table 2).

3.5.4 *Grain size measurements*

Grain size measurements were taken throughout the core at 3 cm intervals using a laser diffraction Malvern machine. This technique is destructive and fairly slow. As with the point counting technique, the sampling resolution is a trade off between the time taken to perform the analyses, the desirability of not consuming a high proportion of the core material and the need for adequate sampling frequency to detect potential tephra layers. The use of 3 cm resolution in this study was clearly not adequate to accomplish the last objective as this technique only identified five of the potential nine visual tephra horizons. In addition, the signal of tephra is ambiguous, because volcanic clasts can be either coarser, finer or the

same grain size as background hemipelagic sediment (Figures 6 and 7). This technique is, however, cost-effective and can provide information about the sedimentology of the core that is useful for such tasks as detecting turbidite sequences. This technique is also useful in conjunction with the XRF core scanning technique (Figure 6) as the signal from the latter can be affected by changes in grain size. Grain size technique was given a detection rating of 2.

3.5.5 *X-radiography*

The results of the X-radiography are presented as an X-ray image of the core (Figure 6). This technique allows for an analysis of sedimentary structures within the core, such as cross bedding and planar laminations. The sampling resolution is very good, it is non-destructive and it can be used as a proxy for density changes in the core, which may indicate the presence of volcanic ash. However, it is a qualitative technique and difficult to interpret in some places. In addition, it is particularly susceptible to picking up pseudo-sedimentary textures such as cracks in the sediment and other coring artefacts. Overall, the X-radiography images did not provide an unequivocal signal of tephra within the core, although some tephra layers detected using the other techniques were coincident with darker areas on the radiograph; as a result the detection rating is 1 (Table 2).

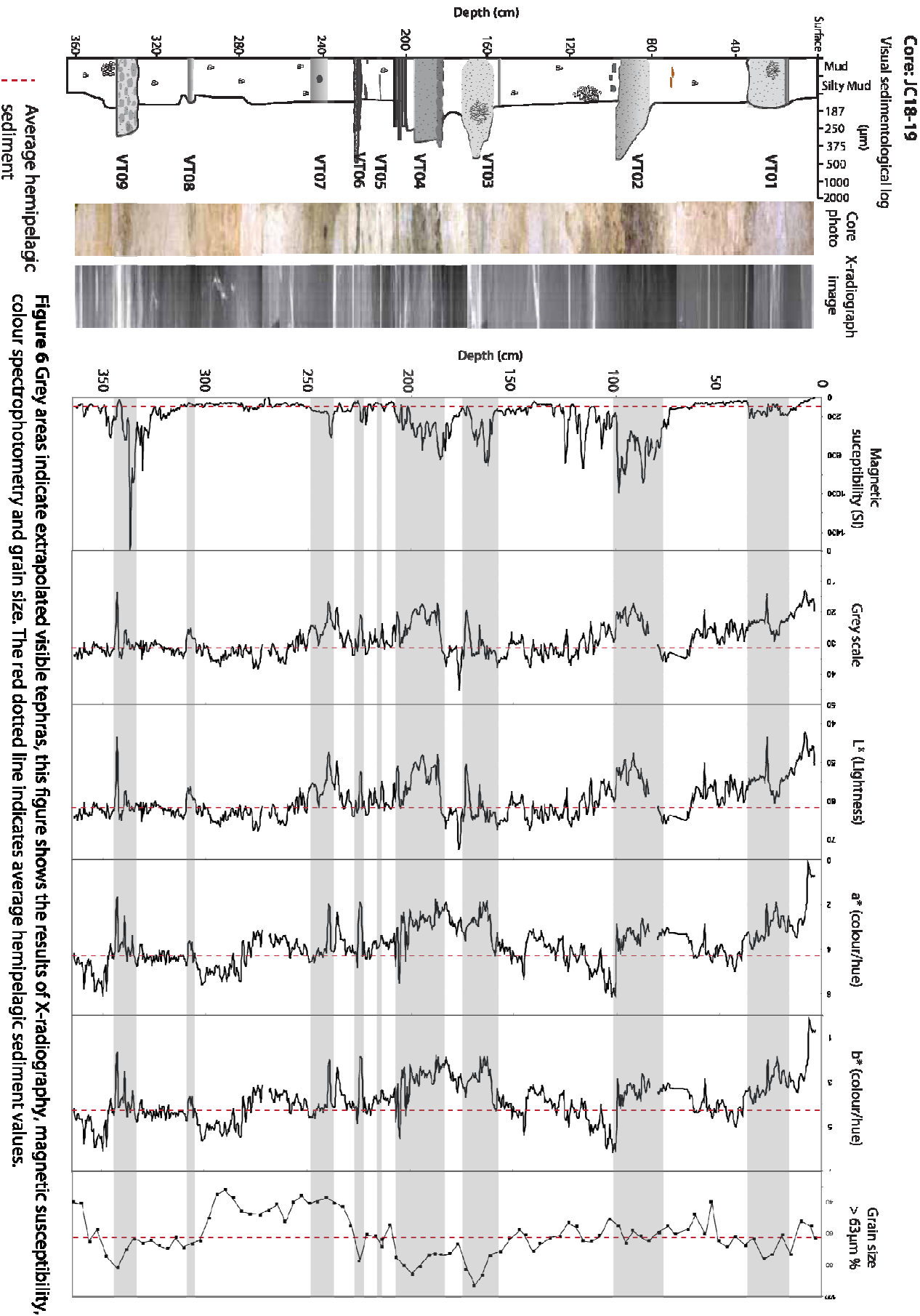


Figure 6 Grey areas indicate extrapolated visible tephra, this figure shows the results of X-radiography, magnetic susceptibility, colour spectrophotometry and grain size. The red dotted line indicates average hemipelagic sediment values.

3.5.6 XRF core scanning

This study used the IRAX instrument at NOC to measure bulk geochemical profiles (semi-quantative) down the core. XRF core scanning is non-destructive, and has an excellent sampling resolution (0.2-1 mm), which can help in the detection of thinner tephra and even cryptotephra. This technique was successful in detecting all eight of the visible tephra horizons within the range scanned (the first 70 cm was not scanned, and therefore did not cover the first visible tephra, VT01). Different tephra layers yielded stronger signals for different element ratios (Figure 7). For example, layer VT-08 does not yield a strong Ti/Sr peak, but it does produce clearly recognizable Mn/Sr and Mn/Ca signals. In contrast, VT-07 has a sharp Ti/Sr, Fe/Sr and Fe/Ca peaks towards the top of the unit, but the Mn/Sr and Mn/Ca peaks are much broader. While it is tempting to ascribe these patterns to geochemical processes, such as diagenetic Mn reduction and diffusion as a result of low pore water oxygen concentrations associated with ash deposition (Hembury et al., 2012), it is important to recognise that the XRF data are semi-quantitative and strongly dependent on surface roughness of the sediment surface and the sediment grain size. Despite these caveats, it is evident that the XRF core scanning is very successful in identifying the visual tephra layers. A detection rating of 5 was, therefore given for this technique.

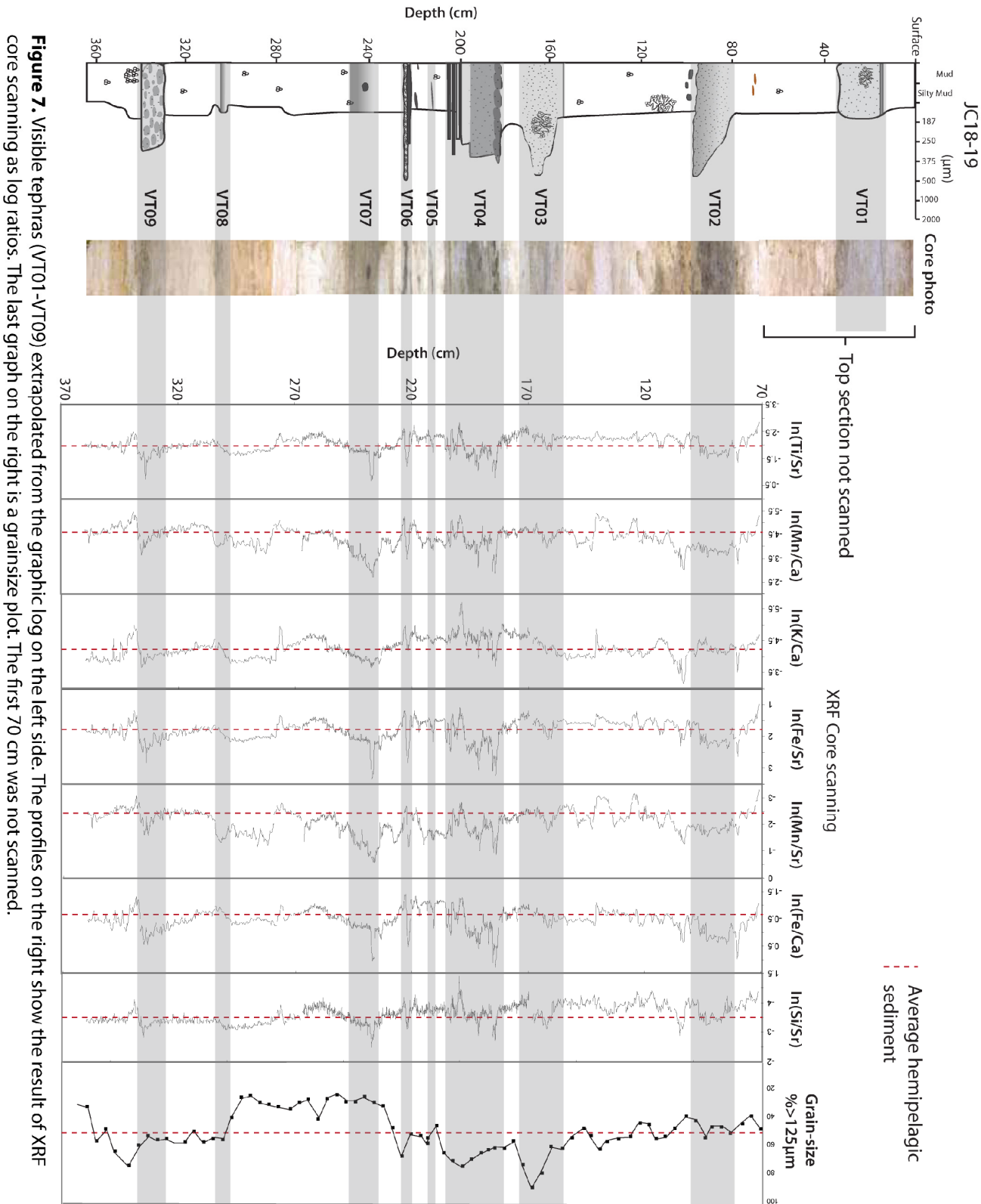


Table 2. Summary of most effective tephra detection methods

Technique	Visual tephra identified	Benefits	Limitations	Detection rating (1-5)
Magnetic susceptibility	8/9	Fast and cost effective, non-destructive, sampling resolution is good	Sampling resolution is satisfactory, but may only detect thick units	4
Colour Spectrophotometry (Grey scale, L*, a* & b*)	8/9	Fast and cost effective, non-destructive, sampling resolution is good	Signal not always unambiguous	3
X-radiography	Ambiguous	Can image sedimentary structures, fast, provides density change information, non-destructive, sampling resolution is excellent	Information is qualitative and noisy signal, very sensitive to cracks and other core artefacts	1
Grain-size	5/9	Cost effective, provides sedimentological information, e.g. grading and sorting.	Signal may be ambiguous, tephra layers can be both fine and coarse, so not definitive. Poor resolution, slow and destructive	2
Component analysis/point counting	5/9	Provides important characterization information, can help distinguish a primary tephra from a reworked tephra	Poor resolution and very slow, destructive, dilution effects, noisy signal due to difficulty in defining background values	2
XRF core scanning	8/8	Good tephra detection, can help distinguish between volcanic and non-volcanic deposits, excellent sampling resolution, fast, non-destructive	Semi-quantative, costly, grain size and water content can have major impacts	5

3.6 *Cryptotephra detection*

Having tested the tephra detection methods on visible layers, the same techniques were used to scan for any cryptotephra within the hemipelagic sediments between the visible layers. Average hemipelagic values for magnetic susceptibility, colour spectrophotometry and XRF core scanning were estimated based on a relatively undisturbed hemipelagic sediment section (at 300-330 cm). Any deviations from this average, and any peaks in the component analysis, a list of potential cryptotephra depths and the methods used to detect them was compiled (Table 3). The potential cryptotephra were given a score (weighted according to the technique's detection rating (Table 2)), by adding up of the detection rating of each of the techniques used to identify them (Table 2). A score of 5 or above was determined a potentially legitimate signal. Some potential cryptotephra, whose scores were above 5 were discounted if they showed signs that they were non-volcanic, for example higher abundances of Ca over Fe in the XRF core scanning profiles and coincident bioclastic maxima observations (Figure 5). These deposits are more likely to be dominated by bioclastic material sourced from remobilised sediment. Thus, the magnetic susceptibility peak at 115 cm was discounted due to the high Ca/Fe and Ca/Mn XRF peaks. Using this scoring process eight cryptotephra were detected, named CYP01-CYP09 (Table 3).

A previous marine tephrochronological record from this area used component analysis to identify cryptotephra (Le Friant et al., 2008). Component analysis was also performed to detect potential hidden tephra layers in core JC18-19 (Figure 5), but out of the 8 potential cryptotephra identified in Table 3, component analysis could only detect 4 (CYP01, CYP03, CYP06 CYP07). It also detected 2 'false' signals at 163 cm and 250-265 cm, which were deemed not to represent tephra layers, because these were shown to be reworked bioclastic deposits (Table 3). It is important to note, however, that different techniques are likely applicable to different settings. For example, Gudmundsdottir et al. (2011) were successful in applying component analysis and grain size changes to detect cryptotephra in marine sediment cores from the North Icelandic shelf. We conclude that component analysis by point counting alone is limited in its ability to define cryptotephra stratigraphy.

Table 3. Potential Cryptotephra

Depth in the core	Methods that detected them	Weighted score (must ≥ 5 to be considered)	Volcanic deposit layer? Why?
7 cm	Colour spectroscopy	= 3	No, not high enough rating to be considered
40 cm	Point counting and colour spectroscopy	2 + 3 = 5	Yes (CYP01). A score of ≥ 5 was recorded
42-60 cm	Colour spectroscopy	= 3	No, not high enough rating to be considered
58 cm	Colour spectroscopy and grain size	3 + 2 = 5	Yes (CYP02). A score of ≥ 5 was recorded
115 cm	Magnetic susceptibility, x-radiography	4 + 1 = 5	No, it sits at a bioclastic maxima (identified by microscope) and XRF core scanning shows it is enriched in Ca versus Fe and other volcanic elements, suggests a bioclastic origin and not principally volcanic
122 cm	Magnetic susceptibility, Grain size	4 + 2 = 5	No, XRF core scanning shows it is enriched in Ca versus Fe and other volcanic elements, suggests a bioclastic origin
127 - 133 cm	XRF core scanning, Point counting	5 + 2 = 7	Yes (CYP03). A score of ≥ 5 was recorded
140 - 148 cm	XRF core scanning, Grain size	5 + 2 = 7	Yes (CYP04). A score of ≥ 5 was recorded
163 cm	Point counting	= 2	No - not high enough rating to be considered and also at bioclastic maxima
227 cm	XRF core scanning	= 5	Yes (CYP05). A score of ≥ 5 was recorded
250-265 cm	Grain size, Point counting and colour spectroscopy	2 + 2 + 3 = 7	No, XRF core scanning shows an increase in Ca over Fe-probably bioclastic origin
270 cm	Point counting, Colour spectroscopy, XRF core scanning	2 + 3 + 5 = 10	Yes (CYP06). A score of ≥ 5 was recorded
280 - 290 cm	X-radiography, point counting, grain size, XRF core scanning	1 + 3 + 2 + 5 = 11	Yes (CYP07). A score of ≥ 5 was recorded
318 cm	X-radiography	= 1	No, not high enough rating to be considered
363 cm	Grain size, XRF core scanning	2 + 5 = 7	Yes (CYP08). A score of ≥ 5 was recorded

3.7 *Primary or reworked*

The identified visible and cryptotephra horizons, VT01-VT09 and CYP01-CYP08, were sampled, cleaned and their carbonate content dissolved. Microscopic analysis was then used to sort the clasts according to their angularity, sphericity, sorting and compositional maturity (Tables 4 & 5). These criteria were then used to assess whether the volcanic deposits were primary or reworked (Figure 8). For the visible tephtras, sedimentological features were also taken into consideration, such as the presence of erosive bases, and tractional structures which are usually associated with flow deposits. Volcanic deposits which were well-sorted, compositionally mature (dominance of one clast type), and had clasts of low sphericity but high angularity were concluded to be primary. Deposits showing rounded, highly spherical clasts, which were poorly-sorted and comprised a large range of components were deemed to be reworked subaerial volcanoclastic deposits. As a result of this qualitative analysis, five of the visible tephra units were classified as reworked volcanoclastic deposits and the remaining four were termed as primary pyroclastic fall and flow deposits (Table 4). Of the cryptotephtras, four were deemed to be reworked and four were interpreted as primary ash fall tephtras (Table 5). This method is limited in its usefulness however, as it is only a qualitative exercise. In addition, exceptions may exist in the criteria, for example, a primary volcanic deposit may be poorly-sorted if ash is transported at different levels in the atmosphere with differing wind trajectories, as in the 1991 Pinatubo eruption (Wiesner et al., 2004). Furthermore, aggregation of clasts of varying sizes is thought to commonly occur within ash plumes, leading to poorly-sorted airfall deposits (Carey and Sigurdsson 1982; Stevenson et al. in press). Determining whether a deposit is of primary or reworked origin is an important consideration, as volcanoclastic flow deposits, e.g. from turbidity currents, debris flows, or landslides, do not necessarily coincide with an eruption, therefore, eruption histories can be artificially inflated by including non-primary deposits.

Table 4. Visual tephra - Primary or reworked?

Sample Name	Depth (cm)	Average clast size (mm)	Sorting	Degree of Angularity and Sphericity of clasts	Dominant clast type(s)	Compositional maturity	Sedimentological evidence for emplacement	Conclusion
VT01	15	0.35	Moderate	Sub angular, high sphericity	Glass shard, vesicular juvenile clasts, crystal fragments	Moderate to well	Lots of fragmented bioclastic material	Reworked bioclastic-rich flow
VT02	85	0.8	Poor	Sub rounded, moderate to high sphericity	Dense and poorly vesiculated clast, altered dome clasts	Very poor	Erosive base, grading, oxidised (red) appearance, very thick deposit	Reworked volcaniclastic-rich turbidite
VT03	159	0.4	Moderate to well	Sub angular, low to moderate sphericity	Glass shard, vesicular juvenile clasts	Moderate	No defining features, bioclasts well-preserved	Primary explosive eruption
VT04	189	0.4	Well	Sub angular, high sphericity	Dense and poorly vesiculated clasts, mafic clasts, altered dome clasts, glass shards	Poor	Deposit is thick and vertically heterogeneous with pod-like deposits of volcanic material	Reworked but well-sorted, low-concentration, volcaniclastic-rich turbidite
VT05	219	0.4	Moderate to Poor	Sub rounded, high sphericity	Glass shards, altered dome clasts, crystal fragments, dense and poorly-vesiculated clasts	Poor	Very thin dark layer with lots of fragmented bioclasts material	Reworked volcaniclastic flow
VT06	220	0.45	Well	Sub angular, moderate sphericity	Glass shards, dense and poorly vesiculated clasts, altered dome clasts	Moderate	No defining features, thin deposit, with disturbed upper boundary, prominent dark ash layer	Primary, possibly a large dome-related eruption
VT07	236	0.25	Very well	Sub angular, low sphericity	Glass shards, dense and poorly-vesiculated clasts, Vesicular juvenile clasts	Moderate to well	Pod-like volcanic material and diffuse volcanic deposit	Primary, pyroclastic flow deposit, possibly dome-related eruption
VT08	303	0.45	Poor	Angular clasts, low sphericity	Glass shards, crystal fragments, altered dome clasts	Moderate to poor	Diffuse deposit, no defining signs from appearance- some	Reworked volcaniclastic flow

Table 5. Cryptotephra - Primary or reworked?

Sample Name	Depth (cm)	Average clast size	Sorting	Degree of Angularity and Sphericity of clasts	Dominant clast type	Compositional maturity	Conclusion
CYP01	40	0.3	Well	Sub angular, moderate sphericity	Glass shards, altered dome clasts	Moderate to poor	Reworked
CYP02	58	0.3	Moderate to poor	Angular, high sphericity	Glass shards, dense and poorly vesiculated clasts, altered dome clasts	Poor (Immature)	Reworked
CYP03	129	0.2	Well	Very angular, low sphericity	Glass shards, crystal fragments	Well (mature)	Primary, explosive eruption.
CYP04	141	0.5	Moderate to well	Angular, low to moderate sphericity	Glass shards and vesicular juvenile clasts	Moderate to well	Primary, explosive eruption
CYP05	227	0.3	Poor	Sub angular, moderate sphericity	Glass shards, altered dome clasts, crystal fragments, mafic clasts	Poor	Reworked
CYP06	270	0.25	Moderate to well	Sub-angular, low to moderate sphericity	Glass shards, vesicular juvenile clasts	Well	Primary, explosive eruption
CYP07	288	0.25	Well	Very angular, low to moderate sphericity	Glass shards	Very well	Primary, explosive eruption
CYP08	363	0.4	Moderate to poor	Sub angular, moderate sphericity	Glass shards, crystal fragments, vesicular juvenile	Moderate to poor	Reworked

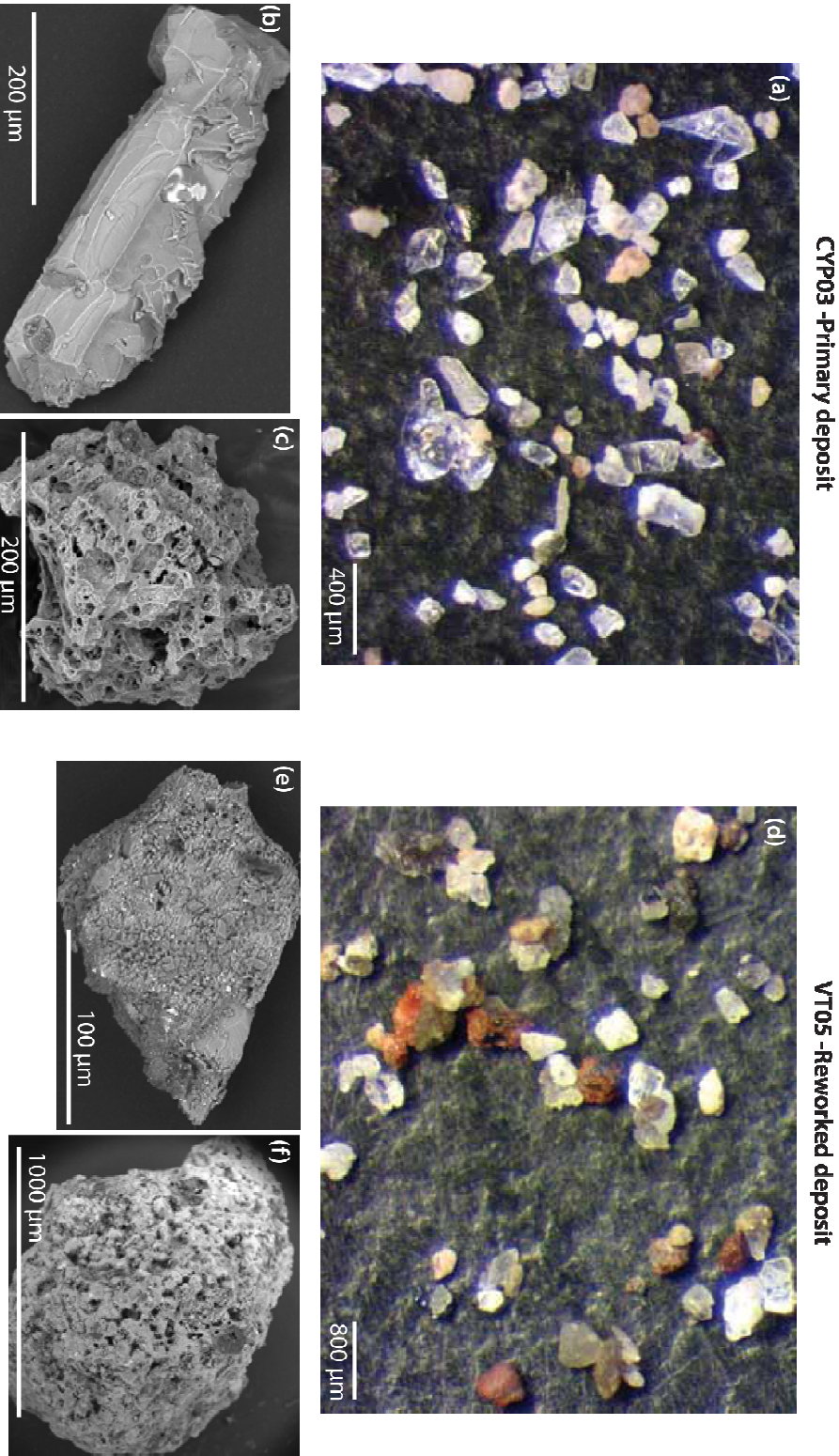


Figure 8. (a) Microscopic image of a typical primary ash deposit (CYP03). The clasts are angular, elongate and the compositional maturity i.e. variation in clast type is mature, shown by the dominance of well sorted glass shards. (b) An SEM image of an elongate and angular glass shard. (c) An SEM image of a vesicular juvenile clast, which can be common in primary volcanic ash fall deposits. (d) A microscopic image of typical reworked deposit (VT05). The clasts are poorly sorted, more spherical and rounded and the variation in clast type is vast (compositionally immature). With oxidised red altered dome clasts, non vesicular dome clasts and mafic clasts, suggesting clasts have been derived from multiple different eruptions. (e) An SEM image of dense and poorly vesiculated clast, with smaller clasts adhered to its surface. (f) An SEM image of a well rounded and spherical mafic clast, with differing mineral assemblage to the other clasts.

3.8 *Nature of volcanic activity*

The nature of the source volcanic activity responsible for the tephra deposits is difficult to discern based solely on observations made under the microscope on samples from a distal core. Inferences, where made, were based on the thickness of the deposit, the average clast size and the type of clasts present; for example a high proportion of vesicular juvenile clasts suggests an explosive event, whereas dominance of non-vesicular juvenile and dome clasts is more suggestive of a dome-related eruption e.g. Le Friant et al. (2008) (Tables 4 & 5). Glass shards were abundant in most of the deposits; making it difficult to deduced much about the eruptive style from their mere presence.

4. Discussion

4.1 *What is the most effective way of detecting and identifying tephra layers?*

Fast, non-destructive and high spatial resolution techniques should be chosen first when attempting to detect potential cryptotephra. Of the techniques employed here, XRF-core scanning, magnetic susceptibility and colour spectrophotometry fall into these categories. It is important to recognise, however, that these techniques only help identify areas which require further investigation. Nevertheless, of these three techniques, XRF-core scanning was found to be the most efficient for detecting cryptotephra, although the more techniques used, the more likely it is that an unequivocal tephra signal will be obtained. All of these core scanning techniques will only help detect areas of possible tephra accumulation. These areas then require further investigation.

Component analysis and grain size variations were ineffective tools for detecting cryptotephra on their own as they lack the practical sampling resolution and are destructive. Component analysis is, however, an important tool for confirming the identity of potential cryptotephra, and whether they are primary volcanic events or reworked from older eruptions. This study confirms that a combination of detection and identification procedures will yield the best results. A weighted score system and specific microscopic criteria are presented (Tables 2, 3, 4 & 5), wherein the use of fast, non-destructive techniques lessens the initial work load of fine-scale sampling an entire core for component analysis. Then once likely volcanic tephra horizons have been identified, a more focused sampling campaign can proceed. This protocol will produce faster results and makes for more efficient use of limited core samples.

4.2 *Inherent problems and limitations of detecting tephra in marine sediment records*

Bioturbation is a common feature within marine tephra sequences, and thin tephra layers in particular are prone to disturbance by this process (Wetzel, 2009). Tephra layers

are often typified by the presence of sharp bases, but gradational upper (bioturbated) contacts (Manville and Wilson, 2004). Evidence from other studies (e.g. Wetzel 2009) suggest that sub centimetre tephra layers are too thin to suppress benthic biota activity and therefore prevent post-depositional bioturbation (Manville and Wilson, 2004). The preservation of a tephra layer of any thickness, however, is heavily dependent on the background hemipelagic sedimentation rate, with a high burial rate able to preserve 1-4 cm thick tephra deposits, although this also depends on environmental conditions such as the nature of the background sediments and bottom water oxygen concentrations (Wetzel, 2009; Hembury et al. 2012).

Volcanic ash layers can also be observed as lenses or 'pods' in marine sediments, as a result of burrowing by benthic dwellers, reworking by strong ocean currents or slumping on steep seafloor topography (Hunt and Najman, 2003). The presence of bioturbation can often be detected by a blotchy appearance in sediment cores, however on occasion bioturbation is so extensive it produces a seemingly homogenous sediment pile. Bioturbation may thus distort an originally thick and visible tephra layer into a diffuse cryptotephra (Hunt and Najman, 2003; Manville and Wilson, 2004), illustrating the importance of using multiple techniques to detect such horizons.

Erosion is another important factor to consider when reconstructing events within the marine realm. Erosion at the base of submarine mass flow is especially in submarine channels and proximal to source locations, but it can also occur more distally. For example, the sediment sampled by JC18-19, 55 km offshore Montserrat preserves evidence of erosion of at least 14 cm of underlying hemipelagic sediment beneath the VT01 event. This is represented as the erosion of 33.3 kyrs of material (using a sedimentation rate of 2.3 cm ka^{-1} from Le Friant et al. (2008)), during which time the record of geologically significant events may have also been removed. Such erosion may remove entire tephra layers, leading to an incomplete volcanic record.

In most cases, airfall deposits evenly mantle marine bathymetry, analogous to ash fall horizons in subaerial topography. This is evidenced by ground penetrating radar and multiple cores sampled from lake sediments in New Zealand (Green and Lowe, 1985; Lowe, 1985), however tephra fallout from the Campanian ignimbrite eruption preserved in marine cores sampled in the Mediterranean Sea, suggest that tephra thickness varies according to surrounding bathymetry (S. Engwell Pers. Comm. 2012). Submarine flows are likely to be channelized in depressions, as a result, airfall tephra may be preserved from erosion when emplaced on bathymetric highs.

Variable weather conditions, e.g. wind strength and direction, and pervasive precipitation, may also affect volcanic fallout within ash plumes and has a strong control on tephra preservation in any one location. For these reasons, it is preferable that multiple cores

are sampled at varying proximities and directions from source, to increase the likelihood of finding tephra from a particular source. Geophysical mapping of the seafloor would also allow bathymetric lows to be selectively cored for likely flow deposits and bathymetric highs to be selectively cored for potential airfall deposits. This procedure would reduce the risk of an ash unit being missed in the reconstruction as wide geographic coverage increases the likelihood of finding tephra that have been distributed into a variety of environments by varying weather conditions.

4.3 Other tephra detection methods not explored in this study

There are other methods for detecting tephra deposits which were not tested in this study due to time constraints. These techniques include those used to detect tephra in lacustrine, peat and terrestrial cores, but which may have useful applications for studying marine cores. Some of the techniques used to detect tephra in peat cores, such as total organic carbon measurements, are not appropriate for volcanoclastic marine core studies, but are discussed in detail by Gehrels et al. (2008).

The study by Kutterolf et al. (2007) used magnetic susceptibility, p-wave velocity and sediment densities from gamma-ray attenuation to detect distal ash units in marine cores derived from Central American volcanoes. This study was successful in identifying several tephra layers which could not be visually identified, and of the methods employed, magnetic susceptibility proved to be the most insightful. Remnant magnetism is often used to supplement magnetic susceptibility measurements (although not usually used in its own right), but the signal acquired is quite similar to magnetic susceptibility (Gomez et al., 2007; Venuti and Verosub, 2010). X-ray diffractograms have been used to detect tephra successfully in marine cores, particularly for sediment intervals with high glass shard contents, in which case basaltic and rhyolitic ash compositions can sometimes be distinguished in situ (Andrews et al. 2006). Lim et al. (2008) used high-resolution trace element analysis by Instrumentation Neutron Activation Analysis (INAA) to detect and characterise ash deposits. Although it is especially useful in detecting alkaline volcanic material through Ta/Sc ratios and rhyolitic material using Cr/Sc ratios, it is also a destructive technique with limited resolution. Biological proxies may also be useful in searching for ash fall layers, for example mass mortality of pteropods is seen in sediment cores after ash fall from eruptions from the Soufrière Hills volcano, Montserrat. This mortality is thought to be caused by local volcanogenic ocean acidification via the release of acid bound to the volcanic ash (Frogner et al., 2001; Jones and Gislason, 2008; Wall-Palmer et al., 2011).

Laser Ablation Inductively Coupled Plasma Mass Spectrometry (LA-ICPMS) and Electron Microprobe (EMP) analyses of glass shards are also commonly used to identify and correlate volcanic deposits (Froggatt, 1992; Pearce et al., 1999, 2004), but these techniques

are only employed after a tephra horizon has been detected. In which case, they are also useful to help distinguish primary volcanic deposits; which should exhibit limited chemical variation between glass shards compared to reworked volcanoclastic deposits.

Volcanic material can be dated by fission-track and Ar-Ar among others methods (Pillans et al., 1996), but this direct method of dating will not provide an age of sediment emplacement. Isotope systems such as ^{210}Pb and ^{137}Cs can be used to date young deposits, and magnetostratigraphy is more applicable to older deposits (Lowe et al., 2011).

4.4 The volcanic history of Montserrat

In this study six major volcanic units were identified and correlated in proximal deposits (7-15 km from the shore) to the south and south west coast of Montserrat. These deposits likely record the SSH period of volcanism which was emplaced ca 130 ka (Harford et al., 2002; Le Friant et al. 2008), suggesting that the proximal cores record events occurring within the past 130 ka. This proximal record mainly records flow events, such as pyroclastic density currents and bioclastic and volcanoclastic clast-rich landslides, many of which are not observed in subaerial records (Harford et al., 2002; Smith et al., 2007), cores sampled in the south east (Trofimovs et al., 2010) or cores sampled more distal to source (Le Friant et al., 2008). This includes a widespread dome collapse deposit at ~8.4 ka, a voluminous shelf collapse at 8.4-35 ka, an pyroclastic eruption at ~ 75 ka shortly followed by a lahar-induced turbidity current.

In the distal core record, using a core sampled 55 km south west offshore Montserrat, eight primary events were recorded between 37 ka to ~135 ka (Figure 9). The main periods of activity were ~40-43 ka, during which three primary explosive volcanic eruptions were identified. This concurs with an event at 43 ka recognised in the distal marine record by Le Friant et al. (2008), and is consistent with pyroclastic deposits found on land dated at 38 ± 8 ka (Soufrière Hills Subunit III; Harford et al., 2002). Another primary volcanic dome-related eruption at ~75 ka correlates well to an event at 77 ka from Le Friant et al. (2008) and with an Ar-Ar date from on-land at 75 ± 10 ka (Soufrière Hills subunit II; Harford et al. 2002). A dome-related eruption at ~100 ka, does not match the record from Le Friant et al. 2008, but it may correspond to their dome forming event at 115 ka and Galways dome eruption from the subaerial record at 112 ± 9 ka. Another period of intense explosive activity is found at ~123-130 ka, when three primary eruptions are recorded. These relate to the activity of the Soufrière Hills and SSH which erupted at overlapping time periods (Cassidy et al., 2012, in press). The event nearest to 130 ka recorded in this study contains an abundance of olivine as a phenocryst phase in the vesicular clasts, this petrology is consistent with rocks found at the SSH volcanic centre (Harford et al. 2002). Overall, this study found four main periods of activity from 37 to 130 ka, that relates well to dated events from subaerial record and are

comparable with the study of Le Friant et al. (2008). However, this study found eight eruptions during the time period when only six were identified by Le Friant et al. (2008). This suggests that a method purely involving component analysis may miss events due to poor sampling resolution.

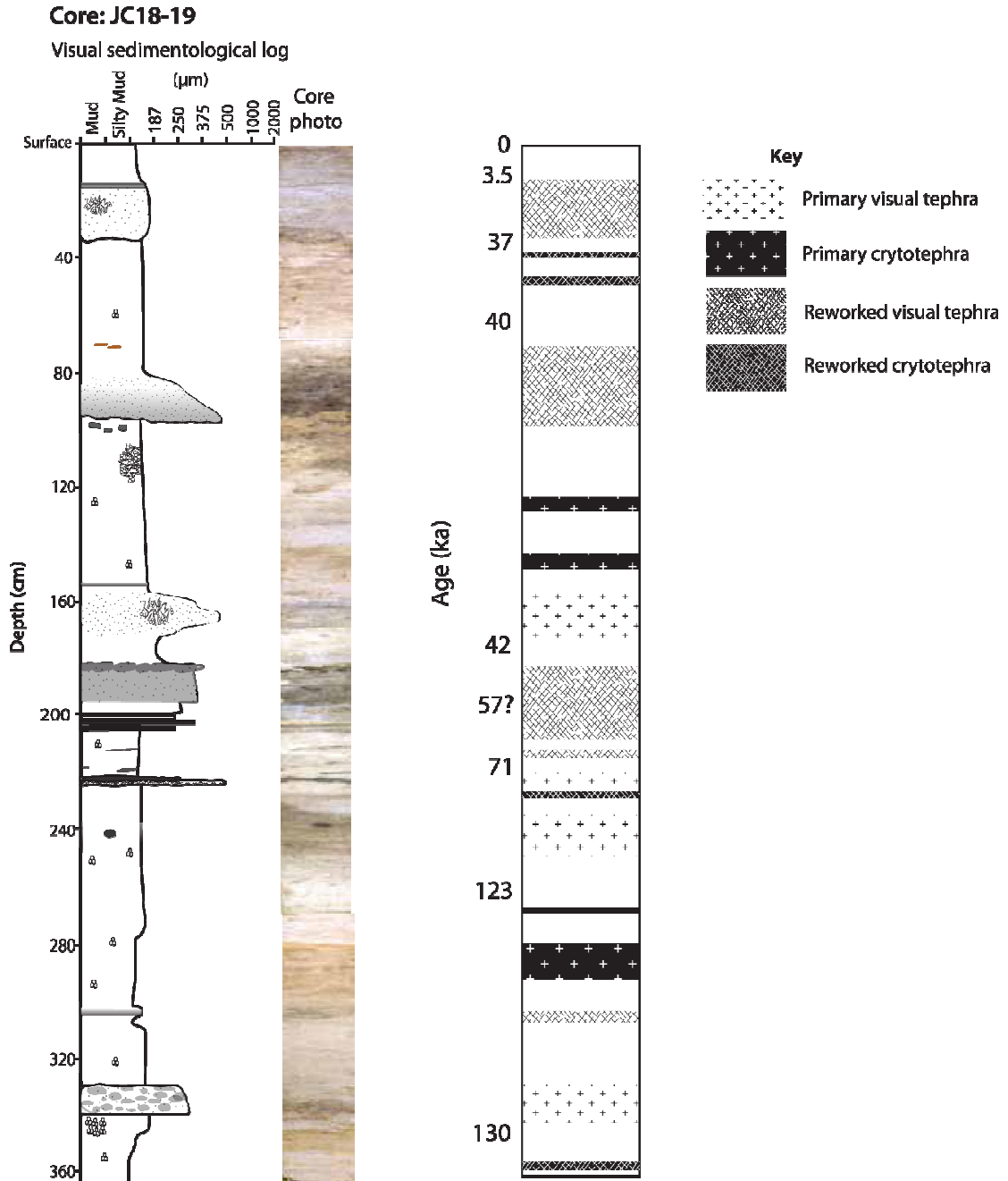


Figure 9. Schematic log shows primary eruption deposits (indicated by crosses) and reworked deposits (indicated by cross-hatch pattern). The visual tephras have white background, whilst the cryptotephra have a black background. Known ages from the core chronology (figure 8) are indicated on the left side of the log. In total, 8 primary ash fall events are recorded from 37 ka to 130 ka.

5. Conclusions

We have tested various methods for detecting tephra layers and cryptotephra in marine sediment cores. The techniques have been judged based on how well they could detect tephra units that had been visually identified, and as a result a detection rating was assigned to each. This provided a weighted score system, which was then used to assess whether potential cryptotephra were legitimate tephra and not part of the background sedimentation. The benefits and limitations of each technique have been explored, and the results show that XRF core scanning is best technique used to detect tephra, but that it should be used in conjunction with other non-destructive scanning techniques such as magnetic susceptibility and colour spectrophotometry for the best possible results. We have dated marine events by analysing hemipelagic sediment through different means such as bulk sediment oxygen isotope, species-specific benthic oxygen isotopes and AMS radiocarbon dating. This has identified 8 primary eruptive events, some of which have not been recorded by previous marine studies that employed different tephra detection methods. The proximal core stratigraphy south and south west (8-15 km offshore) of Montserrat shows five significant events related to subaerial and submarine landslides and primary pyroclastic density currents.

As a result of these studies we make the following suggestions for identifying tephra in marine sediment cores that minimise labour and increase the likelihood of identifying cryptotephra.

- Make a graphic log of the core(s) taking into consideration sedimentological and visual features to create a record of the visible tephra.
- Use fast, non-destructive core scanning techniques, such as XRF core scanning and magnetic susceptibility to detect possible horizons containing tephra. This study found XRF core scanning and magnetic susceptibility to be the most beneficial techniques for identifying mafic to intermediate volcanoclastic material on the basis of their ability to detect the visually-recorded units.
- Use the above techniques to note any points where the signal deviates from average background sedimentation values. Such deviations may highlight primary ash fall layers, turbidites from primary pyroclastic flows or reworked volcanoclastic material.
- After target potential tephra horizons have been identified, these should be sampled using more stringent analytical techniques, such as component analysis and glass shard geochemistry. Use descriptive criteria to judge whether they are reworked or primary tephra deposits. Primary and reworked deposits can be distinguished under

a microscope on the basis of glass shard morphology, compositional maturity and sorting. If possible use EMP and LA-ICP-MS analyses of glass shards, which is especially useful for determining if the shards are from different eruptions and for correlating distal ashes from core to core.

- Date the hemipelagic sediment between the tephra deposits, by AMS radiocarbon dating for sediments <50 ka and produce an oxygen isotope stratigraphy (preferably species-specific) for older deposits.

References

- Allen, J.R.L. (1971) "Instantaneous sediment deposition rates deduced from climbing-ripple cross-lamination" Journal of Geological Society of London **127** 553-561
- Amy, L.A. and P.J. Talling (2006) "Anatomy of turbidites and linked debrites based on long distance (120 x 30 km) bed correlation, Marnoso Arenacea Formation, Northern Apennines, Italy" Sedimentology **53** 161-212
- Andrews, J.T., D.D. Eberl and G.B. Kristjansdottir (2006) "An exploratory method to detect tephra from quantitative XRD scans: examples from Iceland and east Greenland marine sediments" Holocene **16** 1035-1042
- Barclay, J., J. Alexander and J. Susnik (2007) "Rainfall-induced lahars in the Belham Valley, Montserrat, West Indies" Journal of the Geological Society **164** 815-827
- Barclay, J., M.J. Rutherford, M.R. Carroll, M.D. Murphy, J.D. Devine, J. Gardner and R.S.J. Sparks (1998) "Experimental phase equilibria constraints on pre-eruptive storage conditions of the Soufriere Hills magma" Geophysical Research Letters **25** 3437-3440
- Blum, P. (1997) "Physical properties handbook: A guide to the ship board measurement of physical properties of deep-sea cores" In (eds) *ODP Tech. Note 26* Ocean Drilling Program College Station, Tex
- Bonadonna, C., Mayberry, G.C., Calder, E.S., (2002) "Tephra fallout in the eruption of the Soufriere Hills Volcano, Montserrat" In T. H. In Druitt, Kokelaar, B.P. (eds) *The eruption of Soufriere Hills Volcano, Montserrat, from 1995 to 1999* Geological Society of London Memoirs **21** 483-516
- Bond, G., H. Heinrich, W. Broecker, L. Labeyrie, J. McManus, J. Andrews, S. Huon, R. Jantschik, S. Clasen, C. Simet, K. Tedesco, M. Klas, G. Bonani and S. Ivy (1992) "Evidence for massive

discharges of icebergs into the North Atlantic ocean during the last glacial period" Nature **360** 245-249

Boudon, G., A. Le Friant, J.C. Komorowski, C. Deplus and M.P. Semet (2007) "Volcano flank instability in the lesser Antilles arc: diversity of scale, processes, and temporal recurrence" Journal of Geophysical Research-Part B-Solid Earth B08205-1-28

Bouma, A.H. (1962) "Sedimentology of Some Flysch Deposits: A Graphic Approach to Facies Interpretation" Elsevier 168 p

Bouysse, P. and D. Westercamp (1990) "Subduction of atlantic aseismic ridges and late cenozoic evolution of the Lesser Antilles island-arc" Tectonophysics **175** 349-&

Branney, M.J., Kokelaar, B.P., (2002) "Pyroclastic density currents and the sedimentation of ignimbrites" Geological Society of London, Memoirs **27** 152

Branney, M.J. and P. Kokelaar (1992) "A reappraisal of ignimbrite emplacement - Progressive aggradation and changes from particulate to nonparticulate flow during emplacement of high-grade ignimbrite" Bulletin of Volcanology **54** 504-520

Brendryen, J., H. Hafliðason and H.P. Sejrup (2010) "Norwegian Sea tephrostratigraphy of marine isotope stages 4 and 5: Prospects and problems for tephrochronology in the North Atlantic region" Quaternary Science Reviews **29** 847-864

Briden, J.C., D.C. Rex, A.M. Faller and J.F. Tomblin (1979) "K-Ar geochronolgy and paleomagnetism of volcanic-rocks in the Lesser Antilles arc" Geophysical Journal of the Royal Astronomical Society **57** 272-272

Bryn, P., K. Berg, C.F. Forsberg, A. Solheim and T.J. Kvalstad (2005) "Explaining the Storegga Slide" Marine and Petroleum Geology **22** 11-19

Calder, E.S., P.D. Cole, W.B. Dade, T.H. Druitt, R.P. Hoblitt, H.E. Huppert, L. Ritchie, R.S.J. Sparks and S.R. Young (1999) "Mobility of pyroclastic flows and surges at the Soufriere Hills Volcano, Montserrat" Geophysical Research Letters **26** 537-540

Carey, S. (1997) "Influence of convective sedimentation on the formation of widespread tephra fall layers in the deep sea" Geology **25** 839-842

Carey, S. (2000) "Volcaniclastic sedimentation around island arc" In H. Sigurdsson (eds) *Encyclopedia of volcanoes* Academic press 627-642

- Carey, S.N., Sigurdsson, H. (1984) "A model of volcanogenic sedimentation in marginal basins" Journal of the Geological Society London Special Publication **16**
- Carey, S.N. and H. Sigurdsson (1982) "Influence of particle aggregation on deposition of distal tephra from the May 18, 1980, eruption of Mount St. Helens volcano" Journal of Geophysical Research **87** 7061-7072
- Cas, R.A.F., and Wright, J.V. (1987) "Volcanic sucssions" Chapman & Hall, London 528
- Caseldine, C., A. Baker and W.L. Barnes (1999) "A rapid, non-destructive scanning method for detecting distal tephra layers in peats" Holocene **9** 635-638
- Cassidy, M., Trofimovs, J., Palmer, M.R., Taylor, R.N. Moreton, S. (in prep) "A new lava dome collapse into the ocean at the Soufriere Hills volcano, Montserrat, West Indies at ca 8 ka: how submarine stratigraphy can complement subaerial eruption histories"
- Cassidy, M., Trofimovs, J., Watt, S.F.L., Palmer, M.R., Taylor, R.N., Gernon, T.M., Talling, P.J., Le Friant, A. (in press) "Multi-stage collapse events in the South Soufrière Hills, Montserrat, as recorded in marine sediment cores" In G. Wadge, Robertson, R., Voight, B., (eds) *The eruption of Soufrière Hills volcano, Montserrat from 2000 to 2010* Memoir of the Geological Society, London
- Cassidy, M.T., R.N., Palmer, M.R, Cooper, R., Stenlake C., Trofimovs, J. (2012) "Tracking the magmatic evolution of island arc volcanism: Insights from a high-precision Pb isotope record of Montserrat, Lesser Antilles" Geochemistry Geophysics Geosystems
- Clark, R.N. (1999) "Chapter 1: Spectroscopy of Rocks and Minerals, and Principles of Spectroscopy" In R. N. Rencz (eds) *Manual of Remote Sensing, Remote Sensing for the Earth Sciences* John Wiley and Sons **3** 3-58
- Cole, P.D., E.S. Calder, T.H. Druitt, R. Hoblitt, R. Robertson, R.S.J. Sparks and S.R. Young (1998) "Pyroclastic flows generated by gravitational instability of the 1996-97 lava dome of Soufriere Hills Volcano, Montserrat" Geophysical Research Letters **25** 3425-3428
- Cole, P.D., E.S. Calder, R.S.J. Sparks, A.B. Clarke, T.H. Druitt, S.R. Young, R.A. Herd, Harford C.L. and G.E. Norton (2002) "Deposits from dome-collapse and fountain-collapse pyroclastic flows at Soufrière Hills Volcano, Montserrat" In T. H. Druitt and B. P. Kokelaar (eds) *The eruption of the Soufrière Hills Volcano, Montserrat 1995 to 1999* The Geological Society of London **21** 231-262

- Cole, R.B. and P.G. Decelles (1991) "Subaerial to submarine transitions in early Miocene pyroclastic flow deposits, southern San Joaquin basin, California" Geological Society of America Bulletin **103** 221-235
- Couch, S., R.S.J. Sparks and M.R. Carroll (2001) "Mineral disequilibrium in lavas explained by convective self-mixing in open magma chambers" Nature **411** 1037-1039
- Couch, S., R.S.J. Sparks and M.R. Carroll (2003) "The kinetics of degassing-induced crystallization at Soufriere Hills volcano, Montserrat" Journal of Petrology **44** 1477-1502
- Croudace, I.W., A. Rindby and R.G. Rothwell (2006) "ITRAX: Description and evaluation of a new multi-function X-ray core scanner" In R. G. Rothwell (eds) *New Techniques in Sediment Core Analysis* The Geological Society of London **267** 51-63
- DeMets, C., P.E. Jansma, G.S. Mattioli, T.H. Dixon, F. Farina, R. Bilham, E. Calais and P. Mann (2000) "GPS geodetic constraints on Caribbean-North America plate motion" Geophysical Research Letters **27** 437-440
- Deplus, C., A. Le Friant, G. Boudon, J.C. Komorowski, B. Villemant, C. Harford, J. Segoufin and J.L. Cheminee (2001) "Submarine evidence for large-scale debris avalanches in the Lesser Antilles Arc" Earth and Planetary Science Letters **192** 145-157
- Druitt, T.H. and B.P. Kokelaar (2002) "The eruption of the Soufrière Hills Volcano, Montserrat 1995 to 1999" The Geological Society Memoirs, London **21**
- Dugmore, A.J. and A.J. Newton (1992) "Thin tephra layers in peat revealed by X-radiography" Journal of Archaeological Science **19** 163-170
- Feuillet, N. (2000) "Sismotectonique des Petites Antilles, liason entre activite sismique et volcanique = Sismotectonics of Lesser Antilles, relationship between seismic activity and volcanism." Rene Diderot University PhD Thesis 283 pp
- Feuillet, N., F. Leclerc, P. Tapponnier, F. Beauducel, G. Boudon, A. Le Friant, C. Deplus, J.F. Lebrun, A. Nercessian, J.M. Saurel and V. Clement (2010) "Active faulting induced by slip partitioning in Montserrat and link with volcanic activity: New insights from the 2009 GWADASEIS marine cruise data" Geophysical Research Letters **37** 6
- Fine, I.V., A.B. Rabinovich, B.D. Bornhold, R.E. Thomson and E.A. Kulikov (2005) "The Grand Banks landslide-generated tsunami of November 18, 1929: preliminary analysis and numerical modeling" Marine Geology **215** 45-57

Fisher, R.V., Schmincke, H.U. (1994) "Volcaniclastic sediment transport and deposition" Blackwell Scientific Publications 351-388

Fisher, R.V. and G. Heiken (1982) "Mt Pelee, Martinique - May 8 and 20, 1902, Pyroclastic flows and surges" Journal of Volcanology and Geothermal Research **13** 339-371

Freeman, S.P.H.T., A. Dougans, L. McHargue, K.M. Wilcken and S. Xu (2008) "Performance of the new single stage accelerator mass spectrometer at the SUERC" Nuclear Instruments & Methods in Physics Research Section B-Beam Interactions with Materials and Atoms **266** 2225-2228

Freundt, A. (2003) "Entrance of hot pyroclastic flows into the sea: experimental observations" Bulletin of Volcanology **65** 144-164

Froggatt, P.C. (1992) "Standardization of the chemical analysis of tephra deposits, Report of the ICCT working group" Quaternary International **13-14** 93-96

Froggatt, P.C. and D.J. Lowe (1990) "A review of late Quaternary silicic and some other tephra formations from New Zealand: their stratigraphy, nomenclature, distribution, volume, and age" New Zealand Journal of Geology and Geophysics **33** 89-109

Frogner, P., S.R. Gislason and N. Oskarsson (2001) "Fertilizing potential of volcanic ash in ocean surface water" Geology **29** 487-490

Garcia, M.O. (1996) "Turbidites from slope failure on Hawaiian volcanoes" Geological Society London Special Publication **vol. 110** 281-294

Gehrels, M.J., R.M. Newnham, D.J. Lowe, S. Wynne, Z.J. Hazell and C. Caseldine (2008) "Towards rapid assay of cryptotephra in peat cores: Review and evaluation of various methods" Quaternary International **178** 68-84

Gomez, B., L. Carter and N.A. Trustrum (2007) "A 2400 yr record of natural events and anthropogenic impacts in intercorrelated terrestrial and marine sediment cores: Waipaoa sedimentary system, New Zealand" Geological Society of America Bulletin **119** 1415-1432

Green, J.D. and D.J. Lowe (1985) "Stratigraphy and development of c. 17000 year old Lake Maratoto, North Island, New Zealand, with some inferences about postglacial climatic change" New Zealand Journal of Geology and Geophysics **28** 675-699

- Gudmundsdottir, E.R., J. Eiriksson and G. Larsen (2011) "Identification and definition of primary and reworked tephra in Late Glacial and Holocene marine shelf sediments off North Iceland" Journal of Quaternary Science **26** 589-602
- Hampton, M.A. (1975) "Competence of fine-grained debris flows " Journal of Sedimentary Petrology **45** 834-844
- Hampton, M.A. (1979) "Buoyancy in debris flows" Journal of Sedimentary Petrology **49** 753-758
- Harford, C.L., Pringle, M.S., Sparks, R.S.J., Young S.R. (2002) "The volcanic evolution of Montserrat using $^{40}\text{Ar}/^{39}\text{Ar}$ geochronology." In T. H. Druitt, Kokelaar, B.P. (eds) *The eruption of Soufrière Hills Volcano, Montserrat, from 1995 to 1999* Geological Society of London Memoirs **21** 93-113
- Heinrich, H. (1988) "Origin and Consequences of Cyclic Ice Rafting in the Northeast Atlantic Ocean during the Past 130,000 Years" Quaternary Research **29** 142-152
- Hembury, D.J., Palmer, M.R., Fones, G.R., Mills, R.A., Marsh, R. and Jones, M.T. (2012) "Uptake of dissolved oxygen during marine diagenesis of fresh volcanic material" Geochimica et Cosmochimica Acta **84** 353-368
- Herd, R.A., M. Edmonds and V.A. Bass (2005) "Catastrophic lava dome failure at Soufriere Hills Volcano, Montserrat, 12-13 July 2003" Journal of Volcanology and Geothermal Research **148** 234-252
- Hodgson, D.A., C.L. Dyson, V.J. Jones and J.L. Smellie (1998) "Tephra analysis of sediments from Midge Lake (South Shetland Islands) and Sombre Lake (South Orkney Islands), Antarctica" Antarctic Science **10** 13-20
- Houghton, B.F., Wilson, C.J.N., Pyle, D.M. (2000) "Pyroclastic fall deposits" In H. Sigurdsson (eds) *Encyclopedia of Volcanoes* Academic Press 555-570
- Hsu, K.J. (2004) "Physics of Sedimentology" Springer
- Hunt, J.B., Najman, Y.M.R. (2003) "Tephrochronological and tephrostratigraphical potential of Pliocene-Pleistocene volcanoclastic deposits in the Japan Forearc, ODP Leg 186" In K. Suyehiro, Sacks, I.S., Acton, G.D., Oda, M. (eds) *Proceedings of the Ocean Drilling Program. Scientific Results* **186** 1e29

- Hunt, J.E., R.B. Wynn, D.G. Masson, P.J. Talling and D.A.H. Teagle (2011) "Sedimentological and geochemical evidence for multistage failure of volcanic island landslides: A case study from Icod landslide on north Tenerife, Canary Islands" Geochemistry Geophysics Geosystems **12**
- Ilstad, T., A. Elverhoi, D. Issler and J.G. Marr (2004) "Subaqueous debris flow behaviour and its dependence on the sand/clay ratio: a laboratory study using particle tracking" Marine Geology **213** 415-438
- Imbrie, J., Hays, J.D., Martinson, D.G. (1984) "The orbital theory of Pleistocene climate: support from a revised chronology of the marine 180 record" In A. L. Berger, Imbrie, J., Hays, J.D., Kukla, G., Saltzman, B. (eds) *Milankovitch and Climate, Part 1* 269-305
- Iverson, R.M. (1997) "The physics of debris flows" Reviews of Geophysics **35** 245-296
- Jones, M.T. and S.R. Gislason (2008) "Rapid releases of metal salts and nutrients following the deposition of volcanic ash into aqueous environments" Geochimica Et Cosmochimica Acta **72** 3661-3680
- Kneller, B. and C. Buckee (2000) "The structure and fluid mechanics of turbidity currents: a review of some recent studies and their geological implications" Sedimentology **47** 62-94
- Kneller, B.C. and M.J. Branney (1995) "Sustained high-density turbidity currents and the deposition of thick massive beds" Sedimentology **42** 607-616
- Kneller, B.C. and W.D. McCaffrey (2003) "The interpretation of vertical sequences in turbidite beds: The influence of longitudinal flow structure" Journal of Sedimentary Research **73** 706-713
- Kokelaar, P. and S. Koniger (2000) "Marine emplacement of welded ignimbrite: the Ordovician Pitts Head Tuff, North Wales" Journal of the Geological Society **157** 517-536
- Kuenen, P.H. (1966) "Matrix of turbidites: experimental approach" Sedimentology **7** 267-297
- Kutterolf, S., A. Freundt, W. Perez, T. Moerz, U. Schacht, H. Wehrmann and H.U. Schmincke (2008) "Pacific offshore record of plinian arc volcanism in Central America: 1. Along-arc correlations" Geochemistry Geophysics Geosystems **9**
- Kylander, M.E., E.M. Lind, S. Wastegard and L. Lowemark (2012) "Recommendations for using XRF core scanning as a tool in tephrochronology" Holocene **22** 371-375

Le Friant, A., C. Deplus, G. Boudon, N. Feuillet, J. Trofimovs, J.C. Komorowski, R.S.J. Sparks, P. Talling, S. Loughlin, M. Palmer and G. Ryan (2010) "Eruption of Soufriere Hills (1995-2009) from an offshore perspective: Insights from repeated swath bathymetry surveys" Geophysical Research Letters **37**

Le Friant, A., C. Deplus, G. Boudon, R.S.J. Sparks, J. Trofimovs and P. Talling (2009) "Submarine deposition of volcanoclastic material from the 1995-2005 eruptions of Soufriere Hills volcano, Montserrat" Journal of the Geological Society **166** 171-182

Le Friant, A., C.L. Harford, C. Deplus, G. Boudon, R.S.J. Sparks, R.A. Herd and J.C. Komorowski (2004) "Geomorphological evolution of Montserrat (West Indies): importance of flank collapse and erosional processes" Journal of the Geological Society **161** 147-160

Le Friant, A., E.J. Lock, M.B. Hart, G. Boudon, R.S.J. Sparks, M.J. Leng, C.W. Smart, J.C. Komorowski, C. Deplus and J.K. Fisher (2008) "Late Pleistocene tephrochronology of marine sediments adjacent to Montserrat, Lesser Antilles volcanic arc" Journal of the Geological Society **165** 279-289

Lebas, E., A. Le Friant, G. Boudon, S.F.L. Watt, P.J. Talling, N. Feuillet, C. Deplus, C. Berndt and M.E. Vardy (2011) "Multiple widespread landslides during the long-term evolution of a volcanic island: Insights from high-resolution seismic data, Montserrat, Lesser Antilles" Geochemistry Geophysics Geosystems **12**

Lim, C., K. Ikehara and K. Toyoda (2008) "Cryptotephra detection using high-resolution trace-element analysis of Holocene marine sediments, southwest Japan" Geochimica Et Cosmochimica Acta **72** 5022-5036

Lisiecki, L.E. and M.E. Raymo (2005) "A Pliocene-Pleistocene stack of 57 globally distributed benthic delta O-18 records" Paleoceanography **20**

Lovholt, F., G. Pedersen and G. Gisler (2008) "Oceanic propagation of a potential tsunami from the La Palma Island" Journal of Geophysical Research-Oceans **113** 21

Lowe, D.J. (1985) "Application of impulse radar to continuous profiling of tephra-bearing lake sediments and peats: an initial evaluation" New Zealand Journal of Geology and Geophysics **28** 667-674

- Lowe, D.J. (1988) "Stratigraphy, age, composition, and correlation of late Quaternary tephras interbedded with organic sediments in Waikato lakes, North Island, New Zealand" New Zealand Journal of Geology and Geophysics **31** 125-165
- Lowe, D.J., Hunt, J.B. (2001) "A summary of terminology used in tephra-related studies" Les Dossiers de l'Archaeo-Logis **1** 17-22
- Lowe, D.J. (2011) "Tephrochronology and its application: A review" Quaternary Geochronology **6** 107-153
- Lowe, D.R. (1982) "Sediment gravity flows 2. Depositional models with special reference to the deposits of high-density turbidity currents" Journal of Sedimentary Petrology **52** 279-298
- Manville, V. and C.J.N. Wilson (2004) "Vertical density currents: a review of their potential role in the deposition and interpretation of deep-sea ash layers" Journal of the Geological Society **161** 947-958
- Masson, D.G., C.B. Harbitz, R.B. Wynn, G. Pedersen and F. Lovholt (2006) "Submarine landslides: processes, triggers and hazard prediction" Philosophical Transactions of the Royal Society a-Mathematical Physical and Engineering Sciences **364** 2009-2039
- Masson, D.G., A.B. Watts, M.J.R. Gee, R. Urgeles, N.C. Mitchell, T.P. Le Bas and M. Canals (2002) "Slope failures on the flanks of the western Canary Islands" Earth-Science Reviews **57** 1-35
- Melnik, O. and R.S.J. Sparks (1999) "Nonlinear dynamics of lava dome extrusion" Nature **402** 37-41
- Moore, J.G., D.A. Clague, R.T. Holcomb, P.W. Lipman, W.R. Normark and M.E. Torresan (1989) "Prodigious submarine landslides on the Hawaiian Ridge" Journal of Geophysical Research-Solid Earth and Planets **94** 17465-17484
- Moore, J.G., W.R. Normark and R.T. Holcomb (1994) "Giant Hawaiian landslides" Annual Review of Earth and Planetary Sciences **22** 119-144
- Mulder, T. and J. Alexander (2001) "The physical character of subaqueous sedimentary density flows and their deposits" Sedimentology **48** 269-299
- Mulder, T. and P. Cochonat (1996) "Classification of offshore mass movements" Journal of Sedimentary Research **66** 43-57

Murphy, M.D., R.S.J. Sparks, J. Barclay, M.R. Carroll and T.S. Brewer (2000) "Remobilization of andesite magma by intrusion of mafic magma at the Soufriere Hills Volcano, Montserrat, West Indies" Journal of Petrology **41** 21-42

Murphy, M.D., R.S.J. Sparks, J. Barclay, M.R. Carroll, A.M. Lejeune, T.S. Brewer, R. Macdonald, S. Black and S. Young (1998) "The role of magma mixing in triggering the current eruption at the Soufriere Hills volcano, Montserrat, West Indies" Geophysical Research Letters **25** 3433-3436

Nederbragt, A., Dunbar, R.B., Osborn, A.T., Palmer, A., Thurow, J.W., Wagner, T. (2006) "Sediment colour analysis from digital images and correlation with sediment composition" In R. G. Rothwell (eds) *New techniques in sediment core analysis* Geological Society, London Special Publications **267** 99-112

Palike, H., N.J. Shackleton and U. Rohl (2001) "Astronomical forcing in Late Eocene marine sediments" Earth and Planetary Science Letters **193** 589-602

Palike, H., N.J. Shackleton and U. Rohl (2001) "Astronomical forcing in Late Eocene marine sediments" Earth and Planetary Science Letters **193** 589-602

Pearce, N.J.G., J.A. Westgate, W.T. Perkins, W.J. Eastwood and P. Shane (1999) "The application of laser ablation ICP-MS to the analysis of volcanic glass shards from tephra deposits: bulk glass and single shard analysis" Global and Planetary Change **21** 151-171

Pearce, N.J.G., J.A. Westgate, W.T. Perkins and S.J. Preece (2004) "The application of ICP-MS methods to tephrochronological problems" Applied Geochemistry **19** 289-322

Pillans, B., B.P. Kohn, G. Berger, P. Froggatt, G. Duller, B. Alloway and P. Hesse (1996) "Multi-method dating comparison for mid-Pleistocene Rangitawa Tephra, New Zealand" Quaternary Science Reviews **15** 641-653

Piper, D.J.W., P. Cochonat and M.L. Morrison (1999) "The sequence of events around the epicentre of the 1929 Grand Banks earthquake: initiation of debris flows and turbidity current inferred from sidescan sonar" Sedimentology **46** 79-97

Pyle, D.M. (1989) "The thickness, volume and grainsize of tephra fall deposits" Bulletin of Volcanology **51** 1-15

- Pyle, D.M., G.D. Ricketts, V. Margari, T.H. van Andela, A.A. Sinitsyn, N.D. Praslov and S. Lisitsyn (2006) "Wide dispersal and deposition of distal tephra during the Pleistocene 'Campanian Ignimbrite/Y5' eruption, Italy" Quaternary Science Reviews **25** 2713-2728
- Rasmussen, T.L., S. Wastegard, E. Kuijpers, T.C.E. van Weering, J. Heinemeier and E. Thomsen (2003) "Stratigraphy and distribution of tephra layers in marine sediment cores from the Faeroe Islands, North Atlantic" Marine Geology **199** 263-277
- Rea, J.W. (1974) "The volcanic geology and petrology of Montserrat, West Indies" J. Geol. Soc. Lond. **130** 341-366
- Reid, R.P., S.N. Carey and D.R. Ross (1996) "Late quaternary sedimentation in the Lesser Antilles island arc" Geological Society of America Bulletin **108** 78-100
- Roobol, M.J. and A.L. Smith (1998) "Pyroclastic stratigraphy of the Soufriere Hills volcano, Montserrat - Implications for the present eruption" Geophysical Research Letters **25** 3393-3396
- Rothwell, R.G. (1992) "Late quaternary evolution of the Madeira Abyssal plain, NE Atlantic" Basin Research **4** 103-131
- Rothwell, R.G., Rack, F.R. (2006) "New techniques in sediment core analysis: an introduction" In R. G. Rothwell (eds) *New techniques in sediment core analysis* Geological Society of London Special Publications **267** 1-29
- Shackleton, N.J., J. Backman, H. Zimmerman, D.V. Kent, M.A. Hall, D.G. Roberts, D. Schnitker, J.G. Baldauf, A. Desprairies, R. Homrighausen, P. Huddlestun, J.B. Keene, A.J. Kaltenback, K.A.O. Krumsiek, A.C. Morton, J.W. Murray and J. Westbergsmith (1984) "Oxygen isotope calibration of the onset of ice-rafting and history of glaciation in the North Atlantic region" Nature **307** 620-623
- Siebert, L. (1984) "Large volcanic debris avalanches: Characteristics of source areas, deposits, and associated eruptions" Journal of Volcanology and Geothermal Research **22** 163-197
- Sigurdsson, H., R.S.J. Sparks, S.N. Carey and T.C. Huang (1980) "Volcanogenic sedimentation in the Lesser Antilles arc" Journal of Geology **88** 523-540
- Slota, P.J., A.J.T. Jull, T.W. Linick and L.J. Toolin (1987) "Preparation of small samples for C-14 accelerator targets by catalytic reduction of CO" Radiocarbon **29** 303-306

- Smith, A.L.R., M.J. Schellekens, J.H. & Mattioli, G.S. (2007) "Prehistoric stratigraphy of the Soufriere Hills–South Soufriere Hills volcanic complex, Montserrat, West Indies" Journal of Geology **115** 115-127
- Sparks, R.S.J., Sigurdsson, H. and Carey, S. (1980) "The entrance of pyroclastic flows into the sea. II. Theoretical considerations on subaqueous emplacement and welding. " J. Volcanol. Geoth. Res. **7** 97-105
- Sparks, R.S.J., M. I. Burski, S. N. Carey, J. S. Gilbert, L. S. Glaze, H. Sigurdsson, A. W. Woods (1997) "Volcanic Plumes" Wiley 1-590
- Sparks, R.S.J., M.D. Murphy, A.M. Lejeune, R.B. Watts, J. Barclay and S.R. Young (2000) "Control on the emplacement of the andesite lava dome of the Soufriere Hills volcano, Montserrat by degassing-induced crystallization" Terra Nova **12** 14-20
- Sparks, R.S.J., H. Sigurdsson and S.N. Carey (1980) "The entrance of pyroclastic flows into the sea I. Oceanographic and geologic evidence from Dominica, Lesser Antilles" Journal of Volcanology and Geothermal Research **7** 87-96
- Sparks, R.S.J., S.R. Young, J. Barclay, E.S. Calder, P. Cole, B. Darroux, M.A. Davies, T.H. Druitt, C. Harford, R. Herd, M. James, A.M. Lejeune, S. Loughlin, G. Norton, G. Skerrit, M.V. Stasiuk, N.S. Stevens, J. Toothill, G. Wadge and R. Watts (1998) "Magma production and growth of the lava dome of the Soufriere Hills Volcano, Montserrat, West Indies: November 1995 to December 1997" Geophysical Research Letters **25** 3421-3424
- Stanton, T., I. Snowball, L. Zillen and S. Wastegard (2010) "Validating a Swedish varve chronology using radiocarbon, palaeomagnetic secular variation, lead pollution history and statistical correlation" Quaternary Geochronology **5** 611-624
- Stevenson, J.A., C. Rae, J. S. Gilbert, S. Harangi, R. Lukács B. Højgaard, U. Árting, S. Pyne-O'Donnell, A. MacLeod, S. Loughlin, A.E. Milodowski and M. Cassidy (in press) "Observations of Distal Tephra From the Eyjafjallajökull 2010 Summit Eruption" Journal of Geophysical Research - Solid Earth
- Takemura, K., A. Hayashida, M. Okamura, H. Matsuoka, M. Ali, Y. Kuniko and M. Torii (2000) "Stratigraphy of multiple piston-core sediments for the last 30,000 years from Lake Biwa, Japan" Journal of Paleolimnology **23** 185-199

Talling, P.J., R.B. Wynn, D.G. Masson, M. Frenz, B.T. Cronin, R. Schiebel, A.M. Akhmetzhanov, S. Dallmeier-Tiessen, S. Benetti, P.P.E. Weaver, A. Georgiopoulou, C. Zuehlsdorff and L.A. Amy (2007) "Onset of submarine debris flow deposition far from original giant landslide" Nature **450** 541-544

Trofimovs, J., Fisher, J. K., Macdonald, H. A., Talling, P. J., Sparks, R. S J., M. B. Hart, C. W. Smart, G. Boudan, C. Deplus, J.C. Komorowski, A. Le Friant, S. G. Moreton, M. J. Leng (2010) "Evidence for carbonate platform failure during rapid sea-level rise; ca 14 000 year old bioclastic flow deposits in the Lesser Antilles" Sedimentology **57** 735 - 759

Trofimovs, J., L. Amy, G. Boudon, C. Deplus, E. Doyle, N. Fournier, M.B. Hart, J.C. Komorowski, A. Le Friant, E.J. Lock, C. Pudsey, G. Ryan, R.S.J. Sparks and P.J. Talling (2006) "Submarine pyroclastic deposits formed at the Soufriere Hills volcano, Montserrat (1995-2003): What happens when pyroclastic flows enter the ocean?" Geology **34** 549-552

Trofimovs, J., C. Foster, R.S.J. Sparks, S. Loughlin, A. Le Friant, C. Deplus, L. Porritt, T. Christopher, R. Lockett, P.J. Talling, M.R. Palmer and T. Le Bas (2012) "Submarine pyroclastic deposits formed during the 20th May 2006 dome collapse of the Soufriere Hills Volcano, Montserrat" Bulletin of Volcanology **74** 391-405

Trofimovs, J., R.S.J. Sparks and P.J. Talling (2008) "Anatomy of a submarine pyroclastic flow and associated turbidity current: July 2003 dome collapse, Soufriere Hills volcano, Montserrat, West Indies" Sedimentology **55** 617-634

Turner, M.B., S.J. Cronin, R.B. Stewart, M. Bebbington and I.E.M. Smith (2008) "Using titanomagnetite textures to elucidate volcanic eruption histories" Geology **36** 31-34

Ui, T., Takarada, S., Yoshimoto, M. (2000) "Debris Avalanches" Academic Press 617-627

Ui, T., H. Yamamoto and K. Suzukikamata (1986) "Characterization of debris avalanche deposits in Japan" Journal of Volcanology and Geothermal Research **29** 231-243

Valentine, G.A., Fisher, R.V. (2000) "Pyroclastic surges and blasts" In H. Sigurdsson (eds) *Encyclopedia of volcanoes* Academic Press 571-581

Vallance (2000) "Lahars" In H. Sigurdsson (eds) *Encyclopedia of Volcanoes* Academic Press 601-617

Venuti, A. and K.L. Verosub (2010) "Paleomagnetic record of basaltic volcanism from Pukaki and Onepoto maar lake cores, Auckland Volcanic Field, New Zealand" New Zealand Journal of Geology and Geophysics **53** 71-79

Vogel, H., G. Zanchetta, R. Sulpizio, B. Wagner and N. Nowaczyk (2010) "A tephrostratigraphic record for the last glacial-interglacial cycle from Lake Ohrid, Albania and Macedonia" Journal of Quaternary Science **25** 320-338

Voight, B., R.S.J. Sparks, A.D. Miller, R.C. Stewart, R.P. Hoblitt, A. Clarke, J. Ewart, W.P. Aspinall, B. Baptie, E.S. Calder, P. Cole, T.H. Druitt, C. Hartford, R.A. Herd, P. Jackson, A.M. Lejeune, A.B. Lockhart, S.C. Loughlin, R. Lockett, L. Lynch, G.E. Norton, R. Robertson, I.M. Watson, R. Watts and S.R. Young (1999) "Magma flow instability and cyclic activity at Soufriere Hills Volcano, Montserrat, British West Indies" Science **283** 1138-1142

Wadge, G. (1984) "Comparison of volcanic production-rates and subduction rates in the Lesser Antilles and Central America" Geology **12** 555-558

Walker, G.P.L., L. Wilson and E.L.G. Howell (1971) "Explosive Volcanic Eruptions-I. The rate of fall of pyroclasts." Geophysical Journal of the Royal Astronomical Society **22** 377-&

Walker, R.G. (1969) "Geometric analysis of ripple-drift cross-lamination" Canadian Journal of Earth Science **6** 683-691

Wall-Palmer, D., M.T. Jones, M.B. Hart, J.K. Fisher, C.W. Smart, D.J. Hembury, M.R. Palmer and G.R. Fones (2011) "Explosive volcanism as a cause for mass mortality of pteropods" Marine Geology **282** 231-239

Ward, S.N. and S. Day (2001) "Cumbre Vieja Volcano - Potential collapse and tsunamis at La Palma, Canary Islands" Geophysical Research Letters **28** 3397-3400

Watt, S.F.L., Talling, P.J., Vardy, M.E., Heller, V., Hühnerbach, V., Urlaub, M., Morelia, S., Sarkar, S., Sudipta, Masson, D.G., Henstock, T.J., Minshull, T.A., Paulatto, M., Le Friant, A., Lebas, E., Berndt, C., Crutchley, G., Karstens, J., Stinton, A. and Maeno, F. (2012) "Combinations of volcanic-flank and seafloor-sediment failure offshore Montserrat, and their implications for tsunami generation" Earth and Planetary Science Letters **319-320** 228-240

Weltje, G.J. and R. Tjallingii (2008) "Calibration of XRF core scanners for quantitative geochemical logging of sediment cores: Theory and application" Earth and Planetary Science Letters **274** 423-438

- Wetzel, A. (2009) "The preservation potential of ash layers in the deep-sea: the example of the 1991-Pinatubo ash in the South China Sea" Sedimentology **56** 1992-2009
- White, M.J. and J. McPhie (1997) "A submarine welded ignimbrite crystal-rich sandstone facies association in the Cambrian Tyndall Group, western Tasmania, Australia" Journal of Volcanology and Geothermal Research **76** 277-295
- Whitham, A.G. (1989) "The behaviour of subaerially produced pyroclastic flows in a subaqueous environment: evidence from the Roseau eruption, Dominica, West Indies" Marine Geology **86** 27-40
- Wiesner, M.G., A. Wetzel, S.G. Catane, E.L. Listanco and H.T. Mirabueno (2004) "Grain size, areal thickness distribution and controls on sedimentation of the 1991 Mount Pinatubo tephra layer in the South China Sea" Bulletin of Volcanology **66** 226-242
- Wilson, C.J.N., Houghton, B.F. (2000) "Pyroclastic transport and deposition" In H. Sigurdsson (eds) *Encyclopedia of Volcanoes* Academic Press
- Wilson, L. and G.P.L. Walker (1987) "Explosive volcanic-eruptions .6. Ejecta dispersal in plinian eruptions - the control of eruption conditions and atmospheric properties" Geophysical Journal of the Royal Astronomical Society **89** 657-679
- Wynn, R.B.M., D. G. (2003) "Canary island landslides and tsunami generation: can we use turbidite deposits to interpret landslide processes." Kluwer Academic Publishers **325-332**
- Xu, S., R. Anderson, C. Bryant, G.T. Cook, A. Dougans, S. Freeman, P. Naysmith, C. Schnabel and E.M. Scott (2004) "Capabilities of the new suerc 5MV AMS facility for C-14 dating" Radiocarbon **46** 59-64
- Young, S.R., R.S.J. Sparks, W.P. Aspinall, L.L. Lynch, A.D. Miller, R.E.A. Robertson and J.B. Shepherd (1998) "Overview of the eruption of Soufriere Hills volcano, Montserrat, 18 July 1995 to December 1997" Geophysical Research Letters **25** 3389-3392
- Zachos, J., M. Pagani, L. Sloan, E. Thomas and K. Billups (2001) "Trends, rhythms, and aberrations in global climate 65 Ma to present" Science **292** 686-693
- Zellmer, G.F., C.J. Hawkesworth, R.S.J. Sparks, L.E. Thomas, C.L. Harford, T.S. Brewer and S.C. Loughlin (2003) "Geochemical evolution of the Soufriere Hills volcano, Montserrat, Lesser Antilles volcanic arc" Journal of Petrology **44** 1349-1374

Zielinski, G.A., J.E. Dibb, Q.Z. Yang, P.A. Mayewski, S. Whitlow, M.S. Twickler and M.S. Germani (1997) "Assessment of the record of the 1982 El Chichon eruption as preserved in Greenland snow" Journal of Geophysical Research-Atmospheres **102** 30031-30045

CHAPTER 6

CONCLUSIONS AND FUTURE WORK

This thesis documents a comprehensive geochemical stratigraphy throughout Montserrat's 2.6 Ma history. The work particularly focuses on the SSH volcanic centre, with its distinctive geochemical signatures and significant mass wasting events, as recognised from subaerial exposures and submarine sediment cores. The thesis remainder focuses on reconstructing the most significant events in the submarine sedimentological record to the south and southwest of Montserrat, including reworked volcanoclastic flows, pyroclastic flows and airfall tephra deposits in the sea. The synthesis chapter assesses and reviews different techniques used to detect, characterise and date tephra in submarine sediment cores, using Montserrat as a case example. This contribution aims to advance the protocol for generating volcanic records developed from marine sediment cores globally. Therefore, the work within this thesis has implications beyond Montserrat volcanism. This includes a greater understanding of magma genesis in the Lesser Antilles, further recognition of the processes involved with submarine and subaerial collapses from volcanic islands and the application of the Montserrat case study to help construct volcanic records in other locations.

1. Key conclusions and returning to the original thesis questions

1.1 Chapter 2 - Tracking the magmatic evolution of an island arc volcano: Insights from a high-precision Pb isotope record of Montserrat, Lesser Antilles

(Q2.1) Have the composition of magmas beneath Montserrat been consistent throughout its history?

The composition of the magmas beneath Montserrat remained similar throughout the Silver and Centre Hills eruptive episodes, and into the early Soufrière Hills evolution, which equates to a time period >2 Myr. However, this was interrupted by a rapid shift in trace element, Pb and Nd isotopic compositions during the formation of SSH Suites A and B at ~130 ka, which possibly corresponds to regional transtensional tectonic changes, which may have extracted magma from a shallower source than typically observed prior to this episode. Subsequent to the SSH eruption, volcanism returned to more consistent isotopic compositions, continuing today at the currently active, Soufrière Hills volcano. The

composition of magma sources for the current phases of activity at Soufrière Hills on Montserrat during the last 15 years has remained fairly stable. The island of Redonda and Kahouanne, submarine volcano SE of Montserrat have compositions similar to the SSH, but it is not yet known when these were active.

(Q2.2) What implications does this geochemical study on Montserrat have on the factors controlling the composition magmas at other volcanoes in the Lesser Antilles?

With the use of high-precision Pb isotopes I have shown that Montserrat (and the Lesser Antilles arc) is not a simple two component system, but is affected by bulk sediment addition, sediment melt, slab fluids, altered oceanic crust and Galapagos plume components. These same components in different proportions are likely influencing the magma compositions of the other volcanoes in the Lesser Antilles.

The SSH suite on Montserrat has the least radiogenic Pb isotopes reported from the Lesser Antilles, and represents a distinct composition within this volcanic arc. This study hypothesises that this results from regional tectonics affecting the compositions of magma at Montserrat. The differences between the Pb isotope and other geochemical characteristics of the SSH and rest of volcanic centres on Montserrat suggests they were generated from sources with distinct compositions, arising from variations in the relative contribution of sediment and fluid components derived from the subducted slab. This evidence is made more intriguing by the fact that the Soufrière Hills and SSH volcanoes were active at overlapping time periods and located only 2 km apart. The islands of Redonda and Kahouanne, located 30 km north west and 15 km south east respectively have almost identical geochemistry to the SSH volcanic centre which suggests that magma variation between the Soufrière Hills and SSH is unlikely to be resultant of small scale differences in the sediment supply from the slab, instead it suggests that there may be a regional control influencing magma compositions. Transtensional faults within the area can reach down to the lower crust and upper mantle (Bowman et al. 2003) and are located adjacent to Kahouanne, SSH and Redonda volcanoes. These faults provide local extension forces that can draw up slab-fluid-rich magmas from shallower portions of the mantle wedge, which have not been so heavily influenced by sediment addition or mantle depletion, and thus yield the distinct geochemical characteristics observed in the SSH, Redonda and Kahouanne samples. My hypothesis is that these faults may be sampling the shallower derived fluids and not the slab sediment compositions.

1.2 Chapter 3 - Multi-stage collapse events in the South Soufrière Hills, Montserrat, as recorded in marine sediment cores

(Q3.1) What was the chronostratigraphic evolution of the South Soufrière Hills volcanic complex?

Detailed field and petrographic observations coupled with SEM image analysis shows that the SSH volcanic products preserve a complex record of magmatic activity. The SSH erupted volcanics from multiple magmatic pulses, comprising two main geochemical signatures termed, SSH Suite A and SSH Suite B. Both Suites preserve evidence of episodic explosive eruptions of andesitic pumice, followed by weakly explosive eruptions of poorly vesiculated basaltic scoria and dacitic and basaltic lava flows. The occurrence of magma mingling between andesite and basalt suggests that the explosive andesitic eruptions were likely triggered by pulses of mafic magma disturbing a differentiated magma chamber. Geochemical provenance studies have shown that a unit derived from the Soufrière Hills volcano yet exposed within the basal stratigraphy of the SSH volcanic centre. Ages of this unit provided by Harford et al. (2002), reveal that volcanism at the Soufrière Hills and SSH was likely contemporaneous.

(Q3.2) How did such flank collapse(s) and resulting sediment flow(s) behave?

Sedimentological and geochemical analyses of submarine deposits sampled in sediment cores suggest that they were formed by large multi-stage flank failures of the subaerial SSH edifice into the sea. This is evidenced by bathymetric and seismic imaging of a debris avalanche and thick bedded turbidite deposits found within sediment cores sampled south of Montserrat, the material of which is identical geochemically with SSH units found on land. This study has identified two distinct geochemical suites within the SSH succession on the basis of trace element and Pb isotope compositions. Volcaniclastic turbidites in the submarine cores also preserve these chemically heterogeneous rock suites. However, the subaerial chemostratigraphy is reversed within the submarine sediment cores. Sedimentological analysis suggests that the edifice failures produced high-concentration turbidites and that the collapses occurred in multiple stages, with an interval of at least ~2 kyr between the first and second failure. As these failures progressed they eroded back into older, chemically distinct strata, subsequently reversing the subaerial chemostratigraphy within the submarine environment.

1.3 Chapter 4 - A new lava dome collapse into the ocean at the Soufrière Hills volcano, Montserrat, West Indies at ca 8 ka: how submarine stratigraphy can complement subaerial eruption histories

(Q4.1) Where do the 8 ka Andesitic Volcaniclastic Unit and the Mafic Bioclastic-rich Unit originate from?

The 8 ka Andesitic Volcaniclastic Unit is derived from a primary volcanic eruption, which is evidenced in the submarine cores by the lack of geochemical variation between deposits and the compositionally mature lithofacies. The 8ka Andesitic Volcaniclastic Unit has

characteristics similar to those seen in pyroclastic flow deposits which have entered the sea, for example thick, poorly-sorted and crystal-rich lithofacies. Its lateral extent in the marine cores and geochemical provenance suggests it originated from the south west flank of the Soufrière Hills volcano, likely in the form of a pyroclastic density current from a lava dome collapse. The Mafic and Bioclastic rich Unit, comprises coarse, fragmented bioclastic material and reworked volcanic material from the Soufrière Hills and South Soufrière Hills volcanoes offshore south west of Montserrat. Its componentry and spatial distribution are consistent with a collapse from the submarine shelf surrounding Montserrat.

(Q4.2) What are the processes that led to the emplacement of these flows?

The 8 ka Andesitic Volcaniclastic Unit has characteristics similar to a submarine pyroclastic flow deposit, it was likely formed from a dome collapse from the Soufrière Hills volcano. This pyroclastic flow underwent quench fragmentation as the hot flow interacted with the cold seawater. The flow rapidly mixed with the ocean water to become water-supported gravity-driven density flow, which resulted in a crystal-rich volcaniclastic. The Mafic and Bioclastic-rich Unit was formed from the multiple failures from submarine shelf forming stacked graded beds of high-concentration turbidites.

1.4 Chapter 5 - Advances in the construction of volcanic records from marine sediment cores: A review and case study (Montserrat, West Indies).

(Q5.1) What is the best way of constructing a volcanic record from marine cores?

Using the Montserrat submarine cores, a protocol for identifying and characterising marine tephra layers has been derived. The first step when constructing a marine record is to make a graphic log of the core(s), taking into consideration the sedimentological and macro-scale features such as unit boundaries and contacts, sedimentological structure and preliminary composition analysis. Following this, fast, non-destructive and high-spatial resolution techniques are best used to detect potential cryptotephra, for example XRF-core scanning, magnetic susceptibility and colour spectrophotometry were found to be the most effective methods. These techniques, however, only help identify areas which will require further investigation. After target potential tephra horizons have been identified, these should be sampled using more stringent analytical techniques, such as component analysis and glass shard geochemistry. Inspection of these tephra horizons under a microscope using descriptive criteria such as glass shard morphology, compositional maturity and sorting, will help distinguish primary tephra from reworked volcaniclastic deposits. If it is possible, the use of EMP and LA-ICP-MS analyses on glass shards, is especially useful for determining if the shards are from different eruptions and for correlating distal ashes from core to core.

To obtain chronology information from a marine tephrostratigraphic framework, the hemipelagic sediment between the tephra deposits can be dated by AMS radiocarbon dating for sediments <50 ka and for sediments older than this an oxygen isotope stratigraphy (preferably species-specific) should be produced on as fine a sampling scale as practical.

(Q5.2) Were the volcanic centres on Montserrat more or less volcanically active than previously recognised?

This study shows that the volcanic centres were more active than previously recognised. This is thought to be a result of incomplete eruption sequences in subaerial records and insufficient methodology used to detect tephra in marine sediment cores. This study identifies primary dome collapse at 8 ka not recognised in the previous studies, as well as three ash fall events at 43-40 ka, 75 ka, 100 ka and three eruptions from 130 -123 ka that equate to dated subaerial rocks. As a consequence of this detailed analysis of the submarine sediment cores, this study finds eight eruptions from 37 to 135 ka, whereas Le Friant et al. (2008), notes only six eruptions in their sequence. This highlights the importance of using effective methods to create volcanic records from marine sediment cores.

2. Future perspectives

This study has built our understanding of how volcanism has evolved on Montserrat. It also highlights further questions that would benefit from further research, some of which may be addressed by analysing newly obtained drilled cores from the recent IODP cruise around Montserrat and the Lesser Antilles (IODP Expedition 340).

The second chapter in this thesis underscores the complexity observed within Lesser Antilles island arc geochemistry, and brings to attention some of the following questions:

When were Redonda and Kahouanne volcanoes active? How does this fit in the Montserrat history? (These are currently being dated via Ar-Ar dating by collaborators in Japan)

What can the minerals within the rocks tell us about magmatic storage conditions and if disequilibrium textures are preserved, the timing of magmatic processes associated with SSH volcanism in contrast the Soufrière Hills volcano?

Are there any other volcanoes in the Lesser Antilles that show evidence of transtensional faulting as a mechanism for generating different magma chemistries?

Can one test the hypothesis presented here of different depths of magma generation by looking at geothermometers such as Ce/H₂O ratios in melt inclusions?

How do the volatile budgets of the SSH and Soufrière Hills rocks compare? One might expect the carbon and sulphur inventory to be slightly different between them given the relative

influences of slab fluids and sediment melt. (This study is currently in progress working in collaboration with Marie Edmonds in Cambridge)

Is there any evidence for Galapagos-like mantle source material from other volcanoes in the Lesser Antilles?

In the cases where different isotopic trends can be distinguished in volcanoes close to each other, can tectonics explain the chemistry of magmas here also?

The third and fourth chapters aim to understand flank collapses from the volcanic islands and submarine gravity flows. This brings up several more questions:

What else can the SSH tell us about volcanism on Montserrat if allowed to survey the areas with better exposure?

Using tsunami models, what are the potential wave heights from such collapses? How does a multi-stage collapse affect the wave heights?

How much does erosion play a part in submarine sediment flows? For example, with more core coverage of these deposits, it may be possible to quantify the percentage of bottom sediment that is entrained in the two deposits and how this varies both laterally and vertically, which may allow us to quantify the erosive power of the flows to a greater degree.

The final chapter opens up scope for more validation of this method presented but before we submit this paper for publication, we aim to quantify more of the qualitative and descriptive parameters used to detect and characterise the tephras, this will produce a more objective and robust system for detecting tephras and discerning their primary or reworked origin. For example in the detection of cryptotephras from a signal (e.g. magnetic susceptibility), instead of picking out peaks and troughs by eye, only values 3 times the standard deviation from background hemipelagic may be deemed a tephra signal. We also plan to look at more quantitative parameters to give criteria such as angularity and sphericity a number, to produce an index where primary ash fall deposits can be distinguished from reworked Volcaniclastic deposits. If this method is used in conjunction with more complete and deeper core sampled offshore Montserrat, it may uncover more events from the history of Montserrat. Proposing such a method also asks:

Will this method be successful in constructing volcanic records in other settings globally?

APPENDIX

Appendix A: Chapter 2 Geochemical tables:

Table 1 - Major and trace element geochemical data for all samples analysed

Volcanic region:			Silver Hills					Centre Hills			
Latitude			16.8045	16.7994	16.8020	16.8073	16.8117	16.8019	16.8131	16.7062	16.7552
Longitude			62.2022	62.1958	62.1928	62.1855	62.1926	62.1947	62.2044	62.1485	62.1679
Submarine core I.D.											
Sample depth interval (cm)											
Sample	JB-2	RSD (%)	MVO 144	MVO 755	MGEOL 1	MGEOL 5	SilvH3	SilvH4	MGEOL9	MVO 135	MVO 131
Major elements (XRF)											
SiO ₂	53.72	0.62	57.28	64.06			58.81	60.51			57.28
TiO ₂	1.13	0.14	0.70	0.52			0.57	0.65			0.70
Al ₂ O ₃	14.78	0.51	17.86	17.47			17.59	16.35			17.86
Fe ₂ O ₃	14.09	0.80	7.06	5.84			7.60	8.06			7.06
MnO	0.22	2.08	0.16	0.15			0.19	0.20			0.16
MgO	4.56	0.88	3.89	1.55			3.47	2.83			3.89
CaO	9.76	0.41	8.21	5.22			7.47	6.23			8.21
K ₂ O	0.41	1.70	0.89	0.84			0.64	0.68			0.69
Na ₂ O	2.11	2.49	3.24	3.66			3.06	3.11			3.24
P ₂ O ₅	0.10	2.15	0.13	0.03			0.10	0.11			0.13
Totals	100.89		99.22	99.34			99.48	98.72			99.22
Trace elements	JA-2	% RSD									
Li	30.19	2.42					9.82	9.29			
Sc	18.22	0.68					20.77	20.19			
Rb	77.24	5.68	15.83		17.63	8.20	15.50	16.40	18.37	22.98	14.54
Sr	245.80	1.19	223.20		220.90	322.00	202.60	202.90	192.20	219.10	284.00
Y	17.68	1.68	24.12		23.52	26.02	27.60	27.14	24.04	28.40	23.77
Zr	120.70	5.06	122.20		97.62	82.82	72.23	105.50	107.39	136.70	78.36
Nb	8.93	0.59	2.50		2.15	1.77	2.02	2.48	2.12	3.57	2.74
Cs	5.17	3.58	0.60		0.18	0.04	0.25	0.16	0.26	0.76	0.26
Ba	319.20	0.92	149.26		140.04	126.81	152.40	152.50	163.81	198.20	148.65
La	16.00	0.44	9.14		7.78	8.75	8.77	8.70	10.81	12.10	9.45
Ce	33.28	0.88	22.17		18.93	20.69	19.85	20.62	30.36	28.69	22.90
Pr	3.81	1.94	2.87		2.52	2.83	2.70	2.69	3.05	3.58	2.85
Nd	14.47	1.30	13.17		11.26	13.42	11.78	12.64	13.77	16.41	13.07
Sm	3.11	0.25	3.42		2.95	3.50	2.97	3.31	3.44	4.03	3.33
Eu	0.90	0.92	1.06		0.93	1.19	0.92	1.02	1.00	1.02	1.02
Gd	3.02	0.34	3.57		3.17	3.81	3.51	3.68	3.58	4.07	3.42
Tb	0.48	0.43	0.62		0.56	0.67	0.60	0.64	0.63	0.70	0.59
Dy	2.90	0.12	3.97		3.63	4.13	3.89	4.08	4.02	4.46	3.72
Ho	0.59	1.98	0.86		0.79	0.88	0.87	0.89	0.87	0.96	0.81
Er	1.71	0.20	2.56		2.35	2.62	2.60	2.68	2.58	2.97	2.39
Tm	0.25	1.63	0.40		0.36	0.40	0.40	0.42	0.41	0.48	0.36
Yb	1.70	0.61	2.68		2.57	2.65	2.76	2.96	2.78	3.15	2.39
Lu	0.26	1.33	0.46		0.41	0.42	0.45	0.47	0.47	0.55	0.39
Hf	2.91	0.41	3.11		2.52	2.27	2.08	2.91	2.97	3.50	2.19
Pb	2.21	8.83	2.21		2.48	1.34	2.24	2.12	2.99	2.76	3.19
Th	4.85	2.17	2.25		1.78	1.48	1.83	2.37	2.53	3.08	2.02
U	2.26	1.76	0.60		0.57	0.24	0.60	0.80	0.57	1.10	0.53

Table 1: Continued

	Centre Hills						SSH Suite A				
Latitude	16.7830	16.7691	16.7745	16.7874	16.7962	16.7226	16.7358	16.6761	16.6761	16.6775	16.6933
Longitude	62.2057	62.1735	62.1705	62.2089	62.2100	62.2397	62.3491	62.3272	62.3272	62.1804	62.1484
Core I.D.							JR123-1	JR123-2	JR123-2		
Depth (cm)							388-389	272-273	265-266		
Sample	MVO 147	MVO 809	MVO 831	CH1	CH2	Brands	MC08A	MC02A	MC01G	SSH2C	MVO 830
SiO ₂	60.54	57.03	60.76	53.33	55.85	52.79				52.99	51.71
TiO ₂	0.51	0.66	0.57	0.68	0.69	0.62				0.92	0.83
Al ₂ O ₃	17.49	18.87	17.21	18.84	17.44	17.50				18.50	19.08
Fe ₂ O ₃	7.02	7.32	6.15	9.95	10.14	10.88				9.84	9.45
MnO	0.15	0.19	0.17	0.25	0.27	0.32				0.19	0.16
MgO	2.59	3.40	2.90	4.42	4.27	5.16				4.80	4.82
CaO	6.81	7.83	8.98	8.95	7.60	8.65				9.33	10.20
K ₂ O	0.77	0.42	0.76	0.33	0.41	0.31				0.64	0.61
Na ₂ O	3.44	3.32	3.67	2.89	3.08	2.76				2.97	3.03
P ₂ O ₅	0.10	0.16	0.15	0.09	0.17	0.19				0.20	0.11
Totals	99.22	99.20	99.32	99.72	99.92	99.17				100.48	100.00
Li				7.19	8.36	5.81	7.37	9.69	7.77	5.25	
Sc				19.74	19.34	19.94	41.43	21.02	27.63	17.96	
Rb	12.55	5.35	17.36	6.50	9.14	5.42	7.73	10.95	7.84	8.88	
Sr	245.10	261.10	225.50	292.70	257.50	262.70	223.89	248.50	293.90	237.50	
Y	20.51	22.18	27.79	14.13	22.18	15.97	22.29	22.08	21.33	16.70	
Zr	83.94	108.48	141.46	44.98	77.97	37.70	59.24	74.07	62.59	57.29	
Nb	2.58	2.60	3.50	1.83	2.38	1.44	1.28	1.80	1.14	4.39	
Cs	0.45	0.21	0.52	0.23	0.31	0.19	0.25	0.36	0.27	0.23	
Ba	132.65	99.16	202.33	88.12	110.60	74.16	96.30	127.00	96.20	116.40	
La	8.99	8.10	12.40	6.02	8.93	5.97	4.79	6.40	5.29	7.40	
Ce	18.50	22.88	29.43	12.60	18.94	14.01	11.85	14.72	12.93	16.37	
Pr	2.61	2.66	3.60	1.81	2.97	1.99	1.79	2.23	1.92	2.26	
Nd	11.80	12.70	16.12	7.80	12.98	8.99	8.72	10.26	9.07	9.88	
Sm	2.85	3.31	3.85	1.93	3.20	2.29	2.58	2.77	2.55	2.43	
Eu	0.95	1.09	1.07	0.88	1.03	0.91	0.91	0.97	0.98	0.83	
Gd	2.90	3.36	3.78	2.09	3.38	2.54	3.20	3.18	3.09	2.63	
Tb	0.50	0.57	0.65	0.35	0.56	0.42	0.54	0.53	0.51	0.42	
Dy	3.20	3.54	4.21	2.24	3.55	2.63	3.53	3.47	3.32	2.60	
Ho	0.70	0.75	0.90	0.48	0.75	0.57	0.76	0.76	0.71	0.55	
Er	2.10	2.23	2.71	1.45	2.23	1.67	2.24	2.26	2.13	1.58	
Tm	0.33	0.34	0.43	0.23	0.35	0.26	0.34	0.34	0.32	0.24	
Yb	2.36	2.32	2.95	1.65	2.46	1.86	2.32	2.39	2.20	1.61	
Lu	0.40	0.37	0.47	0.27	0.39	0.30	0.36	0.38	0.35	0.25	
Hf	2.12	2.60	3.59	1.23	2.05	1.08	1.59	1.98	1.64	1.51	
Pb	3.09	2.88	2.20	2.00	1.58	1.75	5.88	3.72	6.11	3.35	
Th	1.99	1.83	3.30	0.99	1.46	0.80	0.77	1.15	0.83	1.57	
U	0.62	0.30	1.04	0.32	0.45	0.26	0.32	0.57	0.33	0.43	

Table 1: Continued

Latitude	16.7358	16.6761	16.7358	16.6431	16.6108	16.6431	16.6108	16.7358	16.5833	16.6762	16.6913
Longitude	62.3491	62.3272	62.3491	62.3017	62.1881	62.3017	62.1881	62.3491	62.1522	62.1682	62.1486
Core I.D.	JR123-1	JR123-2	JR123-1	JR123-4	JR123-45	JR123-4	JR123-45	JR123-1	JR123-46		
Depth (cm)	388-389	272-273	181-182	63-64	148-150	63-64	148-150	181-182	165-166		
Sample	MC08G	MC02G	MC07A	MC18A	MC09A	MC18G	MC09G	MC07G	MC10G	SSH4	SSH5B
<i>SiO₂</i>										50.87	58.77
<i>TiO₂</i>										0.87	0.59
<i>Al₂O₃</i>										19.20	17.95
<i>Fe₂O₃</i>										9.58	7.58
<i>MnO</i>										0.18	0.19
<i>MgO</i>										4.83	3.19
<i>CaO</i>										10.65	7.27
<i>K₂O</i>										0.69	0.60
<i>Na₂O</i>										2.73	3.52
<i>P₂O₅</i>										0.13	0.15
<i>Totals</i>										98.73	99.81
<i>Li</i>	6.48	7.40	9.79	8.88	12.54	8.34	7.54	9.00	7.22	6.20	8.63
<i>Sc</i>	39.72	27.69	33.76	28.12	35.83	33.20	55.58	35.80	31.17	32.75	16.53
<i>Rb</i>	6.55	8.22	11.31	10.19	7.52	7.30	7.89	10.51	7.83	7.99	11.00
<i>Sr</i>	219.85	199.90	242.43	299.78	259.20	271.97	212.26	237.40	283.04	540.80	260.30
<i>Y</i>	21.18	19.84	25.18	16.80	18.90	22.37	22.99	23.31	21.01	17.71	20.68
<i>Zr</i>	54.30	59.43	79.46	49.51	49.04	64.93	55.19	70.94	61.38	61.17	89.96
<i>Nb</i>	1.04	1.57	1.79	1.38	1.00	1.48	1.15	1.58	1.25	2.31	2.10
<i>Cs</i>	0.22	0.28	0.39	0.27	0.23	0.25	0.25	0.34	0.26	0.19	0.30
<i>Ba</i>	78.04	93.62	128.11	128.43	94.24	93.43	82.43	115.80	94.58	128.20	168.00
<i>La</i>	4.26	4.96	6.44	5.42	4.38	5.68	4.45	5.84	5.15	8.31	7.75
<i>Ce</i>	10.79	11.52	15.34	12.69	10.34	13.98	11.18	14.04	12.58	18.79	17.60
<i>Pr</i>	1.65	1.79	2.22	1.77	1.50	2.05	1.70	2.05	1.85	2.60	2.50
<i>Nd</i>	8.10	8.40	10.38	8.02	6.95	9.62	8.35	9.60	8.78	11.36	11.03
<i>Sm</i>	2.44	2.38	2.93	2.19	1.99	2.74	2.56	2.74	2.49	2.68	2.76
<i>Eu</i>	0.89	0.84	1.02	0.84	0.81	1.01	0.91	0.88	0.94	0.94	0.94
<i>Gd</i>	3.07	2.85	3.58	2.54	2.46	3.31	3.35	3.37	3.04	2.92	2.97
<i>Tb</i>	0.52	0.48	0.60	0.42	0.41	0.55	0.57	0.56	0.51	0.47	0.51
<i>Dy</i>	3.36	3.17	3.90	2.67	2.69	3.49	3.70	3.65	3.31	3.00	3.19
<i>Ho</i>	0.72	0.70	0.85	0.57	0.58	0.75	0.79	0.79	0.71	0.63	0.69
<i>Er</i>	2.13	2.04	2.51	1.69	1.71	2.22	2.31	2.35	2.09	1.80	2.07
<i>Tm</i>	0.32	0.30	0.39	0.26	0.26	0.34	0.35	0.36	0.32	0.27	0.32
<i>Yb</i>	2.19	2.13	2.62	1.74	1.81	2.31	2.36	2.47	2.17	1.77	2.27
<i>Lu</i>	0.34	0.33	0.41	0.27	0.28	0.36	0.36	0.38	0.34	0.27	0.37
<i>Hf</i>	1.47	1.64	2.05	1.37	1.31	1.71	1.52	1.88	1.62	1.73	2.25
<i>Pb</i>	6.47	3.34	10.66	5.26	8.29	6.50	4.89	6.63	9.16	1.82	3.05
<i>Th</i>	0.65	0.89	1.19	1.21	0.78	0.94	0.74	1.07	0.84	1.81	1.26
<i>U</i>	0.29	0.53	0.46	0.39	0.29	0.33	0.28	0.41	0.33	0.56	0.45

Table 1: Continued

	SSH A			SSH Suite B						Sulfure	
Latitude	16.6913	16.6922	16.6930	16.6431	16.6431	16.5833	16.5750	16.5833	16.6770	16.6760	16.6761
Longitude	62.1486	62.1479	62.1489	62.3017	62.3017	62.1522	62.0894	62.1522	62.1628	62.1692	62.3272
Core I.D.				JR123-4	JR123-4	JR123-46	JR123-47	JR123-46			JR123-2
Depth (cm)				9394	124-125	187-188	384-385	187-188			17-18
Sample	SSH5Cl	SSH10	SSH11	MC03G	MC06G	MC11G	MC12G	MC11A	MVO 791	SSH3	MC13A
SiO ₂	56.12	62.72	49.29						49.44	49.22	
TiO ₂	0.63	0.40	0.85						0.82	1.00	
Al ₂ O ₃	18.57	16.45	20.87						19.95	18.67	
Fe ₂ O ₃	8.12	5.54	9.82						10.01	10.90	
MnO	0.19	0.18	0.17						0.17	0.18	
MgO	3.19	2.41	4.77						5.50	5.93	
CaO	8.16	6.56	11.03						11.02	10.93	
K ₂ O	0.54	0.96	0.46						0.58	0.63	
Na ₂ O	3.29	4.13	2.48						2.42	2.45	
P ₂ O ₅	0.17	0.10	0.11						0.09	0.12	
Totals	98.98	99.45	99.85						100.00	100.03	
Li	8.19	4.33	5.65	3.89	4.88	4.25	4.22	4.64		4.58	14.35
Sc	15.18	41.89	37.79	68.84	54.27	58.93	60.84	43.48		41.10	12.59
Rb	9.95	5.53	5.55	4.05	4.99	5.49	5.05	7.45	5.17	6.10	18.46
Sr	305.20	394.70	430.20	314.00	461.80	402.23	385.47	374.94	499.90	450.70	285.98
Y	22.88	20.18	20.20	18.76	17.50	17.22	19.22	13.43	18.40	18.21	23.23
Zr	89.40	41.00	39.13	35.47	37.43	39.67	39.27	32.60	41.10	40.81	83.51
Nb	2.08	0.90	0.88	0.81	1.09	0.86	0.83	0.80	0.84	0.74	3.36
Cs	0.32	0.08	0.14	0.10	0.12	0.13	0.13	0.16	0.13	0.13	0.56
Ba	133.40	104.70	112.80	73.45	90.69	99.14	117.01	81.88	84.50	90.50	242.64
La	8.29	3.82	4.13	3.15	3.40	3.49	3.42	2.91	3.82	4.10	11.00
Ce	19.27	9.17	9.56	7.98	8.57	8.95	8.85	7.30	10.11	10.40	24.25
Pr	2.74	1.49	1.66	1.36	1.44	1.40	1.43	1.12	1.46	1.66	3.16
Nd	12.21	7.53	8.15	7.05	7.19	7.06	7.38	5.47	7.52	7.84	13.23
Sm	3.11	2.35	2.50	2.31	2.26	2.18	2.35	1.71	2.26	2.47	3.17
Eu	1.07	0.86	0.92	0.80	0.87	0.84	0.88	0.62	0.87	0.89	1.06
Gd	3.38	2.86	2.97	2.90	2.75	2.74	3.00	2.09	2.72	2.93	3.43
Tb	0.57	0.49	0.50	0.49	0.46	0.45	0.50	0.35	0.48	0.51	0.55
Dy	3.60	3.15	3.23	3.23	3.01	2.89	3.21	2.24	3.01	3.34	3.49
Ho	0.77	0.68	0.68	0.70	0.65	0.61	0.68	0.47	0.65	0.71	0.74
Er	2.29	1.94	1.98	1.99	1.86	1.75	1.96	1.37	1.88	1.97	2.25
Tm	0.36	0.29	0.30	0.28	0.26	0.25	0.29	0.20	0.28	0.31	0.36
Yb	2.48	1.94	1.95	1.89	1.76	1.67	1.88	1.33	1.73	1.88	2.52
Lu	0.39	0.30	0.29	0.28	0.26	0.25	0.27	0.20	0.25	0.30	0.40
Hf	2.26	1.24	1.21	1.15	1.17	1.19	1.21	1.02	1.18	1.17	2.28
Pb	3.03	2.35	2.37	2.10	2.77	7.38	8.47	4.98	1.80	2.08	10.94
Th	1.26	0.57	0.71	0.51	0.52	0.57	0.50	0.65	0.49	0.59	2.73
U	0.43	0.29	0.24	0.34	0.42	0.29	0.28	0.27	0.27	0.29	0.85

Table 1: Continued

Hills	Soufrière Hills										
Latitude	16.7126	16.7399	16.7152	16.7103	16.7145	16.7351	16.7334	16.7064	16.1550	16.7223	16.7257
Longitude	62.1711	62.1527	62.1885	62.1616	62.1526	62.2329	62.1549	62.1831	62.7134	62.1545	62.1548
Core I.D.											
Depth (cm)											
Sample	MVO 104	MVO 127	MVO 152	MVO 154	MVO 777	MVO 785	MVO 819	MVO892	MVO775	MVO1209	MVO1329
SiO ₂	58.37	59.69	58.80	59.74	61.40	63.79	59.96	60.17	58.13	59.30	58.85
TiO ₂	0.69	0.62	0.61	0.65	0.54	0.45	0.56	0.60	0.62	0.53	0.61
Al ₂ O ₃	17.75	17.83	17.68	18.02	17.38	16.82	17.68	16.61	18.43	18.21	19.16
Fe ₂ O ₃	7.99	6.76	7.41	7.12	6.30	5.67	6.75	7.95	8.31	7.30	7.65
MnO	0.18	0.16	0.17	0.17	0.16	0.16	0.17	0.19	0.21	0.19	0.18
MgO	3.18	2.99	4.14	3.05	2.66	2.25	2.91	2.79	2.98	2.93	2.72
CaO	7.84	7.41	6.94	6.70	6.72	8.00	7.27	5.97	7.57	7.62	8.25
K ₂ O	0.68	0.87	0.88	0.84	0.93	1.02	0.88	0.81	0.68	0.75	0.71
Na ₂ O	3.18	3.53	3.42	3.57	3.75	3.71	3.71	3.21	3.39	3.47	3.53
P ₂ O ₅	0.15	0.14	0.15	0.14	0.15	0.13	0.12	0.12	0.14	0.12	0.13
Totals	100.02	100.00	100.00	100.00	99.99	100.00	100.01	98.41	100.46	100.42	101.77
Li								9.26	7.83	12.67	12.19
Sc								12.73	10.35	12.43	13.13
Rb	18.65	20.13	18.94	16.68	20.57	19.96	16.59	11.89	13.06	16.08	15.44
Sr	305.60	238.50	295.30	250.10	270.20	316.00	306.50	244.10	267.80	273.90	307.20
Y	20.00	20.20	22.70	24.50	19.90	19.60	18.40	20.62	15.48	19.86	17.48
Zr	91.60	76.90	105.80	108.70	86.60	49.80	72.00	85.90	73.10	76.04	72.65
Nb	3.20	2.96	3.82	4.96	3.51	3.50	2.70	3.45	2.65	2.68	2.70
Cs	0.63	0.66	0.32	0.10	0.35	0.55	0.64	0.29	0.43	0.54	0.51
Ba	201.30	236.80	240.20	274.80	266.60	242.70	223.90	236.90	184.30	188.10	182.70
La	10.33	10.51	12.13	8.17	12.79	12.07	9.97	12.33	8.66	9.78	9.65
Ce	24.91	23.56	27.85	20.16	28.25	27.97	22.02	26.41	18.30	21.18	20.58
Pr	2.80	2.90	3.19	2.59	3.36	3.34	2.56	3.49	2.37	2.77	2.66
Nd	12.09	12.83	13.84	12.21	14.37	14.39	10.60	14.17	9.75	11.61	10.86
Sm	2.79	3.09	3.24	3.22	3.15	3.23	2.51	3.17	2.22	2.73	2.48
Eu	1.02	0.99	1.02	1.13	0.98	0.98	0.88	0.99	0.82	0.97	0.96
Gd	2.82	3.21	3.26	3.35	3.11	3.12	2.54	3.17	2.30	2.88	2.53
Tb	0.48	0.54	0.56	0.58	0.52	0.50	0.44	0.52	0.38	0.48	0.42
Dy	3.00	3.48	3.62	3.77	3.21	3.06	2.79	3.24	2.35	3.02	2.65
Ho	0.66	0.75	0.77	0.81	0.69	0.64	0.59	0.69	0.51	0.66	0.57
Er	1.96	2.24	2.30	2.46	2.11	1.89	1.79	2.04	1.53	1.97	1.71
Tm	0.31	0.35	0.36	0.40	0.33	0.30	0.27	0.33	0.25	0.31	0.28
Yb	2.16	2.39	2.48	2.73	2.25	1.96	1.85	2.27	1.73	2.22	1.93
Lu	0.34	0.40	0.40	0.45	0.39	0.32	0.30	0.37	0.28	0.35	0.31
Hf	2.31	2.27	2.70	2.85	2.47	1.66	2.02	2.31	1.90	2.09	1.95
Pb	2.88	3.16	3.31	4.32	2.87	3.85	3.06	7.26	2.13	2.64	2.89
Th	2.78	3.18	3.48	3.43	2.81	2.54	3.10	2.78	1.85	2.28	2.20
U	0.90	0.97	1.08	1.05	0.64	0.60	0.95	0.86	0.59	0.70	0.68

Latitude	16.7588	16.7531	16.7202	16.6775	16.6913	16.7185	16.7187	16.7323	16.7351	16.6989
Longitude	62.1553	62.1578	62.2007	62.1804	62.1486	62.2063	62.2061	62.2277	62.2328	62.1447
Core I.D.										
Depth (cm)										
Sample	MVO1547	MVO1587	MVO 1532	SSH2bi	SSH5Cii	StG1	StG2	Gara1	Gara4	MVO 138
<i>SiO₂</i>	56.43	53.55	55.23	52.52	53.82	56.71	56.70	63.40	57.87	53.73
<i>TiO₂</i>	0.67	0.81	0.54	0.83	0.75	0.68	0.73	0.62	0.58	0.75
<i>Al₂O₃</i>	18.96	18.89	21.24	19.38	18.24	18.17	18.08	16.57	18.96	18.89
<i>Fe₂O₃</i>	8.36	9.40	6.64	8.73	10.15	9.01	9.09	6.75	7.04	8.72
<i>MnO</i>	0.20	0.20	0.15	0.17	0.22	0.23	0.21	0.12	0.15	0.16
<i>MgO</i>	2.93	4.22	2.65	4.62	4.16	3.45	3.06	2.14	3.18	4.30
<i>CaO</i>	8.31	9.44	9.36	10.33	8.64	7.60	7.36	6.31	8.34	9.53
<i>K₂O</i>	0.58	0.54	0.47	0.57	0.44	0.60	0.70	1.05	0.70	0.76
<i>Na₂O</i>	3.37	2.85	3.44	3.02	2.84	3.19	3.32	3.56	2.91	3.06
<i>P₂O₅</i>	0.14	0.12	0.11	0.12	0.14	0.19	0.24	0.16	0.16	0.10
Totals	99.94	100.01	99.84	100.29	99.40	99.82	99.49	100.67	99.89	100.00
<i>Li</i>	11.63	10.78	9.88	8.33	7.33	12.93	11.19	10.40	5.61	
<i>Sc</i>	13.34	25.67	13.15	32.16	18.41	14.23	15.84	14.34	20.56	
<i>Rb</i>	11.44	10.59	10.23	12.40	8.04	13.90	11.62	19.63	11.26	14.82
<i>Sr</i>	293.30	293.80	336.30	354.10	307.40	291.20	280.80	225.10	445.20	325.90
<i>Y</i>	17.28	22.45	13.39	19.54	20.61	21.96	21.31	27.70	17.75	18.00
<i>Zr</i>	58.06	68.46	45.87	62.78	74.58	74.53	81.45	134.90	77.49	63.50
<i>Nb</i>	2.33	2.25	1.80	4.68	1.78	3.13	3.08	3.80	2.10	1.81
<i>Cs</i>	0.37	0.36	0.34	0.45	0.27	0.43	0.37	0.22	0.19	0.24
<i>Ba</i>	154.90	134.00	143.30	146.60	110.40	191.70	161.00	235.60	150.10	181.60
<i>La</i>	8.50	7.60	7.29	7.38	6.98	10.79	8.64	13.12	8.07	6.91
<i>Ce</i>	18.46	17.51	15.44	16.30	16.31	23.45	20.39	28.37	18.36	15.97
<i>Pr</i>	2.43	2.46	2.01	2.28	2.35	3.09	2.65	3.82	2.51	2.00
<i>Nd</i>	10.33	10.97	8.32	10.32	10.62	12.92	11.47	16.04	10.73	9.25
<i>Sm</i>	2.44	2.87	1.90	2.76	2.75	3.02	2.83	3.80	2.65	2.45
<i>Eu</i>	0.93	1.00	0.92	1.13	0.98	1.02	1.00	1.09	0.90	0.86
<i>Gd</i>	2.58	3.26	2.04	3.02	3.04	3.24	3.03	4.06	2.77	2.78
<i>Tb</i>	0.43	0.54	0.33	0.50	0.51	0.54	0.51	0.68	0.46	0.48
<i>Dy</i>	2.68	3.50	2.12	3.18	3.25	3.36	3.21	4.27	2.82	3.05
<i>Ho</i>	0.58	0.75	0.46	0.67	0.69	0.72	0.69	0.92	0.59	0.67
<i>Er</i>	1.73	2.23	1.35	1.94	2.06	2.15	2.10	2.76	1.72	1.94
<i>Tm</i>	0.27	0.34	0.21	0.30	0.32	0.34	0.33	0.43	0.26	0.30
<i>Yb</i>	1.90	2.36	1.50	1.99	2.23	2.34	2.31	2.96	1.79	1.95
<i>Lu</i>	0.30	0.37	0.24	0.31	0.35	0.37	0.37	0.46	0.28	0.31
<i>Hf</i>	1.63	1.82	1.32	1.71	1.92	2.06	2.20	3.50	2.07	1.86
<i>Pb</i>	2.56	3.07	2.31	1.82	2.54	3.76	3.24	3.36	3.86	3.52
<i>Th</i>	1.68	1.54	1.49	1.61	1.02	2.11	1.97	3.42	2.04	2.25
<i>U</i>	0.53	0.48	0.44	0.45	0.34	0.73	0.57	1.17	0.73	0.80

	<i>Kahouanne</i>				<i>Redonda</i>	
Latitude	16.6913	16.6913	16.6910	16.6775	16.3764	16.9432
Longitude	62.1486	62.1486	62.1490	62.1800	61.5770	62.3447
Core I.D.					JR123-11	
Depth (cm)					159-161	
Sample	SSH5A	SSH5D	SSH6A	SSH2bii	KAH01	Red01
<i>SiO₂</i>	64.07	54.54	53.27	53.28	50.64	49.83
<i>TiO₂</i>	0.50	0.62	0.62	0.84	0.85	0.82
<i>Al₂O₃</i>	16.04	20.27	20.10	18.20	18.05	19.21
<i>Fe₂O₃</i>	5.94	7.60	8.28	9.09	11.23	11.00
<i>MnO</i>	0.14	0.17	0.19	0.18	0.22	0.19
<i>MgO</i>	2.11	3.36	3.50	4.52	6.08	6.11
<i>CaO</i>	5.79	9.80	9.60	9.17	10.50	10.45
<i>K₂O</i>	1.15	0.78	0.39	0.64	0.42	0.47
<i>Na₂O</i>	3.50	2.59	2.82	3.10	2.41	2.16
<i>P₂O₅</i>	0.10	0.08	0.13	0.19	0.17	0.22
<i>Totals</i>	99.34	98.80	98.91	99.20	100.56	100.47
<i>Li</i>	16.65	11.60	8.01	8.94	5.57	2.83
<i>Sc</i>	11.62	18.51	17.74	25.79	22.25	30.29
<i>Rb</i>	24.55	16.07	7.25	12.90	5.14	3.31
<i>Sr</i>	216.10	287.40	351.40	329.60	297.10	419.40
<i>Y</i>	19.33	13.46	19.57	25.20	12.72	12.34
<i>Zr</i>	94.18	57.65	67.97	83.35	37.16	34.79
<i>Nb</i>	3.32	2.14	1.63	4.55	1.92	0.59
<i>Cs</i>	0.37	0.21	0.24	0.41	0.14	0.07
<i>Ba</i>	286.30	147.30	103.40	169.50	81.89	52.82
<i>La</i>	11.64	6.71	6.55	10.33	4.96	3.71
<i>Ce</i>	23.95	13.80	15.23	23.13	11.46	8.64
<i>Pr</i>	3.01	1.80	2.19	3.22	1.59	1.27
<i>Nd</i>	11.95	7.43	9.91	14.23	7.12	5.88
<i>Sm</i>	2.72	1.80	2.60	3.58	1.80	1.54
<i>Eu</i>	0.85	0.76	0.98	1.18	0.68	0.58
<i>Gd</i>	2.80	1.96	2.84	3.86	1.97	1.77
<i>Tb</i>	0.46	0.33	0.48	0.63	0.33	0.30
<i>Dy</i>	2.93	2.10	3.04	3.92	2.05	1.94
<i>Ho</i>	0.63	0.45	0.65	0.84	0.44	0.42
<i>Er</i>	1.92	1.35	1.93	2.46	1.27	1.24
<i>Tm</i>	0.30	0.21	0.30	0.37	0.19	0.19
<i>Yb</i>	2.17	1.54	2.07	2.52	1.31	1.22
<i>Lu</i>	0.35	0.25	0.33	0.39	0.20	0.19
<i>Hf</i>	2.59	1.59	1.75	2.19	1.04	1.02
<i>Pb</i>	3.64	2.32	2.38	2.97	1.60	1.52
<i>Th</i>	3.68	1.82	0.96	1.95	0.83	0.78
<i>U</i>	1.10	0.54	0.31	0.59	0.26	0.33

Table 2 - Isotopic geochemical data table for all samples analysed

Volcanic tag	Samples	Longitude	Latitude	Core I.D.	Sample depth	⁸⁷ Sr/ ⁸⁶ Sr	SE	¹⁴³ Nd/ ¹⁴⁴ Nd	SE	²⁰⁶ Pb/ ²⁰⁸ Pb	SE	²⁰⁷ Pb/ ²⁰⁸ Pb	SE	²⁰⁶ Pb/ ²⁰⁸ Pb	SE	As/4 Pb	Δ7/4 Pb
Silver Hills	MVO 144	16.8045	62.2022			0.703553	10	0.512981	6	19.0525	13	15.6659	12	38.7876	38	12.6	11.0
	MVO 755	16.7994	62.1958			0.703678	13	0.512975	5	19.0381	9	15.6646	8	38.7739	24	13.0	11.0
	MGEOL 1	16.8020	62.1928			0.703626	11	0.512985	5	19.0430	9	15.6674	8	38.7825	25	13.3	11.2
	MGEOL 5	16.8073	62.1855			0.703570	11			19.0364	9	15.6612	8	38.7665	25	12.5	10.7
	Si/H3	16.8117	62.1926			0.703631	6			19.0344	24	15.6689	22	38.7655	70	12.6	11.3
	MGEOL9	16.8131	62.2044			0.703662	17	0.512980	12	19.0448	12	15.6648	11	38.7812	35	12.9	10.8
	MVO 135	16.7062	62.1485			0.703599	12	0.512961	7	19.0398	10	15.6632	9	38.7777	28	13.2	10.8
	MVO 131	16.7552	62.1679			0.703608	11	0.512945	6	19.0442	23	15.6628	21	38.7748	66	12.3	10.7
	MVO 147	16.7830	62.2057			0.703673	11			19.0383	14	15.6631	13	38.7739	40	12.8	10.8
	MVO 809	16.7691	62.1735			0.703652	10	0.512961	5	19.0359	10	15.6614	9	38.7689	28	12.9	10.7
Centre Hills	MVO 831	16.7745	62.1705			0.703630	14	0.512943	7	19.0447	16	15.6618	14	38.7755	45	12.3	10.6
	CH2	16.7962	62.2100			0.703591	7	0.512967	8	19.0436	19	15.6677	17	38.7890	54	13.8	11.2
	Brands	16.7226	62.2397							19.0426	17	15.6662	16	38.7800	49	13.0	11.1
	MC02A	16.6761	62.3272	JR123-2	272-273	0.703499	78			18.9244	21	15.6324	18	38.6163	58	11.0	9.0
	MC01G	16.6761	62.3272	JR123-2	265-266	0.703641	8			18.9422	23	15.6356	21	38.6378	63	11.0	9.1
	MVO 830	16.6933	62.1484			0.703682	9	0.512981	14	18.9428	14	15.6222	13	38.6190	41	9.0	7.8
	MC08G	16.7358	62.3491	JR123-1	388-389	0.703624	9			18.9259	31	15.6257	32	38.6056	80	9.7	8.3
	MC02G	16.6761	62.3272	JR123-2	272-273	0.703657	8			18.9374	33	15.6363	30	38.6398	94	11.8	9.5
	MVO 1099	16.6881	62.1839			0.703654	9	0.512993		18.9087	17	15.6231	16	38.6162	49	9.4	7.9
	MC07A	16.7358	62.3491	JR123-1	181-182	0.703609	9			18.9115	28	15.6215	31	38.5848	72	9.4	8.0
SSH Suite A	MC18A	16.6431	62.3017	JR123-4	63-64	0.703631	9										
	MC09A	16.6108	62.1881	JR123-45	148-150	0.703636				18.9489	25	15.6315	25	38.6331	58	9.7	8.6
	MC18G	16.6431	62.3017	JR123-4	63-64					18.9241	18	15.6262	15	38.6038	45	9.8	8.4
	MC08G	16.6108	62.1881	JR123-45	148-150	0.703660	12			18.9161	23	15.6236	29	38.5919	68	9.5	8.2
	MC07G	16.7358	62.3491	JR123-1	181-182	0.703614	10										
	SSH5B	16.6913	62.1486			0.703756	35	0.512938	8	18.8937	27	15.6368	25	38.6025	79	13.3	9.8
	SSH5Bb	16.6913	62.1486							18.8809	24	15.6303	25	38.5754	58	12.1	9.3
	SSH10	16.6922	62.1479			0.703601	13	0.513017	7	18.8803	25	15.6018	24	38.5190	74	6.6	6.4
	SSH11	16.6930	62.1489	JR123-4	9394	0.703623	7	0.512997	5	18.8909	31	15.6137	28	38.5547	89	8.9	7.5
	MC03G	16.6431	62.3017	JR123-4	124-125	0.703590	11			18.8732	23	15.5860	19	38.4923	69	4.8	4.9
SSH Suite B	MC06G	16.6431	62.3017	JR123-4	187-188	0.703691	7			18.9098	18	15.6094	21	38.5765	45	9.0	6.9
	MC11G	16.5833	62.1522	JR123-46	384-385	0.703515	34			18.8761	31	15.5926	28	38.5066	77	5.8	5.5
	MC12G	16.5750	62.0894	JR123-47						18.8728	25	15.5887	25	38.4962	60	5.2	5.2
	MC03 [A]	16.6431	62.3017	JR123-4	9394					18.8815	21	15.5896	31	38.5066	71	5.2	5.2
	MC06 [A]	16.6431	62.3017	JR123-4	124-125					18.8881	26	15.6019	32	38.5364	80	7.4	6.3
	MVO 791	16.6770	62.1628			0.703548	12	0.513007	6	18.9019	27	15.6082	21	38.5660	77	8.7	6.8
	SSH3	16.6780	62.1692					0.512989	9	18.8736	27	15.6027	25	38.5240	79	7.9	6.6

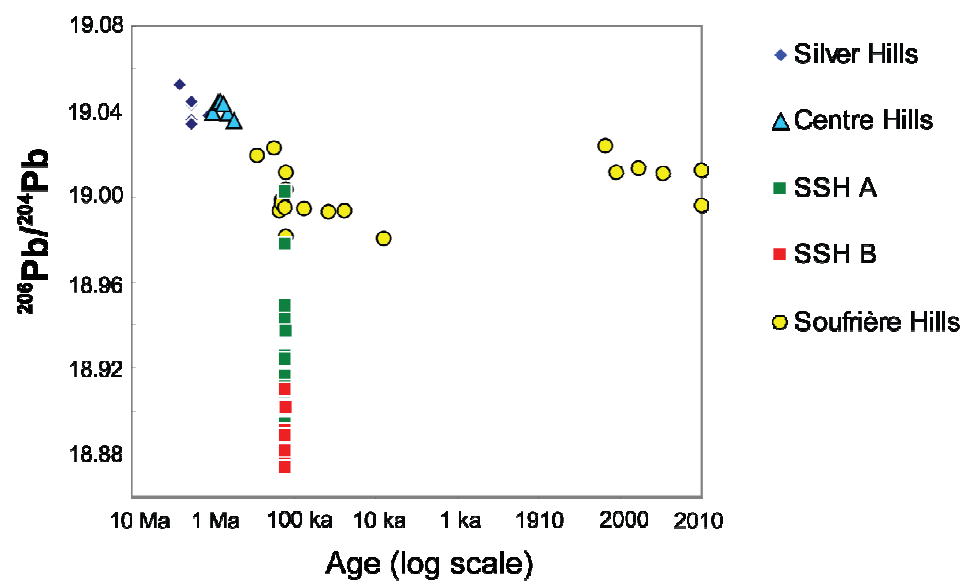
Table 2 Continued																		
Volcanic reg	Samples	Longitude	Latitude	Core I.D.	Sample depth	⁸⁷ Sr/ ⁸⁶ Sr	SE	¹⁴³ Nd/ ¹⁴⁴ Nd	SE	²⁰⁶ Pb/ ²⁰⁸ Pb	SE	²⁰⁷ Pb/ ²⁰⁸ Pb	SE	AS/4 Pb	Δ7/4 Pb			
Soufrière Hills	MC13A	16.6761	62.3272	JR123-2	17-18	0.703550	8			18.9804	24	15.6397	26	38.6770	71	10.3	8.1	
	MVO 104	16.7126	62.1711			0.703613	11	0.512969		19.0240	60	15.6597	55	38.7502	172	12.3	10.7	
	MVO 127	16.7399	62.1527			0.703600	10	0.512964		18.9927	13	15.6523	12	38.7228	37	13.4	10.2	
	MVO 152	16.7152	62.1885			0.703635	9	0.512964		18.9936	11	15.6506	10	38.7166	52	12.6	10.1	
	MVO 154	16.7103	62.1616			0.703647	11	0.512970		18.9933	13	15.6486	12	38.7123	37	12.2	9.9	
	MVO 777	16.7146	62.1626			0.703579	11	0.512969		18.9946	15	15.6484	14	38.7127	43	12.1	9.6	
	MVO 785	16.7351	62.2329			0.703572	10	0.512969		19.0193	27	15.6519	25	38.7367	78	11.5	9.9	
	MVO 819	16.7334	62.1549			0.703635	13	0.512963		19.0230	16	15.6561	15	38.7545	46	12.9	10.3	
	MVO 892	16.7064	62.1831			0.703617	6	0.512949	32	18.9971	31	15.6496	28	38.7155	89	12.1	10.0	
	MVO 775	16.1550	62.7134			0.703574	6	0.512976	9	18.9932	17	15.6508	16	38.7127	50	12.3	10.1	
	MVO 1209	16.7223	62.1545					0.512963	5	19.0114	16	15.6519	15	38.7292	46	11.7	10.0	
	MVO 1329	16.7257	62.1548			0.703598	7	0.512939	10	19.0131	20	15.6547	23	38.7367	65	12.3	10.3	
	MVO 1547	16.7588	62.1553					0.512960	7	18.9958	15	15.6480	14	38.7064	45	11.3	9.8	
	MVO 1587	16.7531	62.1578			0.703608	8	0.512941	8	19.0123	24	15.6506	22	38.7232	70	11.0	9.9	
	MVO 1532	16.7202	62.2007			0.703604	12	0.512978	9	19.0110	20	15.6549	19	38.7327	58	12.1	10.3	
	SSH5CII	16.6913	62.1486								18.9781	26	15.6491	25	38.6989	61	12.7	10.1
	SSH2bi	16.6775	62.1804								19.0022	18	15.6531	15	38.7210	65	12.0	10.2
	SG1	16.7185	62.2063								18.9982	36	15.6505	33	38.7165	105	12.1	10.0
	MVO 136	16.6989	62.1447								18.9947	12	15.6443	11	38.7059	36	11.4	9.4
	SSH5A	16.6913	62.1486								19.0032	23	15.6487	21	38.7151	67	11.3	9.8
	SSH5D	16.6913	62.1486								19.0112	30	15.6530	28	38.7322	87	12.1	10.1
	SSH6A	16.6910	62.1490								18.9815	26	15.6525	24	38.7085	76	13.3	10.4
	KAH01	16.3764	61.5770	JR123-11	159-161		0.703788	11			18.9428	11	15.6385	10	38.6455	31	11.7	9.4
	Red01	16.9432	62.3447								18.8954	11	15.6008	10	38.5414	31	8.2	6.3

Supplementary Table 1 - Ar-Ar, relative stratigraphic and average

Sample Name	Volcanic centre	Age (ka)	Value used ϕ
MVO 144	Silver Hills	2580	Ar-Ar
MVO 755	Silver Hills	1160	Ar-Ar
MGEOL 1	Silver Hills	1870	Average
MGEOL 5	Silver Hills	1870	Average
SilvH3	Silver Hills	1870	Average
MGEOL 9	Silver Hills	1870	Average
MVO 135	Centre Hills	1021	Ar-Ar
MVO 131	Centre Hills	871	Ar-Ar
MVO 147	Centre Hills	663	Ar-Ar
MVO 809	Centre Hills	550	Ar-Ar
MVO 831	Centre Hills	826	Ar-Ar
CH2	Centre Hills	752	Average
MVO 785	Soufrière Hills	282	Ar-Ar
MVO 819	Soufrière Hills	174	Ar-Ar
MVO 152	Soufrière Hills	151	Ar-Ar
StG1	Soufrière Hills	141	Average
MVO692	Soufrière Hills	141	Average
SSH5D	Soufrière Hills	128	Stratigraphic
SSH5A	Soufrière Hills	128	Stratigraphic
SSH6A	Soufrière Hills	128	Stratigraphic
MVO 136	Soufrière Hills	130	Ar-Ar
MC01G	SSH A	129	Stratigraphic
MC02A	SSH A	129	Stratigraphic
MC08G	SSH A	129	Stratigraphic
MC02G	SSH A	129	Stratigraphic
MC07G	SSH A	129	Stratigraphic
MC07A	SSH A	129	Stratigraphic
MC18A	SSH A	129	Stratigraphic
MC18G	SSH A	129	Stratigraphic
MC09G	SSH A	129	Stratigraphic
MVO 830	SSH A	129	Ar-Ar
SSH2bi	SSH A	129	Stratigraphic
SSH5Cii	SSH A	129	Stratigraphic
MVO 1099	SSH A	128	Ar-Ar
SSH5B	SSH A	129	Stratigraphic
SSH10	SSH B	130	Stratigraphic
SSH11	SSH B	130	Stratigraphic
MC11G	SSH B	130	Stratigraphic
MC12G	SSH B	130	Stratigraphic
MC03 [A]	SSH B	130	Stratigraphic
MC06 [A]	SSH B	130	Stratigraphic
MC03G	SSH B	130	Stratigraphic
MC06G	SSH B	130	Stratigraphic
MVO 791	SSH B	128	Ar-Ar
SSH3	SSH B	130	Stratigraphic
MVO 777	Soufrière Hills	75	Ar-Ar
MVO 127	Soufrière Hills	38	Ar-Ar
MVO 154	Soufrière Hills	24	Ar-Ar
MVO775	Soufrière Hills	24	Ar-Ar
MC13A	Soufrière Hills	8.01	AMS radiocarbon
MVO 104	Soufrière Hills	0.015	Real
MVO1209	Soufrière Hills	0.011	Real
MVO1329	Soufrière Hills	0.006	Real
MVO1532	Soufrière Hills	0.003	Real
MVO1547	Soufrière Hills	0.001	Real
MVO1587	Soufrière Hills	0.001	Real

ϕ Ar-Ar dates from Harford et al. (2002)

Average values are taken from the available Ar-Ar dates averaged for AMS radiocarbon date from marine sediment core JCR123-2 used to Stratigraphic dates are based on field relationships between the units



Supplementary figure. This is based on relative and absolute age data (supplementary Table 3)

Table 1 continued

Core I.D.	JR123-4	JR123-4	JR123-1	JR123-1	JR123-4	JR123-45	JR123-4	JR123-45	JR123-1	JR123-46	JR123-45	JR123-4	JR123-46	JR123-1
Latitude	16.643056	16.64306	16.73583	16.73583	16.64306	16.61083	16.64306	16.61083	16.73583	16.58333	16.61083	16.64306	16.58333	16.73583
Longitude	62.301687	62.30167	62.34917	62.34917	62.30167	62.18806	62.30167	62.18806	62.34917	62.15222	62.18806	62.30167	62.15222	62.34917
Depth (cm)	83.5-94.5	124-125	388-389.5	181.5-182	63-64.5	148-150	63-64.5	148-150	181.5-182	165-166.5	148-150	63-64.5	165-166.5	181.5-182.1
Submarine unit	SSH LU	SSH LU	SSH LU	SSH LU	SSH UU	SSH UU	SSH UU	SSH UU	SSH LU	SSH UU	SSH UU	SSH UU	SSH UU	SSH LU
Samples:	MC03F	MC06F	MC08F	MC07A	MC18A	MC09A	MC18G	MC09G	MC07G	MC10G	MC09F	MC18F	MC10F	MC07F
Li	1.78	2.72	3.43	9.79	8.88	12.54	8.34	7.54	9	7.22	4.29	2.23	6.61	6.49
Sc	4.95	4.01	5.44	33.76	28.12	35.83	33.2	55.58	35.8	31.17	3.07	2.06	12.69	9.85
Rb	1.86	2	1.51	11.31	10.19	7.52	7.3	7.89	10.51	7.83	2.28	0.97	3.92	5.27
Sr	531.3	490.6	403.3	242.4	299.8	259.2	272	212.3	237.4	283	433.8	428.9	426.1	382.4
Y	3.28	2.92	3.83	25.18	16.8	16.9	22.37	22.99	23.31	21.01	3.08	1.64	8.5	8.33
Zr	9.8	11.2	10.2	79.5	49.5	49	64.9	55.2	70.9	61.4	10.8	4.9	20.3	17.6
Nb	0.46	0.77	0.26	1.79	1.38	1	1.48	1.15	1.58	1.25	0.3	0.13	0.51	0.78
Cs	0.06	0.04	0.04	0.39	0.27	0.23	0.25	0.25	0.34	0.26	0.06	0.03	0.11	0.17
Ba	37.2	40	31.9	128.1	126.4	94.2	93.4	82.4	115.8	94.6	55.9	15.2	66.6	80
La	1.29	1.43	1.34	6.44	5.42	4.38	5.68	4.45	5.84	5.15	2.17	0.73	2.7	3.21
Ce	2.8	2.99	3.02	15.34	12.69	10.34	13.98	11.18	14.04	12.58	4.28	1.62	6.19	7.02
Pr	0.41	0.43	0.42	2.22	1.77	1.5	2.05	1.7	2.05	1.85	0.53	0.22	0.89	0.96
Nd	1.85	1.88	1.91	10.38	8.02	6.95	9.62	8.35	9.6	8.78	2.17	0.98	4.1	4.21
Sm	0.47	0.47	0.5	2.93	2.19	1.99	2.74	2.56	2.74	2.49	0.46	0.25	1.13	1.08
Eu	0.29	0.33	0.43	1.02	0.84	0.81	1.01	0.91	0.98	0.94	0.58	0.24	0.62	0.69
Gd	0.54	0.5	0.59	3.58	2.54	2.46	3.31	3.35	3.37	3.04	0.5	0.27	1.32	1.23
Tb	0.08	0.08	0.1	0.6	0.42	0.41	0.55	0.57	0.56	0.51	0.08	0.04	0.21	0.2
Dy	0.55	0.49	0.6	3.9	2.67	2.68	3.49	3.7	3.65	3.31	0.48	0.26	1.35	1.31
Ho	0.12	0.1	0.13	0.85	0.57	0.58	0.75	0.79	0.79	0.71	0.1	0.05	0.28	0.28
Er	0.34	0.29	0.37	2.51	1.69	1.71	2.22	2.31	2.35	2.09	0.29	0.16	0.83	0.82
Tm	0.05	0.04	0.06	0.39	0.26	0.26	0.34	0.35	0.36	0.32	0.05	0.02	0.12	0.13
Yb	0.34	0.29	0.38	2.62	1.74	1.81	2.31	2.36	2.47	2.17	0.31	0.16	0.83	0.85
Lu	0.05	0.04	0.06	0.41	0.27	0.28	0.36	0.36	0.38	0.34	0.05	0.02	0.13	0.13
Hf	0.29	0.31	0.27	2.05	1.37	1.31	1.71	1.52	1.88	1.62	0.27	0.13	0.55	0.52
Pb	1.05	1.27	5.19	10.66	5.26	8.29	6.5	4.89	6.63	9.16	4.89	2.69	14.77	5.56
Th	0.26	0.23	0.14	1.19	1.21	0.78	0.94	0.74	1.07	0.84	0.23	0.08	0.38	0.47
U	0.19	0.2	0.06	0.46	0.39	0.29	0.33	0.28	0.41	0.33	0.09	0.03	0.16	0.16

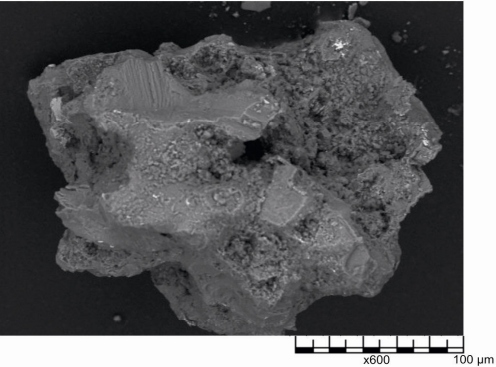
Major elements (wt%)	Sample	Rock Unit	West section	Longitude	Latitude
	SSH2N	PB	West	62.18046	18.6775
	SSH2bii	PB	West	62.18046	18.6775
	SSH2C	WB-F	West	62.18048	18.6775
	SSH3	MSD	West	62.18927	18.67672
	SSH4	MSD	West	62.19326	18.67622
	SSH5A	LDF	East	62.14866	18.66131
	SSH5B	IA-F	East	62.14866	18.66131
	SSH5Ci	PB	East	62.14866	18.66131
	SSH5Cii	PB	East	62.14866	18.66131
	SSH5D	LDF	East	62.14936	18.66131
	SSH6A	PB	East	62.14907	18.66101
	SSH6A	Not instu	East	62.1516	18.66802
	SSH6A	Not instu	East	62.1516	18.66802
	SSH9B	Not instu	East	62.1479	18.66226
	SSH10	UDF	East	62.14699	18.66304
	SSH11		East		

	JIS-2		RSD (%)		JA-2		% RSD										
SiO2	53.72	0.6	52.52	53.277	52.99	49.221	50.872	64.098	58.772	58.117	53.816	54.541	53.273	56.374	49.031	62.723	49.287
TiO2	1.13	0.1	0.9307	0.9363	0.924	0.995	0.8724	0.4997	0.385	0.6258	0.7507	0.6171	0.6185	1.3955	0.9959	0.3971	0.9461
Al2O3	14.78	0.5	19.38	18.199	18.495	18.671	19.2	16.037	17.951	18.555	18.24	20.268	20.079	16.398	18.451	20.873	20.873
Fe2O3	14.09	0.8	8.728	9.093	9.843	10.898	9.593	5.942	7.577	8.12	10.151	7.598	8.291	8.955	10.295	5.537	9.819
MnO	0.22	2.1	0.17949	0.1878	0.1876	0.1778	0.175	0.1412	0.1882	0.1817	0.2223	0.1727	0.1851	0.1531	0.1733	0.1755	0.17449
MgO	4.56	0.9	4.823	4.515	4.897	5.928	2.106	4.384	3.193	3.193	4.16	3.356	3.504	4.328	5.282	2.41	4.772
CaO	9.76	0.4	10.333	9.172	9.328	10.927	10.847	5.787	7.268	8.161	8.842	9.789	9.588	7.419	11.186	6.556	11.031
Na2O	9.76	0.4	10.333	9.172	9.328	10.927	10.847	5.787	7.268	8.161	8.842	9.789	9.588	7.419	11.186	6.556	11.031
K2O	0.41	1.7	0.57	0.635	0.639	0.634	0.681	1.154	0.802	0.541	0.436	2.592	2.822	3.727	2.395	4.129	2.479
P2O5	0.1	2.2	0.116	0.191	0.204	0.124	0.126	0.192	0.151	0.174	0.142	0.077	0.134	0.234	0.086	0.103	0.108
Trace elements (ppm)																	
Li	30.18	2.42	8.33	8.94	5.25	4.58	6.2	16.55	8.63	8.19	7.33	11.6	8.01	21.78	10.72	4.33	5.65
Na	18.22	0.88	32.16	25.79	17.98	4.11	32.75	11.52	18.53	15.18	18.41	18.51	17.74	11.2	19	41.89	37.78
Rb	77.24	12.9	8.88	12.4	8.88	7.54	7.99	24.55	11	9.55	8.04	16.07	7.25	17.29	22.12	5.53	5.55
Sr	245.8	1.2	354.1	329.8	237.5	589.4	540.8	218.1	280.3	305.2	307.4	287.4	351.4	281	352.9	384.7	430.2
Y	17.58	1.66	19.54	25.2	16.7	18.15	17.71	19.33	20.68	22.88	20.51	13.46	19.57	17.5	21.17	20.18	20.2
Zr	120.7	5.06	62.76	83.35	57.29	58.42	61.17	94.18	89.96	89.4	74.58	57.55	67.97	80.34	113.7	41	39.13
Nb	8.83	0.69	4.68	4.55	4.39	2.35	2.31	3.32	2.1	2.08	1.78	2.14	1.53	2.78	13.65	0.9	0.88
Co	6.17	0.23	0.45	0.41	0.16	0.16	0.19	0.37	0.23	0.32	0.27	0.21	0.24	0.45	0.5	0.08	0.144
Ba	319.2	0.9	146.6	189.5	118.4	114.9	128.2	288.3	168	133.4	110.4	147.3	103.4	280.7	254.5	104.7	112.8
La	16	0.44	7.38	10.33	7.4	8.45	8.31	11.54	7.75	8.29	6.98	6.71	6.55	11.7	11.11	3.82	4.13
Ce	33.28	0.88	16.3	23.13	16.37	19.48	18.79	23.95	17.6	19.27	16.31	13.8	15.23	23.22	23.89	9.17	9.56
Pr	3.81	1.94	2.28	3.22	2.26	2.71	2.5	3.01	2.5	2.74	2.35	1.8	2.19	2.9	3.26	1.49	1.66
Nd	14.47	1.3	10.32	14.23	9.88	11.79	11.38	11.56	11.85	12.21	10.62	7.43	9.91	11.46	14.81	7.53	8.15
Sm	3.11	0.25	2.76	3.68	2.72	2.68	2.68	2.72	2.76	3.11	2.75	1.8	2.6	2.51	4	2.35	2.5
Eu	0.9	0.92	1.13	1.18	0.83	0.84	0.84	0.85	0.84	1.07	0.98	0.78	0.98	0.83	1.38	0.88	0.92
Gd	3.02	0.34	3.02	3.86	2.63	2.97	2.92	2.48	2.48	3.38	3.04	1.96	2.84	2.58	4.22	2.86	2.97
Tb	0.48	0.63	0.5	0.63	0.42	0.48	0.48	0.48	0.51	0.57	0.51	0.33	0.46	0.42	0.65	0.49	0.5
Dy	2.9	0.12	3.18	3.92	2.8	3.02	3	2.83	3.19	3.6	3.25	2.1	3.04	2.88	3.77	3.15	3.23
Ho	0.59	1.98	0.67	0.84	0.56	0.63	0.63	0.63	0.69	0.77	0.69	0.45	0.65	0.57	0.73	0.68	0.68
Er	1.71	0.2	1.94	2.46	1.58	1.8	1.8	1.92	2.07	2.29	2.06	1.35	1.93	1.73	2.01	1.94	1.98
Tm	0.25	1.63	0.3	0.37	0.24	0.27	0.27	0.3	0.32	0.36	0.32	0.21	0.3	0.28	0.29	0.29	0.3
Yb	1.7	0.81	1.99	2.52	1.61	1.74	1.77	2.17	2.27	2.48	2.23	1.54	2.07	1.86	1.89	1.94	1.95
Lu	0.26	1.33	0.31	0.39	0.25	0.37	0.27	0.35	0.39	0.39	0.35	0.25	0.33	0.32	0.29	0.3	0.28
Hf	2.81	0.41	1.71	2.19	1.51	1.88	1.73	2.58	2.25	2.28	1.92	1.59	1.75	2.37	2.9	1.24	1.21
Pb	22.1	8.83	1.82	2.97	3.36	1.79	1.82	3.84	3.05	3.03	2.64	2.32	2.38	4.32	2.57	2.35	2.37
Th	4.85	2.17	1.61	1.95	1.57	1.93	1.81	3.68	1.25	1.25	1.02	1.82	0.96	3.32	2.44	0.57	0.5
U	2.28	1.76	0.45	0.59	0.43	0.55	0.56	1.1	0.45	0.43	0.34	0.54	0.31	0.73	0.76	0.29	0.24

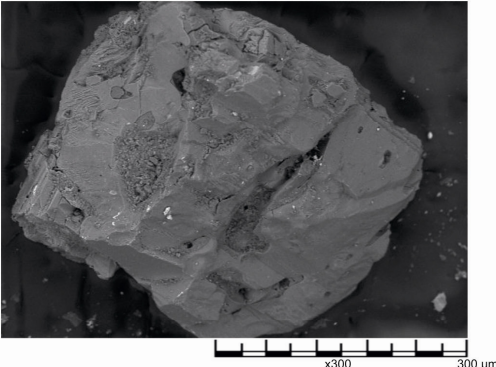
JA= Japanese Andesite (International Standard)
JB-2= Japanese Basalt (International Standard)
RSD= Relative Standard Deviation

Appendix C: SEM images of different components from Chapter 5

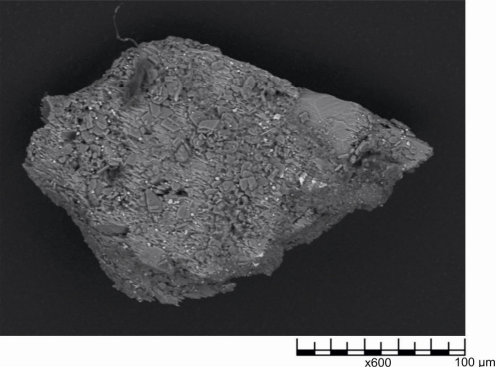
(a) Altered Dome Clast (Sample: B, 15 cm)



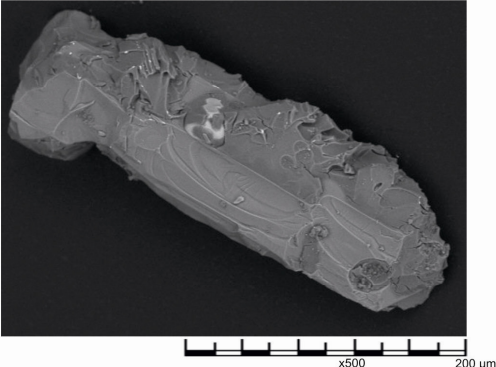
(b) Mafic Clast (Sample: C, 90 cm)



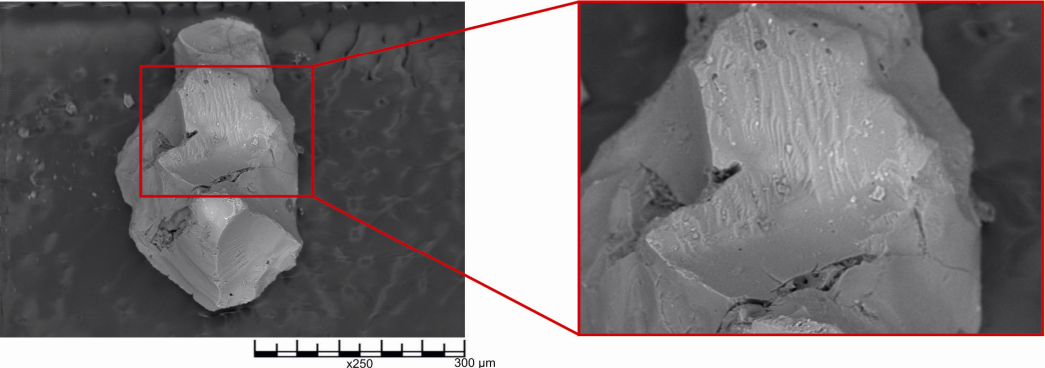
(c) Non vesicular juvenile (Sample: C, 90 cm)



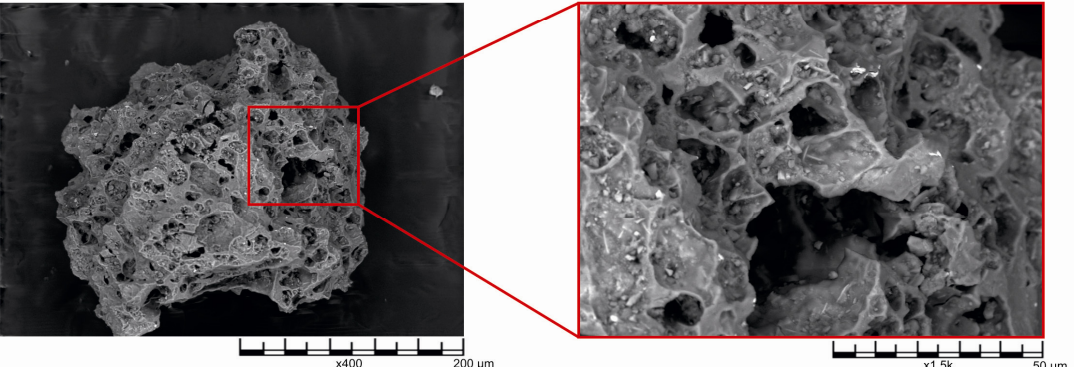
(d) Crystal Fragment (Sample: C, 90 cm)



(e) Glass Shard (Sample: D, 5 cm)



(f) Vesicular Juvenile (Sample: D, 5 cm)



Appendix D: Conference Abstracts**AGU Fall meeting 2011- Poster presentation****Co-existence of two distinct magma sources in an island arc volcano:
evidence from Montserrat, Lesser Antilles Arc**M. CASSIDY^{1*}, R.N. TAYLOR¹, M.J. PALMER¹, J. TROFIMOV¹¹ National Oceanography Centre, Southampton, University of Southampton, Waterfront Campus, European Way, Southampton SO14 3ZH (*correspondance:m.cassidy@soton.ac.uk)

The South Soufrière Hills (SSH), located on the southern tip of the volcanically active island of Montserrat, West Indies, hosts the most complex and interesting volcanic deposits on the island in terms of their geochemistry and volcanic history. In this study we examine the composition of submarine SSH deposits in marine sediment cores and volcanics sampled during subaerial mapping of the SSH and other volcanic centres on Montserrat. SSH volcanism is found to represent an important compositional change in the magmatic evolution of Montserrat with implications for the origin of components in the Caribbean subduction system.

Marine sediment cores and subaerial field mapping of the SSH volcanic centre document voluminous multi-stage flank failures of the SSH, which successively cut into older and chemically distinct stratigraphy as the collapses progressed. Nd, Sr and high-precision double-spike Pb isotopes combined with trace element analyses and SEM imagery of the SSH deposits indicate that this volcano includes multiple injections of mafic magma followed by magmatic differentiation and episodic explosive eruptions of andesitic pumice, which were triggered by fresh mafic pulses.

We demonstrate that the SSH is chemically distinct from the rest of the volcanic centres on the island, suggesting that magmas from the Soufrière Hills and SSH come from entirely separate sources. $^{206}\text{Pb}/^{204}\text{Pb}$ plotted against $\Delta 7/4\text{Pb}$ and $\Delta 8/4\text{Pb}$ show that Montserrat falls along two differing trends; one defined by the SSH volcanic centre and the second comprising the three other volcanic centres (Silver Hills, Centre Hills and Soufrière Hills). Magma generation at these centres (excluding the SSH) reflects an input of pelagic sediment, likely in the form of partial melt as indicated by elevated Th/Nd and lower $^{143}/^{144}\text{Nd}$. However, the SSH has more of slab-fluid rich signature relative to sediment as suggested by lower Ce/Pb, $^{206}\text{Pb}/^{204}\text{Pb}$ and $\Delta 7/4\text{Pb}$ combined with higher $^{87}\text{Sr}/^{86}\text{Sr}$. The low, but stable Nb/Zr values relative to MORB, suggests that the mantle source for each volcanic centre has remained constant despite the deviation in sediment flux reflected during SSH activity. By extension from the high-precision Pb isotope results, we can suggest that subduction fluid, and sediment melt components can be discriminated within a single arc volcano.

Goldschmidt, Prague 2011- Oral presentation**Tracking the magmatic evolution of an island arc volcano: Insights from
a high-precision Pb isotope record of Montserrat, Lesser Antilles**M. CASSIDY^{1*}, R.N. TAYLOR¹, M.J. PALMER¹, J. TROFIMOV¹¹ National Oceanography Centre, Southampton, University of Southampton, Waterfront Campus, European Way, Southampton SO14 3ZH (*correspondance:m.cassidy@soton.ac.uk)

It is rare to have a chance to examine the magmatic evolution of an island arc volcano over a period of millions of years. The volcanic succession exposed on Montserrat provides such an opportunity, extending from the 2 Ma andesites of the Silver Hills complex through to the youngest dome collapse of the Soufrière Hills volcano (February 2010). In this study we present new trace element, Sr, Nd and high-precision double spike Pb isotope data taken through Montserrat's time sequence. As well as from subaerial locations, we have collected samples from marine sediment cores, as significant volumes of pyroclastic material have ended up in the Caribbean Sea.

Each of Montserrat's volcanic groups; South Soufrière Hills (SSH), Soufrière Hills, Centre Hills and Silver Hills, can be clearly discriminated using trace element and isotopic parameters. Furthermore, the SSH can be divided into two suites: A and B, combining trace elements and Pb isotopes.

The trends in trace elements and isotopes suggest some variability in fluid and sediment addition over time. The SSH in particular has a greater slab fluid signature as indicated by elevated Pb/Ce, but less sediment addition than the other volcanic centres. $^{206/204}\text{Pb}$ against $\Delta 7/4$ and $\Delta 8/4$ diagrams show that Montserrat falls along two differing trends, one defined by the SSH volcanic region and the second trend defined by the other volcanic regions on Montserrat (Silver Hills, Centre Hills and Soufrière Hills). Furthermore, the SSH volcanic centre differs noticeably in trace elements and isotope ratios. This demonstrates that the source which generated the SSH magmas is different to the source of the other volcanics on Montserrat. Both isotopic trends point to an enriched mantle source underneath Montserrat. Samples from the current period of activity will be discussed including the presence of mafic enclaves within the current eruption.

VMSG 2011 – Poster presentation

The rise and demise of south Montserrat: Evolution of the South Soufrière Hills

MICHAEL CASSIDY*, JESSICA TROFIMOV, REX TAYLOR AND MARTIN PALMER

[National Oceanography Centre, University of Southampton, Southampton, UK]

(*correspondence: m.cassidy@soton.ac.uk)

On the southern extent of the volcanically active island of Montserrat, West Indies, is an interesting but poorly understood volcanic centre called the South Soufrière Hills (SSH) volcanic complex. Eruptions from the SSH centre are dated at ~128-131 ka [1]. Whereas most of Montserrat is made up of andesitic lavas and pyroclastic deposits, the subaerially exposed outcrops of the SSH volcanic centre are comprised predominantly of basaltic lava flows. This study focuses on sediment cores from the submarine deposits sourced from the SSH. Recent studies have shown that 80 to 90% of volcanic material erupted from the currently active Soufrière Hills volcano on Montserrat ends up in the sea [2]. This illustrates that a better insight into the volcanic history of the SSH can be gained from looking at the marine stratigraphy.

We have discovered new evidence which suggests that there has been a large flank collapse of the SSH edifice into the sea. Sedimentological analysis on stacked graded beds of varying grain-size proportions in the marine sediment cores suggest that the deposit was formed by large retrogressive flank failures of the subaerial SSH edifice.

The geochemical analyses of samples taken from the submarine SSH deposits (trace element and high precision double-spike Pb isotopes) coupled with SEM images illustrate that the SSH volcano contains a record of complex magmatic activity. The activity includes multiple injections of mafic magma followed by magmatic differentiation and episodic explosive eruptions of andesitic pumice, which were triggered by mafic pulses, after this were eruptions of poorly vesiculated basaltic scoria. Significantly, the chemostratigraphic correlations of the subunits within the submarine SSH deposits confirm that the SSH edifice suffered multiple retrogressive collapses of the subaerial edifice. Much of this key information would have been obscured in the on-land record by erosion and burial by later volcanic activity.

[1] Harford, C.L. et al. (2002). The volcanic evolution of Montserrat using $^{40}\text{Ar}/^{39}\text{Ar}$ geochronology. *Geological Society of London, Memoirs*, 93-113 [2] Le Friant, A. et al. (2004). "Geomorphological evolution of Montserrat (West Indies): importance of flank collapse and erosional processes." *Journal of the Geological Society* **161**: 147-160.

International Sedimentology Congress (IAS), Mendoza, Argentina, 2010 – Oral presentation

The rise and demise of South Montserrat: Evolution of the South Soufrière Hills

On the southern extent of the volcanically active island of Montserrat, West Indies, is an interesting but poorly understood volcanic centre called the South Soufrière Hills (SSH) volcanic complex. Eruptions from the SSH centre are dated at ~125-130 ka (Harford *et al.* 2002). Whereas most of Montserrat is made up of andesitic lavas and pyroclastic deposits, the subaerially exposed outcrops of the SSH volcanic centre are composed predominantly of basaltic lava flows. This study focuses sediment cores from the

submarine deposits sourced from the SSH. Recent studies have shown that 80 to 90% of volcanic material erupted from the currently active Soufriere Hills volcano on Montserrat ends up in the sea (Le Friant *et al.* 2009). This illustrates that a better insight into the volcanic history of the SSH can be gained from looking at the marine stratigraphy as deposits on land are commonly eroded or buried by subsequent eruptions.

We have discovered new evidence which suggests that there has been a large flank collapse of the SSH edifice into the sea. Sedimentological analysis on stacked graded beds of varying grain-size proportions in the marine sediment cores suggest that the deposit was formed by large retrogressive flank failures of the subaerial SSH edifice. This is supported by evidence from shallow seismic surveying off the southern Montserrat shoreline, which has identified hummocky morphology interpreted as debris avalanche deposits, the result of volcanic flank collapse, on the sea floor (Le Friant *et al.* 2004).

Chemostratigraphy has been used in this study to provenance clasts to their source regions, to assess the chemical evolution of the magmas, and as a correlative tool to follow the deposits between cores. The geochemical analyses of samples taken from the submarine SSH deposits (trace element, $^{87}\text{Sr}/^{86}\text{Sr}$ and high precision double-spike Pb isotopes) coupled with SEM images illustrate that the SSH volcano contains a record of complex magmatic activity. The activity includes multiple injections of mafic magma followed by magmatic differentiation and episodic explosive eruptions of andesitic pumice, which were triggered by mafic pulses, after this were eruptions of poorly vesiculated basaltic scoria. Significantly, the chemostratigraphic correlations of the subunits within the submarine SSH deposits confirm that the SSH edifice suffered multiple retrogressive collapses of the subaerial edifice. The volcanoclastic turbidites in the cores sample chemically heterogeneous sub-units as the failures successively cut back through older subaerial volcanic deposits from the SSH edifice. Much of this key information would have been obscured in the on-land record by erosion and burial by later volcanic activity. Therefore the record in marine sediment cores provides the best means with which to reconstruct these events.

